HIGH RESOLUTION CHARACTERIZATION AND MODELLING OF AN ARAB-D OUTCROP ANALOG, CENTRAL SAUDI ARABIA

BY

HASSAN ABDALLA ELTOM

A Dissertation Presented to the

DEANSHIP OF GRADUATE STUDIES

KING FAHD UNIVERSITY OF PETROLEUM & MINERALS

DHAHRAN, SAUDI ARABIA

In Partial Fulfillment of the

Requirements for the Degree of

DOCTOR OF PHILOSOPHY

In

GEOLOGY

April, 2013

KING FAHD UNIVERSITY OF PETROLEUM & MINERALS

DHAHRAN- 31261, SAUDI ARABIA

DEANSHIP OF GRADUATE STUDIES

This thesis, written by Hassan Eltom under the direction his thesis advisor and approved by his thesis committee, has been presented and accepted by the Dean of Graduate Studies, in partial fulfillment of the requirements for the degree of **DOCTOR OF PHILOSOPHY IN GEOLOGY.**

Dr. Mohammed Makkawi
(Advisor)

Dr. Abdulaziz Al-Shaibani
Department Chairman

Dr. Osman Abdullatif
(Co-Advisor)

Dr. Salam A. Zummo
Dean of Graduate Studies

Dr. Ahmet Umran Dogan
(Member)

2/5/13
Date

Dr. Mustafa Hariri
(Member)

Dr. Michael Kaminski
(Member)

To my mother

ACKNOWLEDGMENTS

I would like to express my sincere gratitude to King Fahd University of Petroleum & Minerals for giving me the opportunity to pursue PHD study and supporting me for three years to accomplish my PHD degree. I would like also to express my appreciation to the dissertation committee chairman, Dr. Mohammed Makkawi, the co-chair Dr. Osman Abdullatif, Committee members Prof. Ahmet Dogan, Dr. Mustafa Hariri, and Dr. Michael Kaminski. Thanks also to Dr. Wyn Hughes who has considerable participation in the supervision of this dissertation.

I would like to thank the chairman of the Earth Sciences Department, Dr. Abdulaziz Al-Shaibani and faculty in the department and in the research institute for the support and continuing help during different stages of the study. I would like to acknowledge the support provided by King Abdulaziz City for Science and Technology (KACST) through the National Science & Technology Unit at King Fahd University of Petroleum & Minerals (KFUPM) for funding this work under project # 09-Oil767-04 as part of the National Science, Technology and Innovation Plan (NSTIP). Thanks also to my colleagues in Earth Sciences Department and to Sudanese community at KFUPM.

TABLE OF CONTENTS

LIST OF TABLES

LIST OF FIGURES

ABSTRACT (ENGLISH)

Full Name : Hassan Eltom

Thesis Title : HIGH RESOLUTION CHARACTERIZATION AND MODELLING OF AN ARAB-D OUTCROP ANALOG, CENTRAL SAUDI ARABIA

Major Field : Geology

Date of Degree : April, 2013

Outcrop analogs are used to improve characterization of the intra-reservoir stratigraphy, understand subsurface facies architecture, heterogeneity and overcome the limitation associated with large inter-well spacing within individual oil fields. This study characterized and modeled an outcropping strata equivalent to the Upper Jurassic Arab-D carbonate reservoir in central Saudi Arabia. The study presents qualitative and quantitative sedimentological and petrographic descriptions of lithofacies associations and interprets them within a high order stratigraphic framework using geostatistical Modelling, spectral gamma ray, geochemistry, petrography and micropaleontology. The sedimentological studies revealed several lithofacies associations, which are interpreted as a gentle slope platform depositional environments. A total of 44 cycles were identified, with cycle thicknesses ranging from 15.2 cm to 255 cm. These cycles comprise nine high frequency sequences. The biocomponents of the study area show a lower degree of diversity than the subsurface Arab-D reservoir; however, some key biofacies are present and provide paleoenvironment indication. The geochemical results show a strong correlation between the major and trace elements and the reservoir facies and suggest that the concentrations of elements and their corresponding spectral gamma ray logs follow the same general upwards shoaling pattern. The 3-D geocellular model captures small-scale reservoir variability, which is reflected in the petrophysical data distribution in the model. Microporosity and their associated permeability in the analyzed samples range from 0.4% to 6.4 % and 0.02 to 1.2 mD, respectively and their morphology have different characteristics. This investigation increases the understanding of the intra-reservoir stratigraphy of the subsurface Arab-D reservoir and provides a general framework for zonation, layering, and lateral stratigraphic correlations.

ملخص الرسالة

الاسم الكامل: حسن عبدالله التوم مساعد

عنوان الرسالة: دراسة جيولوجية لوصف ونمذجة مكمن العرب- د البترولي باستخدام شبيه سطحي في وسط المملكة العربية السعودية

التخصص: جيولوجيا

تاريخ الدرجة العلمية: ابريل 2013

توفر المنكشفات الصخرية لعصر الجوراسي الأعلي في وسط المملكة العربية السعودية شبيه جيد لمكمن العرب- د تحت سطح الأرض. وهذا بالتالي يساعد على دراسة وتقييم الخصائص الرسوبية والطبقية التي تؤثر على نوعيه ومعماريه المكمن. تعنى هذه الدراسة بوصف ونمذجة مكمن العرب- د باستخدام شبيه سطحي من وسط المملكة العربية السعودية. تهدف الدراسة الى تحديد الخصائص الرسوبية والطبقية والبتروفيزيائية وتأسيس نماذج جيولوجية وجيوإحصائية لمكمن العرب- د. إحتوت الدراسة على تكامل طرق حقلية ومعملية عدة منها تحليل حقلي رسوبي وطبقي وتحاليل رسوبية معملية للسحنات وبتروغرافيه وتحليل المسامية والنفاذية بالاشعه السينيه والمجهر الالكتروني الماسح. تم تأسيس النماذج الجيولوجية والجيوإحصائية التي توفر معلومات تساعد على فهم والتكهن بخصائص مكمن العرب- د ونوعيه صخور المكمن. تشير الدراسة إلى عدة سحنات صخرية وتسع تتابعات سحنية دقيقه في مكون جبيله الأعلى وعضو العرب- د والتي ترسبت على رصيف بحري قليل الميلان.

لقد كشف نموذج المكمن عن توزيع السحنات والمسامية والنفاذية على إمتداد الشبيه السطحى. كما أن نموذج مكمن الشبيه السطحي يوفر رؤيه أفضل للمكمن بمقياس أقل من خليه في نموذج المكمن تحت السطح. يعد تطبيق اشعة قاما المطيافي والتحليل الجيوكيميائي مؤشر جيد لتحديد نوع السحنات ومقارنتها. كما ساعدت ايضاً على تحديد النطاقات في صخور المكمن. كشفت الدراسه الى وجود ثلاثه انواع من المساميه الدقيقة. يشير التنوع في المسامية الدقيقه والنفاذيه المصاحبه الى التنوع فى النظام المسامي كما أكدت ذلك نتائج فحص المجهر الالكتروني الماسح. وفرت هذه الدراسة معلومات ونموذج شبيه سطحى دقيق لمكمن العرب- د ساعد على فهم والتكهن بخصائص ونوعيه ومعماريه مكمن العرب- د لا يمكن أن تتوفر من المعلومات التحت سطحيه. كما أن الدراسة ساهمت ايضًا على توفير وتطوير طرق عمل وتقنية متكاملة لدراسه وفهم خصائص ونوعيه المكامن.

CHAPTER 1

INTRODUCTION

1.1 Introduction

Outcrop analogs have the potential to improve understanding of intra-reservoir stratigraphy (Pringle et al., 2004; Bellian et al., 2005) and provide rock-based data on the vertical and lateral characteristics of their reservoir equivalents (Bellian et al., 2005). Integrated outcrop study leads to a higher order of resolution in characterizing the lithofacies and sedimentary features in the subsurface reservoir analog. This approach improves the understanding of reservoir complexity, facies architecture and heterogeneity within the stratigraphic framework (Girard et al., 2008).

The Arab-D reservoir is considered as the most producing interval in the word (Lindsay et al., 2006) (Figure 1-1). This reservoir comprises the Arab-D Member of the Arab Formation and the Upper Jubaila Member of the Jubaila Formation and is assigned to Upper Jurassic, Kimmeridgian age (Powers, 1962; Meyer et al. 1996; Hughes 1996, 2004a, 2004b,2009). The Arab-D reservoir in Ghawar field has an average thickness of 60 m, an average porosity of 15%, and permeability of several darcys (Lindsay et al., 2006).

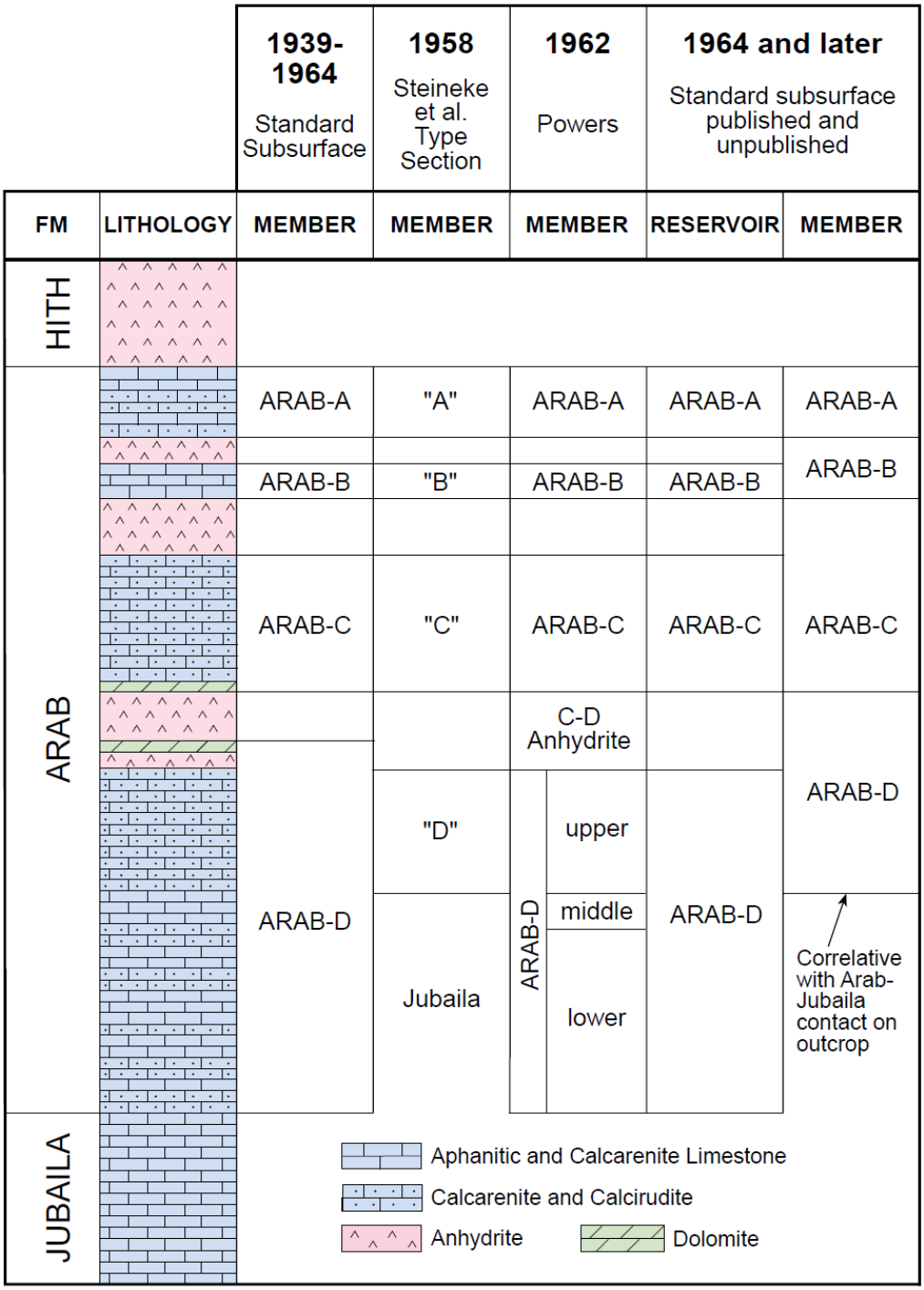

Figure 1-1: Stratigraphic section of the Arab-D reservoir showing the historical evolution of terminology (Meyer et al., 1996).

Sedimentological characterization has been conducted on the major carbonate reservoirs of Saudi Arabia, especially the Arab-D reservoir (Wilson, 1981; Mitchell et al., 1988; Meyer et al., 1996; Hughes, 1996, 2004a, 2004b 2009; Sahin et al., 1998; Cantrell and Hagerty, 1999; Saner and Sahin, 1999; Al-Dhubbeb, 2003; Cantrell et al., 2004a, 2004b; Saner et al., 2005; Lindsay et al., 2006). These studies encompass many aspects of the characterization of the Arab-D reservoir; but a high-resolution stratigraphic model and correlation, which is the main foundation for understanding the reservoir heterogeneity, are still lacking. This limitation is attributed to the relatively large inter-well spacing between oil fields in which major lithofacies changes could occur (Pringle, 2000). In addition, the similarity of the general shoaling upward of the whole upper Jurassic system (Lindsay et al., 2006) may also mask the signature of the Arab-Jubaila formation boundary. Moreover, the existing 3-D reservoir models have large cell volumes (Douglas, 1996) and lack high resolution and likely neglect large facies changes. Therefore, in order to bridge the gaps in reservoir Modelling it is pertinent to construct accurate high-resolution 3-D models of lithofacies stacking patterns.

With the exception of the electron microprobe study of the sub surface Arab-D reservoir (Cantrell, 2005), there has not been any published elemental analysis study carried out on either the outcrop analogs or subsurface Arab-D reservoir. Geochemistry was successfully tested for reservoir zonation, paleogeographic interpretation, and lithofacies mapping (Calvo et al., 1995; Cicero and Lohmann, 2001; Vincent et al., 2006). Chemical stratigraphy is useful for reservoir zonation, particularly, when it is integrated with outcrop Spectral Gamma Ray data (SGR).

This study aims to establish a conceptual high-resolution lithofacies geostatistical model by integrating sedimentological, stratigraphical, palaeoenvironmental and petrophysical data of the Arab-D reservoir analog. It is anticipated that the model will be capable of displaying small-scale facies heterogeneities that could reflect the spatial continuity of the porosity and the permeability in the actual reservoir model. Porosity and the permeability data of the Arab-D reservoir obtained from the literature were superimposed on the equivalent outcrop facies to produce high-resolution 3-D porosity and permeability models with minimal uncertainty. This approach precisely reflects the petrophysical properties of the subsurface reservoir. The porosity and permeability values from outcrop samples were also studied to consider the long period of exposure and diagentical events. The study was also tested the applicability of integrating outcrop spectral gamma ray (SGR) and geochemical analysis to develop a sedimentological and stratigraphic sequence model for carbonate reservoir analogs.

This high-resolution outcrop 3-D geostatistical model may act as a norm or proxy for subsurface exploration and production activities. The model will also improve understanding of the actual reservoir lithofacies stacking patterns and changes in the lateral facies distributions. The model might also provide solutions to some challenges associated with the correlation of intra-reservoir lithofacies and help in the development of a realistic reservoir facies zonation. The study also explores the utilization of new data from the study area such as SGR logs and geochemical analysis data. These data could contribute to the development of a new data-integration approach to understand the characteristics of the hydrocarbon resources of Saudi Arabia.

1.2 Problem Statement

The problem is how to model the sedimentary facies and their sequence hierarchy and stacking pattern at the outcrop analog level with a high order of resolution. Geostatistics, outcrop Spectral Gamma Ray (SGR) logging, and geochemistry are utilized as an integrative toolbox. The study also intends to test the petrophysical parameters of the outcrop analog studied at the same level of facies resolution. This will allow an evaluation of these reservoir parameters in a volume that represents only one cell of the subsurface model and enables the evaluation of the heterogeneity at a finer resolution scale. The toolbox of this research is proposed to answer and explain many research questions that were generated from different assumptions and facts about the Arab-D reservoir.

The motivation to study the reservoir outcrop analog is that compared to the actual geology of the reservoir, the subsurface facies and petrophysical model of Arab-D Reservoir are low in resolution (Meyer et al., 1996). The outcrop analog gives a higher order of facies distribution resolution in both the vertical and horizontal directions (Wilson et al., 2009). The research questions of this part of the study are: how qualitatively describe vertical and lateral variations of the lithofacies and how to apply the reservoir heterogeneity in the outcrop analog scale to provide multiple solution scenarios for hydrocarbon exploration and development of the equivalent reservoir facies in subsurface.

This study also incorporate the concept that lateral facies variations will be expected to affect the stacking patterns of the reservoir units and should therefore be reflected in the

stratigraphic model. The research question to be answered here is to determine how the hierarchy and stacking patterns of the Arab-D reservoir analog would vary along a very closely spaced stratigraphic sections in a single outcrop. The study expect here to be a strong correlation between the lithofacies distribution, the log signature of the SGR for potassium (K), uranium (U), and thorium (Th) and the elemental content. The log signature might reflect relative local marine transgressive and regressive events, where uranium is expected to be higher than the other two radioactive elements. High stand and land progradation would be expected to be marked by higher contents of K and Th and thus higher log values (Bábek et al., 2010; Koptikova et al., 2010; Vacek et al., 2010; Debret et al., 2011; Kalvoda et al., 2011). The question to be answered in this part is whether the correlation of lithofacies, especially the reservoir facies, can be enhanced when using the SGR log integrated with elemental analysis and biofacies.

The study assumes that the sedimentological model generated in the earlier stage of in this study is capable of capturing small scale lithofacies heterogeneities that might affect the spatial continuity of the reservoir porosity and permeability. In this study, the Arab-D reservoir analog was used to build a high resolution model that captures fine-scale sedimentological details. Subsurface reservoir lithofacies were matched with those from the studied outcrop. Porosity values derived from published subsurface core and well logs data from the Ain Dar, Uthmanyah, and Shedgum areas of the Ghawar Field, were assigned to outcrop analog facies (Douglas, 1996; Meyer et al., 1996; Sahin et al., 1998; Cantrell and Hagerty, 1999; Cantrell et al., 2004a; Cantrell et al., 2004b; Cantrell and Swart, 2004). The research question of this part is whether the high resolution facies

model of the outcrop analog can enhance our understanding of petrophysical characteristics when published data are superimposed on the equivalent outcrop facies.

The other aim of petrophysical analysis is to study microporosity. An understanding of the distribution, the origin and the morphology of microporosity is crucial for reservoir characterization and performance (Pittman, 1971; Moshier, 1989; Cantrell and Hagerty, 1999). Microporosity significantly affects logging response, fluid flow properties, capillary forces, irreducible water saturation, and formation evaluation procedure (Budd, 1989).

Finally, the integration of all of these assumptions and research questions is expected to answer the broad question: what are the new views that can be anticipated from this outcrop analog study regarding the improvement of the Arab-D reservoir sedimentary facies, their sequence hierarchy, and the stacking pattern in different Arabian basins. Answering this question could be a valuable contribution for both academic research and the hydrocarbon industry.

1.3 Scope and Objective

The main objective of this dissertation is to establish a high resolution sedimentological, sequence stratigraphic, and geochemical model of the Arab-D reservoir at the outcrop level using geostatistics, sedimentology, and geochemistry as toolboxes for the investigation. The integration of all of these analyses and techniques is expected to result in a high-resolution outcrop-based model, which may act as a norm or proxy for subsurface exploration and production enhancement. This objective was accomplished by performing the following tasks:

- Develop high-resolution, 3-D sedimentological and startigraphical models.
- Establish the paleoenvironment zones by studying macro- and microbiofacies of the outcrop succession.
- Distribute the subsurface porosity and permeability data (extracted from literature) into the high-resolution lithofacies model.
- Describe qualitatively and quantitatively the microporosity and its distribution in the 3-D facies model.
- Characterize the outcrop using Spectral Gamma Ray (SGR) logs and distribute them within the 3-D facies model.
- Analyze the outcrop succession using geochemical analysis.

1.4 Study Area

The outcrop analog of the Arab-D reservoir expose in the Wadi Nisah in central Saudi Arabia,is approximately 90 km long and 2 to 3.7 km wide (Figure 1-2) (Meyer et al. 1996; Weijermars, 1998). At the flank of this graben there are very good exposures of both the Upper Jubaila and Arab-D members, which represent the type section of the Arab-D reservoir in central Saudi Arabia (Okla, 1986). The outcrop also exposes the Arab-C Member that is characterized by a collapsed rocks over the Arab-D carbonate due to dissolution of the Arab-D evaporite dissolution (Figure 1-3). The outcrop is exposed in the strike direction trending N-S. Meyer et al. (1996) performed a lithofacies study of two sections in this outcrop location and described seven lithofacies and their associated porosity and permeability.

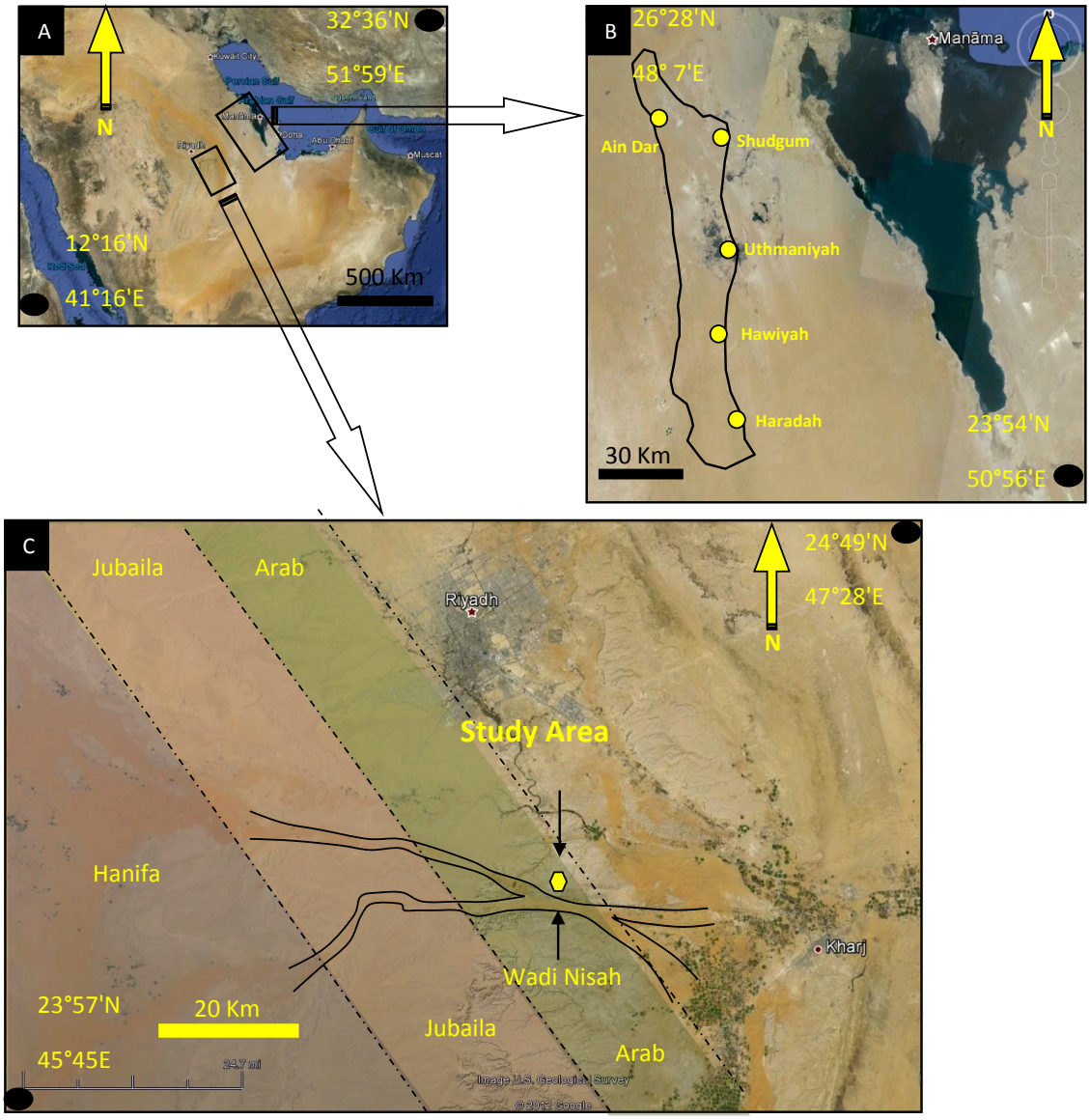

Figure 1-2: A) Map showing the location of Wadi Nisah in central Saudi Arabia, B) Ghawar field including areas within the field from which petrophysical data had been collected, and C) outcrop study area at wadi Nisah southern Riyadh city (Google maps revised February, 2013).

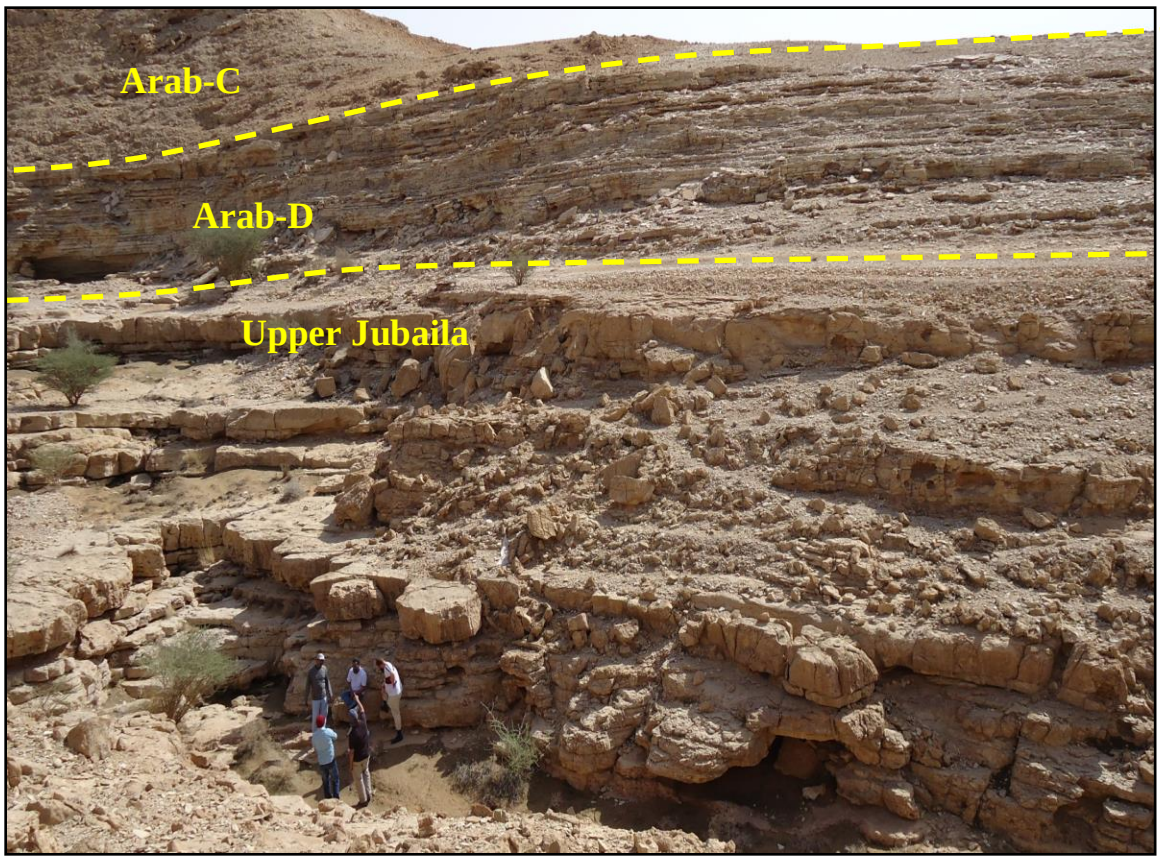

Figure 1-3: Outcrop section in Wadi Nisah. This Arab-D reservoir analog section encompasses the Upper Jubaila Member of Jubaila Formation, and D and C members of the Arab Formation. The Arab-Jubaila contact is clearly defined and confirms of that of Powers et al. (1968).

1.5 Literature Review

The Arabian Plate is one of the largest hydrocarbon regions in the world. It hosts approximately 68% of the oil reserves and approximately 37% of the gas reserves. This region is also considered to be a potential unconventional gas resource. One of the most prolific oil reservoirs in the Arabian Gulf region is the Arab-D reservoir (Lindsay et al., 2006). This reservoir is the major producing interval in Ghawar Field, the largest oil field in the world, and in Khurais field, the largest explored onshore field in the world. In this section of this study, published works on the Arabian plate tectonic history and paleogeography, the geology of the Jurassic succession (Shagra Group), of which Arab-D is one formation, their sequence stratigraphy, the depositional environments and the petroleum system are reviewed. The Arab-D sedimentology, stratigraphy, biofacies, diagenesis, and petrophysical properties are briefly introduced. This section also includes a review of the latest literature on applications of geostatistics, especially at the outcrop level and gives an idea of the integration of SGR logs and geochemistry for geochemical Modelling.

1.5.1 Tectonic Setting

The north trend of the Arabian Plate arches and oil fields were interpreted to be surface reflections of the Precambrian basement configuration (Edgell, 1987). The major events that shape this basement were the Ammar collision, the Najd fault system, Dibba Fault, the Oman Salt Basin and the Wadi Al Batin Lineament (Al-Husseini, 2000) (Figure 1-4). The intersection of the Precambrian structure produced jointed basement fabric, which was reactivated later by subsequent tectonics (Ziegler, 2001) (Figure 1-5).

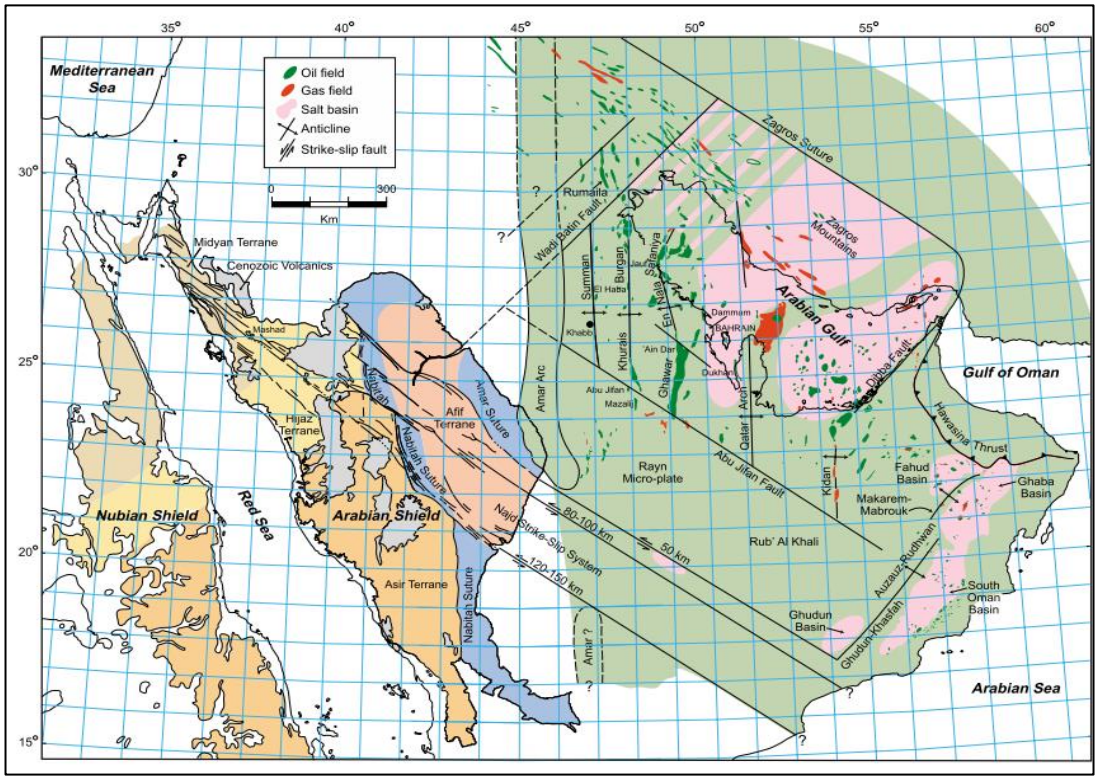

Figure 1-4: Geological map showing the configuration of the Arabian Shield's, the Arabian Arches, and the major fault systems that control the above sedimentary cover in the Saudi Arabia. Note the north trend of the Arabian arches which were controlled mainly by Ammar collision (Al-Husseini, 2000).

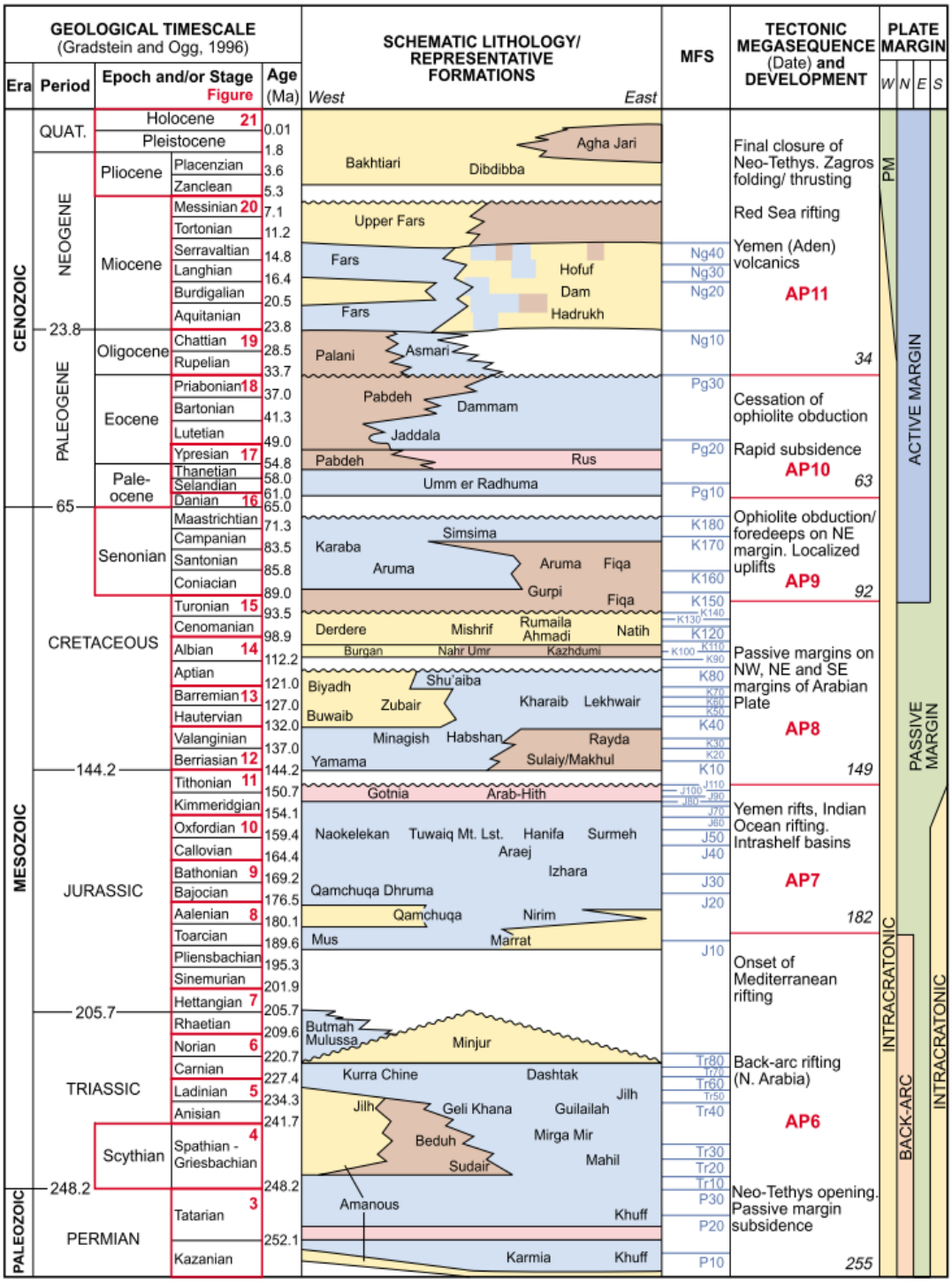

Figure 1-5: Stratigraphic column of the Arabian Plate from Late Permian to Holocene. Note that the Arabian plate had gone through different Plate boundaries during this time (Ziegler, 2001).

The Arabian Plate has evolved through five tectonic settings or evolutionary phases. These phases are plate accretion, intracratonic, back-arc, passive margin plate setting, and active margin setting (Sharland et al., 2001). Currently, the Arabian Plate boundaries are characterized by numerous types of plate boundaries (Konert et al., 2001). In the north and east boundaries, collision with Eurasia occurred during the Late Eocene, followed by the opening of the Red Sea during the late Oligocene to form a divergent margin in the western part. This divergent margin translated to the transform fault of the Dead Sea and the Gulf of Aqaba in the northwest margin of the Arabian Plate during the late Miocene (Hughes et al., 1999; Konert et al., 2001; Ziegler, 2001).

1.5.2 Arabian Plate Paleogeography

The Arabian Plate was located at different positions during the Precambrian and most of the Phanerozoic (Figure 1-6). According to Konert et al. (2001), the Arabian Plate was located close to the equator with an E-W orientation during the Precambrian. It started to move anticlockwise during the Early Paleozoic and reached the maximum south position by the Early Ordovician, the period of glacial deposits in the Arabian Plate. During the Silurian, a time of major transgression, the Arabian Plate moved clockwise towards the equator (Abu Ali et al., 1999).

In the region, another glaciation episode occurred from the Permian through the Carboniferous (Vaslet, 1989; Senalp and Al-Duaiji, 2001). The Arabian Plate was again located near the equator during at the time of deposition of the Arab-D inthe Late Jurassic. The paleogeography of the Arabian Plate during the Early to Late Jurassic was a warm, arid climate representing the southern margin of the Tethys Ocean (Murris, 1981; Le Nindre et al., 1987; Al-Husseini, 1997).

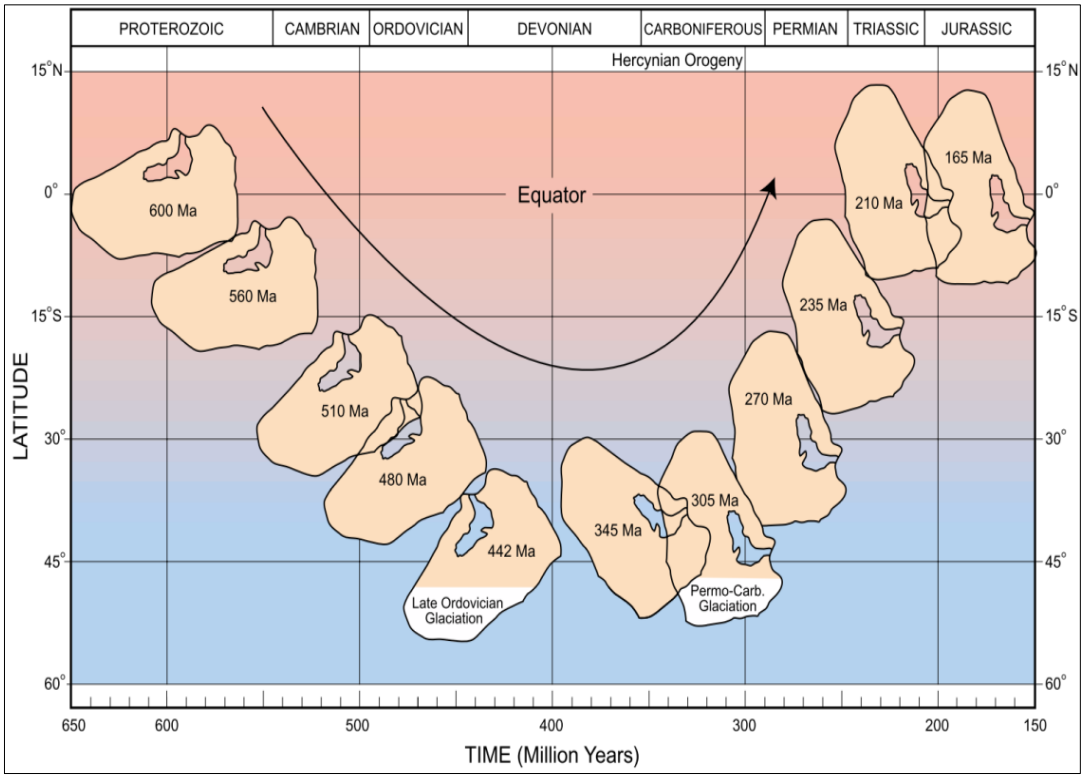

Figure 1-6: Paleolatitude positions of the Arabian Plate from Proterozoic to Jurassic. The Arabian Plate started to move anticlockwise to the south until it reached higher latitude in the Ordovician and Devonian. The plate was completely rotated and started to move north and reached close to the equator in the late Jurassic time (Konert et al., 2001).

The Arabian Plate during Jurassic was occupied by a shallow marine carbonate platform (Al-Husseini 1997; Handford et al., 2002). Tectonic activity during that time created a number of intra-shelf basins in the carbonate platform (Ziegler, 2001). These intra shelf basins are the Arabian, Qotnia, and Al Rub Al Khali basins. During this period, a thick interval of carbonate succession was deposited, the Shaqra Group, which include seven pure carbonate formations. Based on micropaleontological studies, Hughes (2004b) subdivided these Jurassic formations into three possible super sequences of formations that could be differentiated according to their paleoenvironmental setting.

1.5.3 Jurassic Formations (Shaqra Group)

The Jurassic Shaqra Group (Le Nindre et al., 1987) is the most important stratigraphic unit in the Middle East. The sedimentology, stratigraphy, biofacies, paleoenvironment, and reservoir quality of this group have been studied since the middle of the last century (Steineke and Bramkamp, 1952; Powers, 1962; Powers, 1966; Wilson, 1981; Le Nindre et al., 1987; Mitchell et al., 1988; Vaslet et al., 1989; Enay and Mangold, 1994; Le Nindre et al., 1996; Al-Husseini, 1997).

This group comprises seven formations that are, from bottom to top, the Marrat, Dhruma, Tuwaiq Mountain, Hanifa, Jubaila, Arab and Hith formations (Figure 1-7). These seven formations host twelve major hydrocarbon reservoirs in Saudi Arabia; they are, from bottom to top, Marrat, Farida, Sharas, Lower Fadhili, Upper Fadhili, Hadriya, Hanifa, Arab-D, Arab C, Arab B, Arab A, and Manifa (Hughes, 2004a).

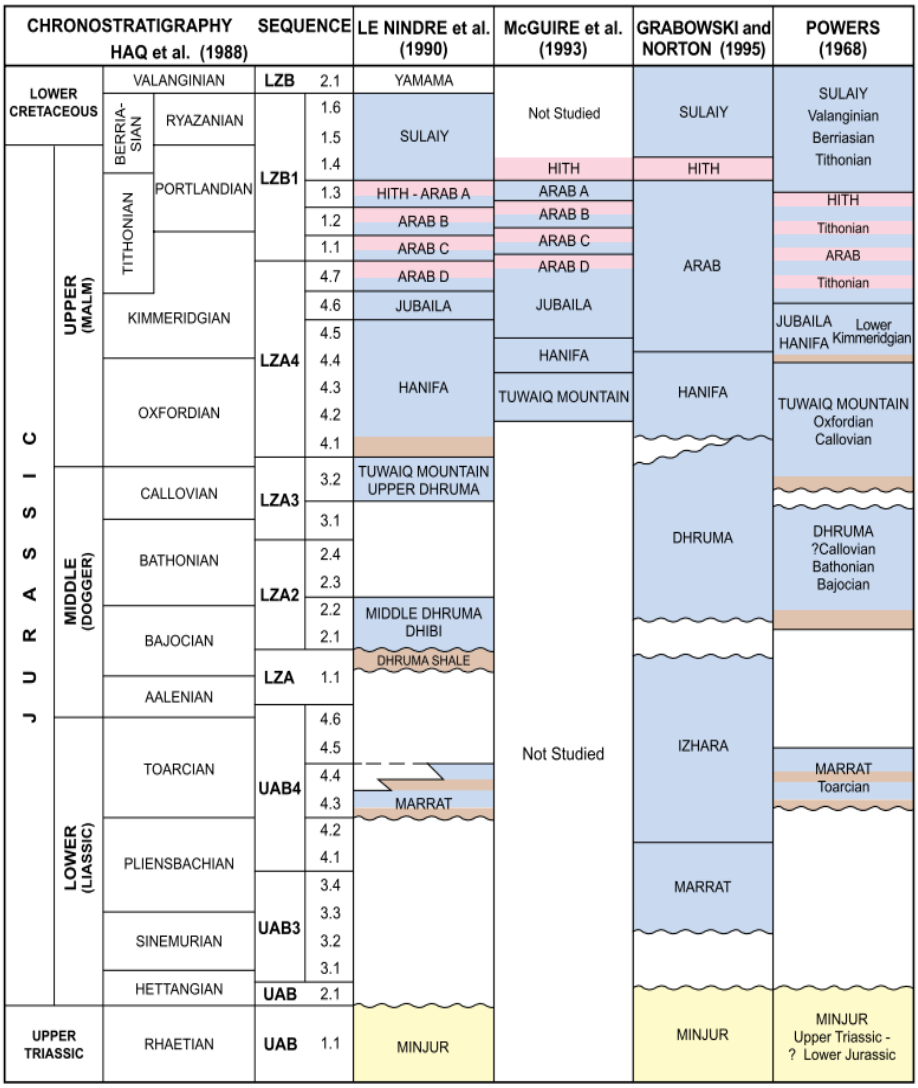

Figure 1-7: Stratigraphic succession of Shaqra Group. This group encompasses seven formation separated by six hiatus (Hughes, 2004a).

Based on exposure description by Enay et al. (1987) the Marrat Formation was interpreted as a shallow to moderately marine condition; the Dhruma Formation was moderately shallow to deep marine; the Tuwaiq Mountain Formation was deep marine to shoal setting; the Hanifa Formation was back shoal to lagoonal; the Jubaila Formation was restricted lagoonal; the Arab Formation was a tidal flat; and the Hith Formation was a salina. It should be noted that east-ward of the outcrop belts described by Enay et al. (1987) intrashelf basins developed such as that described for Hanifa Formation by Hughes et al. (2008).

Based on their micropaleontological data, these formations have been subdivided into five groups (Hughes, 1996, 2004a 2004b, 2009). Each group has a unique biofacies assemblage that indicates a certain paleoenvironment. The sequence stratigraphy framework of the Upper Jurassic formations, including the Jubaila and Arab Formations, has been studied from different perspectives. Le Nindre et al. (1996) suggested a sequence stratigraphic framework based on the global sea level model of Haq et al. (1986) that was followed by Al-Husseini (1997), who established the sequence stratigraphic framework of the Gulf region. By applying the principles of sequence stratigraphy from Galloway (1989) using the maximum flooding surface, Sharland et al. (2001) subdivided the Upper Jurassic sequence into 9 maximum flooding-based stratigraphy (Galloway, 1989), namely they are summarized in Table-1-1.

Arab-D Reservoir

Both the Jubaila and the Arab formations were assigned to the Early Kimmeridgian stage (Figure 1-8). The Jubaila Formation overlays the Hanifa Formation, and it is overlain by

the Arab Formation (Powers, 1962; Powers et al. 1966). The Jubaila Formation is subdivided into the Lower and Upper Jubaila (Vaslet et al., 1989; Meyer et al., 1996). The Upper Jubaila Member is considered to be a part of the Arab-D reservoir (Powers, 1962; powers et al., 1966). The Arab Formation is composed of four members A, B, C, and D each consisting of carbonate-evaporite cycles with the A cycle representing the youngest cycle and topped by a very thick evaporite layer, named the Hith Formation (Hughes, 2004b). The Arab-D Member, along with the underlying Upper Jubaila Formation, composes the most prolific worldwide reservoir, the Arab-D reservoir. On the basis of a biofacies study, Hughes (1996), subdivided the Arab-D reservoir into three zones although subsequent unpublished reports enabled many many more microfacies to be determined (Hughes, personal communication). The basal deep marine zone is represented by the Upper Jubaila Formation D3**.** The middle zone, which includes the Lower Arab-D, represents the relatively shallower marine condition D2. Finally, the upper zone includes the very shallow marine condition and is represented by the upper Arab-D Member. Lindsay et al. (2006) defined five lithofacies for the Arab-D reservoir cores from Shedgam area in the Ghawar field . For the same study area, Lindsay et al. (2006) also defined 8 high frequency sequences, 28 cycle sets, and 120 cycles. The controls on these high resolution sequences were attributed to Milankovitch climatic cycles. Ziegler (2001) discussed the depositional environments, paleogeography, and stratigraphy of the Arab-D reservoir at the subsurface level in Saudi Arabia. Al-Dhubbeb (2003) used biofacies to calibrate the Jurassic Jubaila-Arab contact from the outcrop at Riyadh to the subsurface in central and eastern Arabia. Lindsay et al. (2006) described the Arab-D outcrop reservoir equivalents in central Saudi Arabia around the Riyadh

region. The dolomitization of the Arab-D reservoir was studied by several researchers such as Cantrell et al. (2004a), Swart et al. (2005), and Lehmann et al. (2006) Cantrell et al. (2007). According to these studies, the dolomite in Arab-D was subdivided into non-fabric preserving, fabric preserving, and baroque dolomite. Many researchers (e.g.,Douglas (1996), Meyer et al. (1996), Sahin et al. (1998), Cantrell and Hagerty (1999), and Cantrell et al. (2004a) focused their studies on the porosity distribution and the characterization of the Arab-D reservoir Meyer et al. (2000) presented a detailed description of the permeability distribution patterns in Arab-D-reservoir. Regionally, the Arab-D layers form a significant hydrocarbon reservoir. Its major producing outside Saudi Arabia include UAE, Qatar, and Bahrain. The lithofacies and their paleoenvironment were extensively studied in this region by many researchers (e.g., Wilson,1981, Vaslet et al., 1989, Le Nindre et al., 1996, and Alsharhan and Salah,2001).

1.5.4 Outcrop Geostatistical Modelling

The integration of a geostatistical toolbox to understand reservoir geology has long been used for hydrocarbon production optimization (Al-Khalifah and Makkawi, 2002). but, the subsurface data are still considered coarse and to have very low resolution (Warrlich et al., 2008). Geostatistical outcrop Modelling is increasingly in demand for subsurface reservoir Modelling (Pringle et al., 2006; Warrlich et al., 2008; Leren et al., 2010; Lapponi et al., 2011; Merino-Tomé et al., 2012) because they contribute significantly to exploration and production plans (Palermo et al., 2010). The recent advances in georeferencing and 3-D imaging, such as Light Detection And Ranging (Lidar) and the Differential Global Position System (DGPS), allow for the production of more accurate

3-D geological models from outcrop analogs (Pringle et al., 2004; Bellian et al., 2005; Girard et al., 2008).

The method of 3-D reservoir outcrop analog Modelling was discussed in details by Wilson et al. (2009) and Fabuel-Perez et al. (2010). The resulting model of this method provides a high-resolution model that is capable of capturing small scale sedimentological and stratigraphic features and reservoir qualities, which is expected to address the interwell scale. Outcrop models could be populated by real reservoir petrophysical data to visualize their high resolution distribution (Labourdette et al., 2008; Adams et al., 2009). In these studies, lithofacies from the studied outcrop analogs and the subsurface reservoir were correlated, and similar lithofacies were given similar porosity values.

Subsurface geological Modelling uses non-parametric geostatistics to characterize the spatial variability of lithofacies and the horizontal and vertical zonation (Sahin and Al-Salem, 2001). The main controls for the development of the facies model at the outcrop level are the indicator semivariograms taken from the outcrop stratigraphic sections (Falivene et al., 2006; Wilson et al., 2009; Guo and Deutsch, 2010). Indicator semivariograms were constructed in different directions to determine the directions with the highest and lowest spatial continuity (Dutton et al., 2002). The nugget value, which is defined as the variability at a very low range or at the smaller lag of the data points, should be equal for the three semivariogram directions (major, minor, and vertical) (Frykman, 2001). To calculate the "nugget" value, it is better to begin with the vertical semivariogram because its parameters are better defined.

Table 1-1: Maximum flooding scheme for the Jurassic succession according to Sharland et al. (2001) and Hughes (2009).

MSF	Absolute Age (Ma)	Age	Lithostratigraphy
J110	147	late Tithonian	intra Hith Formation
J100	150.75	late Kimmeridgian	near base of Arab A
J90	151.25	late Kimmeridgian	near base of Arab B carbonate
J80	151.75	late Kimmeridgian	near base of Arab C carbonate
J70	152.75	late Kimmeridgian	lower Jubaila Formation
J60	154	early Kimmeridgian	upper Hanifa Formation
J50	156	mid-Oxfordian	lower Hanifa Formation
J40	162	mid-Callovian	Dhruma Formation, Hisyan Member
J30	168	early Bathonian	middle Dhurma Formation
J20	175	early Bajocian	lower Dhruma Formation
J10	185	late Toarcian	Upper Marrat Formation

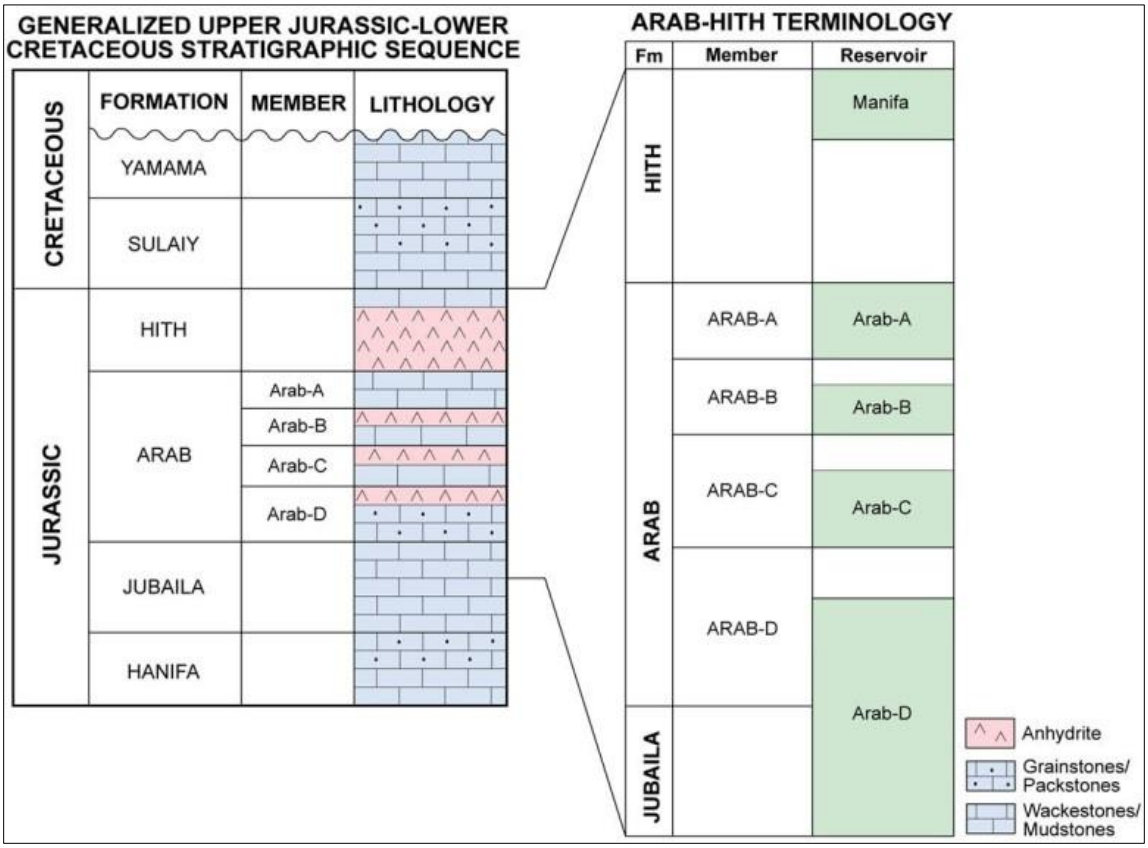

Figure 1-8: Late Jurassic Stratigraphic section showing Hanifa, Jubaila, and Arab formations . The Arab-D reservoir includes both the Upper Jubaila and Arab-D Member of the Arab Formation (Cantrell and Hagerty, 1999).

1.5.5 Outcrop Gamma Ray

Spectral Gamma Ray (SGR) logging of outcrops is an excellent technique to characterize and model reservoirs (Martinius et al., 2002; Krystyniak et al., 2005; Collins et al., 2006). Gamma-ray spectrometry (GRS) logging in outcrops using scintillation spectrometers has wide applications in sedimentological and stratigraphical analysis. The primary logs of SGR logging are potassium K (%), uranium U (ppm), and thorium Th (ppm), which reflects significant rock component information (Slatt et al., 1992). This information is widely used for lithofacies correlation and sequence-stratigraphic interpretations. SGR does not only relate log signatures to actual facies from the outcrop but also provides a potential correlation framework in both two and three dimensions (Evans, et al., 2007).

The integration of SGR with the geochemical data of sedimentary rocks has been used effectively for both carbonate and clastic rocks (Svendsen and Hartley, 2001; Evans et al., 2007). This integration provides much more information regarding the depositional environments in terms of the water depth, the bottom water oxygen conditions, and the terrigenous clastic input. This helps in understanding both vertical and lateral lithofacies stacking patterns and, ultimately, provides a higher order of resolution for reservoir characterization (Dennison, et al., 1997).

1.5.6 Geochemical Analysis

Halverson et al. (2010) stated that "Chemical stratigraphy, or chemostratigraphy, is the study of variations in the chemical compositions of sediments. Chemostratigraphy has diverse applications to the investigation of the rock records. It is used in reconstructing paleoenvironments, determining the tectonic setting of sedimentary basins, indirect dating, and establishing regional or global correlations". A change in chemostratigraphic

signatures might indicate a change in the depositional environment water chemistry or a change in the subsequent diagenetical processes (Bartley et al., 2007).

The integration of the SGR and bulk chemical analyses of an outcrop improves reservoir rock mapping and correlation (Collins et al., 2006; Schnyder et al., 2006; Evans et al., 2007; Koptikova et al., 2010). It may also be utilized to establish a cutoff for the low porosity zones and the permeability barrier. Koptikova et al. (2010) indicated that, once the correlation between elements from the bulk rock analysis and the outcrop SGR is established confidently, the SGR log could give valuable information about the outcrop and downhole lithology.

Stable isotope analysis is the most widely used chemostratigraphic tool to determine the paleoenvironment, diagenetic environments, and sea water chemistry (Cantrell et al., 2004a; Collins et al., 2006; Bartley et al., 2007; Halverson et al., 2010). On the basis of morphology, fabric preservation, and carbon and oxygen isotopes, the dolomite beds in Arab-D reservoir have been classified into five types (Cantrell et al., 2001). Carbon and oxygen isotopes play a major role in establishing the dolomitic environment model for Arab-D reservoir.

The Th/U ratio is an excellent indicator of water chemistry in term of oxidizing and reducing conditions (Koptíková et al., 2010) and can be used to interpret the water depth of the depositional environment and the associated lithofacies. Thorium (Th) is considered a detrital element characterized by a relatively high degree of insolubility; therefore, its high concentration is always associated with a high concentration of other detrital elements fractionated from silicate minerals and indicates a proximal shallow

depositional environment (a high degree of terrigenous clastic input). Uranium (U) is considered more soluble with a relatively higher degree of mobilization, which allows for leaching and concentrations in deep water conditions, and it is always associated with very low concentrations of detrital elements (a low degree of terrigenous clastic input).

CHAPTER 2

METHODOLOGY

2.1 Sedimentological and Stratigraphic Analysis

Several stratigraphic sections were described, measured, and sampled sedimentologically. A sedimentary log for each section was established and sampled for each bed to ensure high resolution for the facies model. Facies logging was performed using the following criteria: micrite percentages, grain types and grain percentages, the textural classification of Dunham (1962), sedimentary fabric, minerology, macro- and micropaleontology, and other carbonate components (Figure 2-1). Photographs and information for each facies in the stratigraphic sections were archived and saved for further analysis. The planned rock sampling procedure is to collect approximately 350 samples distributed in 14 stratigraphic sections in the study area.

During laboratory analysis, all collected samples were slabbed and redescribed for sedimentology. Half of the samples were preserved for thin section analysis and for further microfacies identification. In order to differentiate between carbonate minerals types, some of these thin sections were stained using alizarin Red (Dickson, 1996). Interpretation of the depositional environments were based on field and laboratory observation made from sedimentary structures and texture of the rocks aided with macro- and microbiofacies investigation. Palaeoenvironmental analysis of macro- and microbiofacies of the outcropping succession of the Arab-D reservoir is based on an

interpretation of 120 thin sections. The Palaeoenvironmental reconstruction followed those zones proposed by Hughes (2004a, 2004b, 2009).

2.2 Geochemical Analysis

Out of the 350 samples collected from the study areas, 200 representative samples were selected for geochemical analyses based on bed by bed sampling system. . These samples represent 6 outcrop profiles in which complete individual sections were sampled and logged by full SGR spectrometry. The samples were selected to cover the whole range of lithofacies in the study area (Figure 2-2).

Specifically the following analyses were conducted:

- 120 samples covering 7 stratigraphic sections were studied petrographically.
- 200 samples were analyzed by Inductively Coupled Plasma-Mass Spectrometry (ICP.-MS).
- 56 samples were analyzed by Energy Dispersive Spectroscopy (SEM-EDS), and powder X-ray Diffraction (XRD). These samples were also analyzed for Oxygen and Carbon Stable isotopes. These samples covered two sections that include the Upper Jubaila and Arab-D members.
- 22 samples were analyzed for strontium isotopes (Sr^{87}/Sr^{86}). This covered one section that include the upper Jubaila and Arab-D members

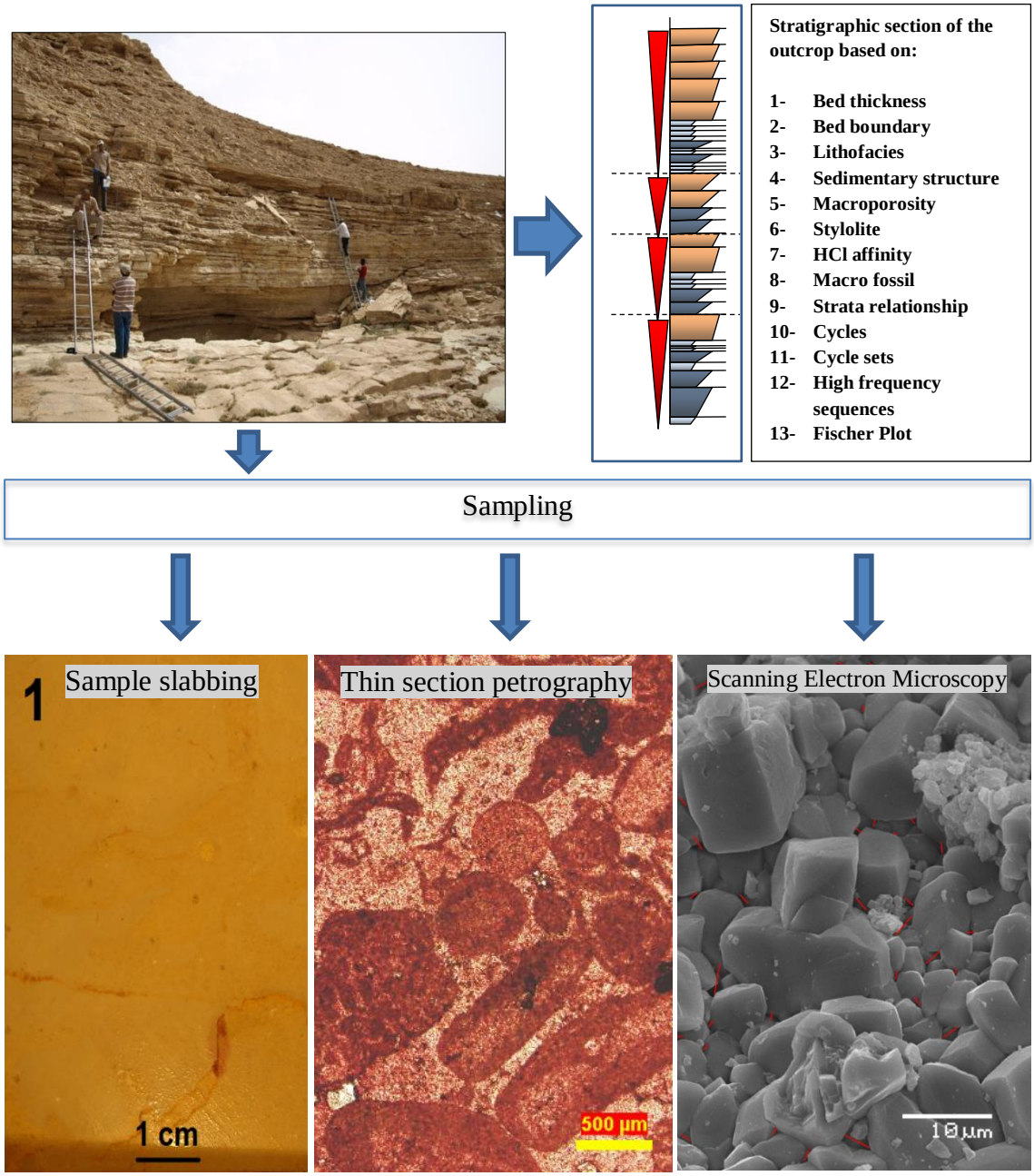

Figure 2-1: Workflow for sedimentology and stratigraphy characterization.

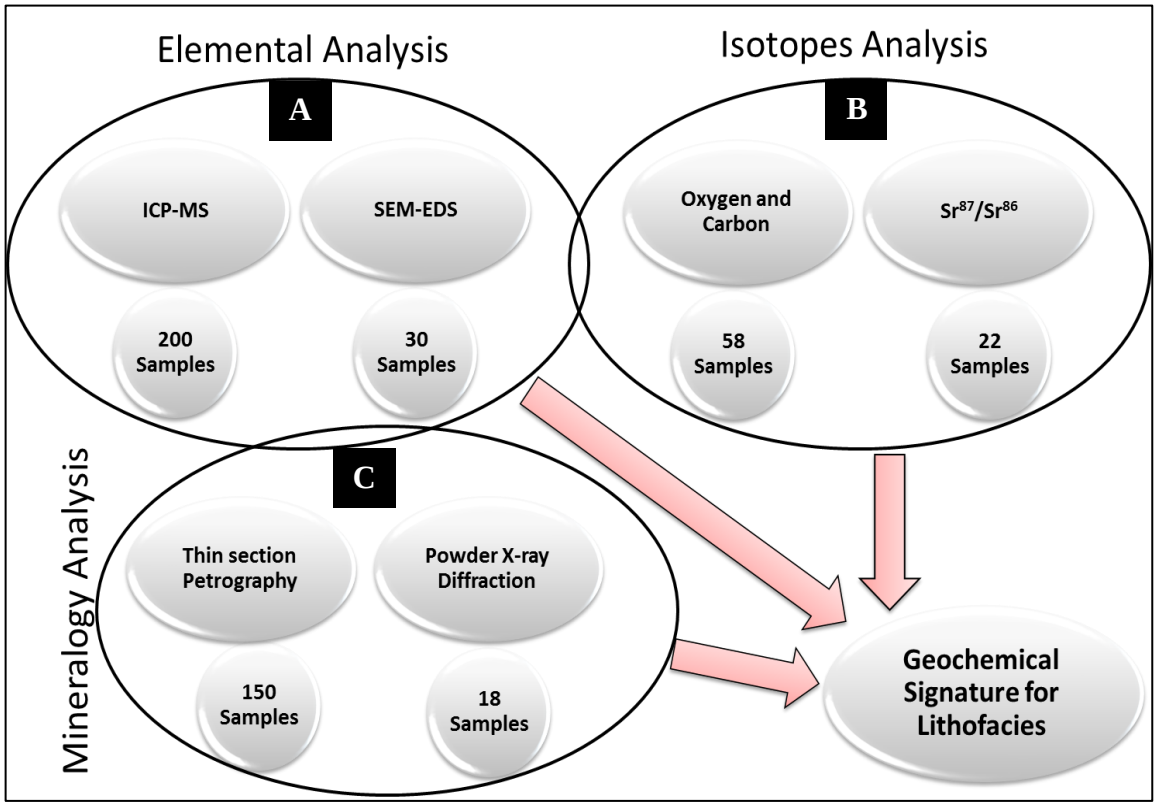

Figure 2-2: Diagram showing selected numbers of samples for different geochemical analysis. A) elemental analysis by inductively coupled plasma mass spectrometry (ICP-MS) and scanning electron microscope (SEM) and energy dispersive spectroscopy (EDS). B) Isotopes analysis includes carbon and oxygen stable isotopes and strontium ration. C) Mineralogical analysis conducted using thin section petrography and powder X-ray diffraction.

2.3 SGR Logging

SGRs are naturally emitted from the more radioactive sediments, which contain the elements U, K, and Th. The radiation was measured in the field using a 512-channel portable SGR spectrometer (Gamma Surveyor model manufactured by Geofyzika, Czech Republic) (Figure 2-3). This spectrometer is equipped with a 3- x 3-inch NaI (TI) scintillation detector and was used to measure the total SGR emissions and the individual levels of each of the three radioactive elements. The SGR spectrometer records count per second (CPS) within a distinct time window defined here as the time over which counts are accumulated. The SGR readings were collected vertically every 20 cm up the face of the outcrop for each stratigraphic section.The sampling time window was selected after measuring the same point 33 times for durations of 10, 20, 30, 40, 50, 60, 120, 180, and 240 seconds to evaluate reading variability among these time windows. This study used 33 measurements because populations with 30 samples represent the boundary between small and large samples and have statistical parameter values with low variability that are reasonably representative of the whole population. This conclusion was reached after conducting 115 measurements of the same point at the outcrop with a 50-second time window to accumulate CPS readings. The number of samples in the population was accumulated every five samples to get 23 populations with sample numbers from 5 to 115 at 5-sample intervals. The mean, standard deviation, and variance were plotted for each population (Figure 2-4). Using these statistical parameters for assessment, the populations with fewer than 30 samples were found to be highly variable, whereas the populations with more than 30 samples were considerably less variable and showed values for each of their statistical parameters that tended to form plateaus in Figure 2-4 indicative of extremely low variation. Therefore, populations with 33 samples were used to test

gamma-ray variability because this size provides a buffer of three samples over the 30-sample boundary above which all populations exhibit similar values for each of the statistical parameters. Figure 2-5 shows histograms and Figure 2-6 shows matrices and coefficients of variation (CVs) for the SGR measurements, which indicated that the longer the readings, the less variable the measurements. Among these measurements, the 240-second reading showed the least variability; however, from a practical viewpoint, a minimal sampling time with an acceptable variability is needed in a study area with a thick logging stratigraphic interval. Acceptable variability is defined in this study as variability that shows little change as the duration of the SGR measurements at single points increase. The histograms and the CVs show that among the tested time windows, the 10-, 20-, 30-, and 40-second readings have higher variability than the 120-, 180-, and 240-second readings. Thus, 60 seconds is the best duration over which to accumulate the SGR counts in the field because the histogram for this duration shows acceptable variability. In addition, 60 seconds is a reasonable time because the CV % plots showed that this duration coincides with a major change in slope beyond which little difference in the measured values is observed. Therefore, the study concluded that the 60-second time window is the shortest one with acceptable variability, and it is considered sufficient for the measurements. Stratigraphic sections of 8 m were logged using an SGR tool and sampling times of 30, 60, and 240 seconds to evaluate the SGR tool reading against two stratigraphic units with different lithofacies associations and a distinctive stratigraphic boundary. For this purpose, 3 points were measured per meter along 8 m of the outcrop face for each sampling time.

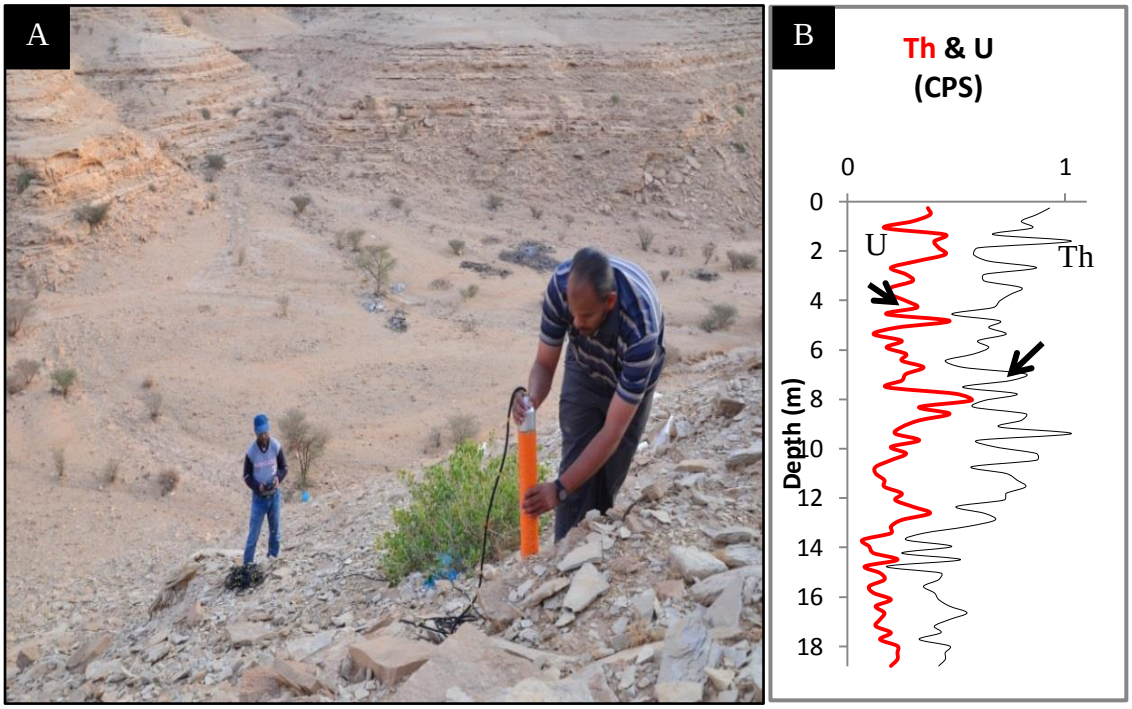

Figure 2-3: (A) Spectral Gamma Ray (SGR) measurements of the Arab-D reservoir outcrop analog (B) logs vertical representation of the outcrop in count per second (CPS).

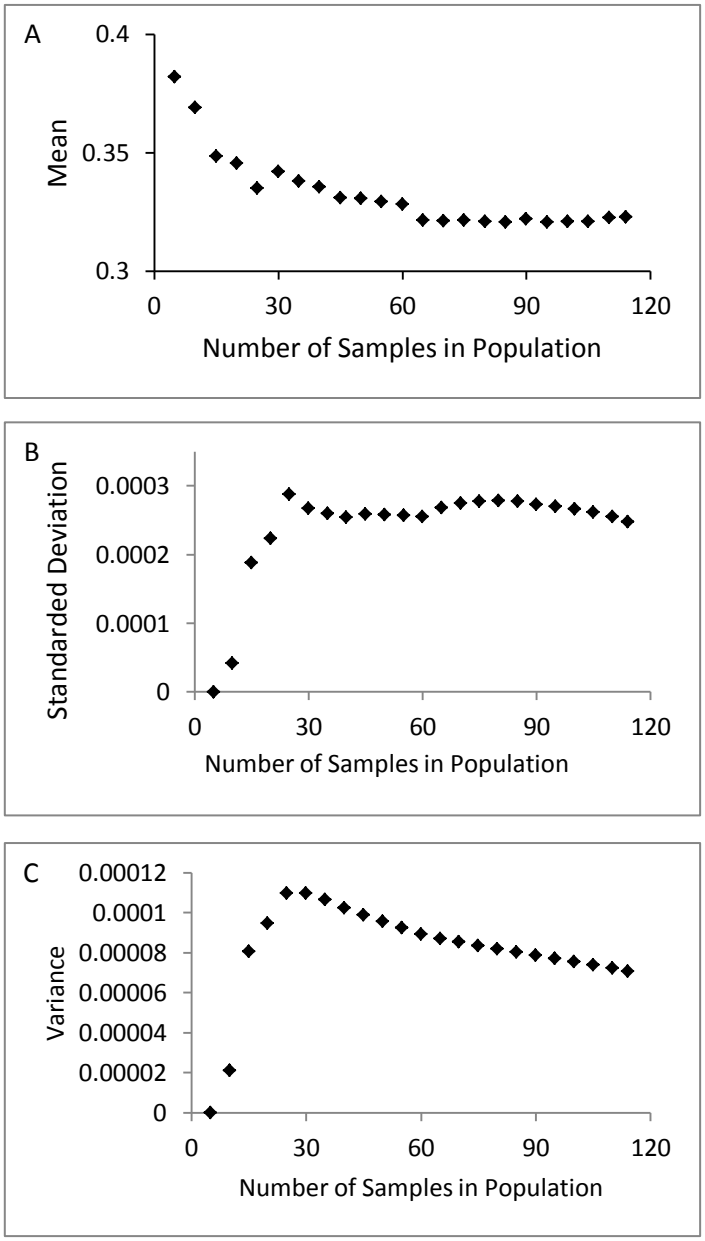

Figure 2-4: Cross plot of populations with different sample numbers accumulated every five samples versus their A) means, B) standard deviations, and C) variances. Note that a population with 30 samples represents the boundary between large and small populations.

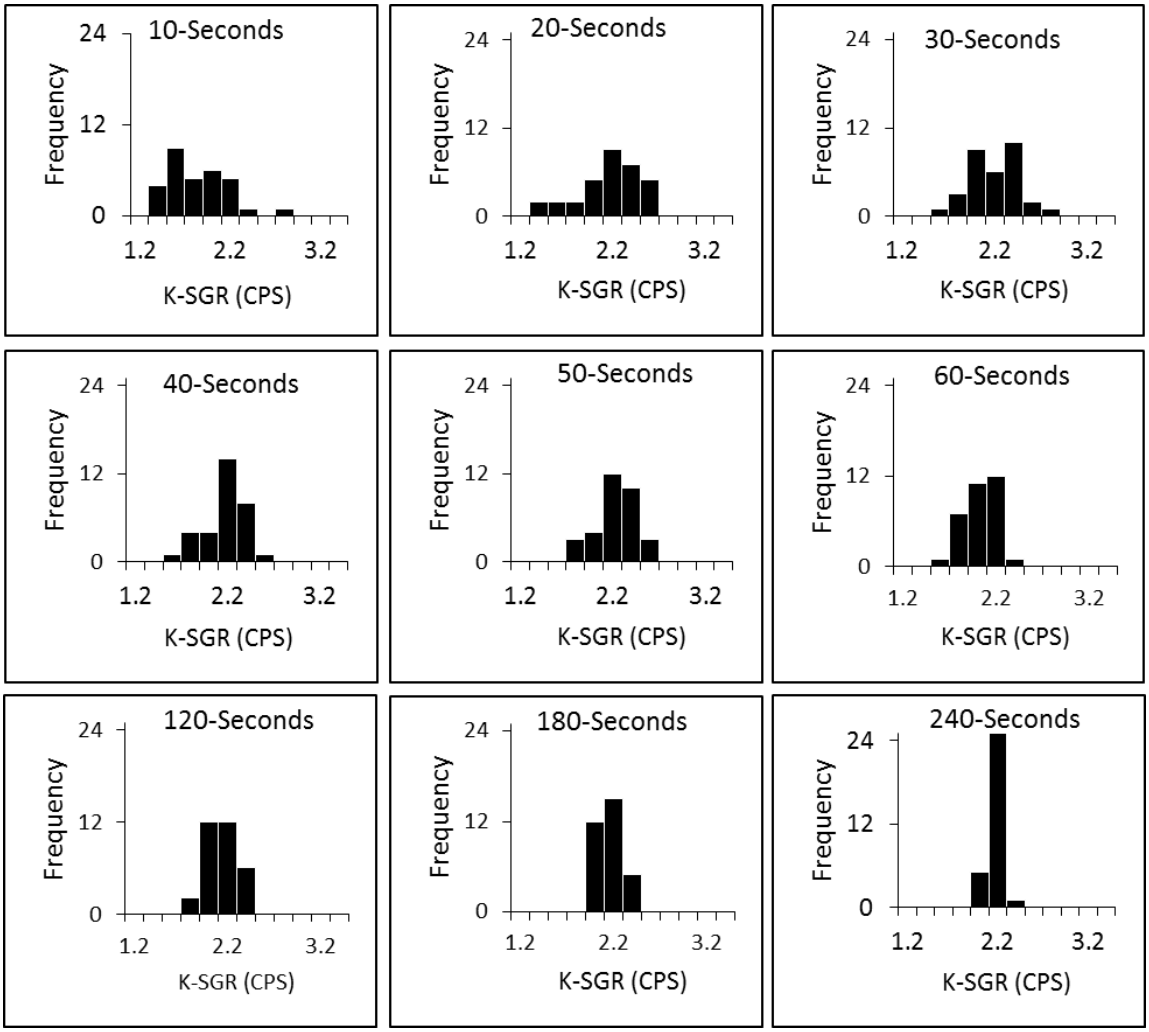

Figure 2-5: Histograms for single-point K-SGR readings using different sampling time windows.

K-SGR	A								
Time Window	10 s	20 s	30 s	40 s	50 s	60 s	120 s	180 s	240 s
Min	1.300	1.250	1.570	1.550	1.660	1.600	1.790	1.83	1.870
Max	2.800	2.550	2.800	2.450	2.580	2.400	2.330	2.32	2.220
Mean	1.803	2.097	2.116	2.080	2.173	2.004	2.056	2.07	2.071
St.dev	0.320	0.327	0.265	0.217	0.205	0.179	0.120	0.14	0.075
Variance	0.103	0.108	0.070	0.047	0.042	0.032	0.018	0.02	0.006
CV%	17.776	15.591	12.538	10.424	9.440	8.916	5.819	6.77	3.604
Th-SGR	**B**								
Time Window	**10 s**	**20 s**	**30 s**	**40 s**	**50 s**	**60 s**	**120 s**	**180 s**	**240 s**
Min	0.000	0.100	0.100	0.130	0.200	0.180	0.240	0.230	0.230
Max	0.900	0.700	0.470	0.430	0.400	0.420	0.460	0.370	0.360
Mean	0.270	0.347	0.300	0.278	0.281	0.285	0.304	0.301	0.294
standard deviation	0.167	0.134	0.087	0.085	0.063	0.067	0.053	0.041	0.033
Variance	0.028	0.018	0.008	0.007	0.004	0.004	0.003	0.002	0.001
CV%	61.826	38.517	28.960	30.688	22.569	23.543	17.478	13.481	11.249
U-SGR	**C**								
Time Window	**10 s**	**20 s**	**30 s**	**40 s**	**50 s**	**60 s**	**120 s**	**180 s**	**240 s**
Min	0.000	0.250	0.330	0.380	0.300	0.400	0.400	0.430	0.450
Max	0.900	0.900	0.800	0.800	0.700	0.780	0.780	0.700	0.700
Mean	0.565	0.536	0.566	0.566	0.541	0.586	0.586	0.581	0.585
Standard deviation	0.200	0.167	0.134	0.117	0.105	0.094	0.094	0.067	0.063
Variance	0.040	0.027	0.018	0.014	0.011	0.009	0.009	0.004	0.004
CV%	35.385	31.167	23.764	20.705	19.368	15.977	15.977	11.478	10.683

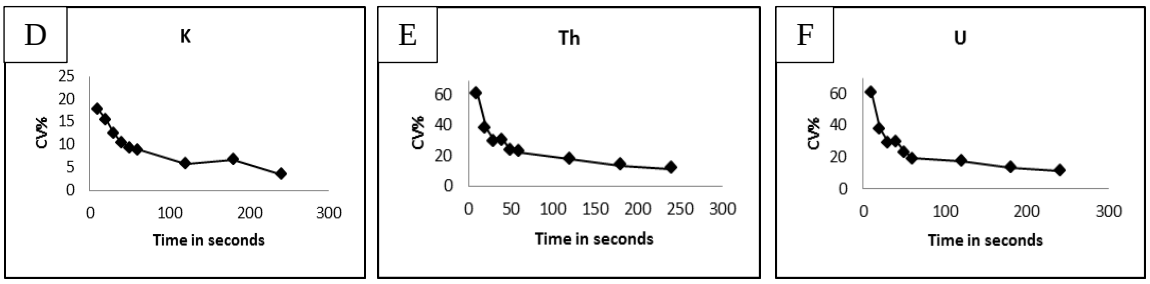

Figure 2-6: Three matrices show statistical parameters for A) K SGRs, B) Th SGRs, and C) U SGRs when accumulating counts per second using 10, 20, 30, 40, 50, 60, 120, and 240 seconds as the time window to measure spectral gamma rays at a single point. Each point was measured 30 times to obtain these statistical parameters. The plots at the bottom show coefficient of variation percentages (CV %) plotted against time-window durations for D) K SGRs, E) Th SGRs, and F) U SGRs. These plots and the matrices were used to select the best duration for the field measurements. Note the high variability in the spectral gamma rays due to their random temporal occurrence.

The points were measured in succession first for 30 seconds each, followed by a set of 60-second measurements and then a final set of 240-second measurements (Figure 2-7). Although the 30-second time window produced a somewhat inconsistent pattern of the SGR logs regarding the stratigraphic units and their boundary, the 60- and 240-second time windows showed reasonable correlation of these logs with the stratigraphic sections and distinctive peaks between the two stratigraphic units. These results confirm the appropriateness of the 60-second time window for logging the stratigraphic sections in this study.

2.4 Stratigraphy from SGR Neural Network and Fischer Plot

An Artificial Neural Network (ANN) is a mathematical model designed to be similar to a human neural network. Two types of ANN are used for facies analysis: unsupervised ANNs and supervised ANNs. In an unsupervised ANN, the user supplies input data and the number of classes that the data should be subdivided into, while in the supervised ANN, the user directs the software to a given correction. The input data for the ANN in this study was the four SGR logs, which reflect the outcrop's high degree of cyclicity. The unsupervised ANN was used to produce the cycle's thicknesses, which were then later used as the inputs for the Fischer Plots. Fischer Plots were defined by Husinec et al. (2008) as "plots of accommodation (derived by calculating cumulative departure from mean cycle thickness) versus cycle number or stratigraphic distance (proxies for time), for cyclic carbonate platforms". Husinec et al. (2008) also provided a template to calculate Fischer plots in excel format, where the only input data for the calculation are the thicknesses of the cycles. In this case, the thicknesses were derived from the SGR logs by the ANN.

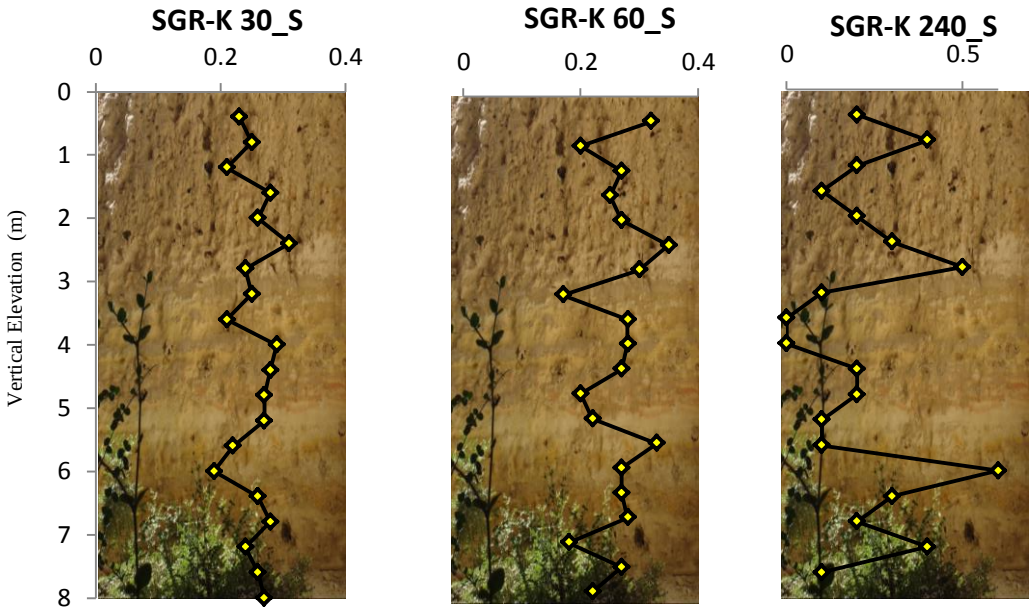

Figure 2-7: SGR logging of 8-m stratigraphic sections using sampling times of 30, 60, and 240 seconds to evaluate the SGR tool reading against the stratigraphic units.

The cycles' thicknesses for this reservoir were extracted from the core description of the Arab-D reservoir by Lindsay et al. (2006). The results are displayed on the same vertical scale as the outcrop stratigraphic profiles to enable an accurate comparison between the subsurface and outcrop cyclicities.

2.5 Petrophysical Analysis

Table 2-1 shows the lithofacies associated porosity data of the Arab-D reservoir from the Ain Dar, Uthmanyah, and Shudgum areas of Ghawar Field in Eastern Saudi Arabia. The data was extracted from the published core measurements and the porosity logs of the Arab-D reservoir (e.g., Douglas 1996; Meyer et al. 1996; Sahin et al. 1998; Cantrell and Hagerty 1999; Cantrell et al. 2004a). The maximum, minimum, and average porosity values for the individual lithofacies were extracted for each of the three oil field areas. The lithofacies from the studied outcrop analog and the Arab-D subsurface reservoir were correlated, and similar lithofacies were given similar porosity values. A total of nine porosity values were assigned to each lithofacies based on the three oil fields and the three porosity values (maximum, minimum, and average) for each field.

2.6 Microporosity Measurement

Choquette and Pray (1970) defined microporosity as porosity with dimensions less than 62.5 micron, but other definitions were given by Anselmetti et al. (1998); Pittman (1971) and Weger et al. (2009). This study uses the definition of Cantrell and Hagerty (1999), who defined microporosity as the difference between core-plug porosity and point-count porosity from thin sections of the same sample. Porosity measurements on core plugs were performed in the laboratory using a saturation method, which is based on the injection of a fluid with a known density into the plug.

The pore volume was determined by subtracting the saturated sample from the dry sample. Permeability measurements were performed using a manually-operated Bench Top Permeability system (TBP 804). The system was operated using 500 psi confining pressure applied to measured samples in which water pump deliver steady flow. A pressure transducer was used for differential pressure measurement . The two methods were suitable for the measurement of porosity in tight samples with very low porosity values. SEM image analysis was performed using JMicroVisionMT software. Images were calibrated to their original scale and then 1D and 2D measurement were performed for micro particles and micro pore areas, respectively.

2.7 Geostatistical Modelling

Geostatistical model was built following standard surface-based modelling workflow described by Pringle (2006). The model was constructed using 14 stratigraphic sections (Figure 2-8).

2.7.1 Data Analysis

Data analysis is an essential step before developing geocellular Modelling. Preliminary analysis was conducted on the facies, the petrophysical parameters and the SGR logs of the outcrop to test normality and other statistical parameters. If the acquired raw data are not normally distributed, a normal score transformation is performed on the data set before any further geostatistical analysis.

2.7.2 Spatial Analysis

Spatial analysis was conducted using semivariograms, which were constructed in different directions to determine the major and minor trends of the data variability.

Vertical semivariograms was computed for all data sets. The search radius of the semivariograms was computed using 0.5 of the data domain size to minimize the edge effect. Using the resulting semivariograms, a geological interpretation was performed regarding isotropy versus anisotropy, continuity and the internal variability.

2.7.3 3-D Model

3-D geostatistical Modelling was conducted using the Petrel™ packages software, which is licensed to the Earth Sciences Department of King Fahd University of Petroleum & Minerals by Schlumberger Overseas as an academic license. The detailed Modelling workflow is described below.

2.7.3.1 Data Geo-Referencing

The stratigraphic sections were assigned to their geo-reference locations, which is an essential step to spatially correlate all geological data of one section to a particular geographical location.

2.7.3.2 Data Arrangement

For each section, the lithofacies log, the stratigraphic horizons, the petrophysical data, and the outcrop Gamma Ray were digitized. Following which, the ASCII files format were formatted for the outcrop sections. The geographical coordinates for each outcrop section was generated according to the reference GPS data coordinates.

2.7.3.3 Surface Modelling

The surfaces are the lithofacies boundaries between the beds and the bed sets. In this step, the standard procedure for outcrop Modelling (Pringle, 2006) was followed. The conditions they used for zonation procedure were carefully followed. but, different

algorithms were used for surface mapping to select the most suitable realization that matche the outcrop structure.

2.7.3.4 Dimensions and Gridding

The potential outcrop sections that were chosen for the high-resolution model cover an area of approximately 250 by 250 m (equivalent to one cell in the Ghawar field subsurface model). The gridding procedure assumes a controlling polygon that surrounds the area under investigation and the top and bottom of the outcrop sections. In the scaling up procedure, the software matches the already constructed grid cell that is penetrated by the sections and the values of the property measured along the same section, in this case, the GR and facies log. For each cell that meets the intersection, the values of the GR or facies code were averaged according to the selected algorithm to produce one value for that cell. Eventually, the discrete values of the log were generated at the grid cell scale.

2.7.3.5 Facies and Property Modelling

The lithofacies distributions in the generated 3-D grids were distributed using the simulation algorithms available in the software such as Sequential Indicator Simulation (SIS) for facies and Sequential Gaussian Simulation (SGS).

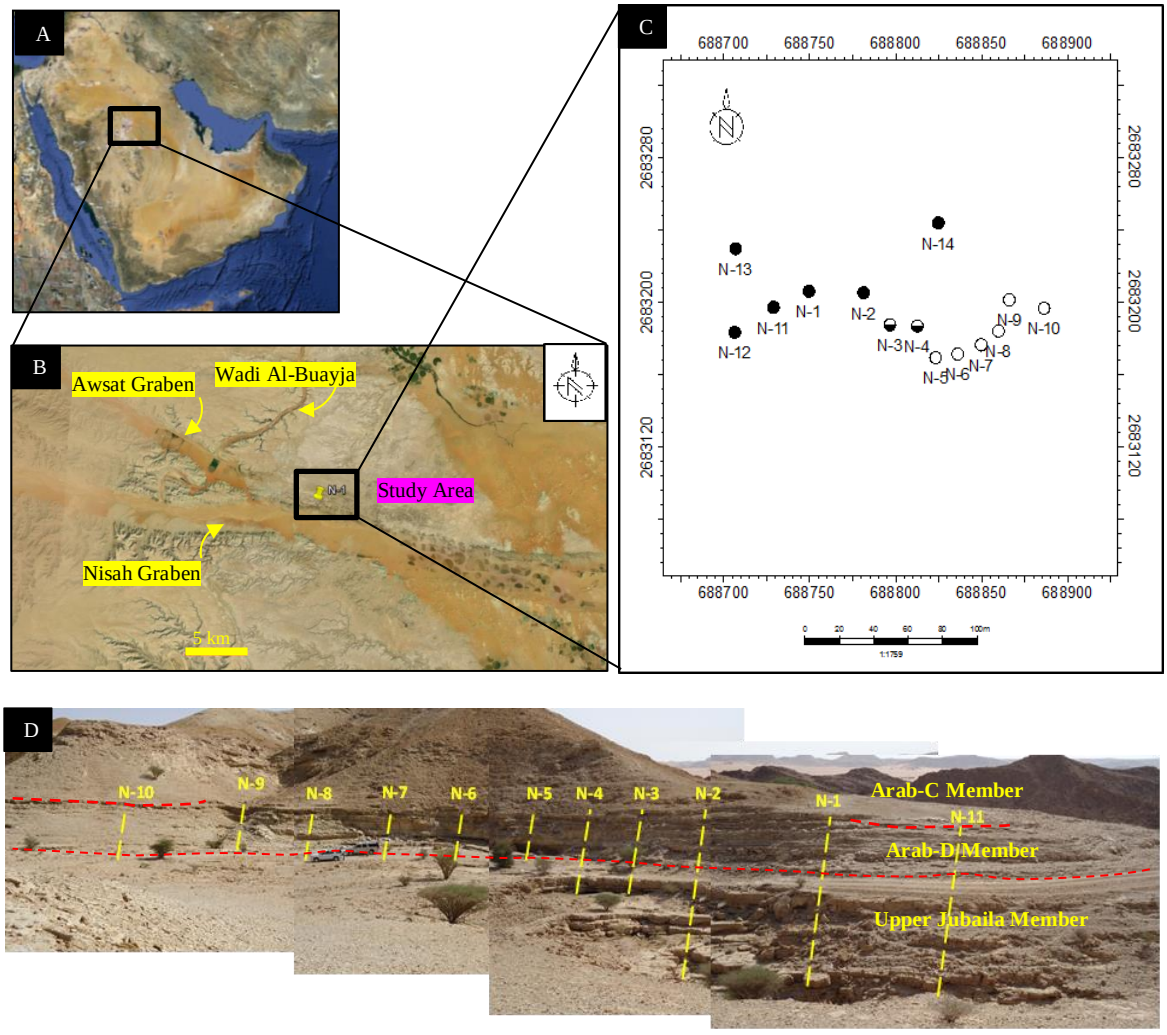

Figure 2-8: Map showing the study area in the central area of Saudi Arabia; B) map showing Wadi Nisah; C) base map showing the location of the 14 stratigraphic sections, with the complete black filling indicating that the stratigraphic section encompasses both the entire Upper Jubaila Member and the Arab-D Member, the partial black filling indicating that only a few beds of the Upper Jubaila Member and the Arab-D Member are present, and the circles without filling indicating that only the Arab-D Member is present; and D) photomosaic showing the three stratigraphic units of the studied outcrop with locations of 11 stratigraphic sections.

Table 2-1: Porosity values of three major producing areas in Ghawar Field as extracted from Literature.

Facies Matching		Porosity Value		Oilfields			
Subsurface Facies	**Outcrop Facies**			**Ain Dar (Douglas, 1996)**	**Shugum (Cantrell et al. 2003)**	**Uthmaniyah (Saner and Sahin, 1999)**	**Ghawar (Lucia et al., 2001)**
Laminated Mudstone	Micritic	Porosity	Min	-		2.8	1.25
			Average	**-**	**13**	**9.2**	**7**
			Max	-		18.8	17.5
Dolomitic Mudstone	Dolomitic Mudstone	Porosity	Min	-		2.8	1.25
			Average	**17.5**	**10.2**	**9.2**	**7**
			Max	-		18.8	17.25
Dolomitic Wackestone	Dolomitic-Wackestone	Porosity	Min	-		2.6	1.25
			Average	**17.5**	**16.3**	**16.5**	**10**
			Max	-		28.7	17.5
Stromatoporoid Wackestone and Packstone	Stromatoporoid Packstone	Porosity	Min	-		19.3	1.25
			Average	**20.7**	**12.64**	**26.55**	**17**
			Max	-		32.5	27.5
Wavy Laminated Sandy Grainstone	Mix skeletal Grainstone	Porosity	Min	-		19.3	3.75
			Average	**25.9**	**25**	**26.55**	**15**
			Max	-		32.5	22.5
Peloidal Fossiliferous Grainstone	Mix skeletal Grainstone	Porosity	Min	-		19.3	3.75
			Average	**25.9**	**25**	**26.55**	**15**
			Max	-		32.5	22.5
Breccia and Mud-clasts	Micritic	Porosity	Min	-		2.8	1.25
			Average	-	**13**	**9.2**	**7**
			Max	-		18.8	17.5

CHAPTER 3

SEDIMENTOLOGY AND STRATIGRAPHY

3.1 Introduction

Facies description is an essential step for reservoir characterization and Modelling. The thickness of the Upper Jubaila and Arab-D members in Wadi Nisah ranges from 17 to 19 m. Facies analyses conducted on fourteen stratigraphic sections identified three seven lithofacies and three lithofacies associations. Lithofacies descriptions, sedimentary structures and their possible depositional environments are summarized in Table 3-1**.** These seven depositional lithofacies defined in this location, form the basis of the subsequent petrophysical investigation, geochemical analysis, and geostatistical Modelling.

The lithofacies identified in this study are characterized based on their hierarchy and stacking patterns by considering them within a sequence stratigraphic model. Both the Upper Jubaila and the Arab-D members are assigned to be two different composite sequences. These composite sequences are comprised of several High Frequency Sequences (HFSs) which are in turn, subdivided into cycles and cycle sets following the scheme of Lindsay et al. (2006)

This study also investigates the diagenetic overprints of the outcropping Arab-D succession in the study area. These digenetic imprints modified the initial porosity and permeability significantly. This study show that the cementation processes caused total

occlusion of pore system. It has been possible to trace the diagenetic paragensis through the geological time of the succession. Major diagenetic processes of the outcrop strata equivalents of the Arab-D reservoir include: 1) micritization ; 2) marine cementation; 3) dissolution; 4) early dolomitization; 5) equant blocky calcite cementation; 6) micrite recrystallization; 7) Compaction; 8) late dolomitization; 9) dedolomitization; 10) meteoric cementation; and 11) fracture filling.

3.2 Facies Description and Interpretation

Sedimentological and stratigraphic investigation revealed seven lithofacies following Meyer et al. (1996) outcrop description. These lithofacies grouped in three lithofacies associations, namely they are:

- Stromatoporoid Lithofacies Association (Figure 3-1)
    - Dolomitic Mudstone and Dolomitic Wackestone
    - Stromatoporoid Wackestones and Packstones
- Skeletal Bank Lithofacies Association (Figure 3-2)
    - Burrowed Fossiliferous Wackestones
    - Peloidal Fossiliferous Grainstones
- Tidal Flat Lithofacies Association (Figure 3-3)
    - Laminated Mudstones
    - Wavy Rippled Sandy Grainstones
    - Breccia

3.2.1 Stromatoporoid Lithofacies Association

3.2.1.1 Dolomitic Mudstones and Wackestones

Observations: This lithofacies occurs at the base of the lower section of the exposed Upper Jubaila Member. It is composed of 20 to 50 cm-thick beds of burrowed mudstones and wackestone with moderate to low biofacies content. Thin-section analysis shows that all molds of skeletal grains have been leached and replaced by coarse and microcrystalline calcite. Crystallisation varied from very fine to very coarse grained. Thin sections stained with Alizarin Red following the procedure of Dickson (1966), show 50% red colour (calcite) and 50% grey colour (dolomite). Microfossil preservation is masked by heavy leaching and dolomitization, but monaxon sponge spicules are well preserved in the studied samples. Bivalve molds and brachiopods are well preserved.

Interpretation: The observed fine muddy facies of the burrowed dolomitic mudstones and wackestone and the lack of high current sedimentary structures, as well as the scarcity of biofacies, suggest that this lithofacies was deposited below wave base in an upper slope depositional environment. The mud-dominated facies was interpreted to have been deposited on the lower slope. This environment can be differentiated from the overlying wackestone facies by the absence of biofacies and the higher lime mud content.

3.2.1.2 Stromatoporoid Wackestones and Packstones

Observations: This lithofacies occurs as thick beds at the top of sequences -1, -2 -3 and -4 of the Upper Jubaila Member, has a maximum thickness of 150 cm, and underlies the dolomitic mud-dominated section. The lithofacies contains scattered stromatoporoid fragments that form wackestones or floatstones. These fragments decrease gradually

upwards and form packstoness or rudstones fabrics when intraclasts are present. The oncoids have different orientations and sizes. Thin section analysis of this lithofacies shows high biofacies diversity, which includes benthic foraminifera, crinoid fragments and shell fragments.

Interpretation: Debris of stromatoporoid and coral fragments and accompanying biofacies like *Kurnubia palastiniensis* and *Nautiloculina oolithica* (Hughes, 2004a, 2004b, 2009) indicate that this section was deposited in a ramp crest to lower-slope environment. The massive beds and the grain orientations suggest intensive reworking from the ramp crest to the upper-slope environment. Forams and bivalve shell fragments indicate shallowing of the depositional environment into the shallower part of the ramp crests to a distal lagoon.

3.2.2 Skeletal Bank Lithofacies Association

3.2.2.1 Burrowed Fossiliferous Wackestones

Observations: This lithofacies occurs above stromatoporoids wackestones and packestones and interbedded with peloidal fossiliferous grainstones. This lithofacies varies in thickness from 30 to 60 cm and shows heavy burrowing. Shell fragments and pellets found floating in a muddy matrix forming mud-supported wackestones or floatstones textures. The biofacies in this unit include foraminifera, shell fragments, and echinoid plate debris.

Interpretation: The domination of mud, of this lithofacies indicate relatively low-energy conditions and a quite water environment that is possibly below storm wave base. Possible depositional environments for this lithofacies is proximal lagoon.

3.2.2.2 Fossiliferous Peloidal Grainstones

Observations: This lithofacies occurs immediately above the laminated mudstones and extends over the entire study area; it can be traced over more than 2 km^2. The lithofacies varies in thickness from 20 to 50 cm and shows small-scale cross bedding. Shell fragments and pellets represent the major component of this lithofacies and form grain-supported grainstone or rudstone textures. This lithofacies contains small to moderate size intraclasts at the base that increase upward in size and quantity. The biofacies in this unit are better preserved than in the other lithofacies and include foraminifera, shell fragments, and oncoid debris.

Interpretation: The lack of mud, abundance of fauna, and peloidal grains of this lithofacies indicate relatively high-energy conditions and an agitated water environment that is possibly above storm wave base. Possible depositional environments for this lithofacies is shallow water skeletal bank.

3.2.3 Tidal Flat Lithofacies Association

3.2.3.1 Laminated Mudstones

Observations: This lithofacies comprises most of the Arab-D Member in the study area. Cycle thickness varies from 90 to 150 cm. The lithofacies contains alternating cycles of platy laminated mudstones with very thin beds of coarse wavy ripples sandy grainstones. This lithofacies includes very thinly laminated mudstones as well as thinning upward beds, and the beds contain very poorly preserved microfossils.

Interpretation: The thickness and the lamination of this lithofacies suggests deposition under low-energy water conditions and possibly in a restricted area with limited

accommodation space such as a proximal lagoon to tidal flat depositional environment. The scarcity of dasyclad, red algae, and low diversity of biofacies suggests that there was a shift of depositional environment from upper lope and ramp crest to proximal lagoon without going through a deep lagoon environment.

3.2.3.2 Wavy Rippled Sandy Grainstones

Observations: This lithofacies occurs immediately above the laminated mudstones and extends over the entire study area; it can be traced over more than 2 km^2. The lithofacies varies in thickness from 20 to 50 cm and shows small-scale cross bedding. Shell fragments and pellets represent the major component of this lithofacies and form grain-supported grainstone or rudstone textures. This lithofacies contains small to moderate size intraclasts at the base that increase upward in size and quantity. The biofacies in this unit are better preserved than in the other lithofacies and include foraminifera, shell fragments, and oncoid debris.

Interpretation: The lack of mud, abundance of fauna, and peloidal grains of this lithofacies indicate relatively high-energy conditions and an agitated water environment that is possibly above storm wave base. Possible depositional environments for this lithofacies is tidal flat channelized flow.

3.2.3.3 Breccia and Mud-Clasts

Observations: This lithofacies consists of clast-supported textures. Individual clasts range from a few millimetres up to 2 cm in size with lime mud mixed with bivalve skeletal fragments. The bed thickness of this lithofacies ranges from 20 to 50 cm. The clasts are elongated, rounded and poorly sorted with no preferred orientation.

Interpretation: The breccia beds vary in grain size and the degree of roundness according to their position in the outcrop succession and their proximity to the shoreline. Breccia beds appear in the Arab-D Member sequences but cannot be correlated. Variations in grain size and the elongation of some clasts indicate that these clasts were not transported for long distances. This lithofacies is interpreted to be deposited in channeled tidal flat mud sheets that seasonally triggered by storm waves in a supratidal to intertidal flat depositional environment.

3.3 Biofacies Zonation

Observations: The boundary between the Jubaila and the Arab formations is defined by the last appearance of stromatoporoid debris (Le Nindre et al., 1990; Hughes, 1996, 2004a, 2004b, 2009). This boundary is clearly defined in the outcrop and is referred to in the further interpretation and discussion in this study. Compared to the subsurface Arab-D reservoir, the studied samples from this outcrop generally show low degrees of biofacies diversity However, some key biofacies are present and provide paleoenvironmental indicators.

Figure 3-4 shows some micro-biocomponents identified from thin sections, and Figure 3-5 shows macro-biocomponents from hand specimens. The stratigraphic distribution of biofacies assemblages is shown in Figure 3-6. The lower section of the exposed Upper Jubaila Member contains a very limited biofacies component in the dolomitic wackestone and mudstone but exhibits good biofacies diversity in the stromatoporoid wackestone and packstone. This section is characterised by the appearance of stromatoporoid fragments, coral fragments, *Lenticulina* spp. and *Valvulin*a spp.

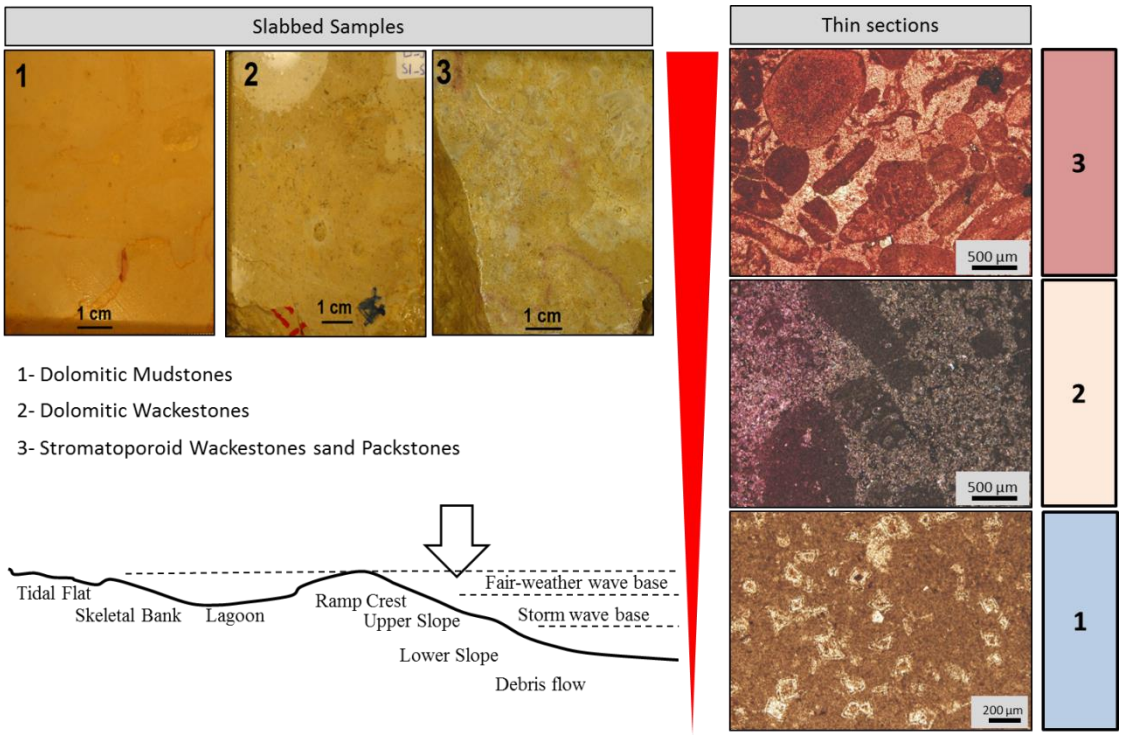

Figure 3-1: Slabbed samples and thin sections photomicrographs showing lithofacies comprise stromatoporoid lithofacies association (shallowing and coarsening upward). The possible interpretation of this lithofacies association is illustrated in the left corner.

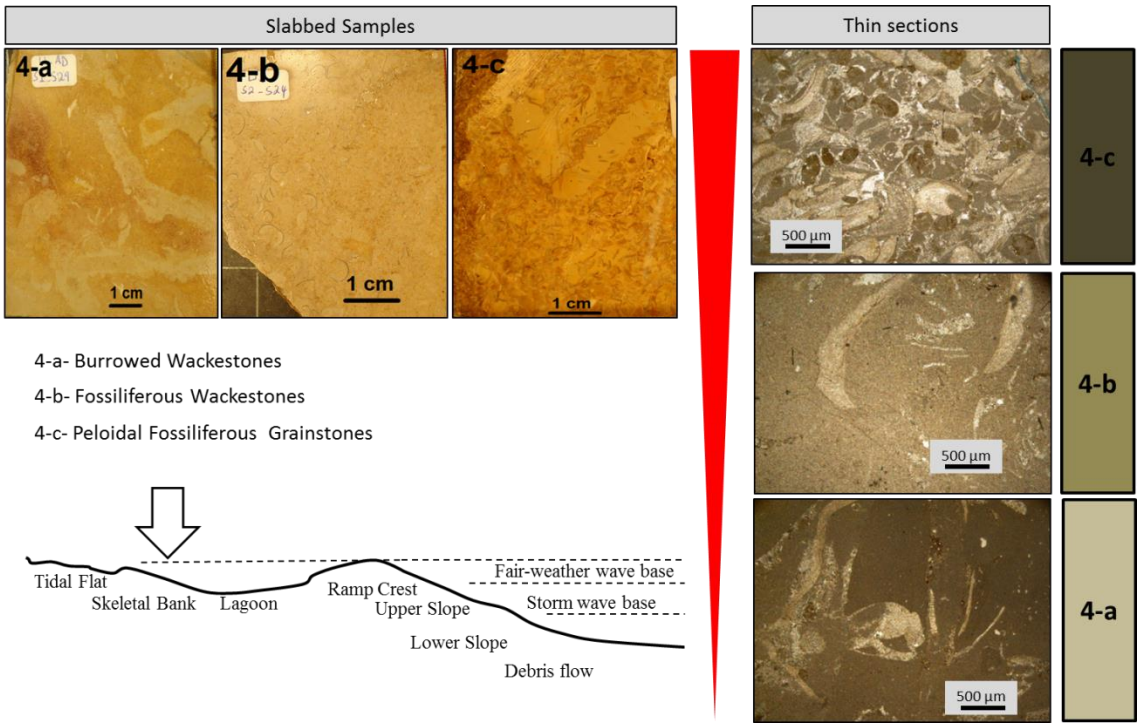

Figure 3-2: Slabbed samples and thin sections photomicrographs showing lithofacies comprise skeletal bank lithofacies association (shallowing and coarsening upward). The possible interpretation of this lithofacies association is illustrated in the left corner. The muddy facies represent more off shore and the grainy facies represent more on shore of skeletal bank.

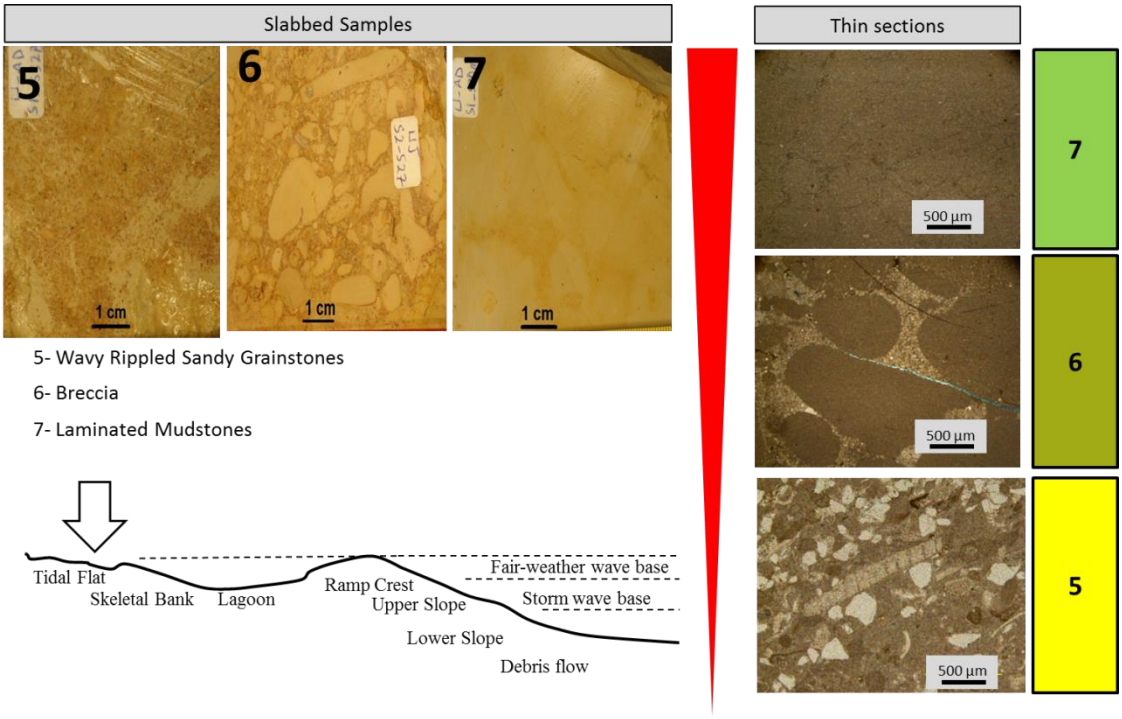

Figure 3-3: Slabbed samples and thin sections photomicrographs showing lithofacies comprise tidal flat lithofacies association (shallowing and fining upward). The possible interpretation of this lithofacies association is illustrated in the left corner. The grainy facies represent subtidal flat channelized flow and the Muddy facies represent thinly laminated tidal flat environment.

Large fossils include stromatoporoid oncoids, echinoid fragments, and bivalve fragments. The upper section of the outcrop (the Arab-D Member) contains limited biofacies in the platy laminated mudstone. In contrast, the laminated sandy fossiliferous grainstone and peloidal sandy grainstone exhibit relatively high diversity of biofacies components. In these lithofacies, the dominant biofacies components are *Pseudocyclammina lituus*, echinoids, ostracods, *Quinqueloculina* spp., gastropods, numerous bivalve fragments, and a few agglutinated foraminifera. Biocomponents like *Nautiloculina oolithica*, *Kurnubia palastiniensis*, spicules, brachiopod fragments, and bivalve fragments are distributed widely in both the Upper Jubaila and Arab-D members.

Palaeoenvironmental Significance:

- Stromatoporoid, coral fragments, and *Lenticulina* spp. are restrict to the Upper Jubaila Member and not present in the Arab-D Member. This assemblage indicates open-marine unrestricted regime (Hughes, 2004a, 2004b, 2009). The possible palaeoenvironmental in the studied outcrop succession is the upper and lower slope to ramp crest where the Upper Jubaila Member was deposited.
- Gastropods, Ostracod, *Pseudocyclammina lituus*, *Quinqueloculina* spp. dominated in the Arab-D Member. This assemblage indicates shallow to very shallow lagoon setting. The corresponding lithofacies for this palaeoenvironment is skeletal bank association.
- *Nautiloculina oolithica*, *Kurnubia palastiniensis*, Echinoid fragments, Brachiopod fragments distributed equally in both units. These could either have a very wide paleoenvironmental tolerance (Hughes, 2004a, 2004b, 2009) or transported by channelized flow (Figure 3-7).

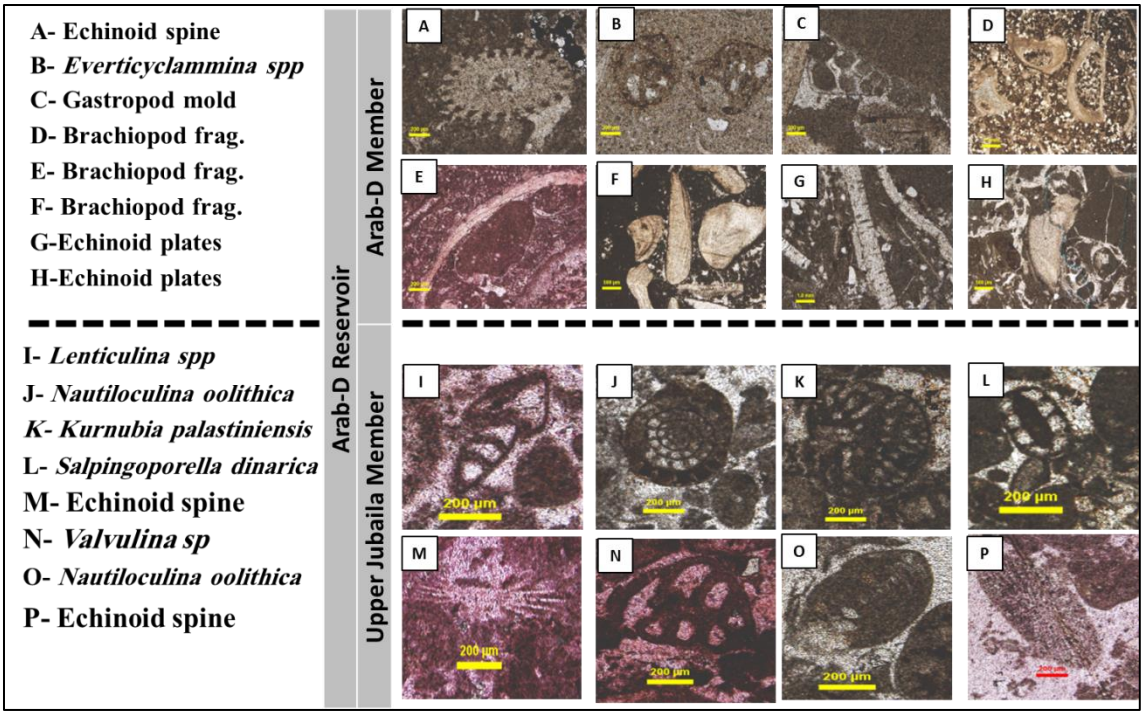

Figure 3-4: Photomicrographs of micro bio-components of outcropping strata equivalent to Arab-D reservoir.

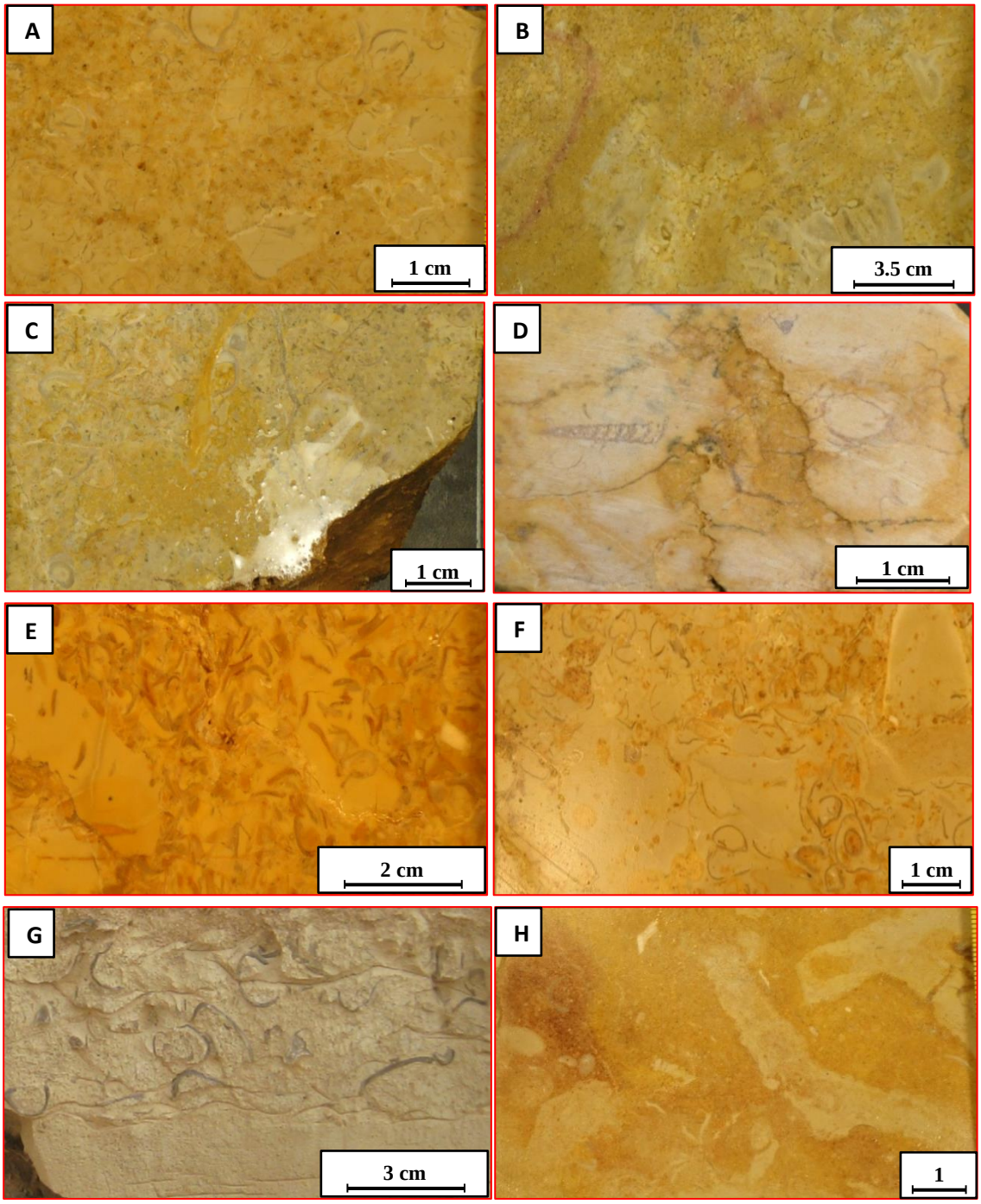

Figure 3-5: Photographs of macro bio-components of outcropping strata equivalent to Arab-D reservoir. A) echinoid spine; B) and C) stromatoporoid debris; D) gastropod mold; E), F), and G) brachiopod fragments; H) burrowed sediments.

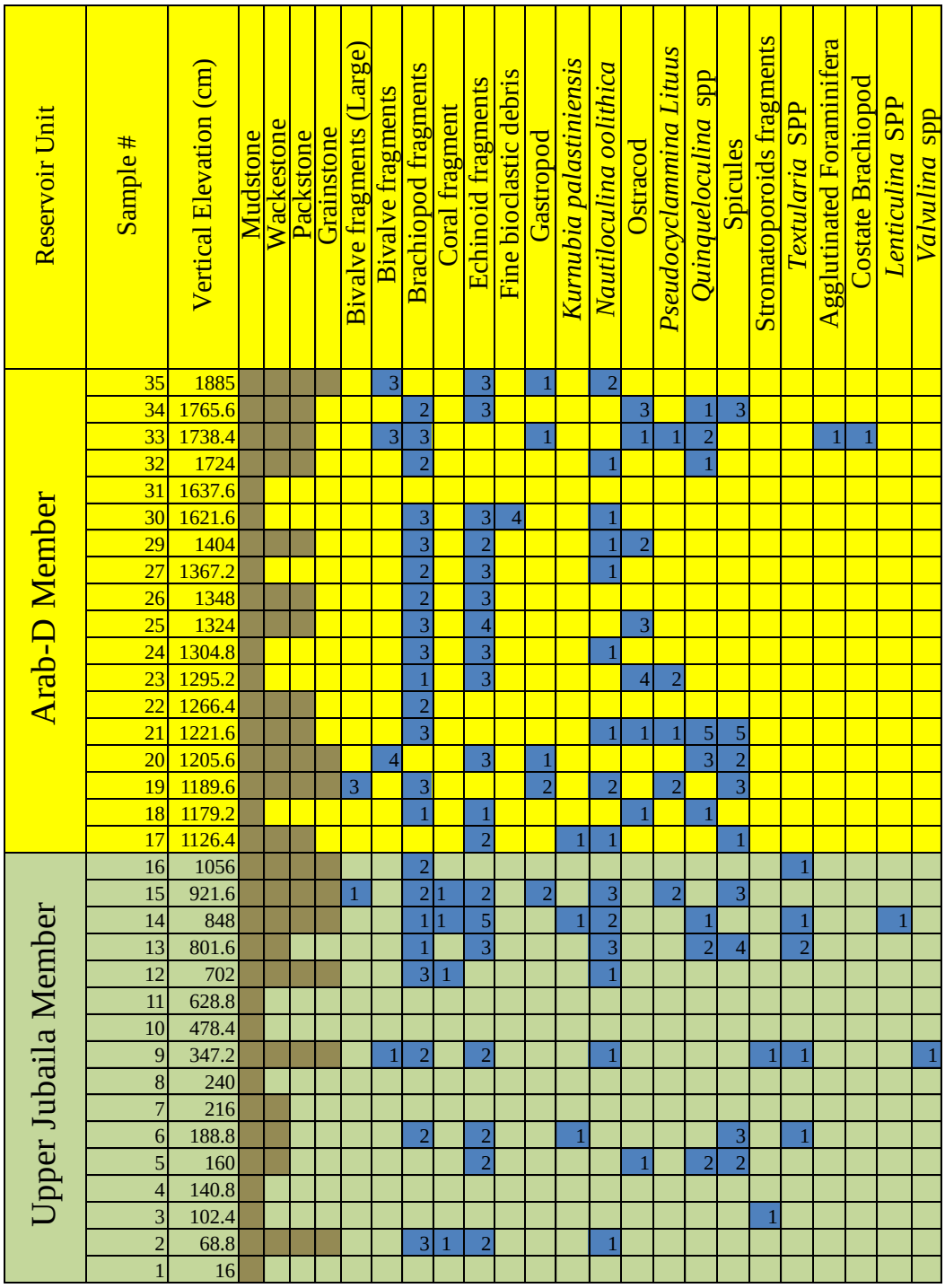

Reservoir Unit	Sample #	Vertical Elevation (cm)	Mudstone	Wackestone	Packstone	Grainstone	Bivalve fragments (Large)	Bivalve fragments	Brachiopod fragments	Coral fragment	Echinoid fragments	Fine bioclastic debris	Gastropod	*Kurnubia palastiniensis*	*Nautiloculina oolithica*	Ostracod	*Pseudocyclammina Lituus*	*Quinqueloculina* spp	Spicules	Stromatoporoids fragments	*Textularia* SPP	Agglutinated Foraminifera	Costate Brachiopod	*Lenticulina* SPP	*Valvulina* spp
Arab-D Member	35	1885						3			3		1		2										
	34	1765.6							2		3					3		1	3						
	33	1738.4						3	3				1			1	1	2				1	1		
	32	1724							2						1			1							
	31	1637.6																							
	30	1621.6							3		3	4			1										
	29	1404							3		2				1	2									
	27	1367.2							2		3				1										
	26	1348							2		3														
	25	1324							3		4					3									
	24	1304.8							3		3				1										
	23	1295.2							1		3					4	2								
	22	1266.4							2																
	21	1221.6							3						1	1	1	5	5						
	20	1205.6						4			3		1					3	2						
	19	1189.6					3		3				2		2		2		3						
	18	1179.2							1		1					1		1							
	17	1126.4									2			1	1				1						
Upper Jubaila Member	16	1056							2												1				
	15	921.6					1		2	1	2		2		3		2		3						
	14	848							1	1	5			1	2			1			1			1	
	13	801.6							1		3				3			2	4		2				
	12	702							3	1					1										
	11	628.8																							
	10	478.4																							
	9	347.2						1	2		2				1					1	1				1
	8	240																							
	7	216																							
	6	188.8							2		2			1					3		1				
	5	160									2					1		2	2						
	4	140.8																							
	3	102.4																		1					
	2	68.8							3	1	2				1										
	1	16																							

Figure 3-6: Bio-components variation of selected forms within section-1 in the study area. Note that the boundary between the Upper Jubaila and Arab-D is define by the last appearance of stromatoporoid. The numbers in the blue squares indicate the abundance of bio-component (1 is low while 5 is very high). Vertical elevation assuming zero elevation at the top of the outcrop and 1885 m at the bottom.

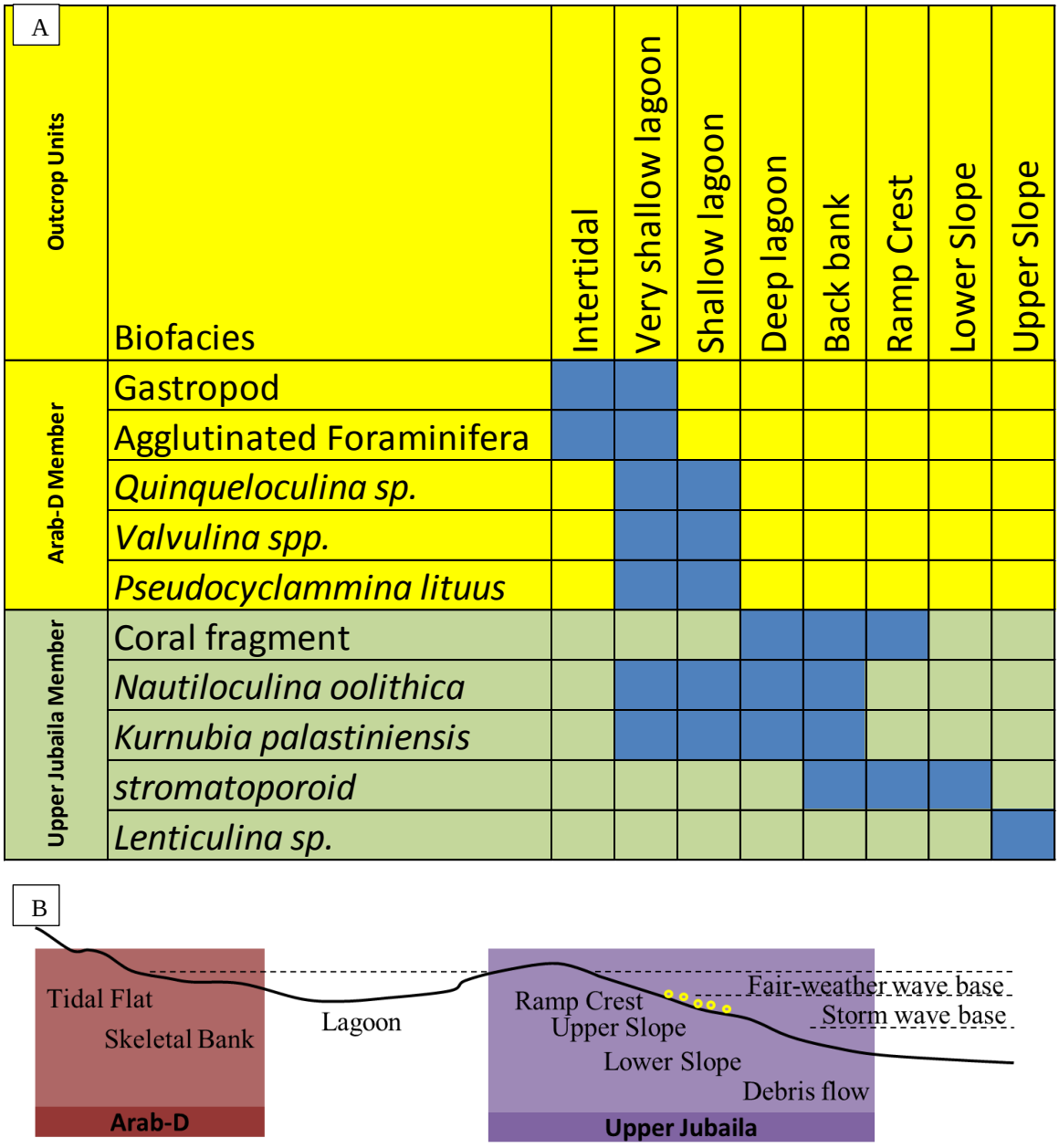

Figure 3-7: A) Palaeoenvironmental model for the Arab-D reservoir outcropping strata at Wadi Nisah using the identified bio-components.; B) Proposed depositional environment of the studied outcropping strata as interpreted by lithofacies association. Note that many of the species from deep lagoon are absence in this strata.

3.4 Stratigraphy Sequence

The measured section of the Arab-D reservoir analog in the study area contains nine high frequency sequences (HFSs). Four of the HFSs are found in the lower part (the Upper Jubaila Member composite sequence) (Figure 3-8) and the remaining five are in the upper section (Arab-D Member composite sequence) of the outcrop (Figure 3-9). He nine HFSs could be categorized into four types which are:

- Typ-1 HFSs (stromatoporoid): This sequences include the four HFSs in the Upper Jubaila Member and show coarsening and shallowing upward strata cyclicity. The lithofacies associations within these sequences range from burrowed dolomitic mudstone and wackestone at the bottom to stromatoporoid wackestone and packstone (rudstone and floatstone) at the top. The boundaries between individual beds within a single HFS are gradational, contain erosive scouring surfaces between different HFSs, and reach more than 30 cm in some places. These four HFSs show similar lithofacies arrangements, biofacies components and, to some extent, thicknesses. Laterally, these HFSs can be correlated along the measured sections.
- Typ-2 HFSs (skeletal bank): This HFSs occur within the Arab-D Member and comprises the two HFSs in the skeletal bank succession. HFSs are also coarsening and shallowing upward and composed of burrowed wackestones, fossiliferous wackestones, and peloidal fossiliferous grainstones mudstone to laminated sandy fossiliferous grainstone.
- Type-3 HFSs (distal tidal flat): This HFSs occur within the Arab-D Member and compose of wavy rippled sandy grainstones of subtidal flat channels, transported

breccia, and laminated mudstone. This type of HFSs occur above type-2 HFSs and comprise of two repeated sequences of fining and shallowing upward.

- Type-4 HFSs (proximal tidal flat): This type of sequence compose of repeated sequences of laminated mudstone and transported mud-clast and breccia. This type of succession occur at the top of the Arab-D succession and also represent fining and shallowing upward. Figure 3-10 shows cross section in the studied outcrop which includes the four types of HFSs and their possible correlation.

3.5 Stratigraphy from Spectral Gamma-Ray Profiles and Fischer Plot

The measured outcrop sections displayed two major SGR profiles in all the logs uranium (U), potassium (K), thorium (Th), and their total counts (TC) (Figure 3-11).These two profiles represent the Upper Jubaila Member in the lower section and Arab-D Member in the upper section of the outcrop. The lower section can be subdivided into four subunits of relatively low SGR troughs separated by sharp peaks of relatively high SGR levels.

The thickness of each of the log profiles varies as the SGR reading increases upward following the change in lithofacies from dolomitic mudstone at the bottom to wackestone and packstone at the top. Table 3-1 shows the thicknesses of the cycles as extracted from the SGR logs. These cycles were used as inputs for the unsupervised Artificial Neural Network (ANN) procedure for cycle identification (Figure 3-12). Using these cycles as the inputs in the Fischer Plot, the Arab-D succession in the outcrop was defined by 44 cycles. The minimum cycle thickness is 15.2 cm, and the maximum thickness is 255.2 cm. A total of 21 cycles are found in the Upper Jubaila Member (5 to 6 cycles for one HFS), while 23 cycles fall within the Arab-D Member of the Arab Formation (2 to 5 cycles for one HFS).

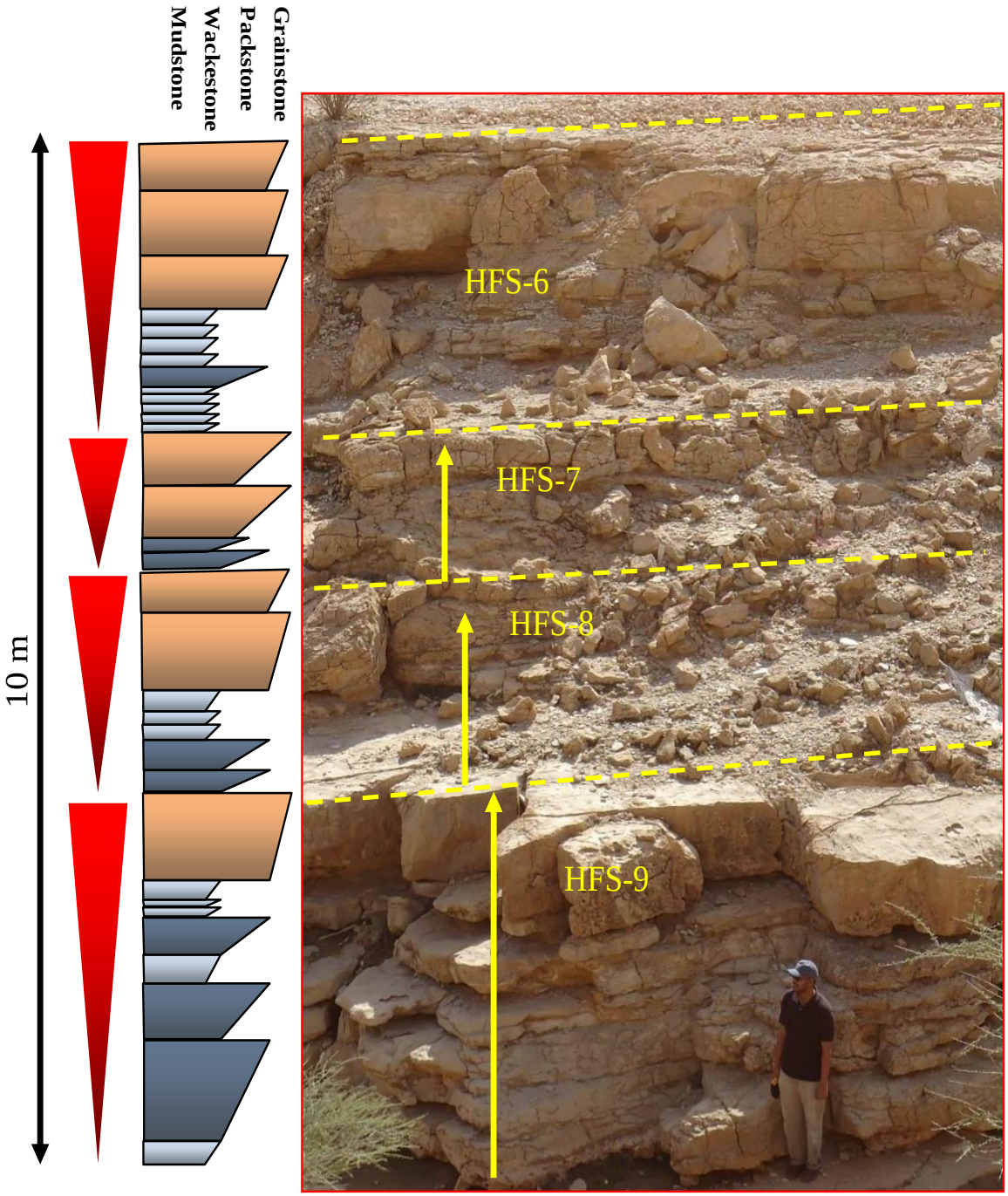

Figure 3-8: Stratigraphic section in the study area, four shoaling up-ward HFSs in the Upper Jubaila Member.

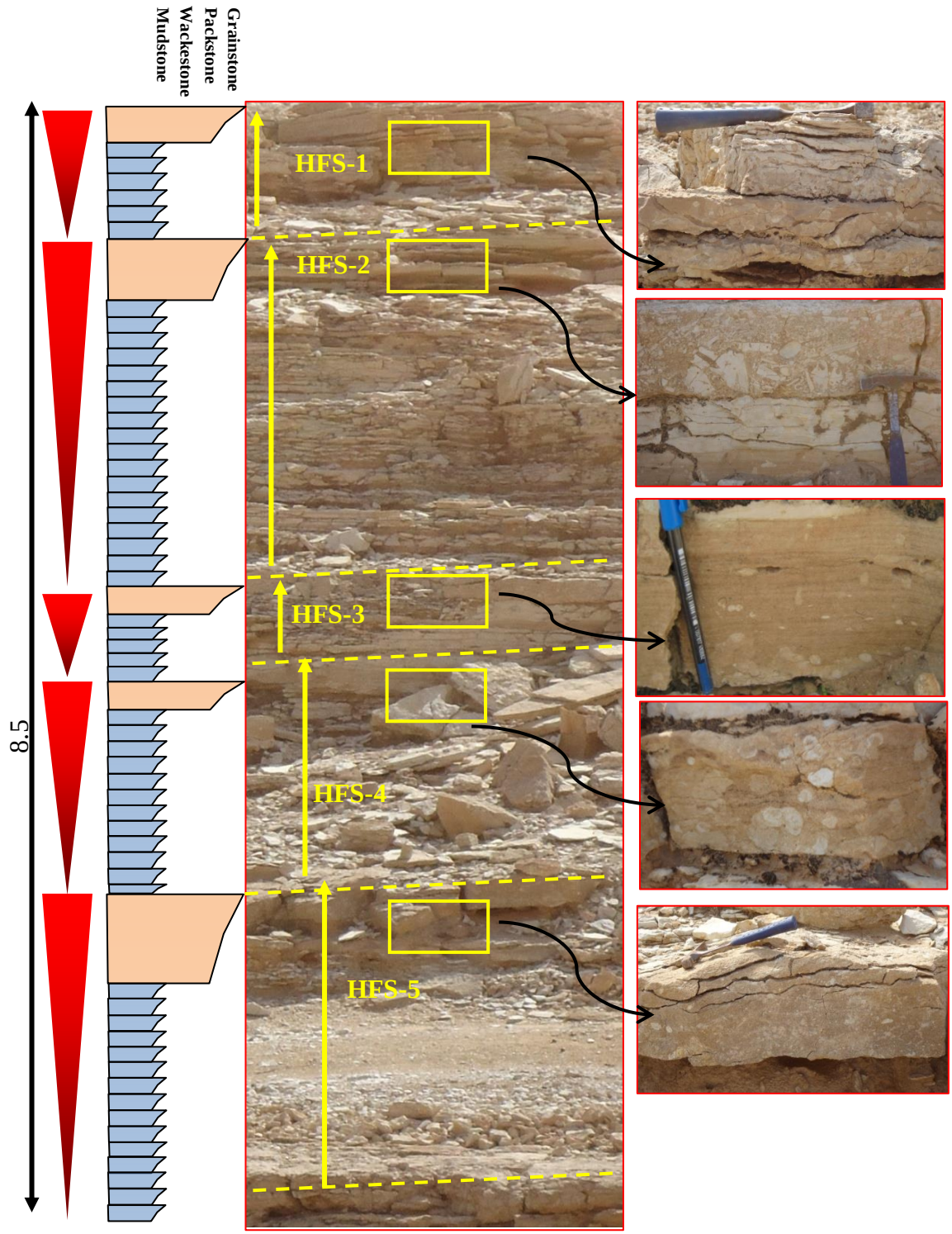

Figure 3-9: Stratigraphic sequences in the study area, five shoaling up-ward HFSs in the Arab-D Member. A very coarse material deposited overlain the muddier facies and represent the top of each HFS.

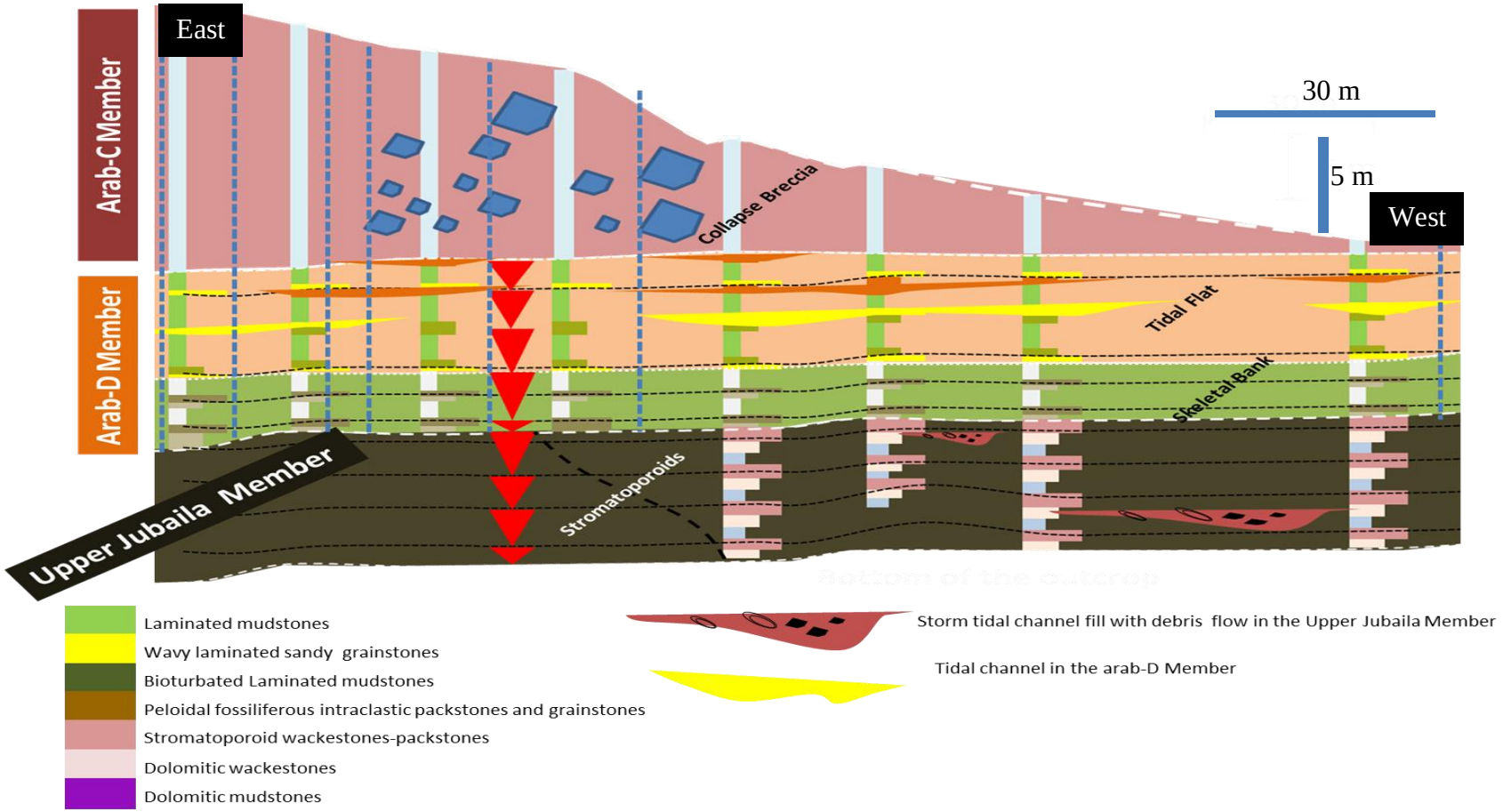

Figure 3-10: Stratigraphic cross section in the study area showing four shoaling upward HFSs in the Upper Jubaila Member and five shoaling upward HFSs in the Arab-D Member. Coarse material deposited overlain the muddier facies and represent the top of each HFS.

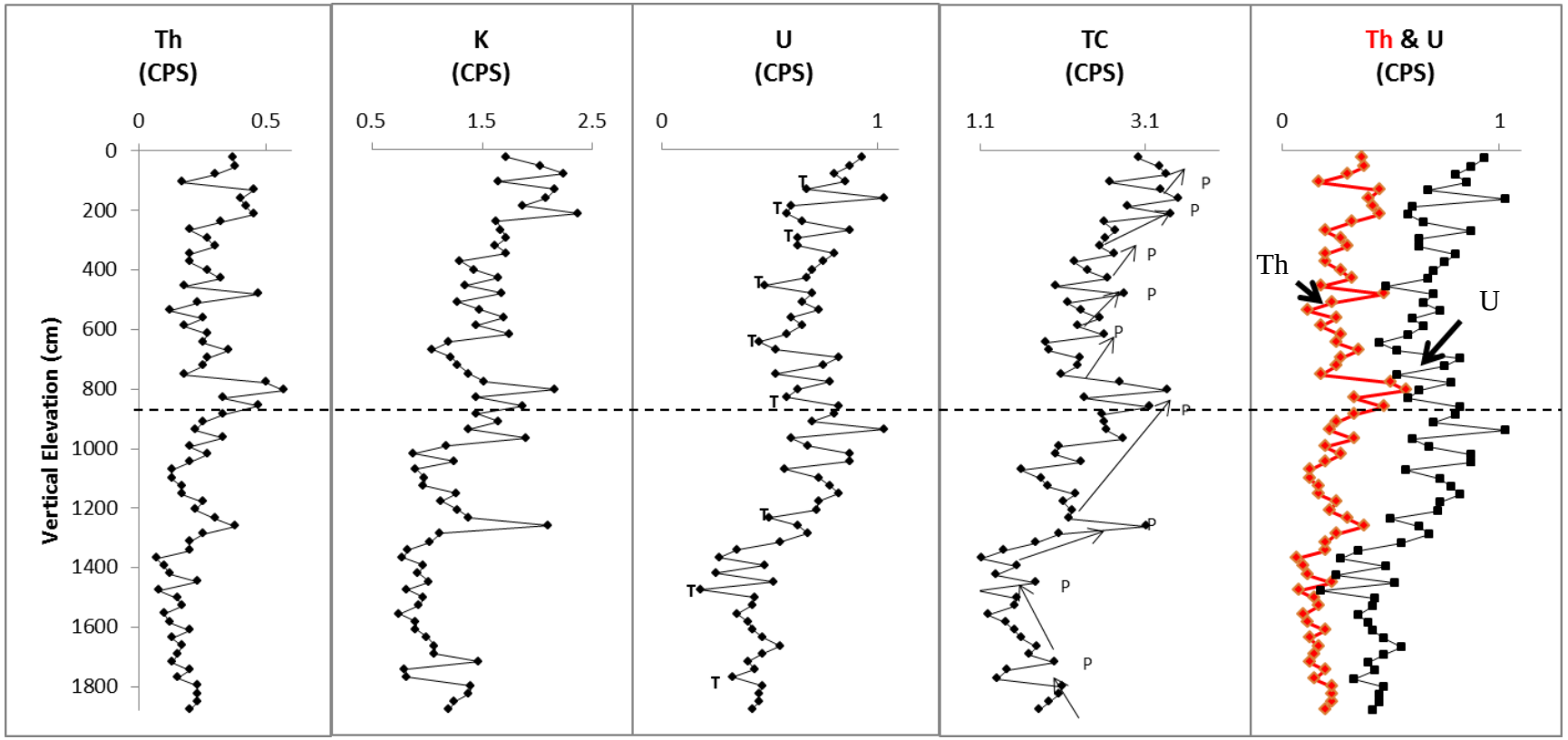

Figure 3-11: SGR Logs profiles in section 11 shows SGR distinctive two major units (the Upper Jubaila Member and the Arab-D Member). The Upper Jubaila Member shows four major sharp SGR peaks (indicated by capital P), while the Arab-D Member shows five to four SGR peaks (indicated by capital P). These peaks correspond to major troughs in the U SGR log (indicated by capital T).

Table 3-1: Data was used for Fischer plot. Note the thicknesses were extracted from the unsupervised artificial neural Network results of SGR.

Cycle NO.	Thickness	Cumulative Thickness (cm)	Cumulative Departure
0	0	0.00	0
1	6.09	6.09	2.31
2	4.58	10.67	3.21
3	1.52	12.19	0.86
4	1.52	13.71	-1.39
5	1.53	15.24	-3.64
6	7.62	22.86	0.21
7	3.05	25.91	-0.52
8	3.04	28.95	-1.25
9	1.53	30.48	-3.5
10	3.05	33.53	-4.22
11	4.57	38.10	-3.42
12	1.52	39.62	-5.68
13	3.05	42.64	-6.41
14	3.05	45.72	-7.13
15	1.52	47.42	-9.39
16	4.57	51.81	-8.59
17	3.05	54.86	-9.32
18	1.53	56.39	-11.56
19	1.52	57.91	-13.82
20	1.52	59.43	-16.07
21	1.53	60.93	-18.32
22	7.62	68.58	-14.48
23	1.52	70.10	-16.73
24	9.15	79.25	-11.36
25	1.52	80.77	-13.61
26	4.57	85.34	-12.82
27	1.53	86.87	-15.06
28	1.52	88.39	-17.32
29	36.58	124.97	15.49
30	3.04	128.01	14.75
31	3.05	131.06	14.03
32	4.57	135.63	14.82
33	1.53	137.16	12.58
34	3.05	140.21	11.85
35	4.57	144.78	12.65
36	4.57	149.35	13.44
37	4.57	153.92	14.24
38	1.53	155.45	11.99
39	1.52	156.97	9.7
40	3.05	160.02	9.01
41	1.52	161.07	6.76
42	1.53	163.07	4.51
43	1.52	164.59	2.26
44	1.52	166.11	0

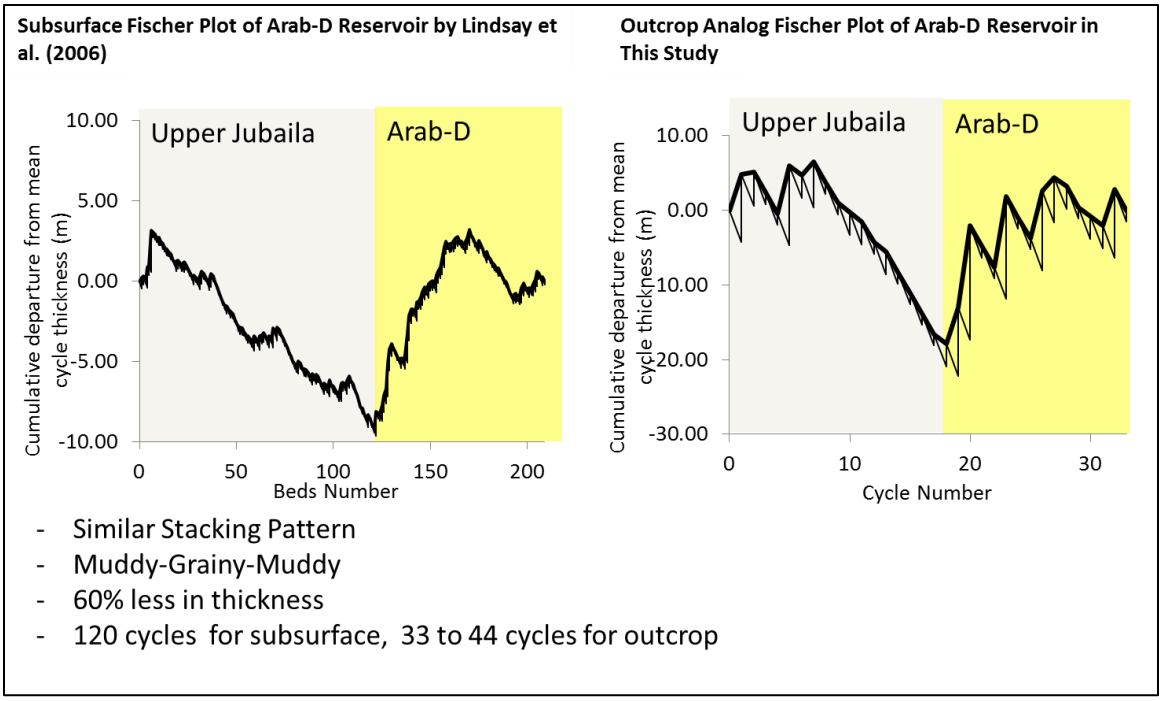

Figure 3-12: Fischer plots show the difference in cycles between subsurface Arab-D reservoir based on cycles extracted from published core data by Lindsay et al. (2006); and the studied outcrop based on SGR logs cycles from section-1. Note the similarity in the stacking pattern and difference in cycle's numbers.

3.6 Diagenesis

The diagenetic features in the outcropping strata equivalent to the Arab-D reservoir include: 1) micritization ; 2) marine cementation; 3) dissolution; 4) early dolomitization; 5) equant blocky calcite cementation; 6) micrite recrystallization; 7) Compaction; 8) late dolomitization; 9) dedolomitization; 10) meteoric cementation; and 11) fracture filling.

3.6.1 Micritization

A micrite envelope coats skeletal grains including bivalves and brachiopods shell fragments, different species of foraminifera, and some dacyclad algae. It was also observed as a coating on non-skeletal grains such a peloids and intraclasts. It was formed by a thin rim around these grains formed by microbial activity (Sanders, 1978). The second type of micritization includes the filling of skeletal grains in the intra pore space that were initially open in the earlier stages of lithofication. Micritization processes assist in porosity preservation because they prevent grain collapse and preserve grain shapes after the grains are completely dissolved, forming moldic porosity. Micritization associated with grainer facies marked the highstand system tracts of all HFSs (Figure 3-13)

3.6.2 Marine Cementation

Marine cementation consists mainly of aragonite and high magnesium calcite. These two forms of cement most likely precipitate in the earlier stage of the rock history. however, It was however, difficult to observe this form of calcite in this ancient carbonate outcrop, where the whole rocks were converted to low a magnesium calcite and dolomite, and can only be indicated by its morphology (Figure 3-14). Basyoni and Khalil, (2011) proposed many investigation tools to recognize the marine cementation in ancient carbonate.

3.6.3 Dissolution

Dissolution includes the leaching of unstable grains of aragonite and high magnesium calcite skeletal frames. This process was mainly caused by early meteoric diagenesis and resulted in the development of secondary porosity (moldic and inter-particle porosities). Micritization that occurred at the earlier stage of diagenesis played a major role in the preservation of skeletal grains, which did not collapse as a result of continuous dissolution. The pore system created at this stage was totally filled by cements during the late meteoric diagenesis stage (Figure 3-13).

3.6.4 Early Dolomitization

This dolomitization process occurs near surface to very shallow burial. Early dolomitization mostly fabric preserving, with fine- to medium-crystalline texture (10 to 50 μm). These dolomite crystals engulfing, and therefore postdating, intra-clasts grains with micrite envelops . dolomite crystals also found filling some dissolved shells fragments (Figure 3-15).

3.6.5 Equant Blocky Calcite Cementation

Dissolution of aragonatic skeletal grains provided solution saturated with calcium carbonate that was recrystallized in the intergranular, intragranular, and moldic pores as equant blocky calcite cements. Dissolution and precipitation processes may continue from shallow burial (eogenesis) through deep burial (mesogenesis) and in when the succession was exposed again (telogenesis) as meteoric cements (Figure 3-16).

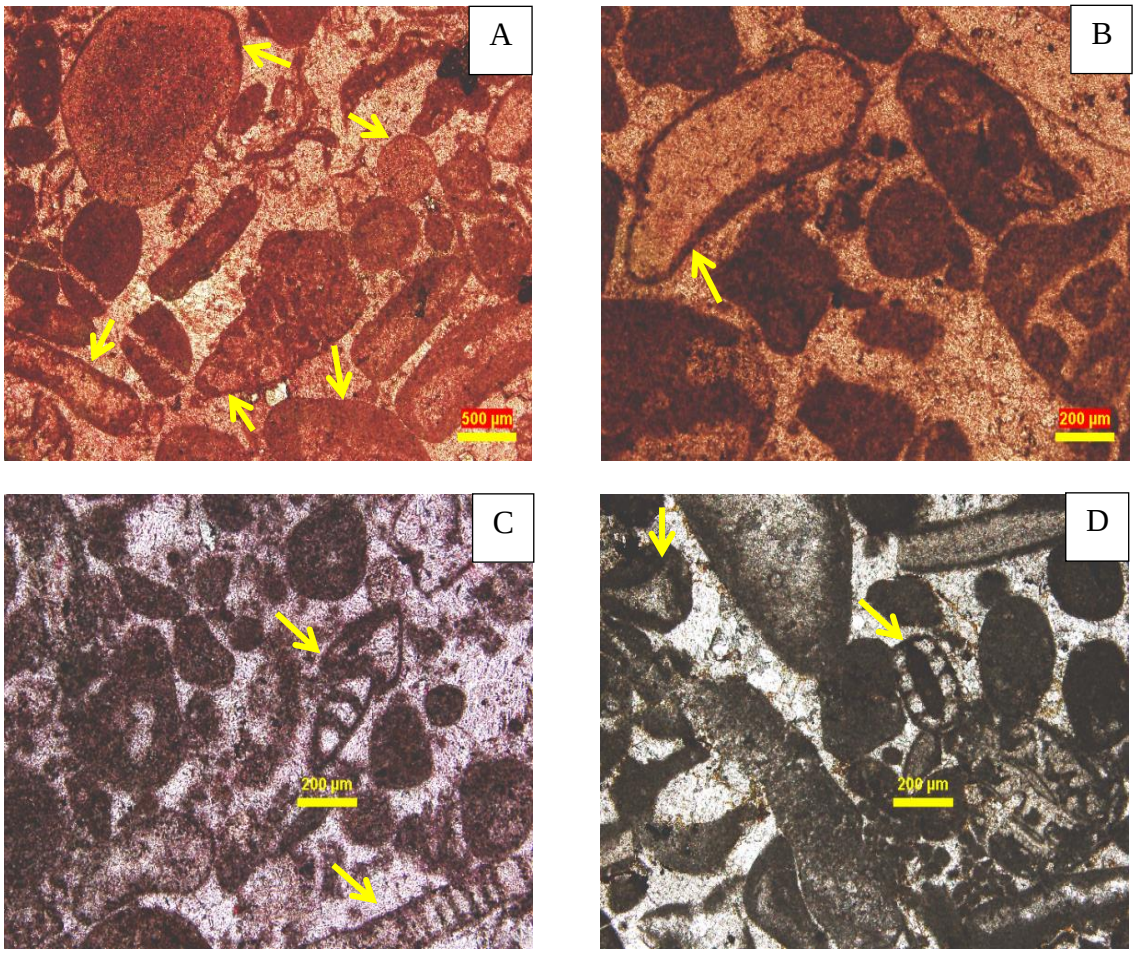

Figure 3-13: Photomicrographs showing (A) Micrite envelope formed as a rim surrounding intra-clast, peloids, and skeletal grains. (B) Completely dissolved skeletal grain with micrite envelope preserved their shape and formed moldic porosity which was filled later by calcite cement. (C) and D) Micrite filled intra-porosity in foraminifera tests and echinoids debris, and Dacyclad algae. The skeletal of these particles was subsequently dissolved and filled by calcite cements.

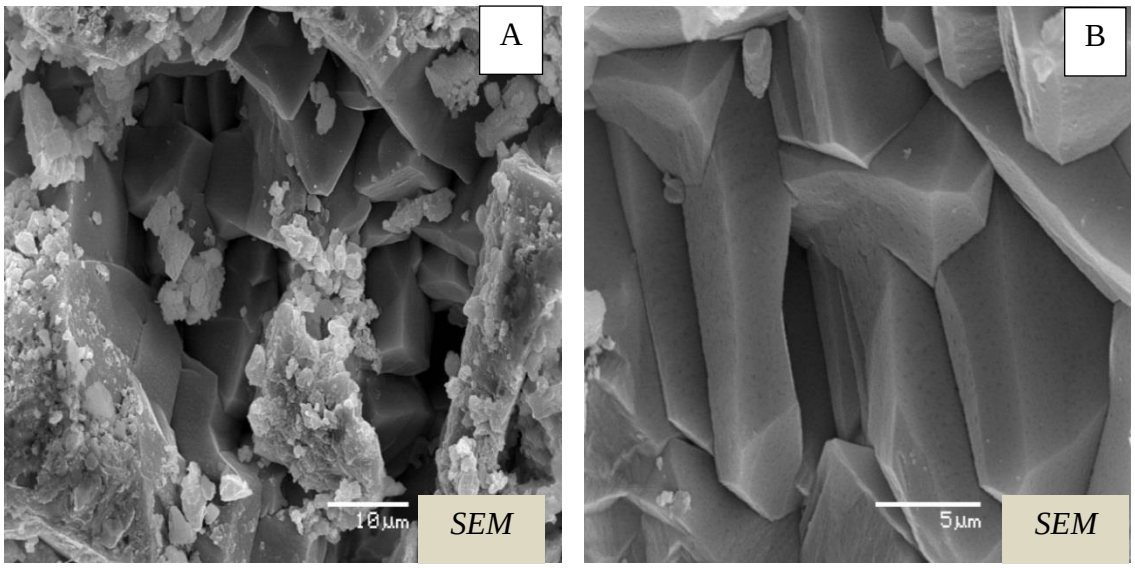

Figure 3-14: SEM image showing two different scales of resolution (A) and (B) for marine calcite cement that have been totally converted from high magnesium calcite to low magnesium calcite but still preserves the original prismatic crystallization morphology of marine cement.

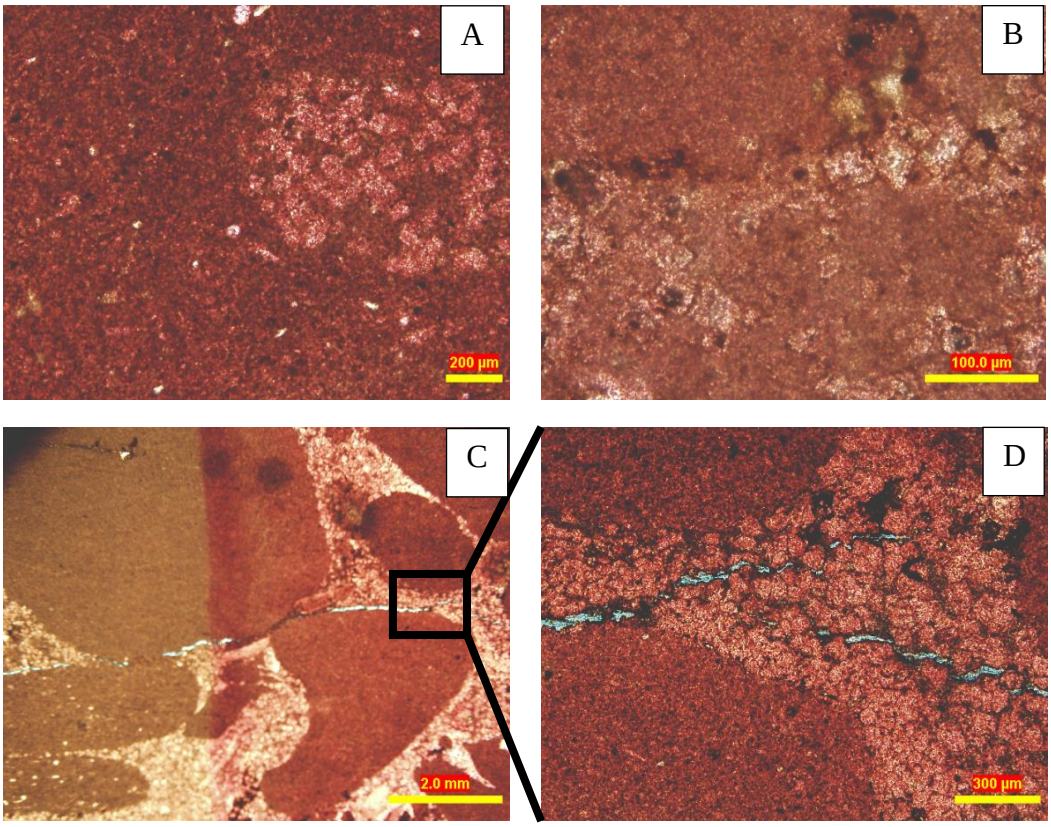

Figure 3-15: Thin section microphotographs showing Fabric Preserving (FP) dolomite filling mold of dissolved skeletal grains A) and B) and occur as a cement filling inter pores space C) and D).

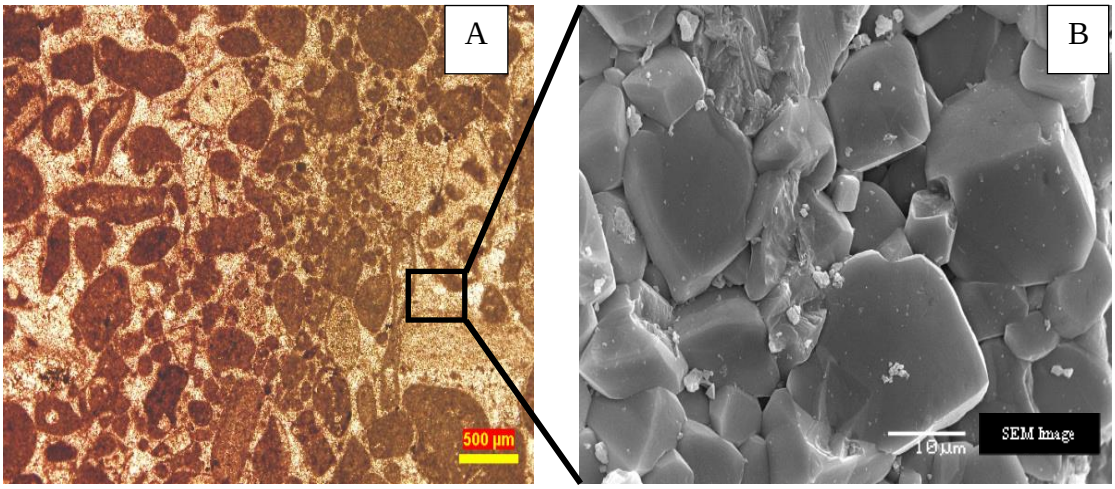

Figure 3-16: (A) Microphotograph showing sparry calcite cement filling grainstone fabric rock of the Upper Jubaila Member (B) SEM image showing very coarse sparry calcite.

3.6.6 Micrite Recrystallization

Recrystallization includes the transition from micrite to micro-spare and pseudo-microspare. This process mostly occurred in the muddier lithofacies of the outcrop succession associated with TST of the HFSs. The recrystallization of micrite to micro-spar and pseudo-microspar occur as rounded, sub-rounded, scaleno-rhombohedral, anhedral compacted, and fused micrites (Figure 3-17). Recrystallization also results to the precipitation of calcite cement between the carbonate grains. The calcite is produced by the the dissolution of unstable aragointe and high magnesium calcite rich carbonate grains.

3.6.7 Compaction

The studied thin sections showed a low to moderate degree of physical compaction. Although the grain contacts (point contact) are present in some thin sections, they are considered as minor and very localized. Compaction, however, results in reduction of the primary porosity in the grainier facies in the HST of the HFSs and the presence of scattered stylolites in the muddier facies of the TST indicate presence of chemical compaction (Figure 3-13 and Figure 3-16).

3.6.8 Late Dolomitization

The type of dolomitization occurs in dolomitic mudstone and wackestone of the Upper Jubaila Member in the outcrop succession (Figure 3-18). The observations in this study showed that this type of dolomite exhibits euhedral crystals, zoning, Planner-S, and crystal size ranging from 50 to 200 µm. This type of dolomite showed both partial dolomitization of mudstone and wackestone and completely dolomized rocks. Large crystals of dolomite have been observed in the thin sections studied (approximately 1 mm

in width), which scattered locally. This type of dolomite has characteristics similar to those of the baroque dolomite. This type of dolomite represent late stage dolomitization associated with hydrothermal solutions.

3.6.9 Dedolomitization

Dedolomitization or calcitization of dolomite is very pronounced in the study area. It was observed that dedolmitization occurred in steps and that all dolomites in the study area had undergone one or more of these dedolomitization steps (Figure 3-19). The steps of dedolomitization as indicated by Basyoni and Khalil (2011) are descending order:

1. Incompletely calcitized dolomite crystals,
2. Well-defined composite calcite rhombohedra as pseudomorphs of calcite after dolomite,
3. The occurrence of palimpsest rhombohedral structures shown by slightly ferric oxide zones that define former dolomite crystals within a new crystalline calcite fabric,
4. The development of some rhombohedral pores is indirect evidence for dedolomitization in limestone.

3.6.10 Fracture Filling

Fractures occur as mega scale regional extended fractures as well as local microscopic fractures. There were a number of fractures that have been observed in the outcrop and under the microscope. The crosscutting relationship indicated that fracturing postdated the earlier cements and compaction of carbonate grains. However, some of the fracture sets with wider apertures were totally filled by calcite cements and therefore predating the later cements (Figure 3-20).

3.6.11 Meteoric Cementation

Meteoric cementation occur as very coarse equant calcite cement and occupies the majority of the original intra-porosity and moldic porosity of the biocomponent. It also occurs as an interparticle porosity filling between different types of carbonate grains in the grainstones, packestones. This meteoric cement found engulfing all othor diagentic features (Figure 3-13). The sequence of diagenetic processes in the studied outcropping succession of the Arab-D reservoir are summarized in (Figure 3-21).

3.6.12 Stable isotopes Composition

3.6.12.1 $\delta^{13}C$ and $\delta^{18}O$ Isotopes

The results of carbon, oxygen, and strontium isotope analysis from outcropping strata equivalent to the Arab-D reservoir at the Wadi Nisah exposure are shown in Figure 3-22 The $\delta^{13}C$ values range from -6.47 to 1.26 while the $\delta^{18}O$ values range from -9.91 to -2.02. The vertical component of both $\delta^{13}C$ and $\delta^{18}O$ shows much lighter (more negative) $\delta^{13}C$ and $\delta^{18}O$ for the Upper Jubaila Member than for the Arab-D Member (Figure 3-23).

3.6.12.2 $^{87}Sr/^{86}Sr$ Isotopic Ratios

Bulk sample analyses reveal that the $^{87}Sr/^{86}Sr$ ratios vary between 0.707167 and 0.707447. Samples from the Upper Jubaila Member have $^{87}Sr/^{86}Sr$ ratios between 0.707167 and 0.707441 while samples from the Arab-D Member have $^{87}Sr/^{86}Sr$ ratios between 0.707224 and 0.707453 (Figure 3-22 and 3-23).

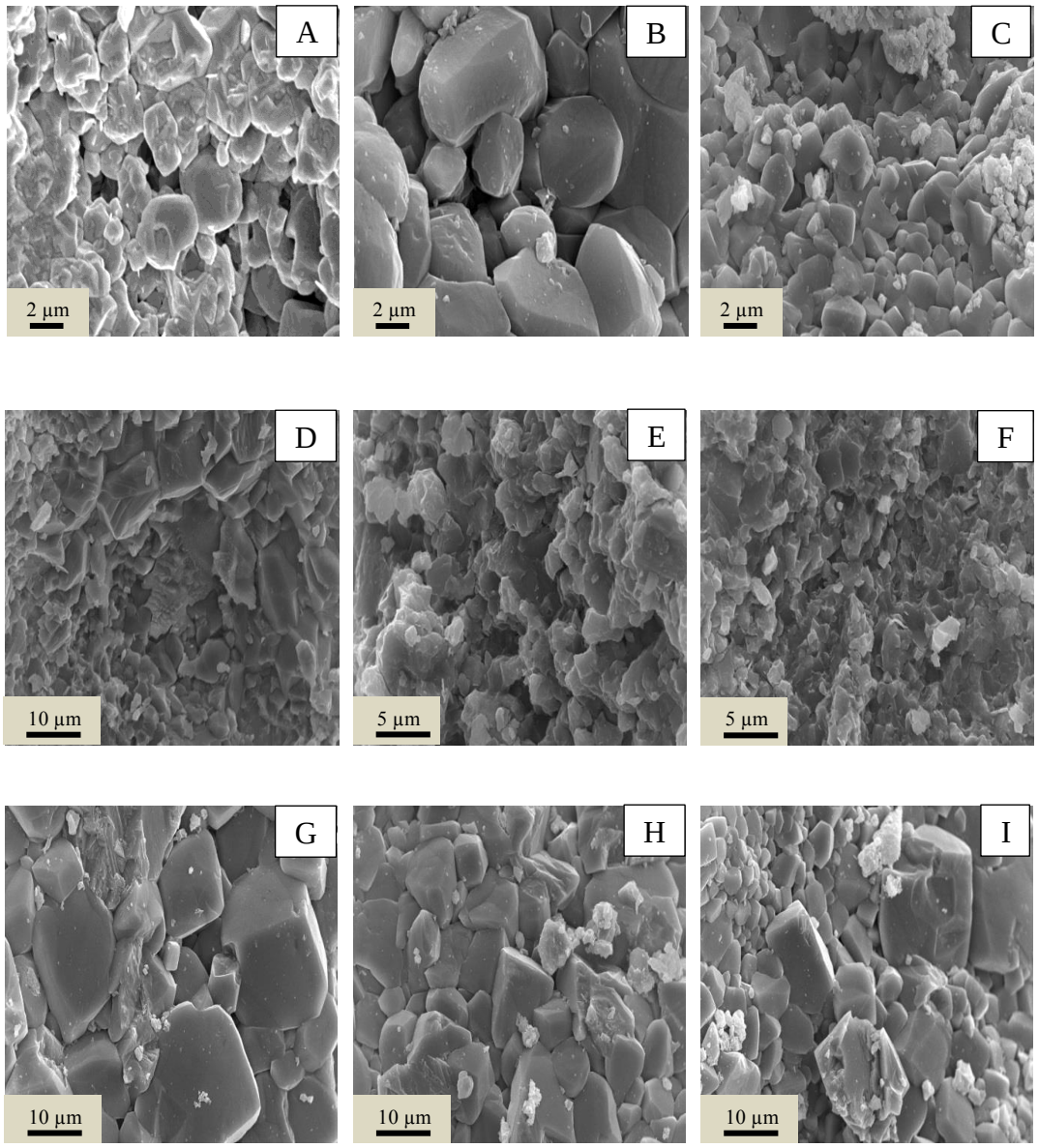

Figure 3-17: SEM images showing recrystlization of micritic limestone into A), B), and C) round and sub round micrite D) scaleno-rhomboedral micrite, E) Anhedral compact micrite, and F) fused micrite.

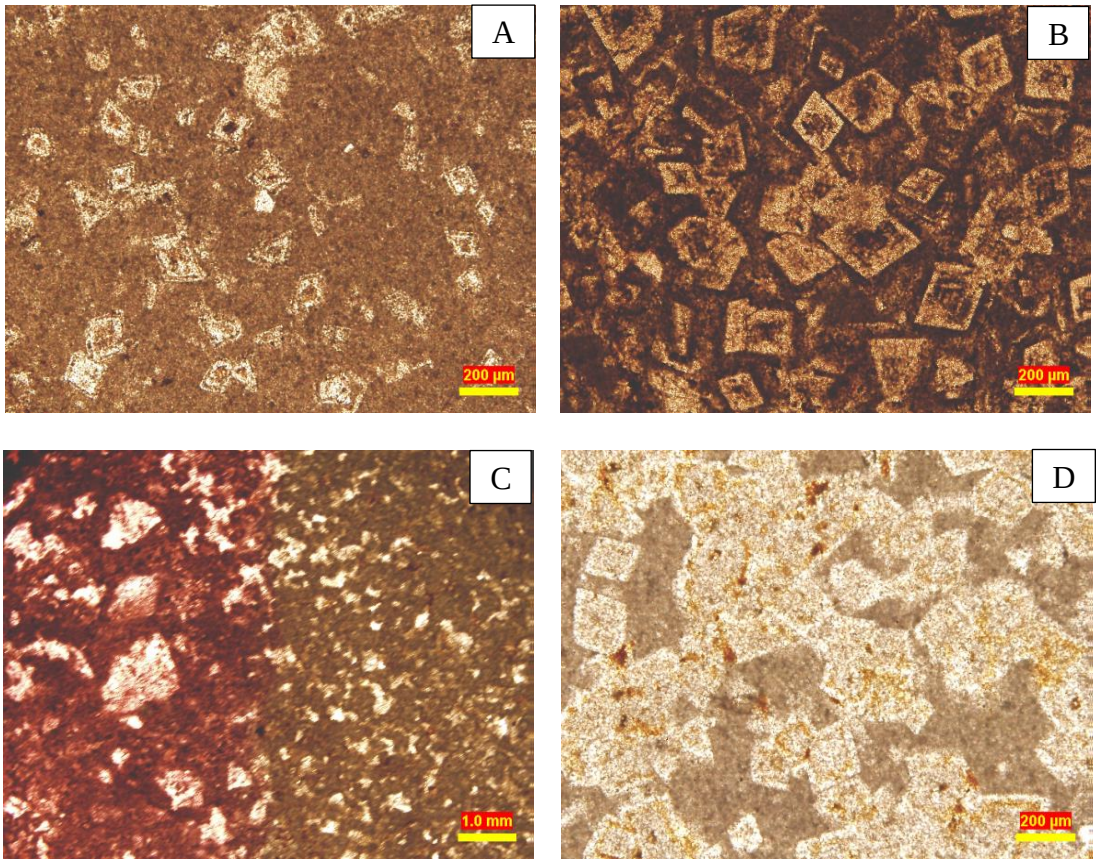

Figure 3-18: Thin section microphotographs showing non-fabric preserving (NFP) dolomite occur as (A) partially dolomitized mudstone and wackestone, (B) completely dolomitized rock, (C) partially dolomitized rock with very large dolomite crystals, and (D) micritic dolomite.

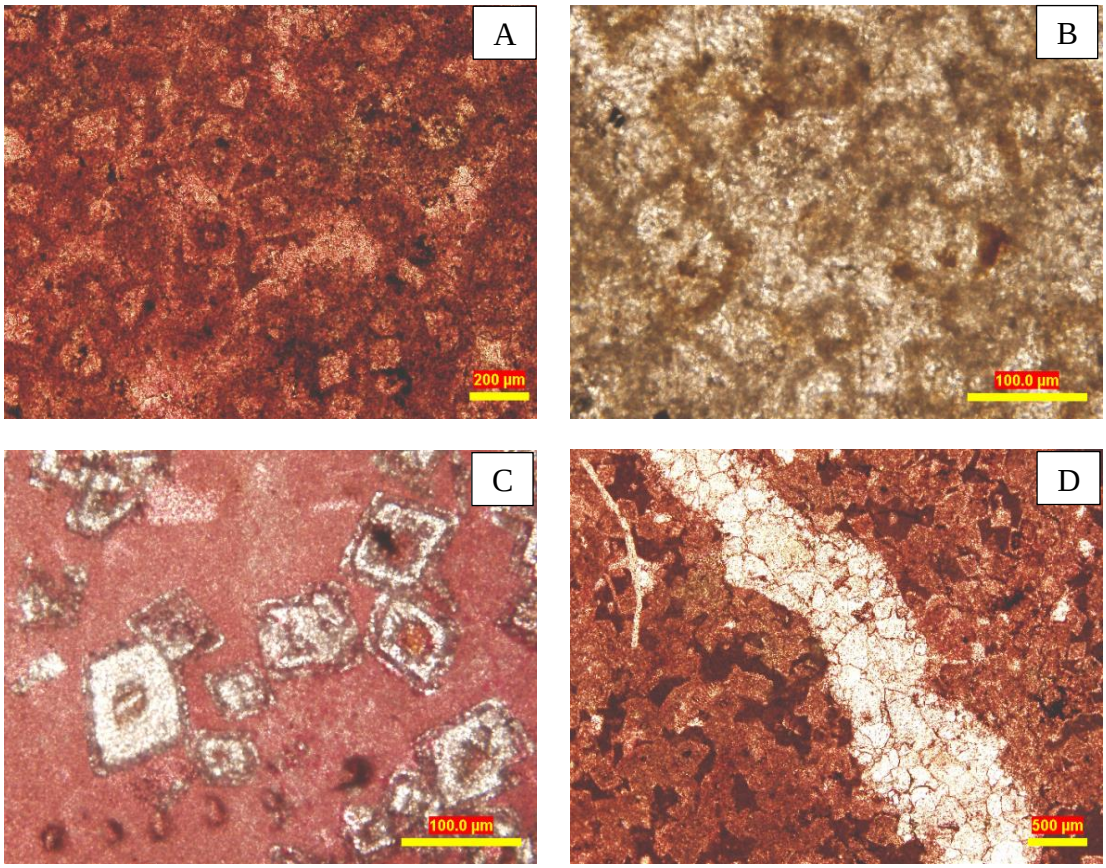

Figure 3-19: A), B), and C) Thin section microphotographs showing dedolomite (calcitized dolomite); D) fracture crossing the microphotograph. This fracture plays major roles in dolomitization and dedolomitization processes.

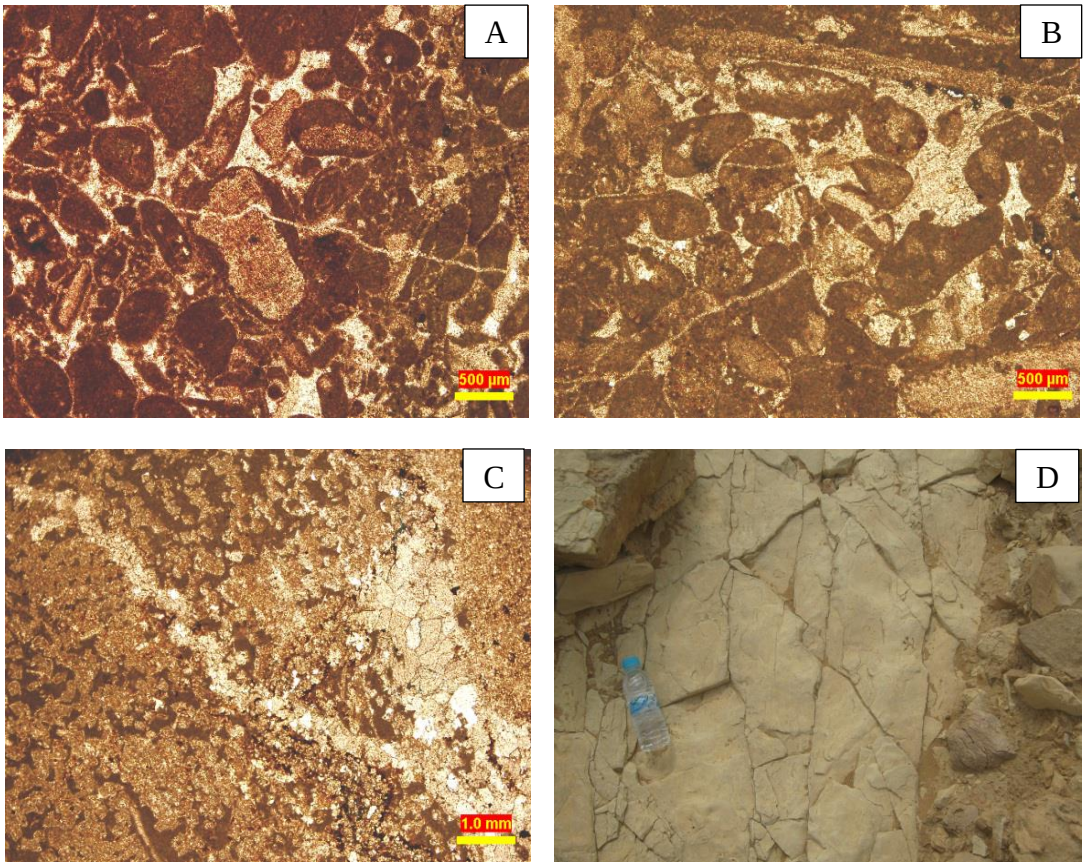

Figure 3-20: (A), B) and (C) microphotographs showing different scales and sets of fractures. (D) Outcrop photograph showing similar sets of fractures as seen in the thin sections.

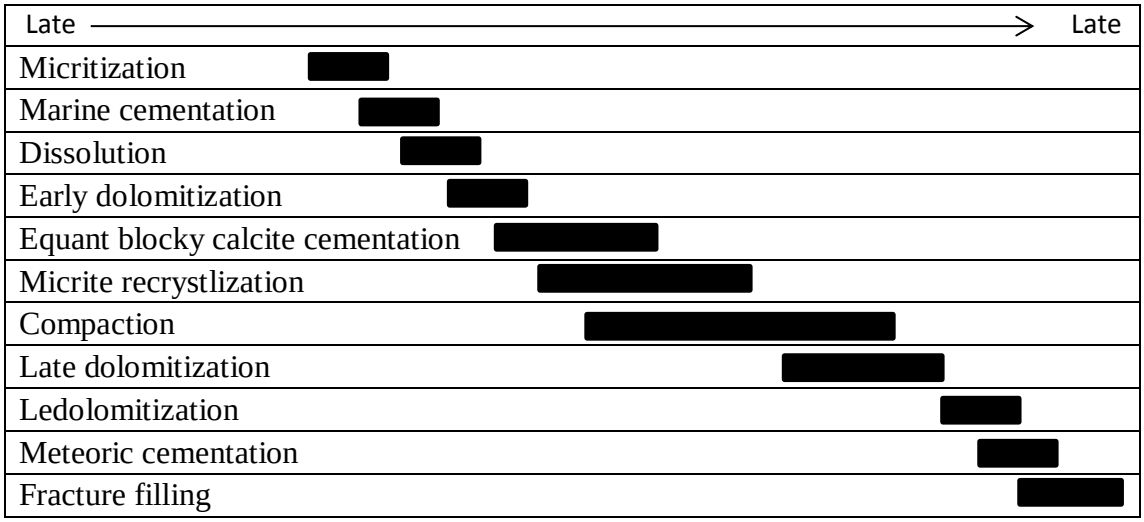

Figure 3-21: Paragenetic sequence reconstructed for the outcropping strata equivalent to the Arab-D reservoir.

Sample	Vertical Elevation (Cm)	Mudstone	Wackestone	Packstone	Grainstone	$\delta^{13}C$ (VPDB)	$\delta^{18}O$ (VPDB)	Sr^{87}/Sr^{86}
35	16					-0.13	-5.08	0.70742
34	68.8					0.52	-4.09	NI
33	102.4					0.54	-3.94	0.70745
32	140.8					0.96	-2.35	0.70736
31	160					0.76	-3.76	0.70758
30	188.8					1.26	-2.35	0.70734
29	216					0.6	-4.4	NI
27	240					1.19	-2.17	0.70744
26	347.2					NI	NI	NI
25	478.4					0.53	-4.36	NI
24	628.8					0.46	-3.83	NI
23	702					1.2	-2.09	0.70722
22	801.6					0.9	-4.15	0.70755
21	848					0.48	-3.8	0.70788
20	921.6					0.77	-3.77	0.70729
19	1056					0.04	-3.98	0.70746
18	1126.4					1.07	-2.59	0.70743
17	1179.2					-0.02	-2.26	0.70746
16	1189.6					NI	NI	0.70755
15	1205.6					-0.7	-4.61	0.70742
14	1221.6					-3.62	-6.4	0.70753
13	1266.4					0.35	-3.75	NI
212	1295.2					0.46	-4.3	0.70751
11	1304.8					-6.29	-9.06	NI
10	1324					-1.64	-4.12	0.7079
9	1348					-1.25	-5.51	0.70736
8	1367.2					-1.59	-5.77	NI
7	1404					-0.21	-3.82	0.70729
6	1621.6					0.35	-3.25	NI
5	1637.6					-0.65	-4.45	NI
4	1724					-0.74	-4.1	0.70751
3	1738.4					0.78	-4.76	NI
2	1765.6					0.01	-5.48	0.70717
1	1885					NI	NI	NI

Figure 3-22: Result of oxygen, carbon, and strontium isotopes analysis with vertical lithofacies component in Wadi Nisah section. Note that samples with no analysis result indicated by NI.

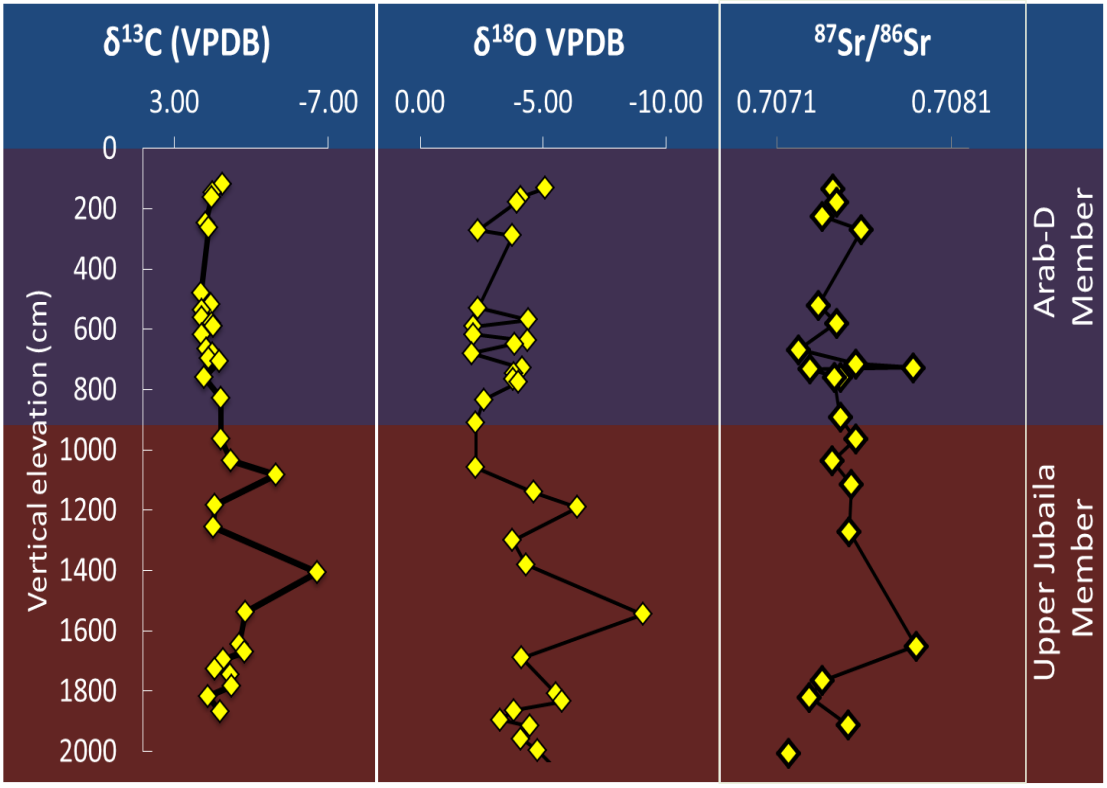

Figure 3-23: Vertical profile along the studied outcrop showing carbon and oxygen isotopes and strontium ratio of both the Upper Jubaila and Arab-D members.

3.7 Discussion

3.7.1 Facies Analysis

In this integrated characterization study of the Arab-D reservoir from equivalent outcropping strata, detailed lithofacies analyses were able to constrain the reservoir's stacking patterns and architectural elements. This study confirmed the similarity of the outcropping strata to the subsurface Arab-D reservoir that was suggested by Meyer et al. (1996). However, the lithofacies succession and sequence stratigraphy can be interpreted in a different context than a general shoaling upward depositional environment, especially for the Upper Jubaila Member. The following observations suggest that the Upper Jubaila Member at the outcrop could have been deposited as fining upward debris:

1- The four HFSs within the Upper Jubaila Member show similar cyclicity patterns and have erosive scour boundary between the HFSs.
2- The boundaries between beds and bed sets within the individual HFSs are gradational and not erosive.
3- Macrofossils, such as stromatoporoid debris, have random orientations.
4- The Fischer Plot constructed from the outcrop SGR logs shows successive finning upward cycles of the Upper Jubaila Member portion of the outcrop.

The layers in the outcrop are approximately one third the thickness of those in the subsurface Arab-D reservoir (60 m for the subsurface Arab-D reservoir, as described by Lindsay et al. (2006) and 20 m for the outcropping strata measured in this study). This may be attributed to a wide intrashelf basin that developed in eastern Saudi Arabia and did not extend to central Saudi Arabia, where the outcrop is exposed (Al-Husseini, 2000). Thus, the accommodation space available for carbonate sedimentation is expected to vary

greatly (Hughes, 2004a). In addition, the dominance of platy laminated mudstone in the study area indicates that the depositional environments shifted toward more of a lagoonal setting. This causes remarkable differences in the lithofacies associations at the outcrop from that of the subsurface reservoir (Table 3-2).

3.7.2 Sequence Stratigraphic Framework

Observations made in this study indicate that the stratigraphic sequence of the outcrop has a similar stacking pattern as the subsurface stratigraphic sequence described by Lindsay et al. (2006). Fischer Plots of the subsurface reservoir and the outcrop have similar shapes of cyclicity but have remarkable differences in the thickness and numbers of cycles. A comparison of this study with that of Lindsay et al. (2006) shows that the subsurface Arab-D reservoir is thicker (19 to 60 m) and has a greater total number of cycles (44 to120), a greater number of cycles within the Upper Jubaila Member (65 to 21), a greater number of cycles within the Arab-D Member (55 to 23), and fewer sequences (8 to 9) than the equivalent outcropping strata (Table 3-3). Four sequences in the Upper Jubaila Member represent a possible episodic regression of the sea and a decrease of accommodation space. These sequences show similar arrangements, starting from lower slope and upper slope burrowed wackestone and mudstone at the bottom of each sequence and overlain by oncoidal stromatoporoid packstone (rudstone) and wackestone (floatstone) that was possibly deposited in a ramp crest to lee side of a distal lagoon environment. The HFSs in the Arab-D Member of the Arab Formation also show a shoaling upward pattern. These HFSs can be categorised into three types of successions. Type-1 HFSs are composed of a sequence of distal lagoon lithofacies to deep lagoon lithofacies to proximal lagoon lithofacies to skeletal bank lithofacies. Type-2

HFSs are composed of a sequence of deep lagoon lithofacies to proximal lagoon lithofacies to skeletal bank lithofacies. Type-3 HFSs are composed of a sequence of proximal lagoon lithofacies to skeletal bank lithofacies to tidal flat lithofacies.

3.7.3 Biostratigraphy

The difference in the accommodation space available to the Arab-D reservoir in the Eastern Arabian Plate that did not extend to the outcrop location is also reflected in the biocomponent diversity of the study area. Table 3-4 compares the subsurface biocomponents and the biocomponents from the outcrop in this study. Although the subsurface Upper Jurassic Arab-D reservoir has excellent biocomponent diversity (Hughes, 1996; 2004a, 2004b, 2009), samples from the outcrop succession show very low biofacies diversity. The scarcity of microfossils and the absence of dasyclad algae indicate different environmental conditions from those of the subsurface Arab-D reservoir and may be related to environmental condition such as elevated salinity.

It is difficult to determine, with accuracy, the age of Jubaila and Arab formation, using micropaleontology. Although there is a limited biofacies component in the study area, key biocomponents are present and support the analogy of this outcrop to the Upper Jurassic Arab-D reservoir. The presence of *Kurnubia palastiniensis*, *Nautiloculina oolithica*, and *Quinqueloculina* SPP. in the outcrop samples suggest a Kimmeridgian age for the succession (Hughes, 2004b). In addition, the last appearance of stromatoporoid that marks the Jubaila-Arab formation boundary is a valuable indicator for the top of the formations.

3.7.4 Link of Porosity Evolution, Diagenetic Alteration and Sequence Stratigraphy

This study is intended to establish a link between the different scales of porosity heterogeneity and their sequence stratigraphic control. The study has also attempted, however, to construct a paragenetic sequence for the main diagenetic overprint and show the impact on the porosity types and distribution. Most of the Middle to Late Jurassic reservoirs is considered as highstand system tracts of high frequency sequences, and the Arab-D reservoir is not an exception. The HST of the stacked shoaling-upward sequences show a succession equivalent to the Arab-D reservoir and consists of very coarse grains between which a high primary porosity developed. The primary porosity evolved through several steps of enhancement and reduction according to both their sequence stratigraphic system tracts and their diagenetic events. The porosity enhancement started with shoaling upward and early meteoric dissolution, which produced most of the moldic and intra-particles porosity in the study area, for which porosity is expected to have higher values. The shoaling upward and the drop down of the relative sea level are expected to develop a dolomitization-prone depositional environment (Morad et al., 2012). According to Cantrell et al. (2001), most of the dolomitic layers within the Arab-D reservoir are suggested to be developed from the subkha reflux model (Cantrell et al., 2001; Morad et al., 2012) . The HST of the HFSs represent a pathway for a highly concentrated Mg^{+2}/Ca^{+2} solution, which later produced partial to completely dolomitic facies within the underlain layers of the TST. Early dolomitization is considered as one of the porosity enhancement factors due to the associated intercrystalline porosity developed between dolomite rhombs. Micritization has two roles in the porosity enhancement-reduction

processes. On one hand, early micritization reduces the primary porosity by infiltrating the primary pores of the skeletal grains. On the other hand, micritization plays a positive role in porosity enhancement because it preserves the skeletal shapes and prevents grain collapse after heavier dissolution due to the passage of meteoric fluid. Mechanical compaction in the studied succession is not pronounced and porosity destruction by grain compaction has not dramatically influenced porosity values, especially for those of skeletal grains, which were protected by a micritization of their skeleton or by development of micrite envelopes.

Early dolomitization is represented by dolomite cements around various carbonate grains within the HST layers. This type of dolomite is considered a destructive porosity factor. Fracturing is a very important process in the porosity enhancement-reduction process, not only because the fracture system by itself enhances the porosity regime but also because the fracture system plays a major role as conduits for highly concentration Mg^{+2}/Ca^{+2} solution through the HST into TST and facilitates the dolomitization procedure (Swart et al., 2005), thus indirectly enhancing porosity. The same fracture system in late stage diagenesis facilitates the infiltration of meteoric solutions with high Ca^{+2}/Mg^{+2} concentrations (Cantrell et al., 2007). This solution is responsible for two processes, one of which is the leaching of dolomite crystals, leaving rhombohedral moldic pores. The other process is to preferentially dedolomitize or calcitize the intact dolomitic rocks. The resulting calcite later fills these fractures as very coarse sparry calcite. The last stage of the diagenetic events is the telodiagenesis meteoric cementation (Cantrell et al. 2007), which completely fills the remaining porosity and leaves only micropore spaces between cements and microcrystalline calcite.

3.7.5 Stable Isotopes

3.7.5.1 $\delta^{13}C$ and $\delta^{18}O$ Analysis

The $\delta^{13}C$ and $\delta^{18}O$ isotope values from this outcropping strata equivalent to the Arab-D reservoir is largely affected by the diagenetic alterations that have changed the original fabric of the outcrop rocks. The $\delta^{13}C$ and $\delta^{18}O$ curve show several negative excursions in general trend of increasing upward from the Upper Jubaila to Arab-D members. These negative excursions are mainly dominant in grain-dominated lithofacies and dedolomitic horizons (Figure 3-24). The negative excursions, may therefore be attributed to meteoric cements filling porosity within and in between these grains. These grain-dominated lithofacies are mainly developed in the Upper Jubaila Member, therefore, this interval shows more negative $\delta^{13}C$ and $\delta^{18}O$ values. The cross-plot of $\delta^{13}C$ and $\delta^{18}O$ shows that several samples of grain-dominated lithofacies in the Upper Jubaila Member have relatively very high negative values comparing to other samples. This could be due to the freshwater diagenesis that decreases both $\delta^{13}C$ and $\delta^{18}O$. the $\delta^{13}C$ and $\delta^{18}O$ values of the mud-dominated lithofacies show relatively narrower range and occur mainly in the Arab-D Member. Figure 3-24 shows a comparison between $\delta^{13}C$ and $\delta^{18}O$ data of the study area and those of the actual Arab-D reservoir in Saudi Arabia (Cantrell et al., 2004) and in the United Arab Emirates (Morad et al., 2012). Based on this comparison, only outcrop samples occur in the mud-dominated interval could be directly compare to the actual subsurface reservoir. Although there is a clear data clustering in $\delta^{13}C$ and $\delta^{18}O$ cross-plot the in which Upper Jubaila and Arab-D could be recognized, this clustering could be attributed to the relatively high negative values caused by meteoric cementation.

3.7.5.2 $^{87}Sr/^{86}Sr$ Ratios Analysis

The $^{87}Sr/^{86}Sr$ ratio of seawater varied from 0.7069 to 0.7067 during the Kimmerdidgian (152 Ma). The determine $^{87}Sr/^{86}Sr$ data of the outcrop samples are clearly higher. The studied samples show biocomponent of Kimmerdidgian and the previous work in this location also indicated same age dating. Dissolution method that preferentially dissolves the carbonate and separated the siliciclastic material from the samples was performed. This test enabled to determine $^{87}Sr/^{86}Sr$ for the carbonate and the residual silisclastic material separately.

Biofacies study suggested that the studied outcrop is Kimmerdidgian time period and therefore should have an age between 151 and 154 Ma (Hughes 1996, 2004a, 2004b, 2009). During this period the seawater $^{87}Sr/^{86}Sr$ curve shows a minimum $^{87}Sr/^{86}Sr$ ratio between 0.7068 and 0.7069 (MacArthur et al. 2001). Lindsay et al. (2006) indicated that $^{87}Sr/^{86}Sr$ of dolomite in Arab-D reservoir range from 0.70712 to 0.70682 while Morad et al. (2012) indicated that the ratio range from 0.70704 to 0.7077. The $^{87}Sr/^{86}Sr$ ratios of the HNO_3 soluble fractions are still higher than expected for the Kimmerdidgian time interval, however, outcrop data show relatively similar value to subsurface Arab-D reservoir.

The possible reasons for this high $^{87}Sr/^{86}Sr$ ratio could be : 1) The rocks are a mixture of carbonate and minor amount of silisclastics. The silicates could have a none seawater isotope signature if they derived from a continental granitic source. 2) Dissolved materials from overlain Cretaceous interval containing a higher amount of $^{87}Sr/^{86}Sr$ precipitated in the studied interval and elevated the $^{87}Sr/^{86}Sr$ ratio than the normal.

Table 3-2: Lithofacies of Arab-D reservoir extracted from core data (Lindsay et al., 2006) and outcropping equivalent strata in the central Saudi Arabia (Meyer et al., 1996) compared to the present study.

Subsurface Facies of Arab-D Reservoir by Lindsay et al. (2006)	**Outcrop Analog Facies of Arab-D Reservoir in This Study**
Anhydrite (nodular bedded, massive, plamate)	Missing
Missing	Breccia
Micrite	Laminated mudstone
Skeletal oolitic grainstones mud-lean packstones	Missing
Stromatoporoid-red and green algae-coral rudstone	Stromatoporoid lithofacies
Cladocoropsis rudstone and floatstones	Missing
Bivalve coated grainstone mud-lean packstones	Skeletal bank lithofacies
Dolomite	Dolomitic-mudstones/wackestones

Table 3-3: Stratigraphic sequences of Arab-D reservoir extracted from core data (Lindsay et al., 2006) and outcropping equivalent strata in the central Saudi Arabia (Meyer et al., 1996) camper to the present study.

		Lindsay et al. 2002			Meyer et al. 1996		This Study	
		HFS	**Cycles Set**	**Cycles**	**Cycles**	**Cycle type**	**HFS**	**Cycles set**
Arab-D Reservoir	**Arab-D Member**	HFS 1	1	5	19	**Thinning Upward**	HFS 1	4
					18			
		HFS 1	3	10	17		HFS 1	3
					16			
		HFS 2	2	10	15		HFS 2	5
					14			
		HFS 3	3	15	13		HFS 3	5
					12			
		HFS 4	2	10	11	**Skeletal Bank**	HFS 4	4
					10			
		HFS 5	2	5	9		HFS 5	2
					8			
	Upper Jubaila Member	HFS 6	4	15	7	**Stromatoporoids**	HFS 6	6
					6			
		HFS 7	6	30	5		HFS 7	5
					4			
		HFS 8	5	20	3		HFS 8	5
					2			
					1		HFS 9	5
		8	28	120			9	44

Table 3-4: Comparing bio-components of Arab-D reservoir extracted from core data (Lindsay et al., 2006) to the present study.

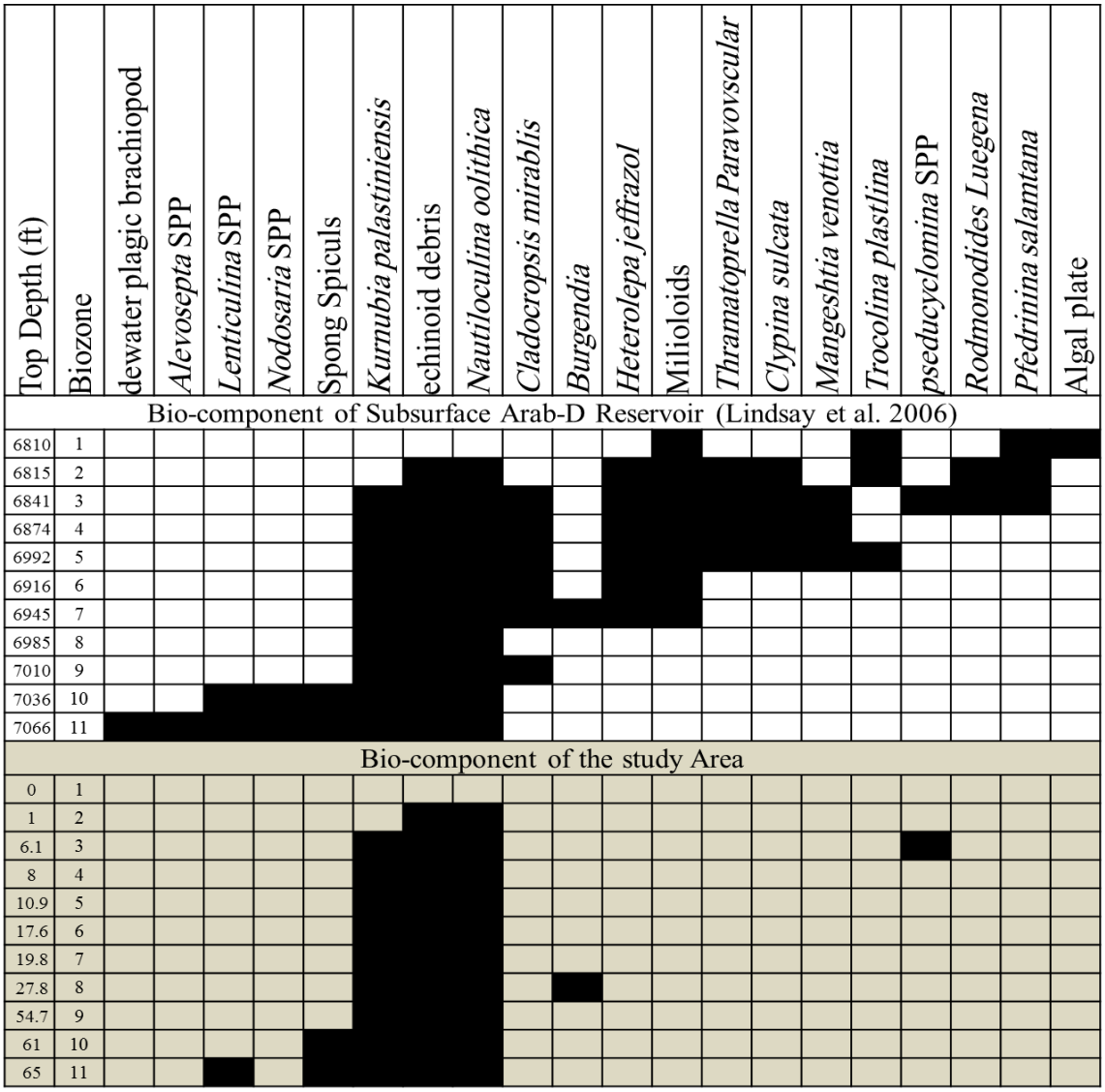

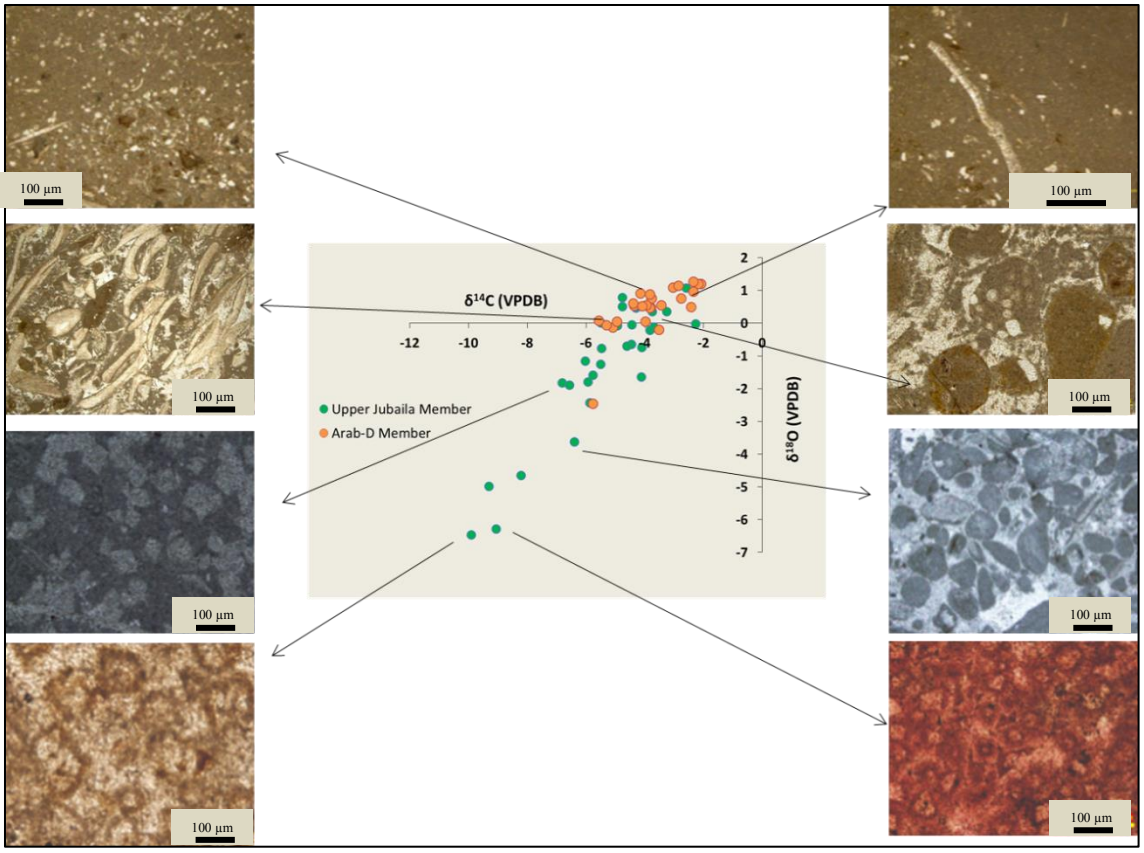

Figure 3-24: Cross plot of carbon versus oxygen isotopes signature of the studied outcrop succession. If excluding the lowest values of the Arab-D member data there will be a good separation between the two members. Light isotopes values (more negative values) in the Upper Jubaila Member associated with high cemented grainstone (meteoric cementation) and dedolomitc layers, while heavy isotopes (less negative values) associated with micritic mudstone.

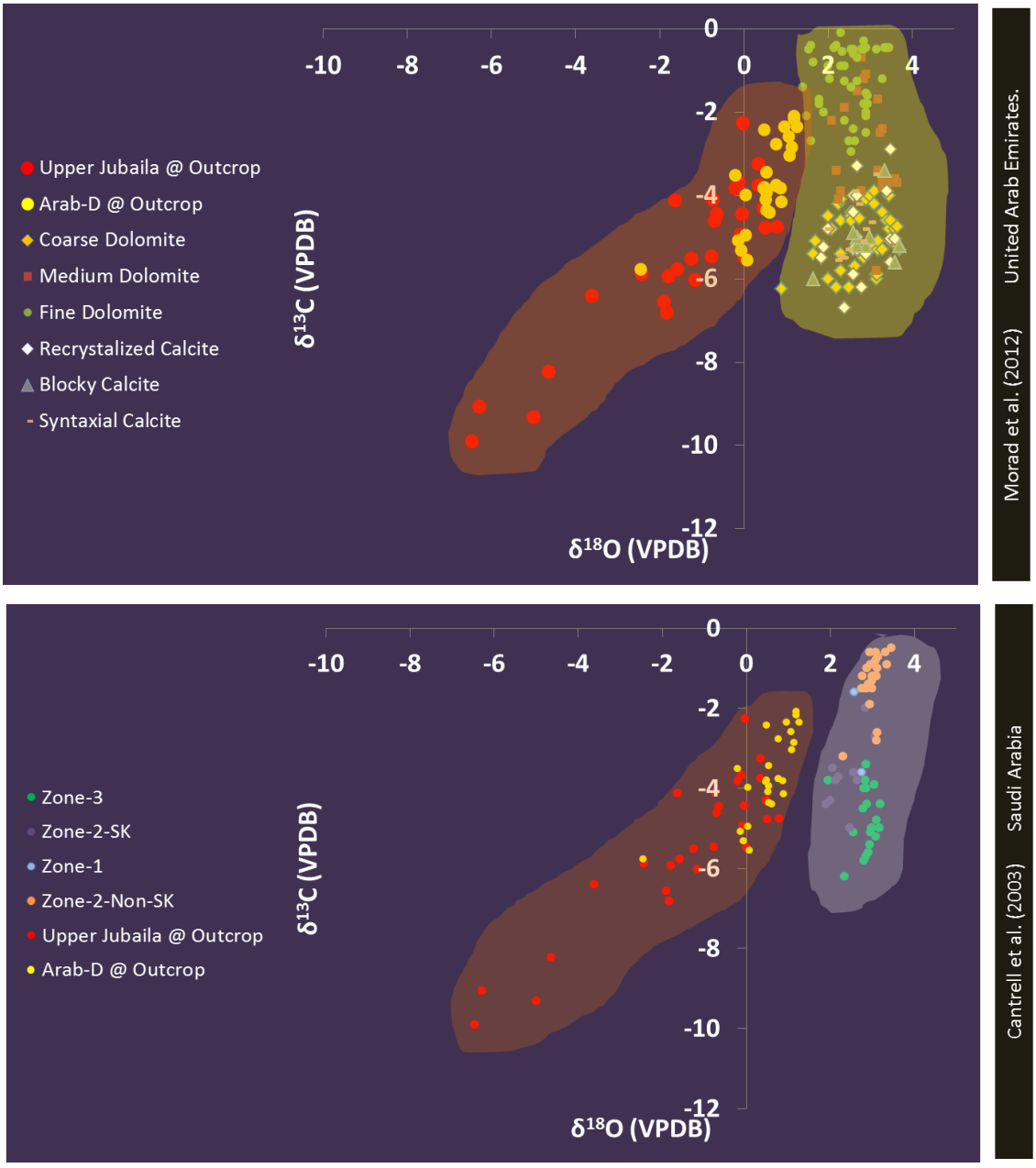

Figure 3-25: Comparison between subsurface and outcrop of the Arab-D reservoir using cross plot of carbon versus oxygen isotopes signature A) comparison between subsurface Arab-D reservoir in the United Arab Emirates and outcrop in the central Saudi Arabia B) comparison between subsurface Arab-D reservoir in the eastern Saudi Arabia and outcrop in the central Saudi Arabia.

CHAPTER 4

THREE-DIMENSIONAL LITHOFACIES AND PETROPHYSICAL MODELLING

4.1 Introduction

When compared to the actual geologic characteristics, subsurface models of hydrocarbon reservoirs are coarse and of low resolution. Understanding of the 3-D architecture of reservoir units is, therefore, often incomplete. Outcrop analogs are commonly used to understand the spatial continuity of reservoir units. In this study, outcrop analog of the Arab-D reservoir was used to build a high resolution model that captures fine geologic details. Subsurface reservoir lithofacies were matched with those from the studied outcrops. Porosity values derived from published core and well logs data from the Ain Dar, Uthmaniyah, and Shedgum areas of the Ghawar Field, eastern Saudi Arabia, were then applied to the equivalent lithofacies in the outcrops. Maximum, minimum, and average subsurface porosity for each lithofacies were distributed in the facies model. Several realizations were run to visualize the variability in each model and to measure the uncertainty associated with the models. The results indicated that potential reservoir zones are associated with grainstones, packstones, and some wackestones layers (Douglas, 1996). Semivariogram analysis of the lithofacies showed good continuity in the N-S direction and less continuity in the E-W direction. The high resolution lithofacies models detected permeability barriers and isolated low porosity bodies within the

potential reservoir zones. This model revealed the porosity distribution in areas smaller than one cell in the subsurface model and highlighted the uncertainty associated with several aspects of the model.

4.2 The Importance of 3-D Outcrop Modelling

Models of the porosity and permeability distributions in oil fields are controlled by information from wells that are often spaced more than 1 km apart. Lateral facies changes are expected between the wells because of these large inter-well distances. These lateral facies variabilities present a challenge for reservoir Modelling (Fabuel-Perez et al., 2009). Because facies is the main factor that controls the distribution of porosity and permeability (Sahin et al., 1998), these parameters are expected to vary along with facies over short distances. The uncertainties in porosity and permeability increase with increased well spacing. Since porosity and permeability depend on facies, the uncertainty about the spatial distribution of facies will, therefore, introduce additional uncertainty to them. In reservoir Modelling, this uncertainty, potentially introduces coarse porosity and permeability estimates and smoothing permeability barriers due to a lack of fine detail. The challenges associated with coarse models can be addressed by studying a reservoir outcrop analog (Pringle et al., 2006; Bellian et al., 2005). Analog models can capture small details of facies that may affect porosity or act as permeability barriers. Surface processes may, however, alter the porosity and permeability of the rocks the outcrop exposures andthese may lead to large differences between the actual subsurface reservoir properties and those of the outcrop analog. To overcome this problem, the porosity and permeability values from the reservoir can be superimposed on the high resolution

outcrop analog model (Labourdette et al., 2008). The integration of a high-resolution outcrop facies model with the actual reservoir properties gives a better understanding of the vertical and lateral porosity and permeability distributions at scales less than the well spacing in the oil field. As indicated earlier, several studies (e.g., Douglas, 1996; Meyer et al., 1996; Sahin et al., 1998; Cantrell and Hagerty, 1999; Cantrell et al., 2004a). have investigated the porosity and permeability of the Arab-D reservoir unit. These studies utilized extensive porosity and permeability data from different areas in the Ghawar Field, such as Ain Dar, Uthmanyah, and Shedgum (Table 4-1). This published data were superimposed on the equivalent outcrop facies to produce high-resolution 3-D porosity and permeability models.

4.3 Grid Construction

Four surfaces were reconstructed from the correlated stratigraphic sections (Figure 4-1), these surfaces are:

- Surface-1. The boundary between Arab-D and Arab-C. This surface is marked by the collapsed breccia;
- Surface-2. The top of the skeletal bank deposits which placed on the transition boundary between relatively thick layers of offshore bank relatively deeper lagoon burrowed mudstones to wackestones and very thinly platy laminated mudstones;
- Surface-3. The top of the Upper Jubaila Member defined by the last appearance of stromatoporoid; and
- Surface-4. The bottom of the exposed strata.

Table 4-1: Porosity values of three major producing areas in Ghawar Field as extracted from Literature review.

Facies Matching		Porosity Value		Oilfields			
Subsurface Facies	Outcrop Facies			Ain Dar (Douglas, 1996)	Shugum (Cantrell et al. 2003)	Uthmaniyah (Saner and Sahin, 1999)	Ghawar (Lucia et al., 2001)
Laminated Mudstone	Micritic	Porosity	Min	-		2.8	1.25
			Average	**13**	**13**	**9.2**	**7**
			Max	-		18.8	17.5
Dolomitic Mudstone	Dolomitic Mudstone	Porosity	Min	-		2.8	1.25
			Average	**17.5**	**10.2**	**9.2**	**7**
			Max	-		18.8	17.25
Dolomitic Wackestone	Dolomitic-Wackestone	Porosity	Min	-		2.6	1.25
			Average	**17.5**	**16.3**	**16.5**	**10**
			Max	-		28.7	17.5
Stromatoporoid Wackestone and Packstone	Stromatoporoid Packstone	Porosity	Min	-		19.3	1.25
			Average	**20.7**	**12.64**	**26.55**	**17**
			Max	-		32.5	27.5
Wavy Laminated Sandy Grainstone	Mix skeletal Grainstone	Porosity	Min	-		19.3	3.75
			Average	**25.9**	**25**	**26.55**	**15**
			Max	-		32.5	22.5
Peloidal Fossiliferous Grainstone	Mix skeletal Grainstone	Porosity	Min	-		19.3	3.75
			Average	**25.9**	**25**	**26.55**	**15**
			Max	-		32.5	22.5
Breccia	Micritic	Porosity	Min	-		2.8	1.25
			Average	**13**	**13**	**9.2**	**7**
			Max	-		18.8	17.5

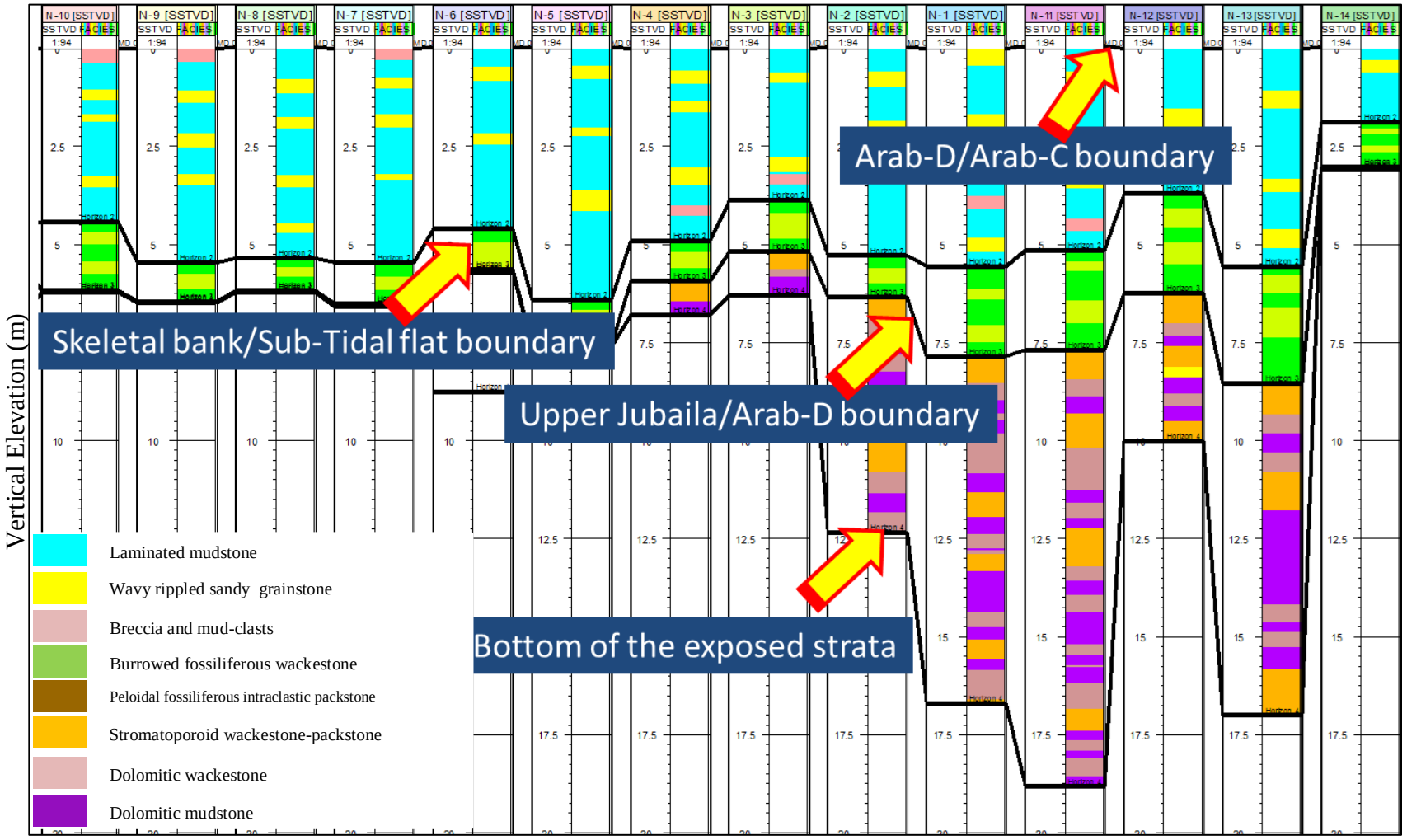

Figure 4-1: Cross section in the study area showing the 14 stratigraphic sections and the four correlated surfaces (time lines). Note that N-1, N-2, …. N-14 are the names of each section; SSTVD refer to true vertical stratigraphic section.

Using the above mention stratigraphic surfaces a three-dimensional gridding system was reconstructed. This gridding system constrained by surface-1 (the Upper limit), surface-4 (the lower limit), and surrounded by a polygon extended 200 m in the east-west direction and 100 m in the North-south direction.

These four surfaces define three zones in the gridding system which are from bottom to top, Stromatoporoids, skeletal bank, and tidal-flat zone. The average number of bed setts in the outcrop is 20, 10, and 10 bed setts for Stromatoporoids, skeletal bank, and tidal-flat respectively. Accordingly, these bed setts were represented by layers in each corresponding zone with a proportional separation between these layers (Figure 4-2). Horizontal girds have spaced 1 m^2. This grid dimension allow for capturing small scale facies heterogeneity in the study area. Table-4-2 shows the properties of the resulting three-dimensional grids. The thicknesses of each of the seven lithofacies in the stratigraphic sections were up-scaled to match the size of grid cells in each layer.

4.4 Variograms Construction

The indicator variograms were constructed for each of the seven lithofacies in the study area. The experimental variograms were computed using thicknesses of lithofacies in the stratigraphic sections up-scaled to the size of grid cells. Horizontal experimental variogram were computed in each zone separately by considering pairs of points belonging to the same grid layer, and with a search radius of 200 and 100 m for E-W and N-S respectively tolerance angle of 45° and a bandwidth of 100 and 50 m for E-W and N-S respectively for the different directions. Vertical variograms were computed by

considering only pairs of lithofacies thickness in the same stratigraphic section. The modeled variograms were constructed by fitting using spherical model.

4.5 Characterization of the Spatial Continuity of the Lithofacies

The main controls for the development of the outcrop facies model are the semivariograms taken from the outcrop stratigraphic sections. Indicator semivariograms were constructed in different directions to determine the direction with the best spatial continuity. The nugget value, which is defined as the variability at a very low range or at the smaller lag of the data points, should be equal for the three semivariogram directions (major, minor, and vertical). To calculate the nugget value, it is better to begin with the vertical semivariogram because its parameters are the best defined. There is a strong link between the differences in the semivariograms and the geologic parameters of the Arab-D reservoir analog. These parameters include vertical layering of the outcrop, lateral facies changes, and topographical control of the outcrop (Sahin et al., 1988). The N-S direction has the best continuity for most of the lithofacies and is considered to be the major axis for the semivariogram. The E-W direction, which has less continuity, is considered to be the minor direction. Generally, the modeled vertical, major, and minor indicator semivariograms for the lithofacies have the following characteristics:

4.5.1 Semivariogram for Dolomitic Mudstones and Wackestones

Semivariogram Shape: The semivariogram for the dolomitic mudstone and wackestone has a good shape, low nugget value, and a sill that is nearly the same in all directions. The range is higher in the major direction than in the minor direction (Figure 4-3).

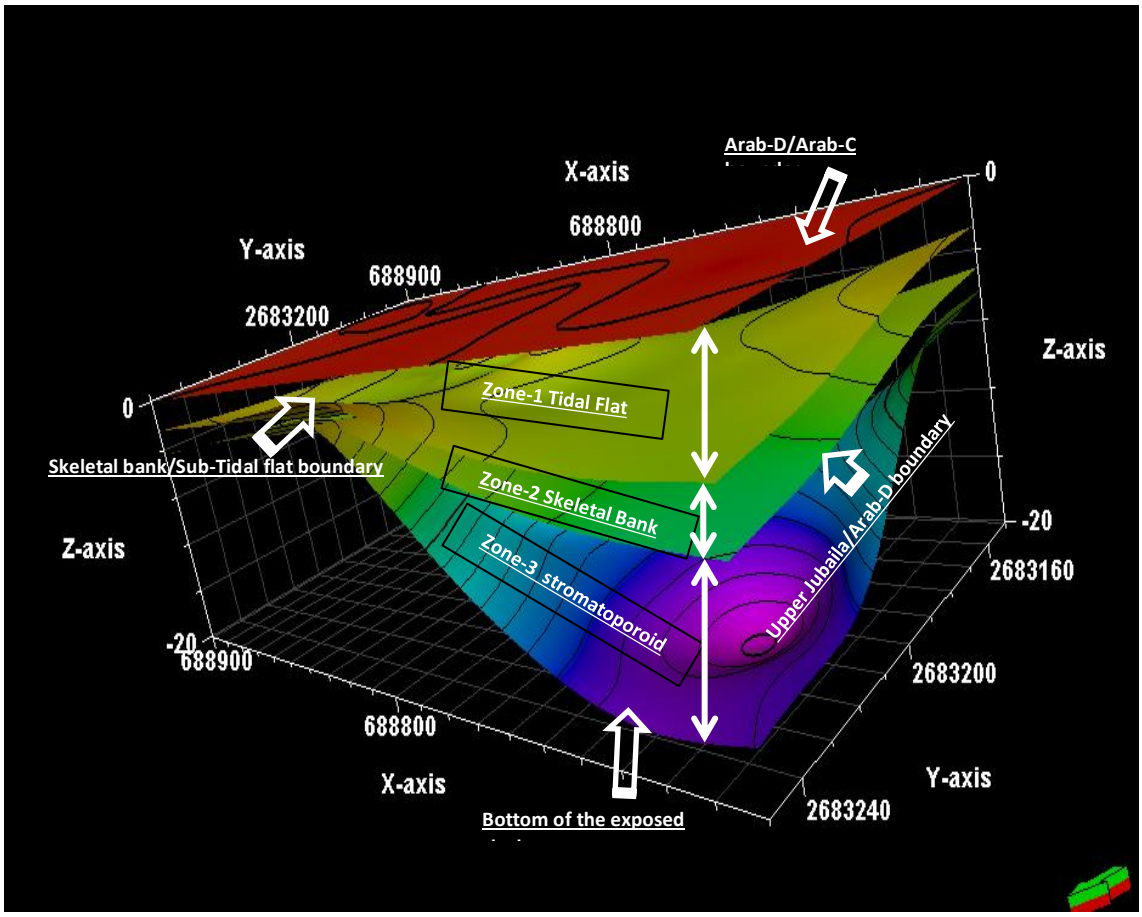

Figure 4-2: Four surfaces reconstructed from the correlated stratigraphic sections. These four surface define three zones, Zone-1 tidal flat, Zone-2 skeletal bank, and Zone-3 stromatoporoid.

Table 4-2: Distribution of cells in different zones in the three-dimensional grid with their corresponding stratigraphic interval in the outcrop.

Gridding System	Stratigraphic Zone	Thickness of zone (m)	Number of Layers	Number of Cells	Average cell thickness
3-D grid of the outcrop	Upper Jubaila and Arab-D	20	40	800000	0.45
Zone-1 grid	Tidal Flat	6.3	10	200000	0.6
Zone-2 grid	Skeletal Bank	2.5	10	200000	0.3
Zone-3 grid	Stromatoporoids	12.00	20	400000	0.6

Geological interpretation: This semivariogram represents lithofacies that has very good vertical and spatial continuity, and is interpreted to have been deposited on the upper slope of a ramp platform in a relatively deep marine setting that has little or no spatial heterogeneity. The different range values indicate geometric anisotropy.

4.5.2 Semivariogram for Stromatoporoid Packestones and Wackestones

Semivariogram shape: The semivariogram model for the stromatoporoid packstone only loosely fits the data in the vertical directions. Major and minor semivariograms show good structural shape. The nugget value is low, and the sill and range are nearly equal in all directions (Figure 4-4).

Geological interpretation: This lithofacies exists only above the dolomitic mudstone and wackestone in four repeated cycles in the lower part of the outcrop. Its presence depends on the allochthonous transportation of the stromatoporoid debris into the upper slope depositional environment, and therefore this facies has a amalgamated.

4.5.3 Semivariogram for Burrowed Fossiliferous Wackestones and Peloidal Fossiliferous Grainstones

Semivariogram Shape: This semivariogram model fairly fitting the data in both the major and minor directions and the vertical semivariogram has very short range structure. The nugget value is relatively low, and the sill and range are nearly equal in all directions (Figure 4-5).

Geological Interpretation: This lithofacies represents skeletal bank deposits that are characterized by nearly continuous layer but have limited vertical extention.

4.5.4 Semivariogram for Wavy Rippled Sandy Grainstones

Semivariogram Shape: This semivariogram model fits the data poorly in both the major and minor directions, and the vertical semivariogram has a very poor structure. The nugget value is very high, and the sill and range are random (Figure 4-6).

Geological Interpretation: There is no continuous layer of this present in the outcrop, and lithofacies geobodies are scattered and random. This lithofacies characterized by small scale channelized flow and that form isolated to small scale channels or amalgamated channels that make up a nearly continuous layer

4.5.5 Semivariogram for Laminated Mudstone

Semivariogram Shape: The semivariogram for the platy laminated mudstone has a good shape and a relatively high nugget value. The sill is nearly equal in all directions, but the range is higher in the major direction than in the minor direction (Figure 4-7).

Geological Interpretation: This lithofacies has very good vertical and spatial continuity, which is reflected in the shape of the semivariogram, and is cut by relatively small scale tidal channels of laminated sandy grainstone that produce internal variability that is expressed by the relatively high nugget values. The difference between the range values in the major and minor directions indicates geometric anisotropy, which suggests rapid lateral facies changes along the E-W dip direction of the carbonate platform.

4.5.6 Semivariogram for Breccia

Semivariogram Shape: The semivariogram of the breccia only loosely fits the data in both the major and minor directions, and the vertical semivariogram has very poor

structure. The nugget value is very high, and the sill and range are nearly equal in all directions (Figure 4-8).

Geological Interpretation: This lithofacies forms patchy layer with high internal variability that is expressed by the high nugget and poor structure fitting of the model. The different sill values in the major, minor, and vertical directions indicate random scatter of this lithofacies. These indicator semiveriograms were related to their distribution in the outcrop to reveal their geological controls (Figure 4-9).

4.6 The 3-D Lithofacies Model

The 3-D lithofacies model was generated using stochastic Sequential Indicator Simulation (SIS) approach. This facies model of the outcrop analog was generated by using 14 stratigraphic sections and semivariogram parameters. A total of 33 equally probable simulated realizations were generated. The average value of each lithofacies was calculated as the representative lithofacies percentage from the study area. Although the model has a layer cake pattern at lower resolutions, it has a higher degree of heterogeneity when viewed at a higher resolution (Figure 4-10). The thicknesses of the layers in this model are very small when compared with the model of the subsurface reservoir. Most of the actual reservoir facies were, however, represented in the outcrop model. The layers representing the upper Jubiala Formation in the model pinch out laterally to the north due to topographical highs and lows. The unit begins with the dolomitic mudstone and wackestone and ends with the last appearance of stromatoporoid packstone. This stratigraphic unit might be equivalent to subsurface reservoir units 2B and 3A (Meyer et al., 1996).

The Upper Jubaila Member represents the coarsest section in the model and composes about 48 % of the total facies and 30 % of the reservoir. The lithofacies layers in the Arab-D member are continuous over the study area and include some tidal channel bodies within the muddier units of the lagoon deposit. The majority of this part of the Arab-D Member represents 52 % of the total facies and 15 % of the reservoir lithofacies (Figure 4-11).

4.7 Validation of the 3-D Facies Model

Since the 3-D facies model is based on scattered 14 stratigraphic sections, the model should be validated to test its applicability to simulate real geology of the study area. This section focuses on the validation of the 3-D facies model by comparing to the outcrop present day topography and stratigraphic observations. The large scale features in the outcrop were visually examined to test satisfaction matching with the 3-D facies model. During this step, it was found that the distribution of the four HFSs in the Upper Jubaila Member closely resembles their outcrop distribution and the 5 HFSs in the Arab-D Member are fairly represented by the model. Despite the fact that the Arab-D Member is more heterogonous than the Upper Jubaila Member, the constructed 3-D facies model adequately reproduce their facies distribution nearly as in the outcrop (Figure 4-12). An ideal way to check the accuracy of the model can be achieved by direct comparison of outcrop high resolution pictures with the model. This could be accomplished by comparing small scale features such as small scale tidal channels in the upper section of the outcrop (Arab-D Member) with the model (Figure 4-13). The result show acceptable distribution of these geo-bodies in the model in similar pattern with the outcrop.

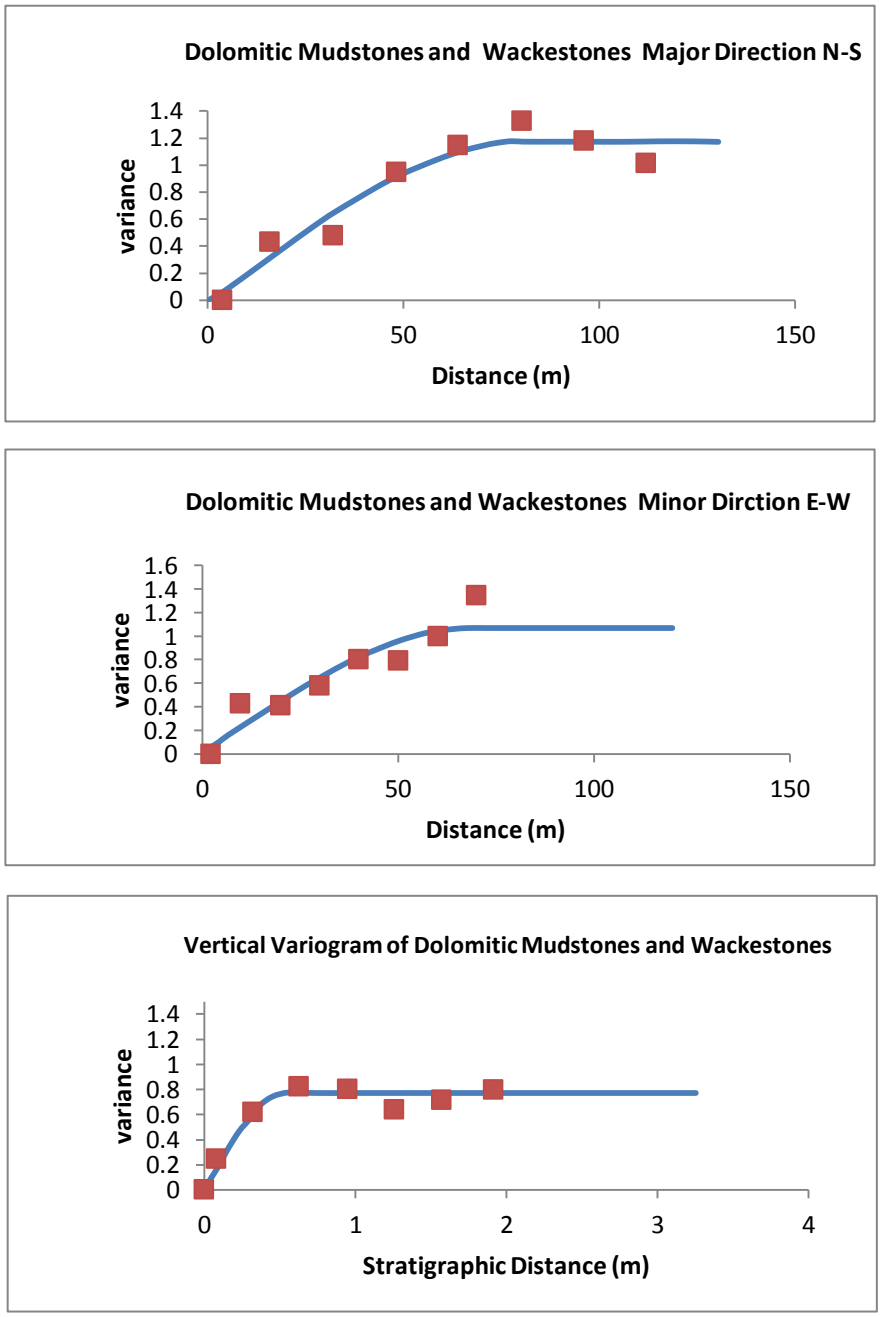

Figure 4-3: Semiverigram for dolomitic mudstones and wackestones.

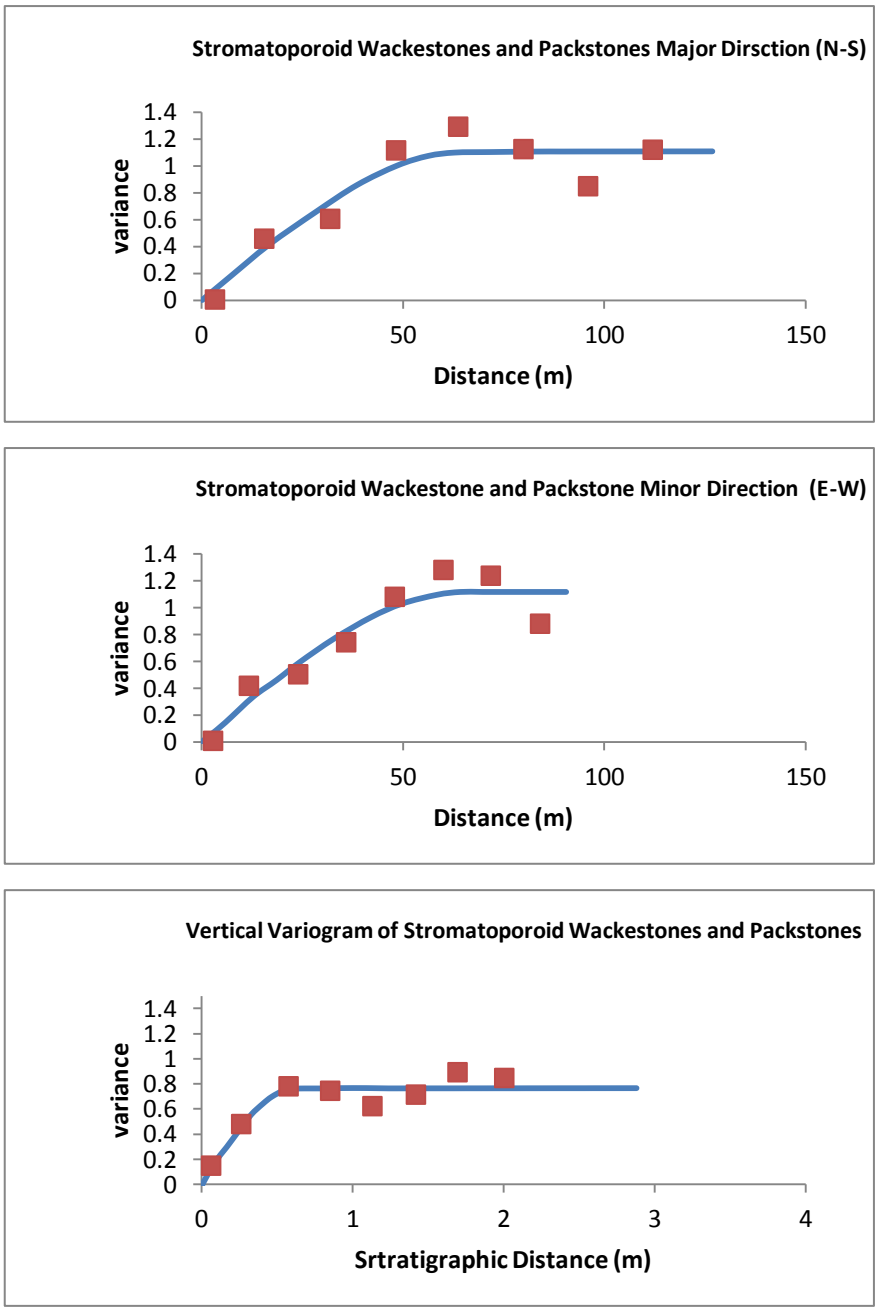

Figure 4-4: Semiverigram for stromatoporoid wackestones and packstones.

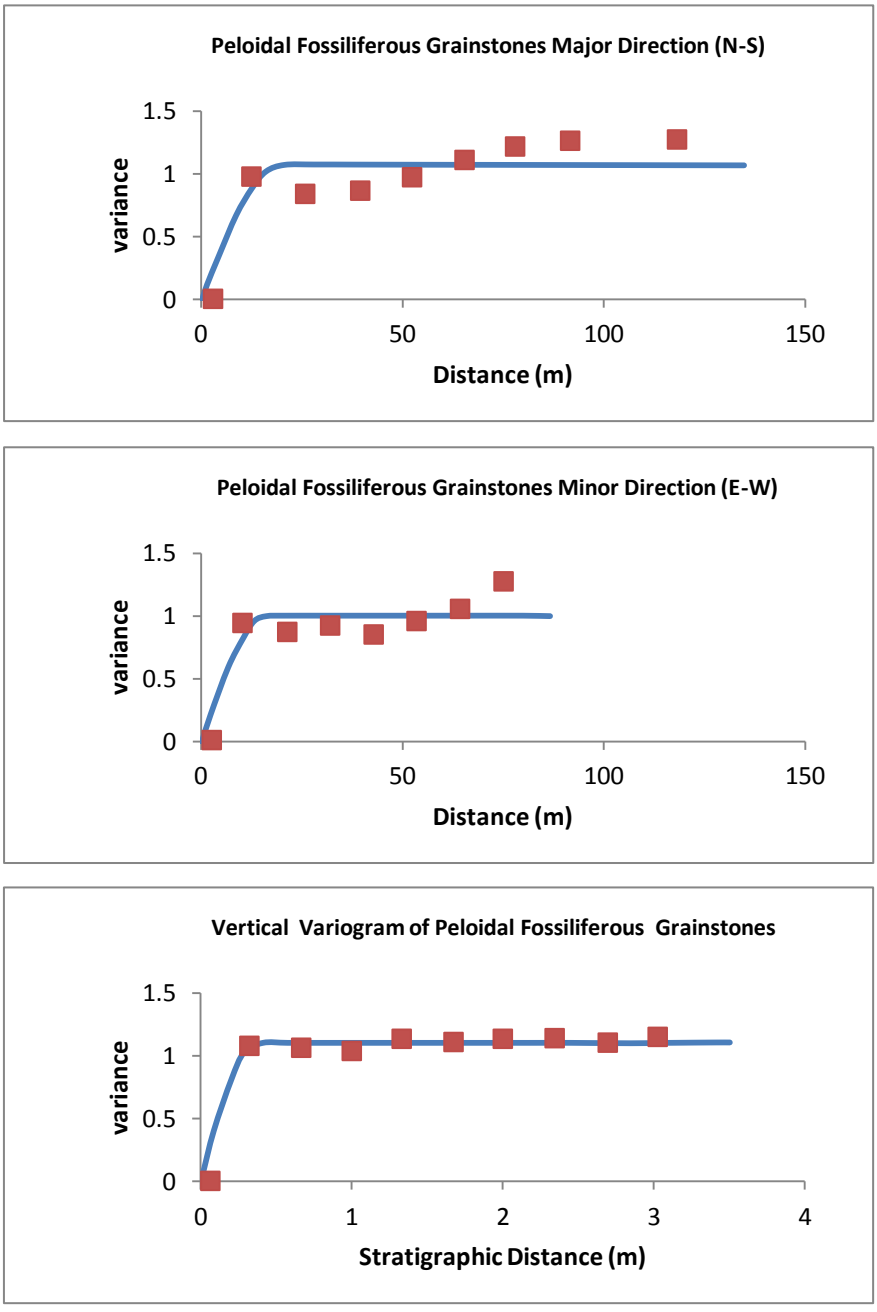

Figure 4-5: Semiverigram for burrowed fossiliferous wackestones and peloidal fossiliferous grainstones. Note that these two lithofacies has the same seiveriogram shape because they are genetically related.

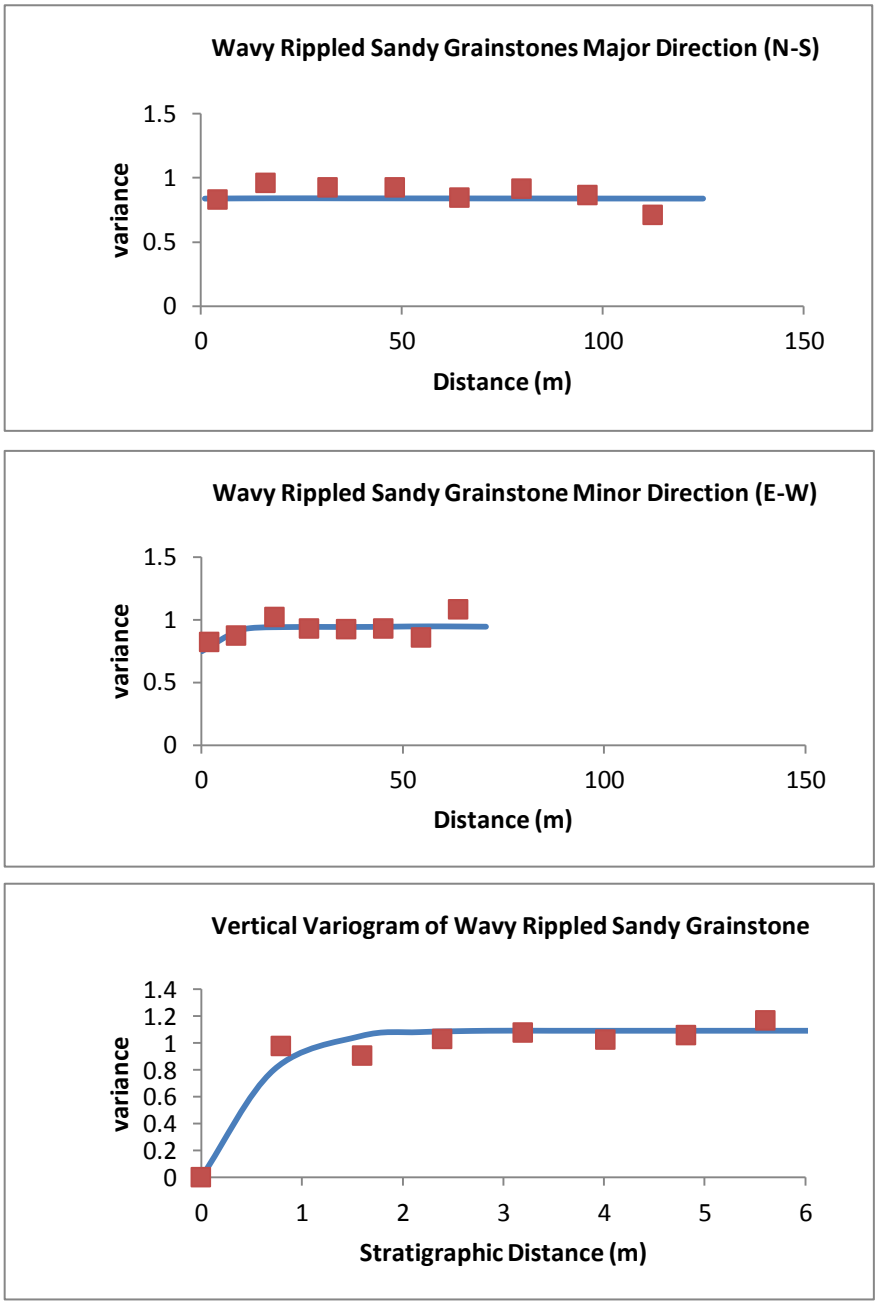

Figure 4-6: Semiverigram for wavy rippled sandy grainstones.

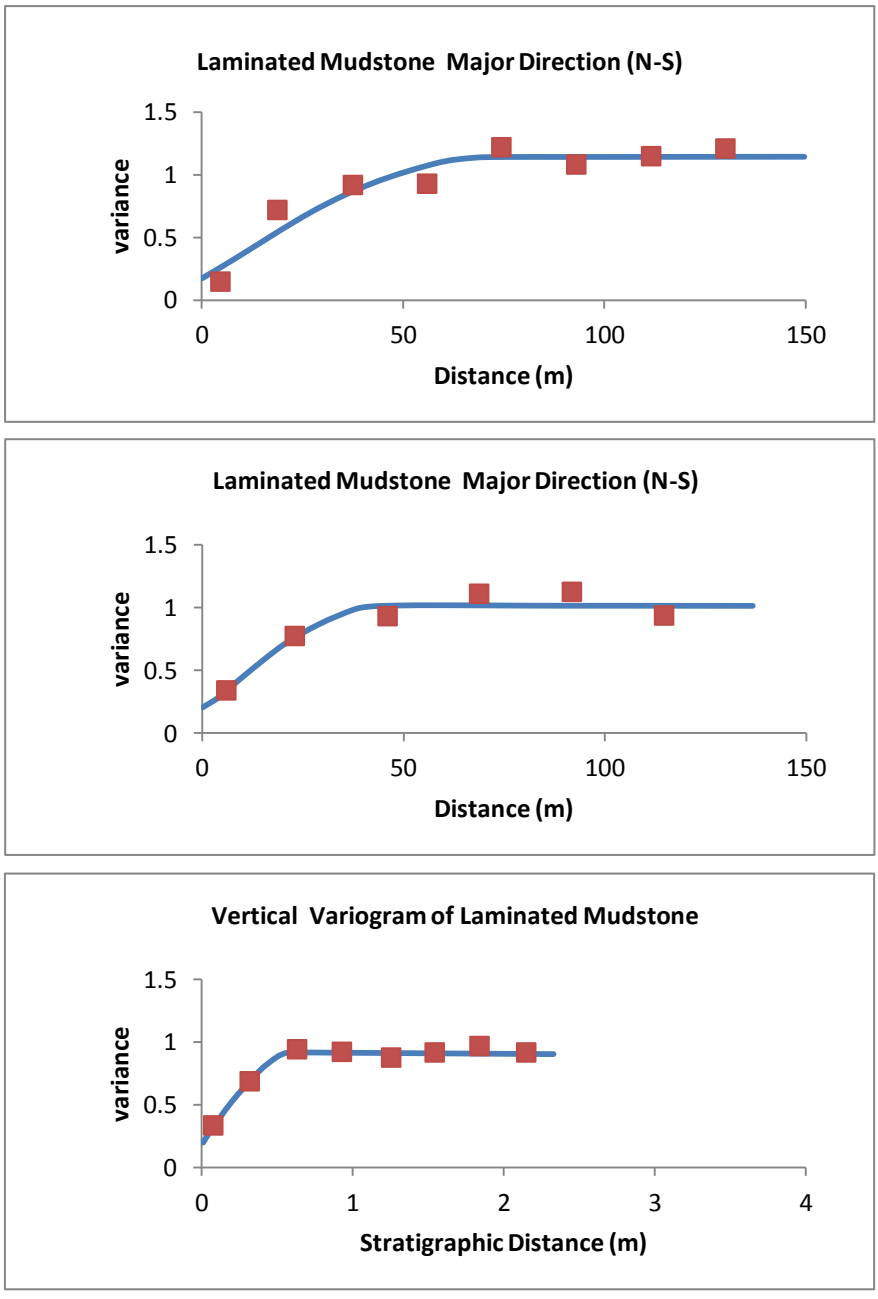

Figure 4-7: Semiverigram for laminated mudstones.

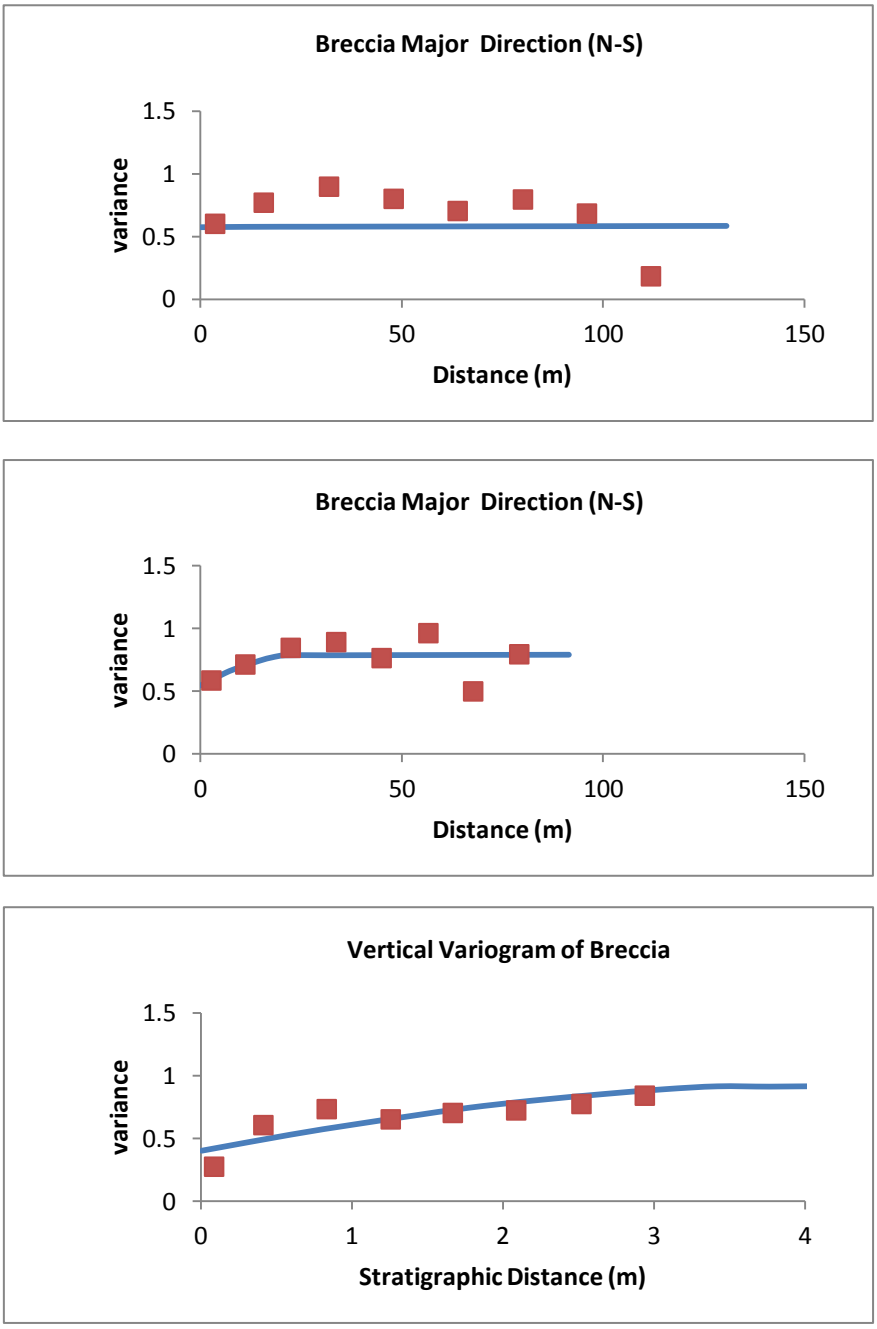

Figure 4-8: Semiverigram for breccia.

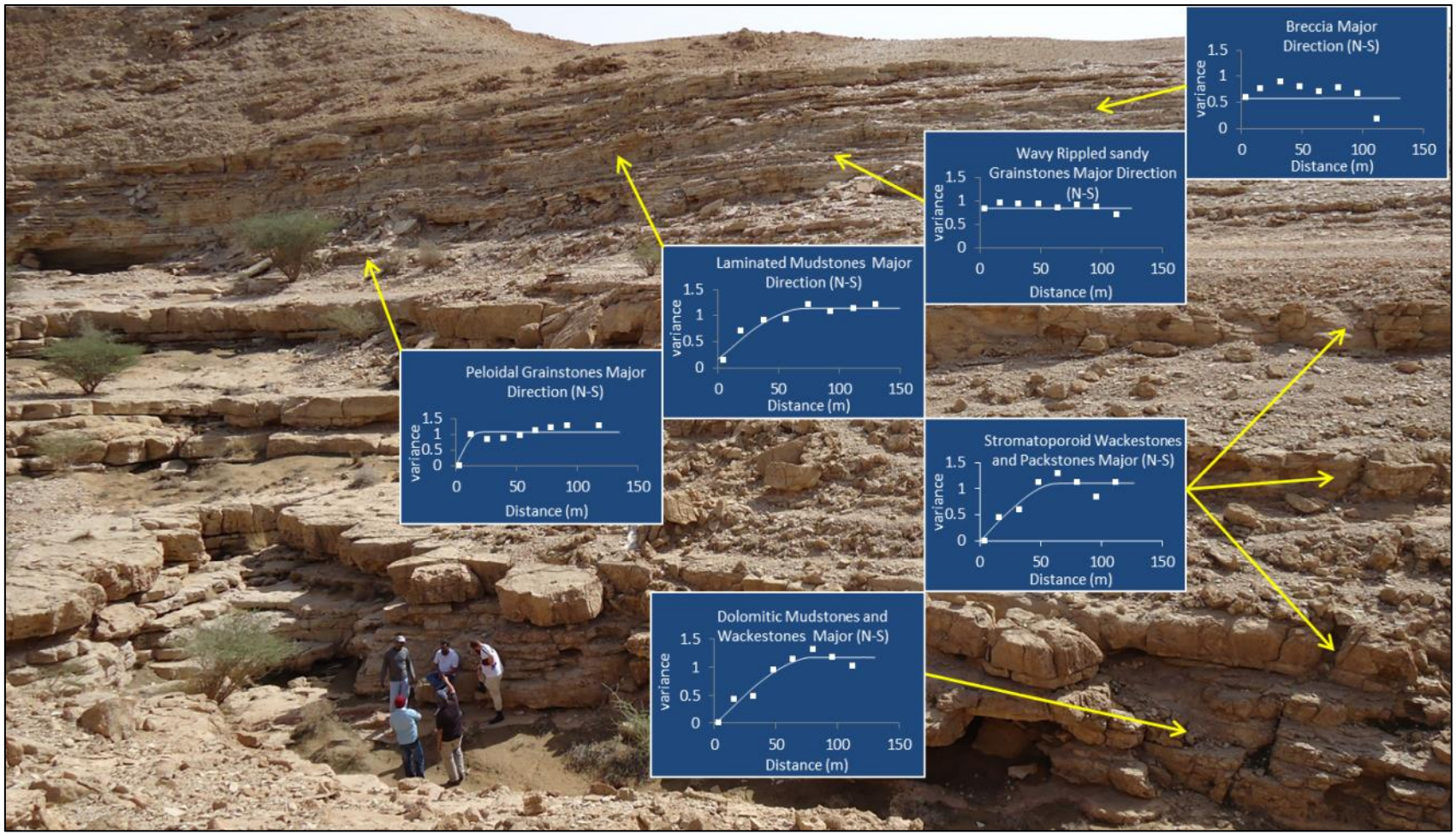

Figure 4-9: Indicator semivariograms for major (N-S) direction of lithofacies matched with their stratigraphic units.

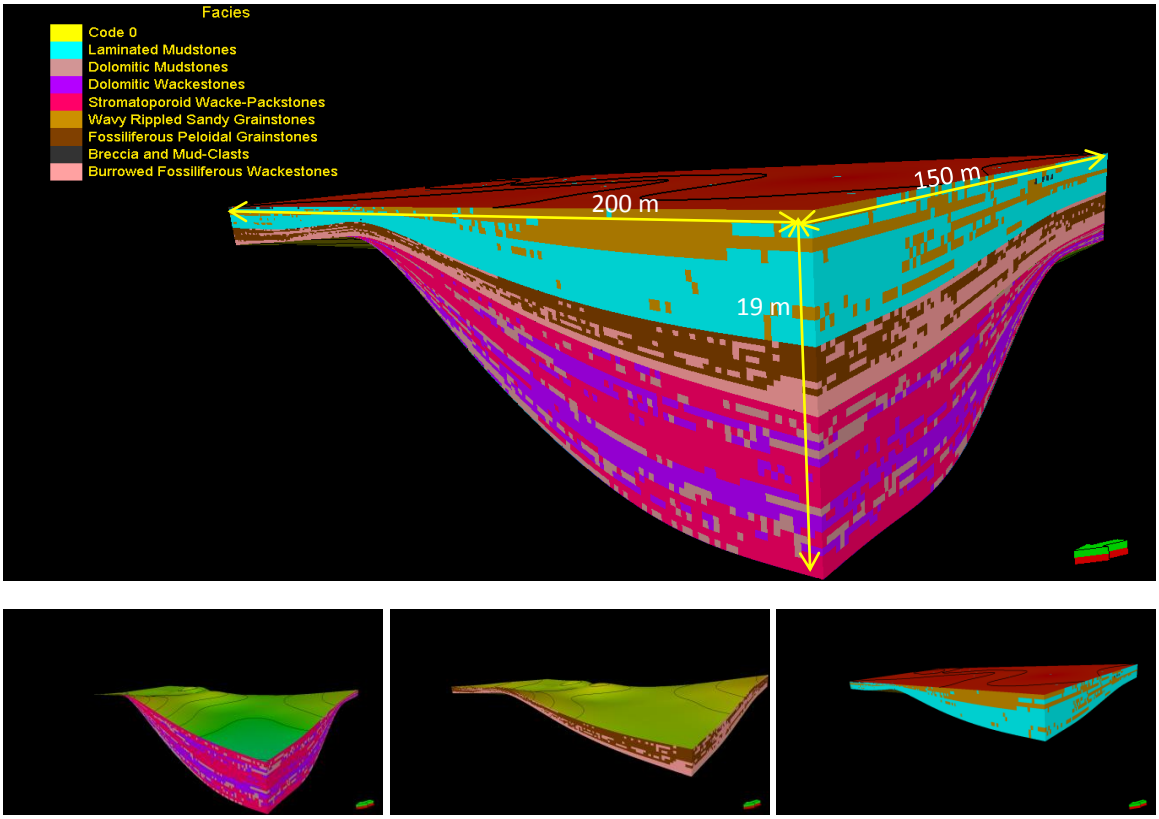

Figure 4-10: 3-D facies model consists of stratigraphic framework through the studied outcrop. Part of this model is truncated laterally due to topographical change at the outcrop site.

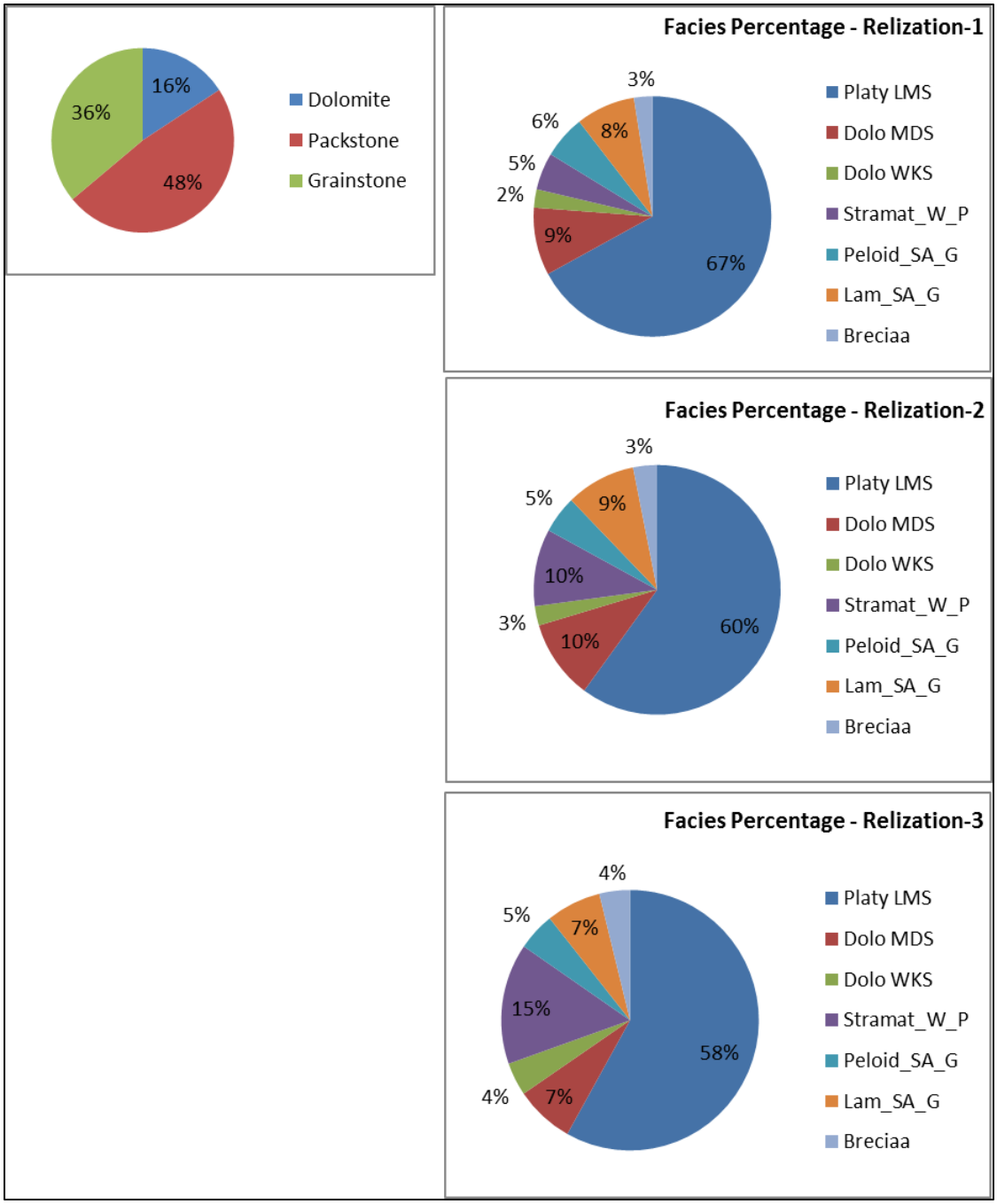

Figure 4-11: Pie diagrams showing lithofacies percentage in the 3-D model for three realizations that run stochastically. The left diagram shows the subsurface lithofacies characterized only by three lithofacies from Douglas, (1996).

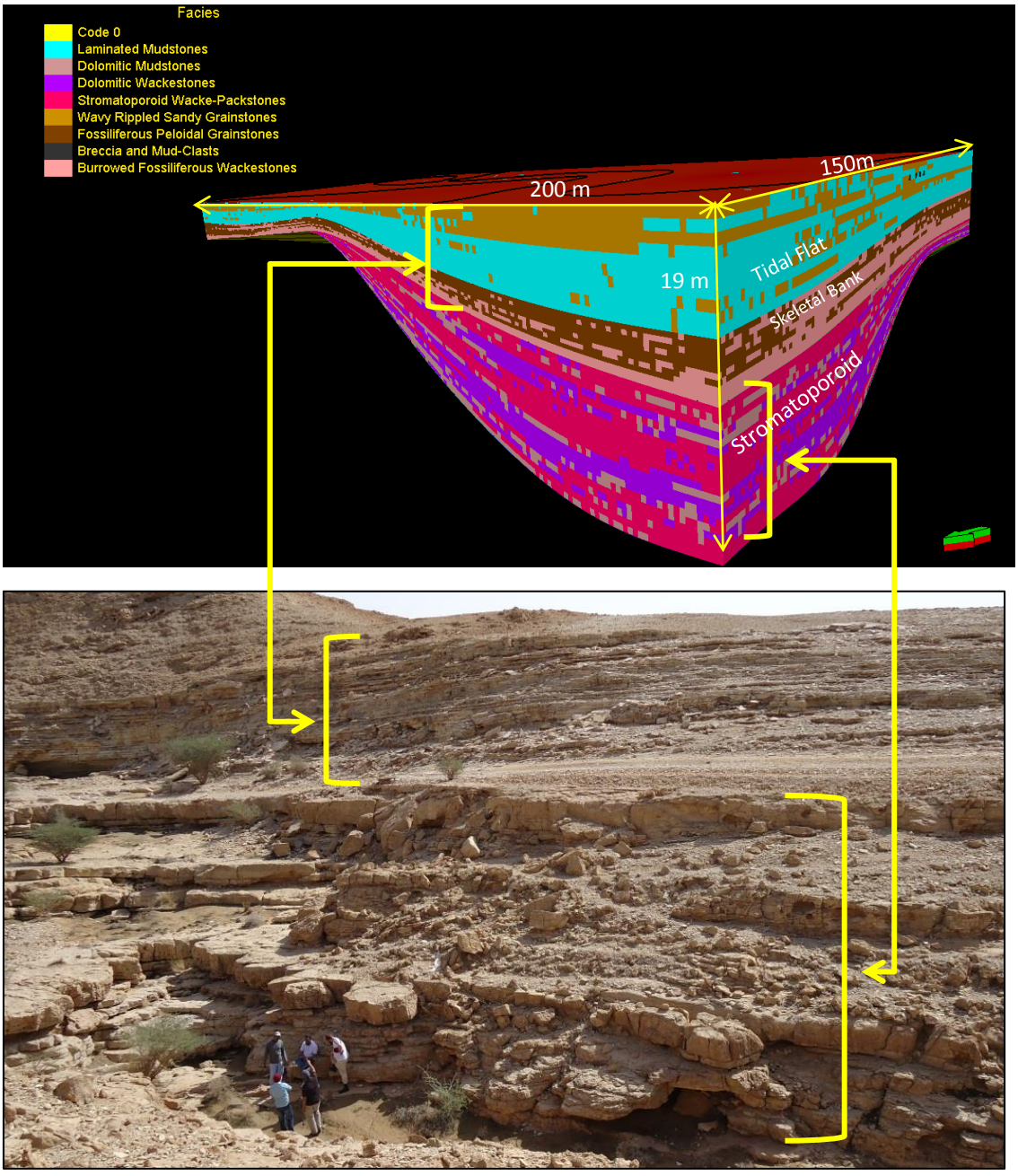

Figure 4-12: 3-D facies model with outcrop stratigraphy. Outcrop picture of Wadi Nisah is compared with the large scale features of the outcrop to the 3-D facies model (the Arrow point to the north).

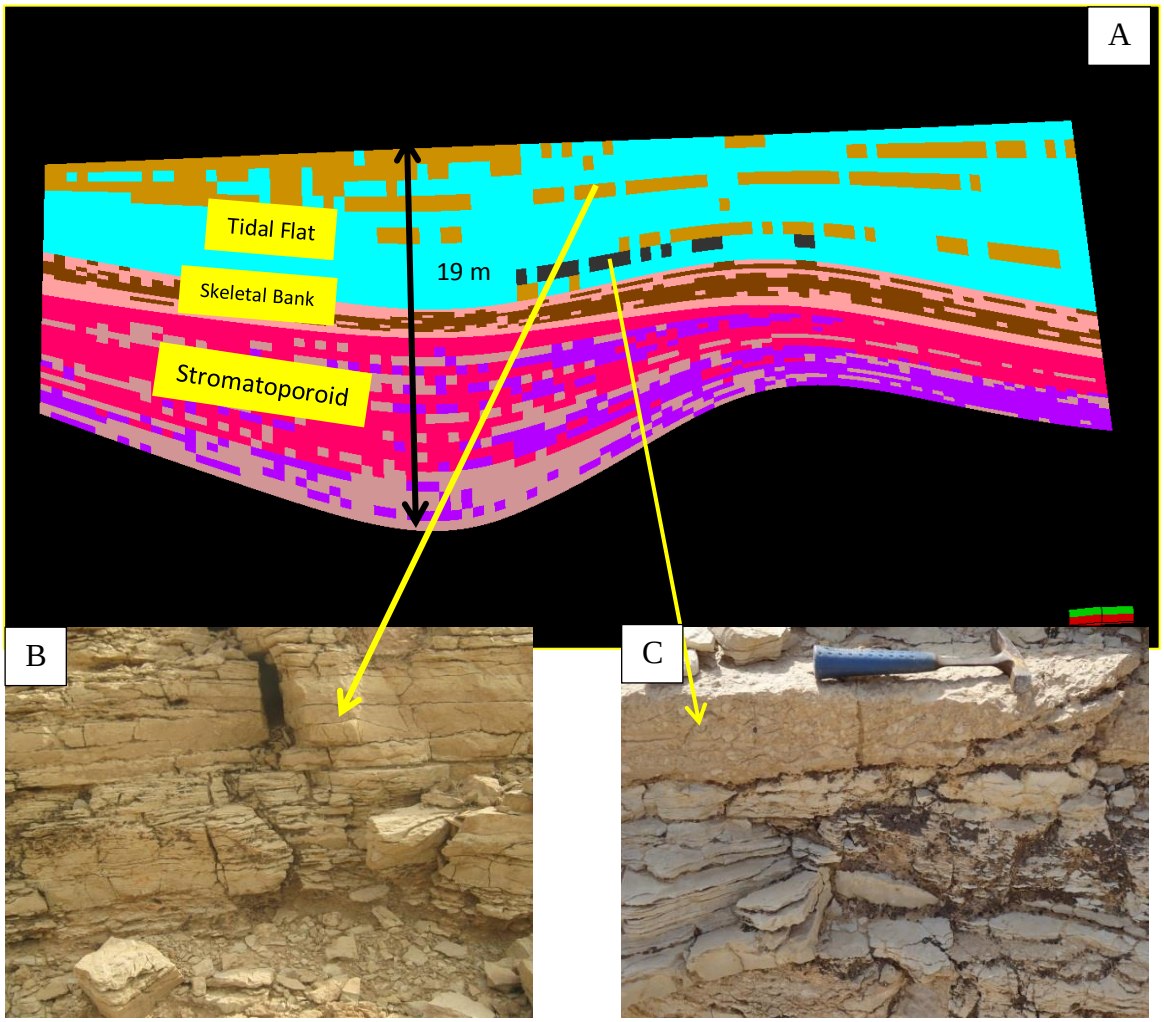

Figure 4-13: A) 3-D facies model with outcrop stratigraphy. Outcrop picture of Wadi Nisah was used to compare the small scale features of the outcrop to the 3-D facies model in this case B) is tidal channel sandy laminated grainstone and C) breccia and mud-clasts. Lithofacies legends are same as in Figure 4-12.

4.8 Petrophysical Model

Because of the effects of meteoric diagenesis and the long surface exposure of the studied outcrop, the petrophysical data of the outcrop samples do not reflect the conditions of the subsurface Arab-D reservoir. The porosity and permeability measurements of the samples collected from the outcrop have very limited ranges. These petrophysical data are not inadequate to simulate the subsurface petrophysical model. Therefore, data from equivalent facies from the subsurface Arab-D reservoir with the same facies component, stratigraphic architecture, and stacking pattern were superimposed on the high-resolution 3-D facies model. Two methods were used to populate subsurface data into the 3-D high resolution facies model and discussed in the following sections.

4.8.1 3-D Petrophysical Model by Assigning Subsurface Values

Petrophysical data from Meyer et al. (2000) were extracted after the subsurface and outcrop facies were correlated. Average porosity and permeability measured from core plugs were extracted for each outcrop lithofacies (Table 4-3). Porosity and permeability 3-D models were generated by assigning the extracted average porosity and permeability values from the lithofacies. The small-scale heterogeneity of the lithofacies created in the lithofacies model was represented by small scale porosity and permeability variability, which could represent high porosity zones or permeability barriers (Figure and 14-4 Figure4-15). The reservoir lithofacies (stromatoporoid rudstone and floatstone, fossiliferous sandy peloidal grainstone and rudstone, and laminated fossiliferous sandy grainstone) have higher porosity and permeability values than the surrounding lithofacies

Table 4-3: Petrophysical data from Meyer et al. (2000) extracted after subsurface and outcrop facies were correlated. For each outcrop lithofacies, averages of horizontal and vertical porosity and permeability were extracted.

Lithofacies from Outcrop analog of Arab-D Reservoir	Lithofacies from Actual Arab-D Reservoir	Average Porosity	Average Permeability
Laminated Mudstone	Micritic	13.4	0.9
Burrowed Dolomitic Mudstone	Dolomitic Mudstone	10.2	0.2
Burrowed Dolomitic Wackestone	Dolomitic-Wackestone	16.9	692.8
Stromatoporoid Wackestone and Packstone	Stromatoporoid Packstone	12.4667	4.2
Wavy Laminated Fossiliferous Sandy Grainstone	Mix skeletal Grainstone	25.95	527.25
Fossiliferous Sandy Peloidal Grainstone and Rudstone	Mix skeletal Grainstone	26	574
Breccia	Micritic	13.4	0.9

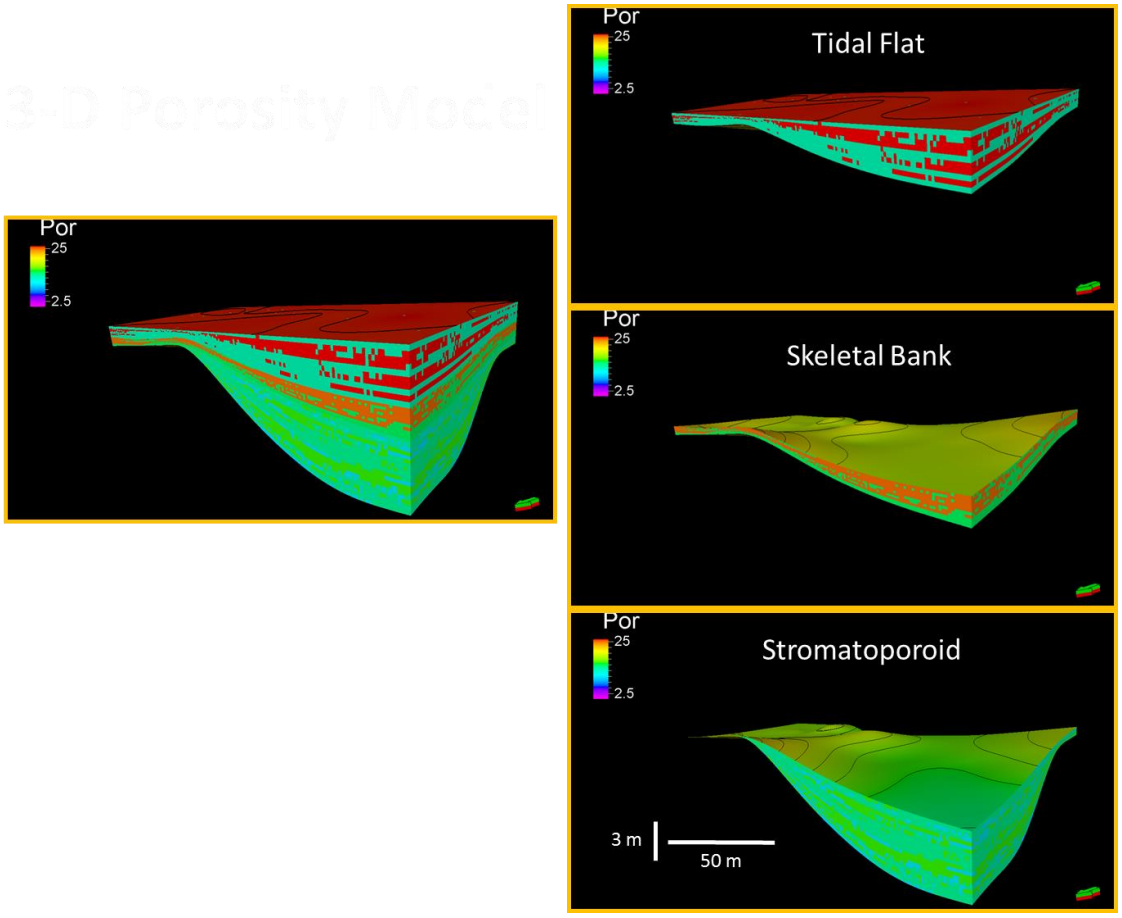

Figure 4-14: 3-D porosity model generated by assigning the extracted average porosity values from Meyer et al. (2000). The small-scale lithofacies heterogeneity created in the lithofacies model was represented by small scale porosity variability.

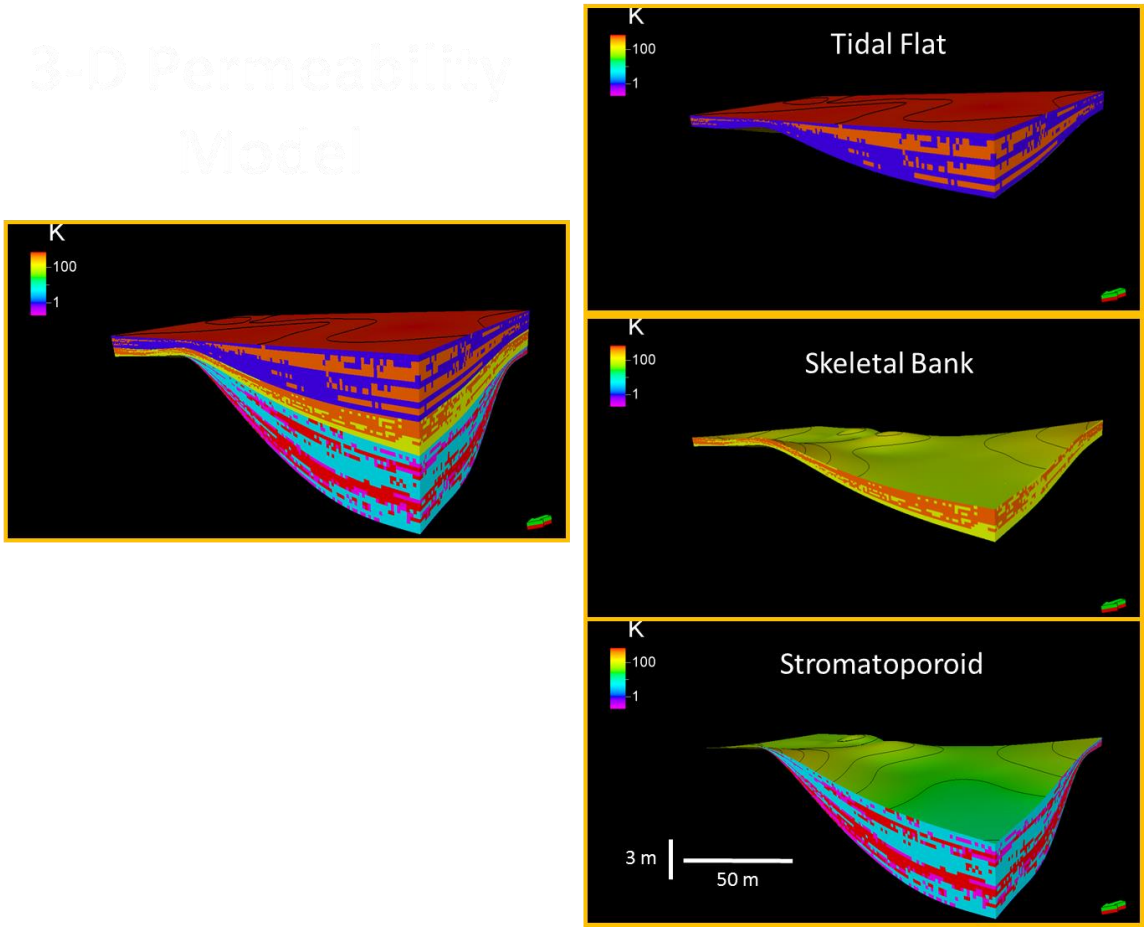

Figure 4-15: 3-D permeability model generated by assigning the extracted average permeability values from Meyer et al. (2000). The small-scale lithofacies heterogeneity created in the lithofacies model was represented by small scale permeability variability.

4.8.2 3-D Petrophysical Model by Generating Logs

The data used to generate the petrophysical model presented in Table 4-1,were extracted from published papers about the Arab-D reservoir (Douglas 1996; Meyer et al. 1996; Sahin et al. 1998 Cantrell and Hagerty 1999; Cantrell et al. 2004a). The porosity data were classified by field location for average porosity, and the subsurface porosities were integrated with those from the equivalent outcrop facies. Porosity logs were generated accordingly and distributed by Sequential Gaussian Simulation (SGS). The main control for SGS are semivariograms generated from stratigraphic sections. Three semivariograms (N-S, E-W, and vertical) were generated for each field data set (Figure 4-16).

Figure 4-17 shows 3-D porosity models of the outcrop that was generated by applying data from the subsurface facies to the outcrop facies. This high resolution model captures fine details such as low porosity values that may represent permeability barriers. The porosity model was compared to the facies model. The facies model shows a high degree of facies continuity, but low porosity patches were also captured in the model, and may represent a potential permeability barriers. Figure 4-18 shows the result of averaging 3-D porosity models of 30 realizations for each field data set.

4.9 Discussion

One of the main goals of this study is to highlight the importance of examining Arab-D reservoir at the inter-well scale. In this regard, the constructed lithofacies model of the study area was intended to be equivalent to one cell of the subsurface reservoir models, assuming that one cell of the reservoir model covers an area nearly represent only one cell of subsurface models (Douglas, 1996; Al-Khalifah and Makkawi, 2002). Studying

outcrops equivalent to the Arab-D reservoir at this higher resolution helps to better understand the reservoir heterogeneity reservoir stacking patterns, the sequence hierarchy, and their lateral correlations. Although the 3-D facies model has a layer cake pattern at a low resolution, it exhibits a higher degree of heterogeneity when examined at a higher resolution. For example, the tidal channel facies that were identified in the upper section of the outcrop are very thin bodies of laminated sandy fossiliferous grainstone that are approximately 1 m wide and a few centimeters thick. These tidal channel bodies are rarely identified in the subsurface model or at the outcrop scale. When petrophysical data of the actual reservoir is superimposed on the high resolution 3-D facies model, the resulting petrophysical model introduces small-scale heterogeneity into the lithofacies model. This small-scale variability can represent features such as zones of high porosity or permeability barriers. Therefore, understanding such small-scale heterogeneity in the outcrop may provide a better understanding of the subsurface reservoir.

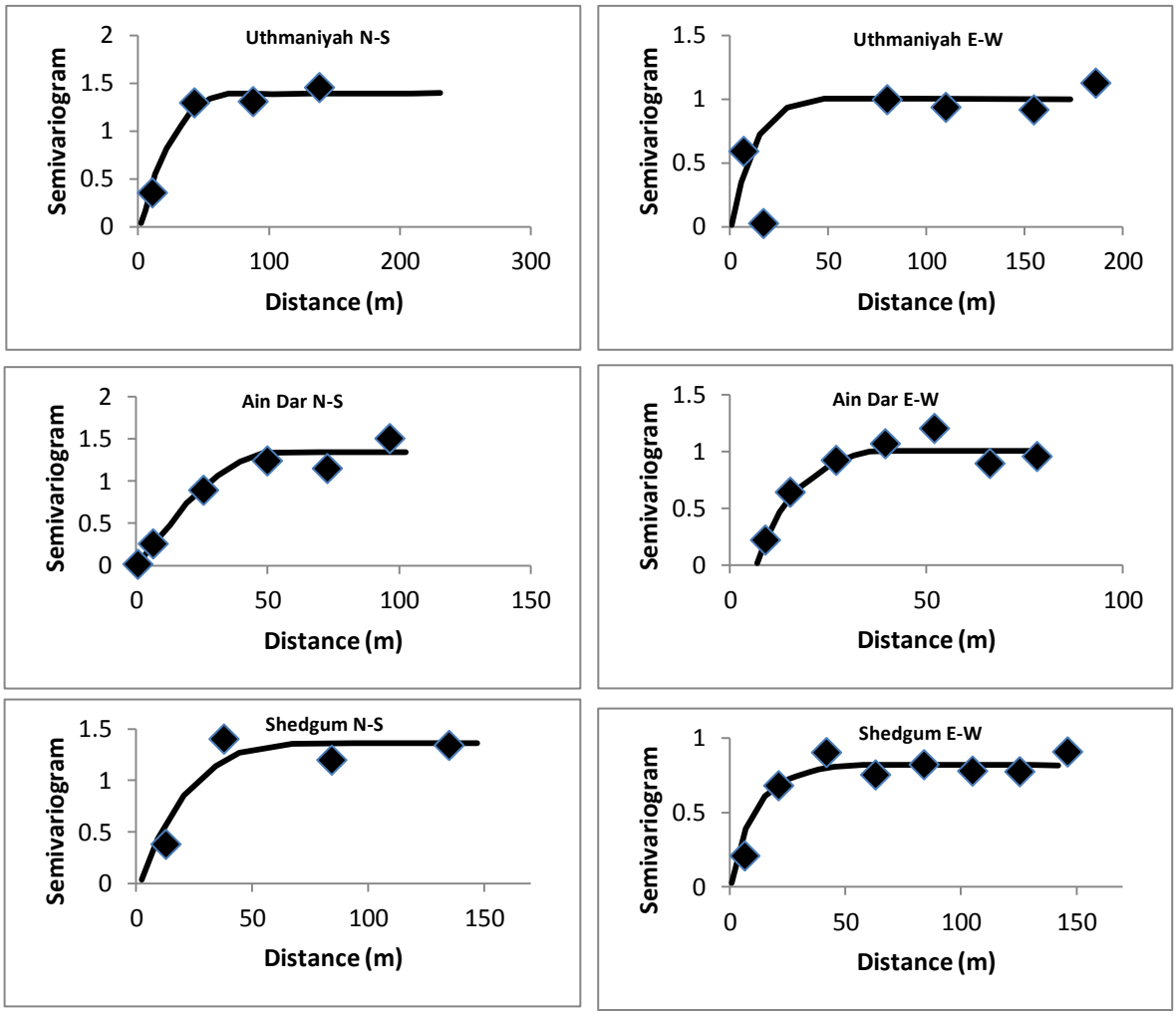

Figure 4-16: Experimental (squares) and modeled (solid lines) semivariograms for outcrop after assigning for each facies in stratigraphic sections porosity data from Ain Dar, Shedgum, and Uthmaniyah areas.

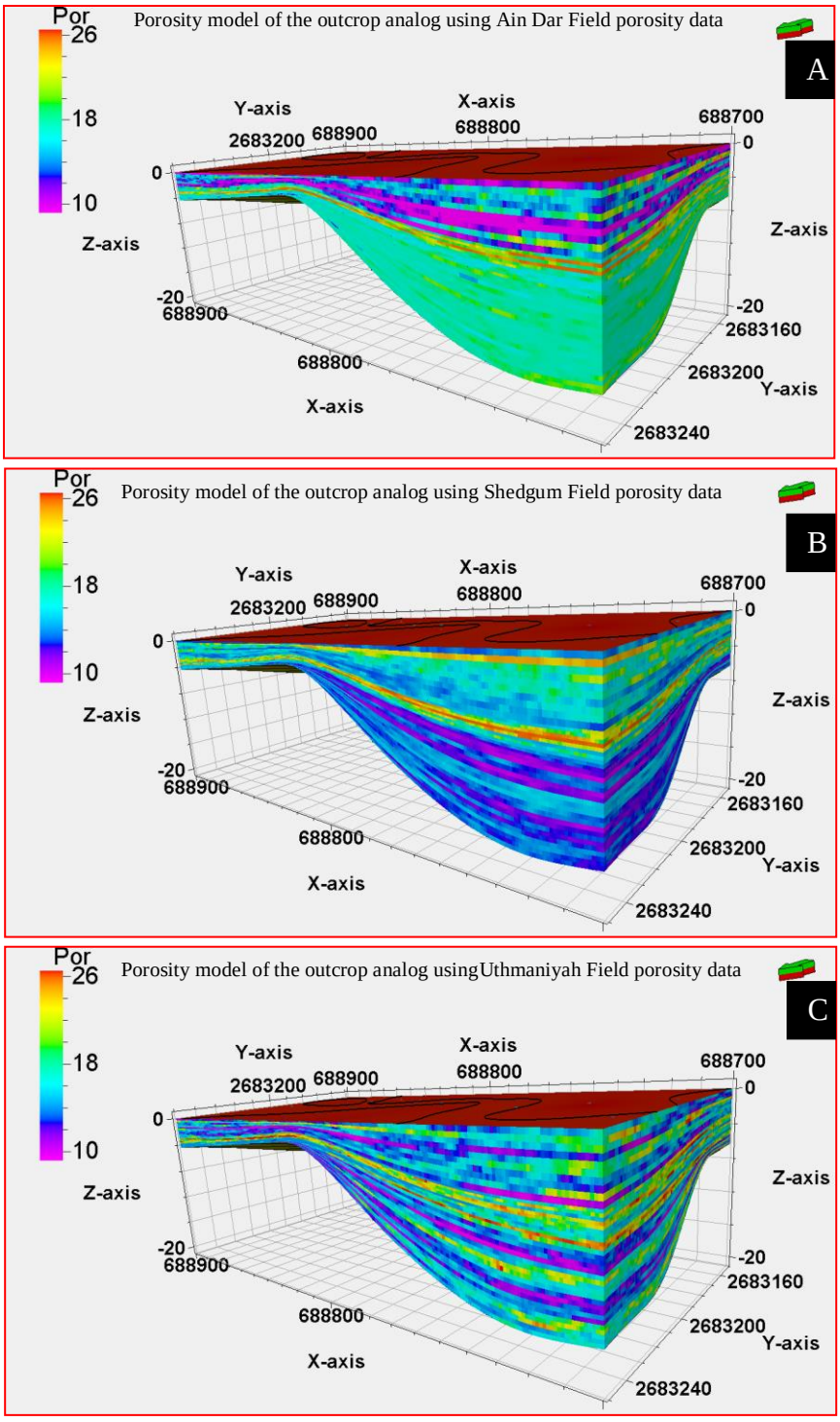

Figure 4-17: 3-D porosity models for the outcrop using subsurface data (realization-1) (A) Ain Dar, (B) Shedgum, and (C) Uthmaniyah areas.

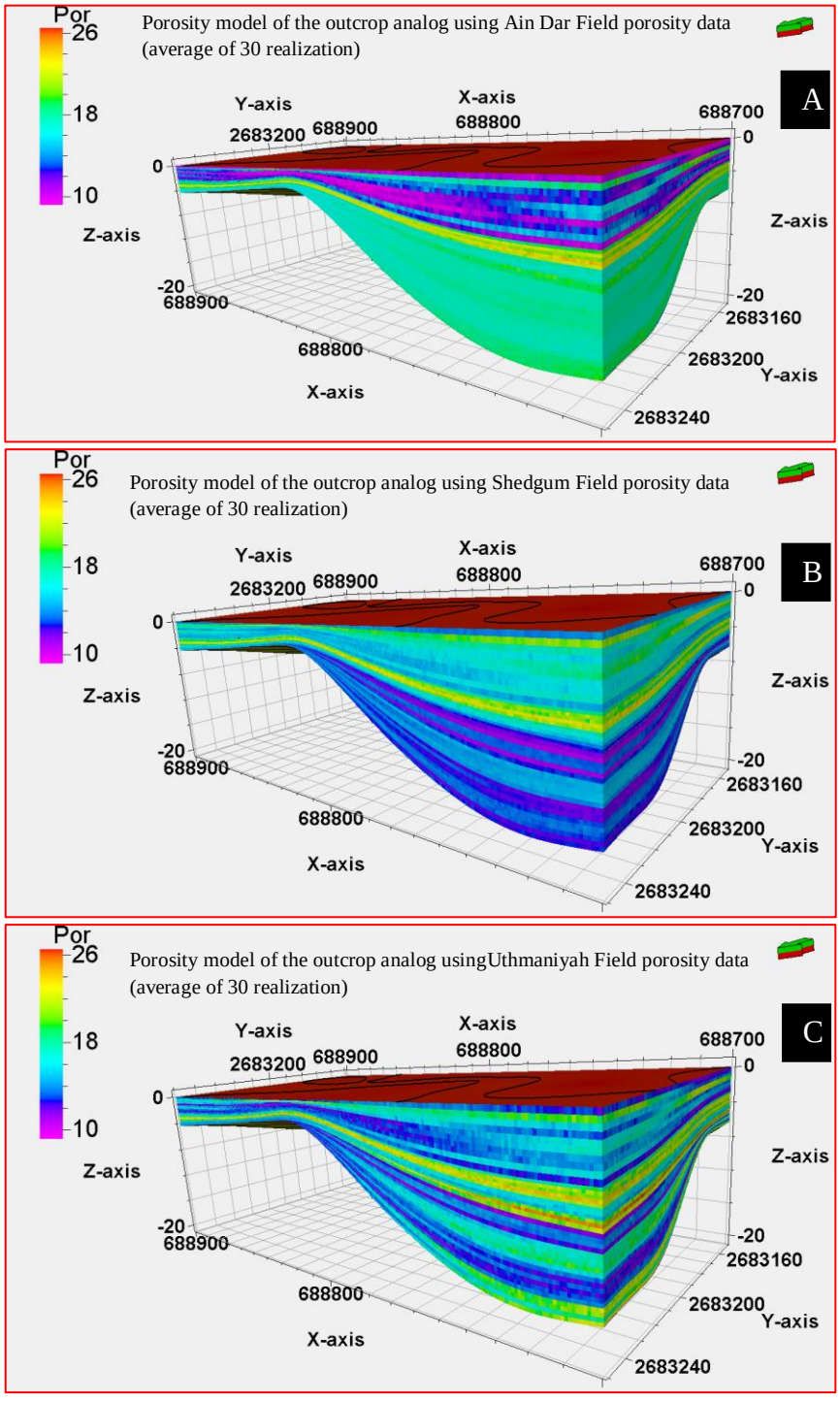

Figure 4-18: 3-D porosity models for the outcrop using subsurface data. Average value for 30 realizations of (A) Ain Dar, (B) Shedgum, and (C) Uthmaniyah areas.

CHAPTER 5

MICROPOROSITY

5.1 Introduction

Understanding the distribution, origin, and morphology of microporosity is crucial for reservoir characterization and performance (Budd, 1989; Moshier, 1989; Dravis, 1989; Maliva et al., 2009a). Microporosity affects well log responses, fluid flow properties, capillary forces, and irreducible water saturations and therefore formation evaluation procedures (Ahr, 1989). Microporosity may reach high proportions when calculated as a percentage of total porosity (Dewever et al., 2007), but it is difficult to predict because it is controlled principally by the characteristics of the reservoir rock (Smith et al., 2003; Lambert et al., 2006; Maliva et al., 2009b; Volery et al., 2009). Some studies have attributed the presence of microporosity to facies and texture, while others (e.g., Deville de Periere et al., 2011) have attributed its occurrence to cementation and micritization.

This chapter focuses on statistical and morphological descriptions of microporosity from an outcrop analog of the Arab-D reservoir rock. It investigates a possible link between microporosity distribution and diagenetic controls (mainly cementation and micritization), and attempts to characterize the permeability associated with the microporosity. Petrographical study of the macroporosity present by visual inspection

showed zero porosity values for all studied outcrop samples, although core plugs of these same samples indicated that significant amounts of porosity are present. This indicates the presence of significant microporosity, calculated as the difference between porosity from core plug measurement and point count porosity from thin sections.

5.2 Microporosity Analysis

Choquette and Pray (1970) defined microporosity as porosity with dimensions less than 62.5 micron, but other definitions were given by Pittman (1971); Anselmetti et al. (1998); and Weger et al. (2009). This study uses the definition of Cantrell and Hagerty (1999), who defined microporosity as the difference between core-plug porosity and point-count porosity from thin sections of the same sample. Visual analyses of thin sections of each lithofacies from the studied outcrop indicated that all samples had zero porosity, and that pore spaces were completely filled by diagenetic cements. There were no differences due to facies variations. However, when the same, however, samples were measured by water saturation methods, certain amounts porosity and permeability were found to be present and were interpreted to be microporosity (Table 5-1). Scanning Electron Microscope (SEM) analysis of the same samples also showed the presence of significant amounts of microporosity. This microporosity are of three types and found:

1) Between macro and micro sparry calcite grains;
2) Between micritic grains, which were of five morphology types (rounded, sub-rounded, scaleno-rhombohedral, anhedral compact and fused); and
3) Within macro dolomite crystals. The three types of microporosity are discussed in the following section.

Table 5-1: Selected microporosity values calculated using water saturation method. The values represent core plugs from collected samples of Arab-D reservoir analog outcrop.

AVERAGE LENGTH	CROSS-SEC. AREA	BULK VOLUME	DRY WEIGHT	SATURATED WEIGHT	BRINE DENSITY	PORE VOLUME	POROSITY Ø	GRAIN VOLUME	GRAIN DENSITY
cm	A (sq.cm)	Vb (cc)	Wd (g)	Ws (g)	ρb (g/cc)	Vp (cc)	%	Vg (cc)	ρg (g/cc)
3.27	4.9323	16.1287	42.28	42.667	1.0042	0.3854	2.389	15.7433	2.686
3.293	4.9678	16.359	43.124	43.525	1.0042	0.3993	2.441	15.9597	2.702
3.335	4.8735	16.253	43.56	43.836	1.0042	0.2748	1.691	15.9781	2.726
3.362	4.8813	16.4109	41.063	42.235	1.0042	1.1671	7.112	15.2438	2.694
3.201	4.9363	15.801	41.961	42.173	1.0042	0.2111	1.336	15.5899	2.692
3.149	4.9678	15.6437	41.011	41.117	1.0042	0.1056	0.675	15.5381	2.639
3.01	4.9481	14.8937	39.594	39.639	1.0042	0.0448	0.301	14.8489	2.666
2.995	4.9363	14.7841	39.45	39.553	1.0042	0.1026	0.694	14.6815	2.687
2.839	4.9441	14.0364	36.951	37.181	1.0042	0.229	1.632	13.8074	2.676
2.625	4.9402	12.968	34.488	34.686	1.0042	0.1972	1.52	12.7709	2.701
2.618	5.2036	13.6231	33.928	34.188	1.0042	0.2589	1.901	13.3642	2.539
3.006	4.9323	14.8266	37.845	38.429	1.0042	0.5816	3.922	14.245	2.657
2.609	4.956	12.9301	33.408	33.758	1.0042	0.3485	2.696	12.5816	2.655
2.589	4.9245	12.7494	34.231	34.378	1.0042	0.1464	1.148	12.603	2.716
2.645	4.9127	12.994	34.312	34.646	1.0042	0.3326	2.56	12.6614	2.71
2.692	4.9323	13.2778	34.773	34.975	1.0042	0.2012	1.515	13.0767	2.659
2.499	4.9127	12.2768	32.048	32.494	1.0042	0.4441	3.618	11.8326	2.708
2.364	4.9402	11.6786	30.321	30.656	1.0042	0.3336	2.856	11.345	2.673
2.289	4.956	11.3442	29.812	30.012	1.0042	0.1992	1.756	11.1451	2.675
2.305	4.9678	11.4508	30.164	30.273	1.0042	0.1085	0.948	11.3423	2.659
2.262	4.9599	11.2193	29.219	29.499	1.0042	0.2788	2.485	10.9405	2.671
2.26	4.9678	11.2273	29.407	29.671	1.0042	0.2629	2.342	10.9644	2.682
2.034	4.9245	10.0163	26.05	26.419	1.0042	0.3675	3.669	9.6489	2.7
1.899	4.9323	9.3665	24.398	24.764	1.0042	0.3645	3.891	9.002	2.71
1.825	4.9402	9.0159	23.792	23.827	1.0042	0.0349	0.387	8.981	2.649
1.809	4.9441	8.944	23.561	23.626	1.0042	0.0647	0.724	8.8792	2.653
1.54	4.9323	7.5958	20.158	20.212	1.0042	0.0538	0.708	7.542	2.673
1.237	4.9323	6.1013	15.701	15.788	1.0042	0.0866	1.42	6.0147	2.61

5.3 Morphological Characteristics of Microporosity

5.3.1 Microporosity in sparry calcite cement

Sparry calcite was defined by Folk (1959) as having a grain size of greater than 4µm. SEM images of the studied samples showed that the average grain diameter of sparry calcites is 15 µm (Figure 5-1 and 5-2). Samples with this type of calcite are concentrated in grain-dominated lithofacies. Sparry calcite cement fills intra- and intergranular pores in grainstones, packstones, and rudstones, and intragranular porosity in wackestones, and floatstones. Two morphological types were recognized: macro-rhombic sparry calcite, and micro- sparry calcite. In the former, crystal size ranges from 4 to 25 µm, and in the latter, it ranges from 2 to 4 µm (Figure 5-3 and 5-4). Image analysis of studied samples showed poor sorting of macro rhombic sparry calcite crystals. This is also shown in the grain size distribution, illustrated by the histogram. Sparry calcite shows perfect preservation of crystal shapes with no fusing of grain boundaries. Pores in macro rhombic calcite range from 0.67 to 6.31 µm. Pore size connectivity increases with increasing sorting and grain size. Pore size in micro rhombic calcite ranges from 1.17 to 4.01 µm. Connectivity between pore size is excellent, especially when the grain size distribution indicates good sorting.

5.3.2 Microporosity in Micrite

Micrite was defined by Folk (1959) as calcite with a grain size of less than 4 µm. In the studied samples, micrite grains have diameters ranging from 0.84 to 3.73 µm (Figure 5-5 and 5-6), and micritic calcite was present in mud-dominated lithofacies such as

wackestones, floatstones, and mudstones. These lithofacies occur in the upper part of the outcrop succession corresponding to the Arab-D Member.

Five morphological types of micrite are present in the study area. Rounded and sub-rounded micrites have considerable microporosity (Figure 5-5 and Figure 5-6)**.** Scaleno-rhombohedral micrites show also considerable amount of microporosity (Figure 5-7 and Figure 5-8). Other types showing none or very small amounts of microporosity are micrites, anhedral compact micrites, and fused micrites (Figure 5-9)**.**

Image analysis of studied samples showed good sorting of rounded and sub-rounded micrites, although some large micrite grains were occasionally present. This was indicated by a nearly normally-distributed histogram of the grain sizes. Crystal shape is rarely preserved and the grains have smooth margins. The pores in rounded and sub-rounded micrite range from 0.087 to 4.81 µm in size. Connectivity depends on the grain contacts and packing relationships. Loose and moderate packing of grains results in good connectivity. Anhedral compact micrites and fused micrites in the Arab-D Member were only present in laminated mudstones.

5.3.3 Microporosity in Dolomite

Dolomite occurs in the outcrop samples in three forms: matrix dolomite without distinctive crystals, fine to medium euhedral crystalline (20 to 55 µm), and coarse euhedral crystalline dolomite (>100 µm) (Figure 5-10, Figure 11, and Figure 12). Elemental analysis from EDS data shows the high Mg content in the samples. Dolomitic samples occur in three intervals in the Upper Jubaila Formation and are associated with burrowed mudstone and wackestones.

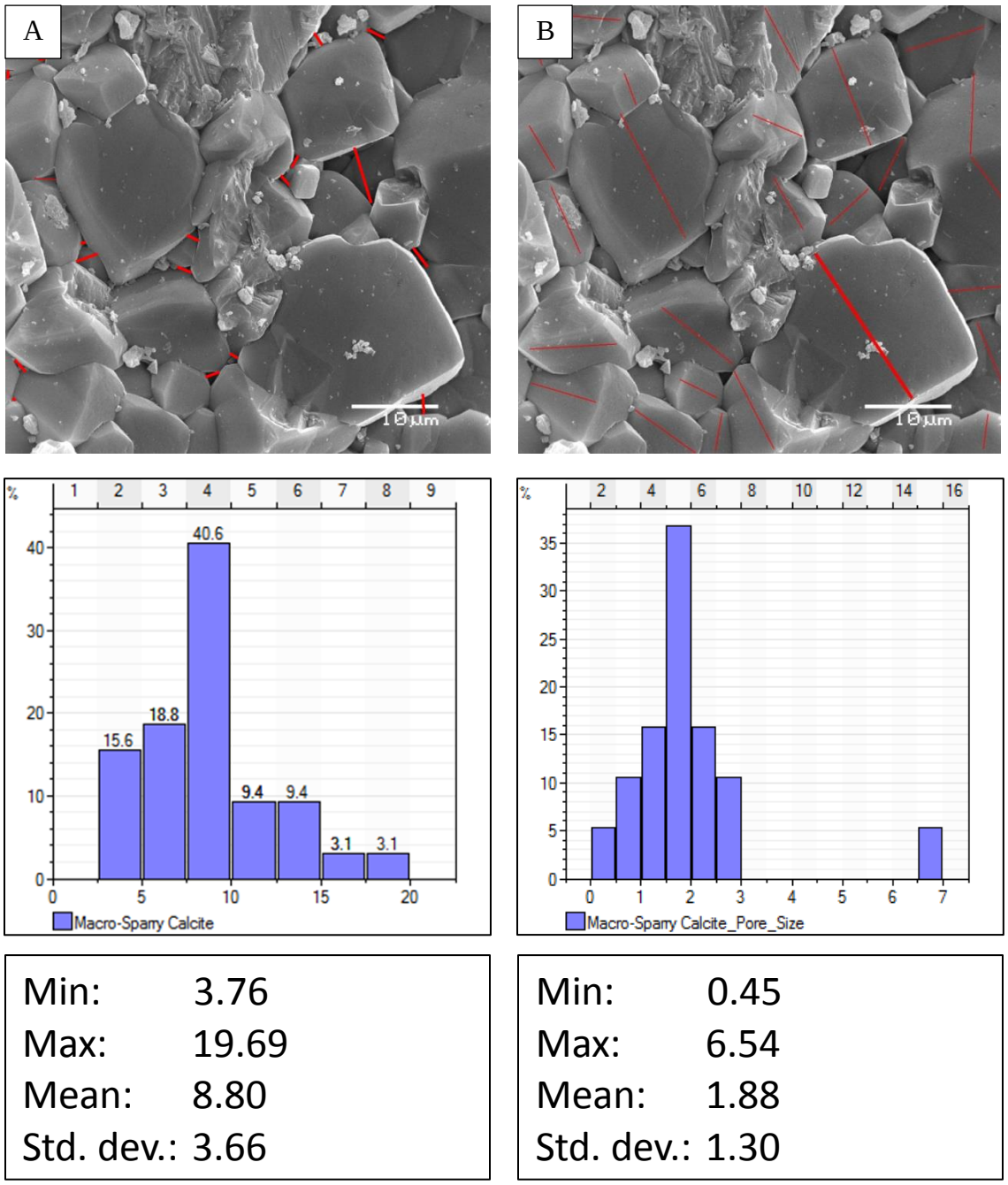

Figure 5-1: SEM image analysis for macro rhombic sparry calcites showing A) the average diameter of the calcite grains using 1-D analysis of JMicrovision software to the bottom a histogram showing diameter distribution in micrometer. B) Showing 1-D area analysis, to the bottomis microporosity distribution for the image.

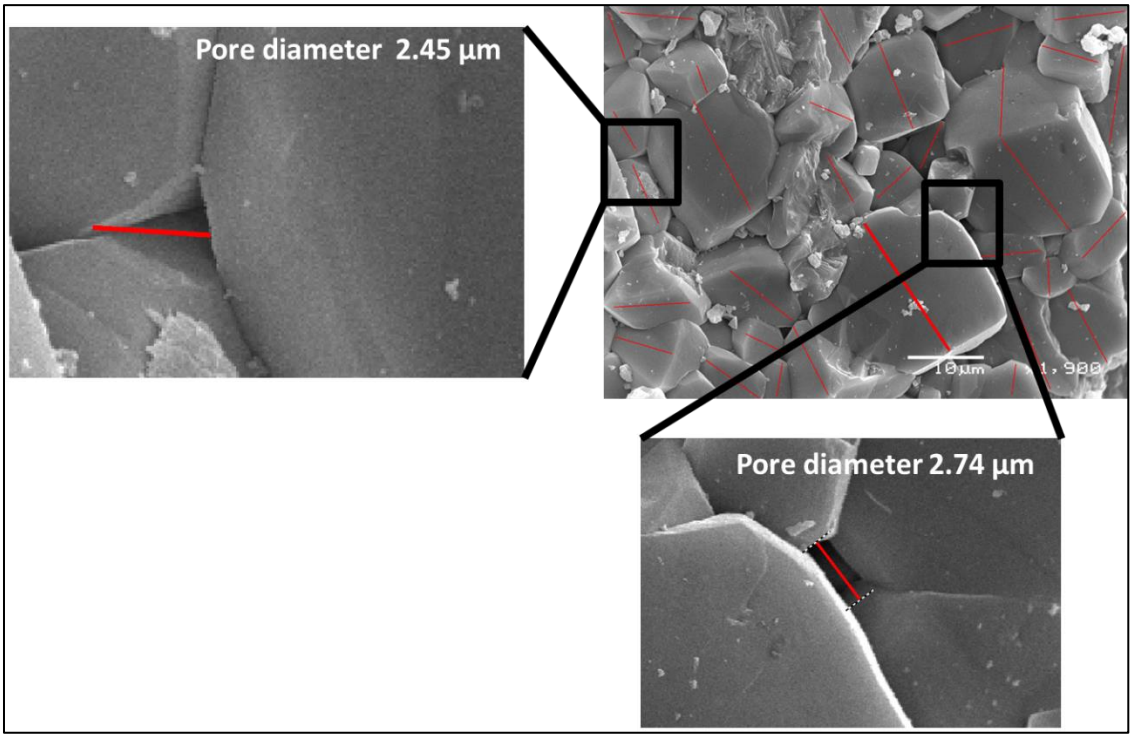

Figure 5-2: High resolution SEM images showing pore diameters in macro rhombic sparry calcites.

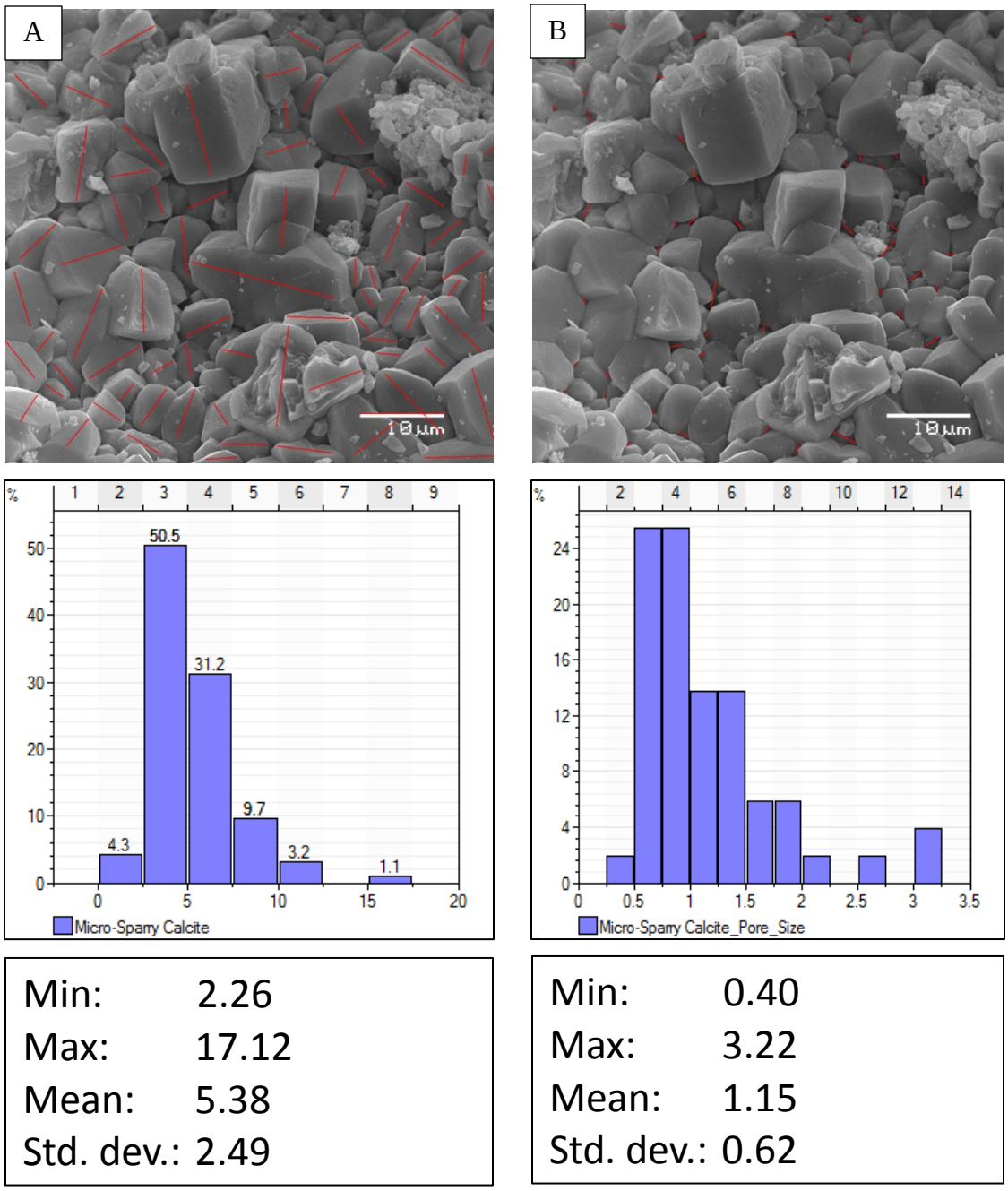

Figure 5-3: SEM image analysis for micro rhombic sparry calcite showing A) the average diameter of the calcite grains using 1-D analysis of JMicrovision software to the bottom a histogram showing diameter distribution in micrometer. B) Shows 1-D area analysis, to the bottom is the porosity calculation for the image.

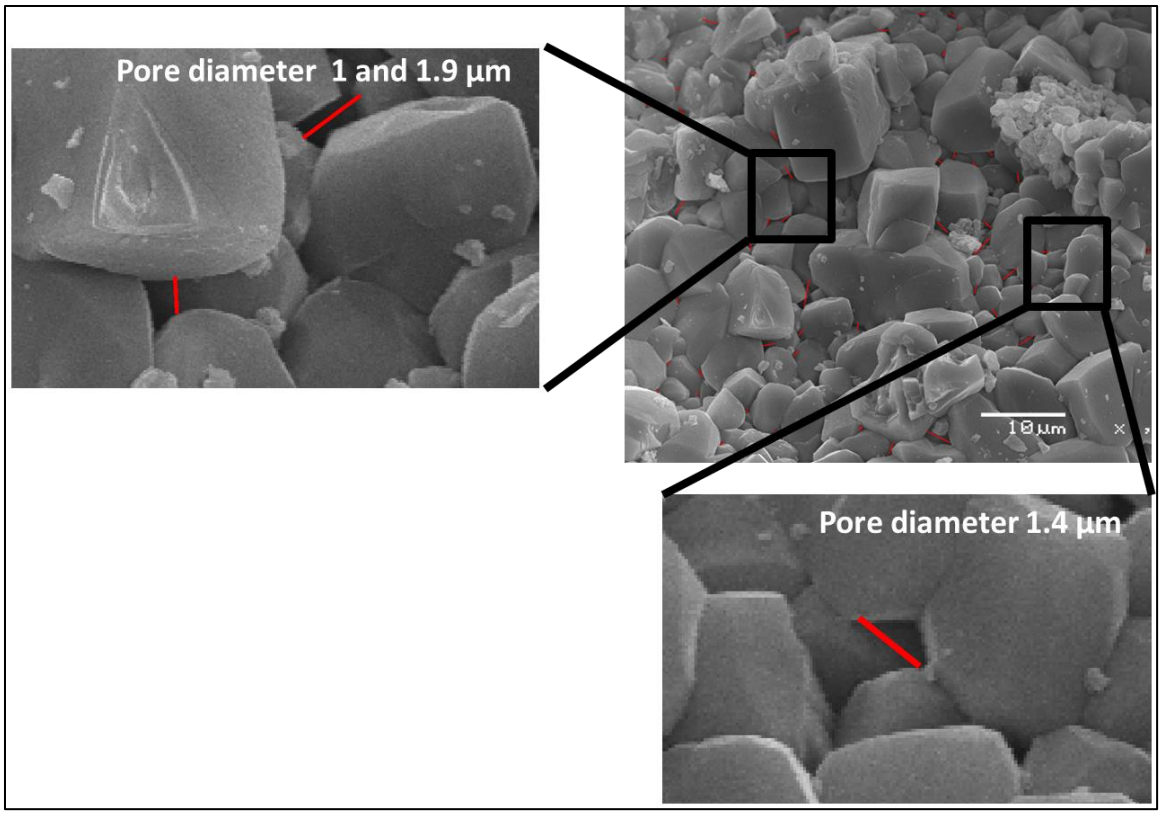

Figure 5-4: High resolution SEM images showing pore diameters in micro rhombic sparry calcites.

.

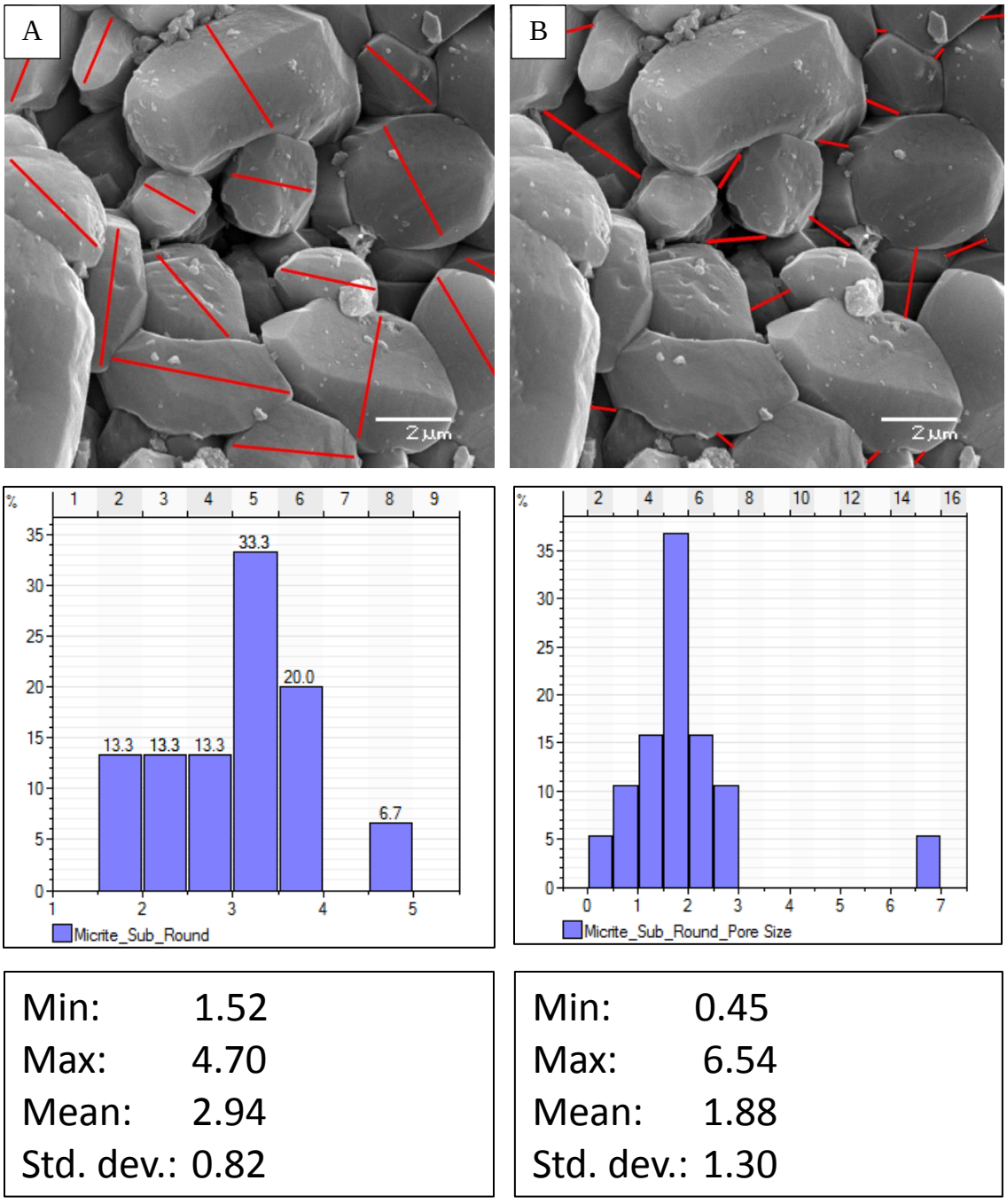

Figure 5-5: SEM image analysis for round and sub round micrite A) Average diameter of the calcite grains using 1-D analysis of JMicrovision software to the bottom histogram showing diameter distribution in micrometer. B) Shows 1-D area analysis the bottom histogram is the porosity calculation for the image.

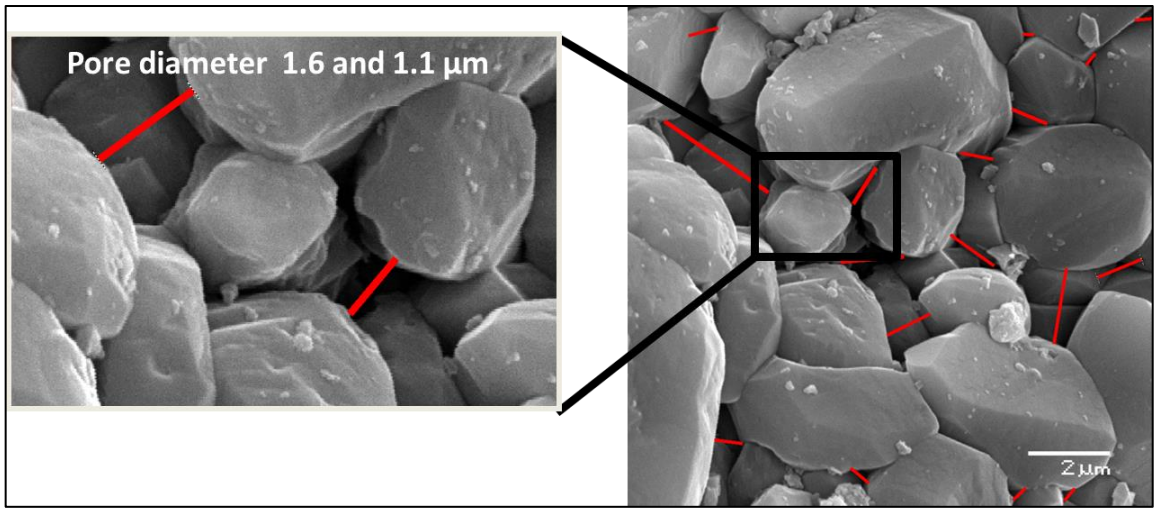

Figure 5-6: High resolution SEM images showing pore diameters in micrometer for round and sub round micrite.

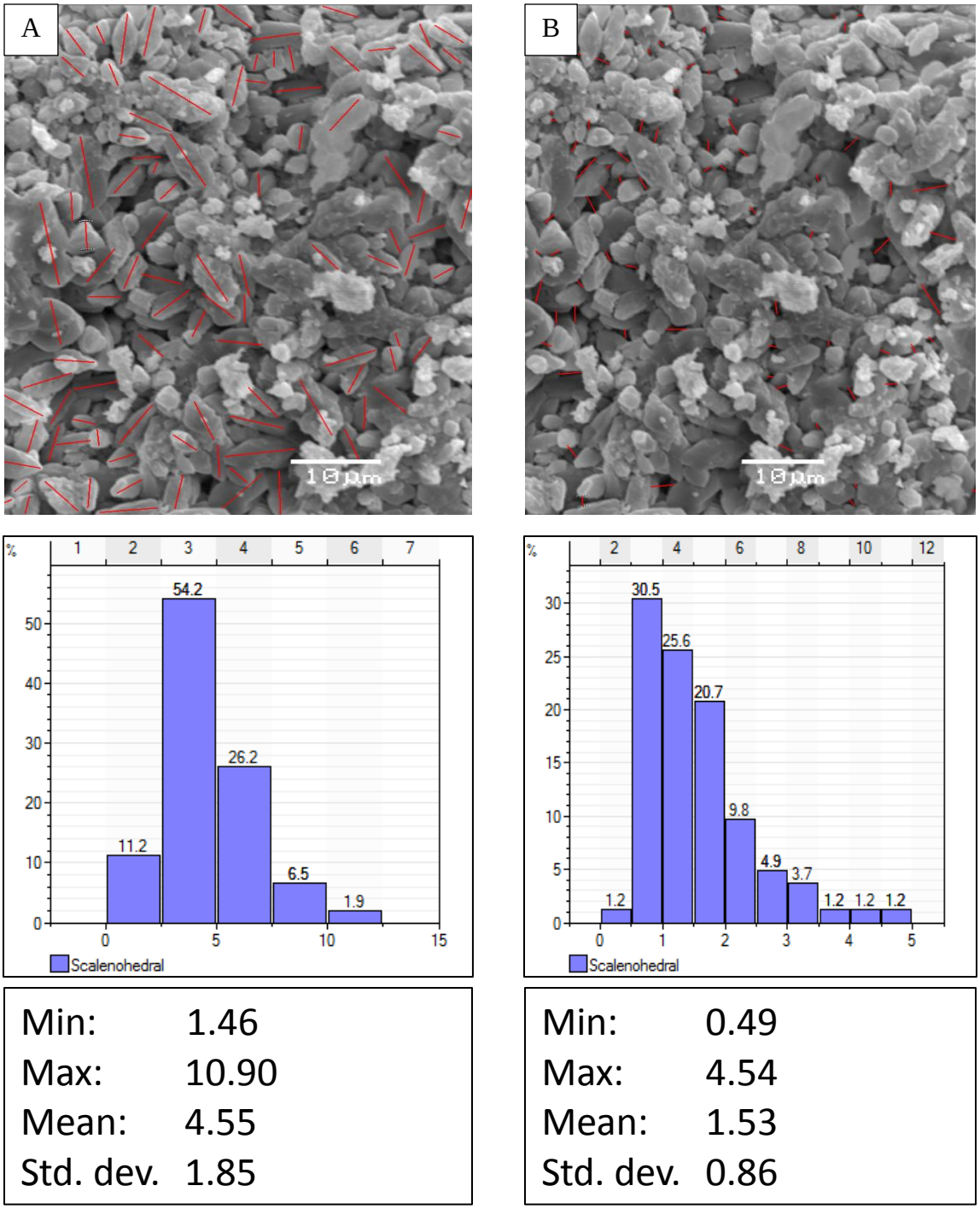

Figure 5-7: SEM image analysis for scaleno-rhomboedral micrites A) Average diameter of the calcite grains using 1-D analysis of JMicrovision software to the bottom histogram showing diameter distribution in micrometer. B) Shows 1-D area analysis, the green 2-D areas; to the right is the porosity calculation for the image.

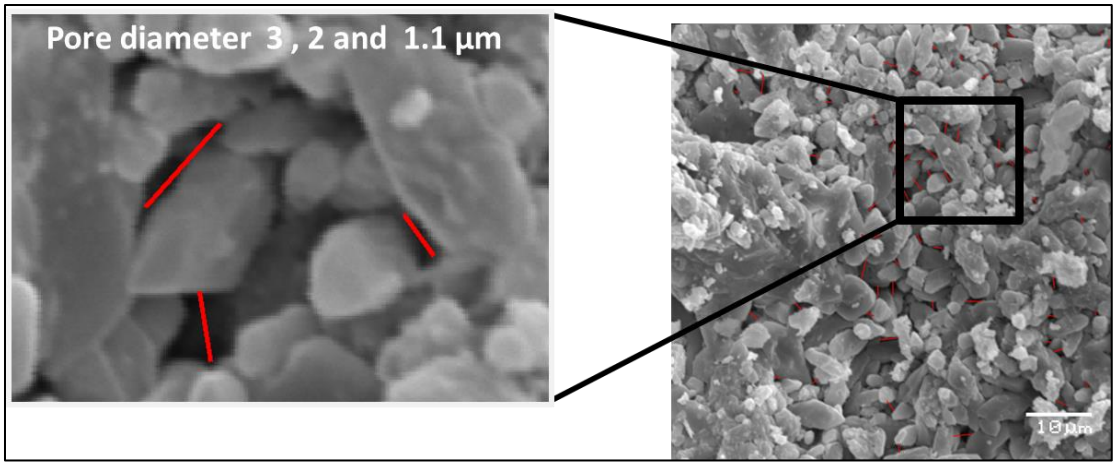

Figure 5-8: High resolution SEM images showing pore diameters in micrometer scaleno-rhomboedral micrites.

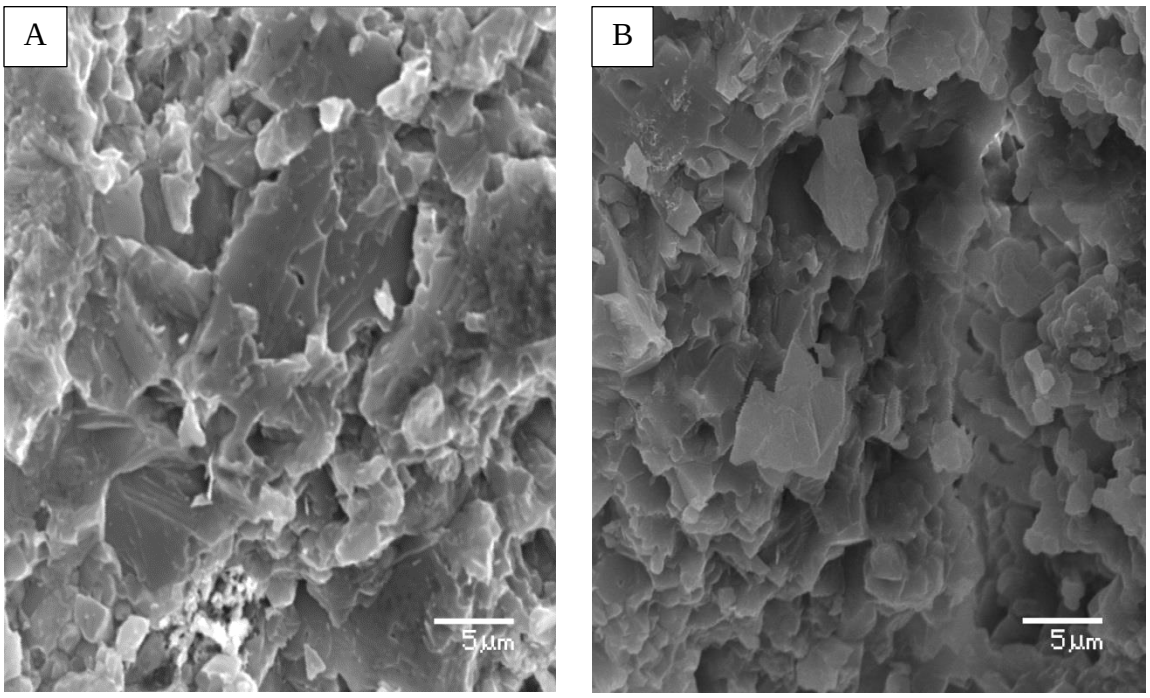

Figure 5-9: SEM images show types of micrites with no or very small amount of microporosity (A) Anhedral compact micrites, and (B) fused micrites.

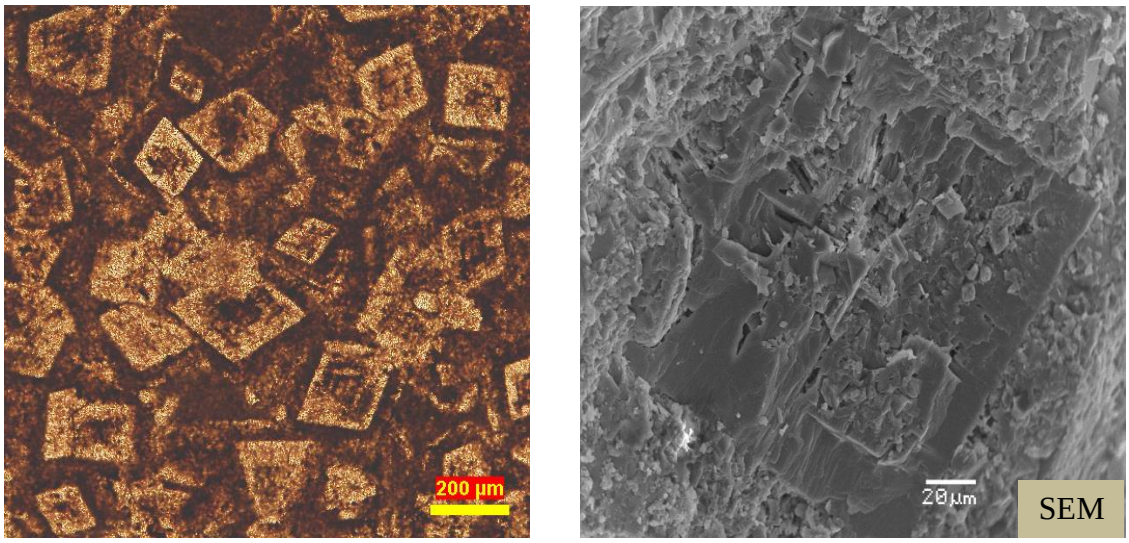

Figure 5-10: Thin section (left hand) and SEM image (right hand) of Dolomite occurs in the study samples.

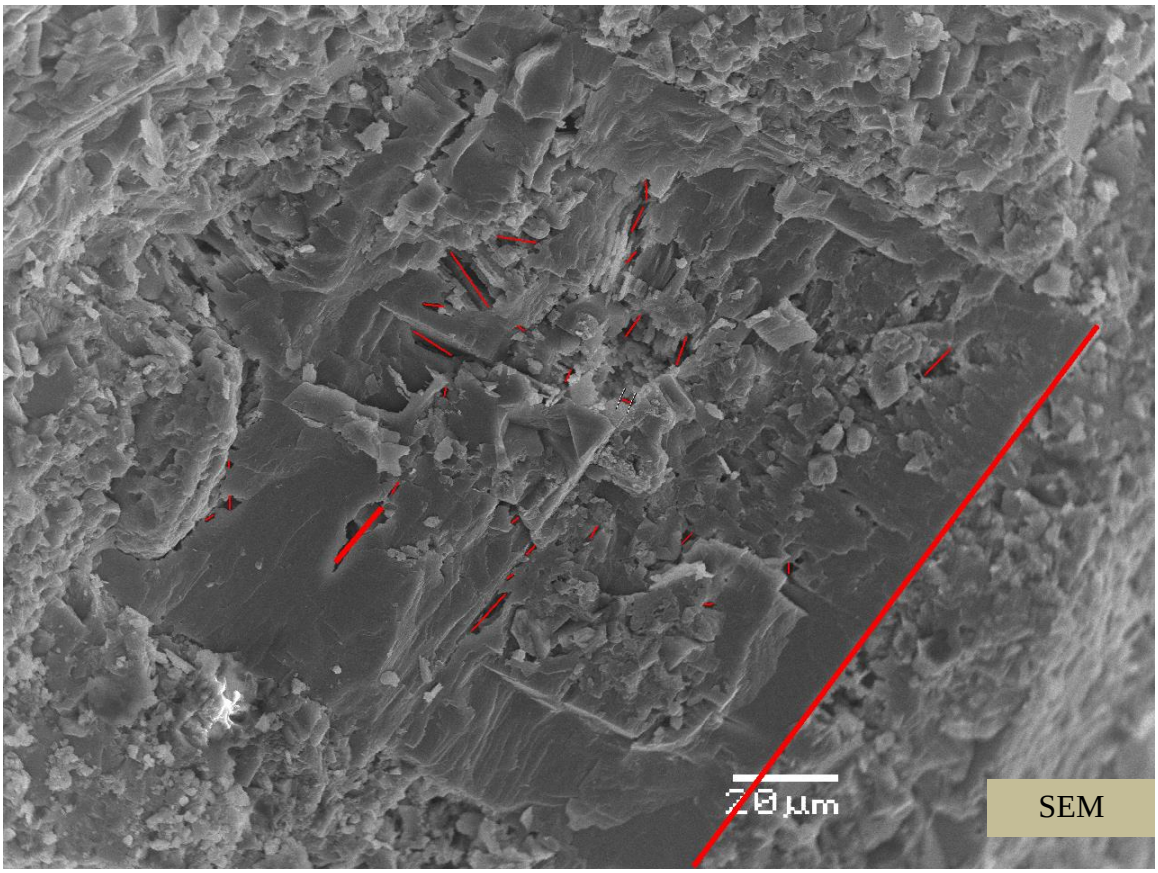

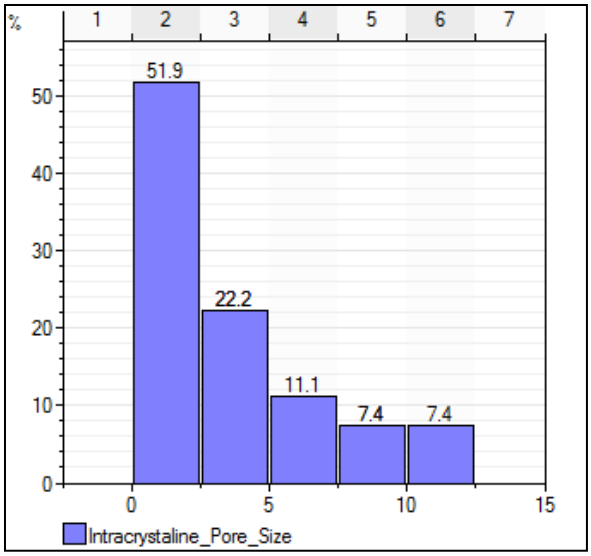

Min:	1.22
Max:	12.24
Mean:	3.91
Std. dev.	3.04

Figure 5-11: SEM image analysis for dolomite crystals A) Average diameter of the calcite grains using 1-D analysis of JMicrovision software to the right a histogram showing diameter distribution in micrometer. B) Shows a 2-D area analysis, the green 2-D areas; to the right is the porosity calculation for the image.

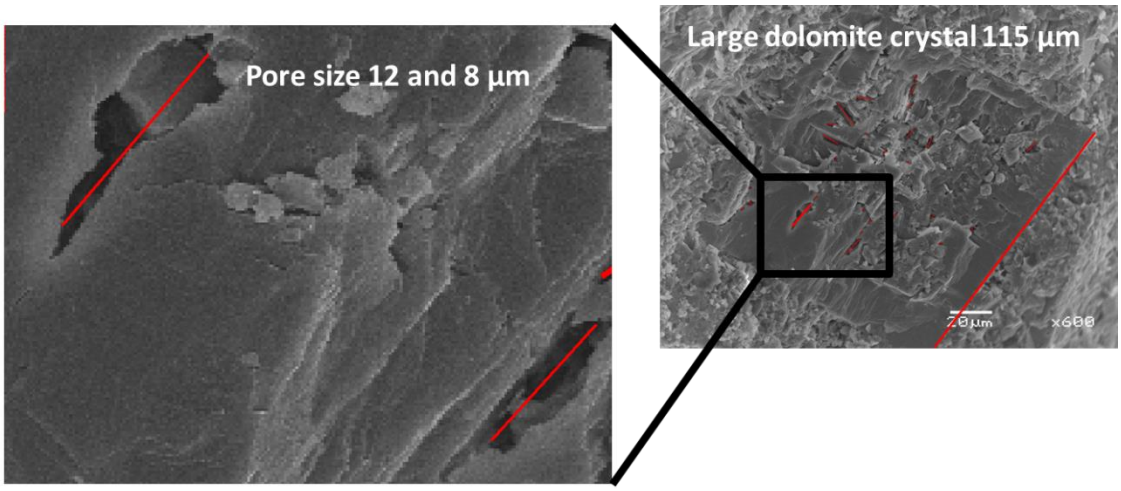

Figure 5-12: High resolution SEM images showing pore diameters in scaleno-rhomboedral micrites.

Micro pores are present in both macro-size euhedral dolomite crystals and dolomite matrix**.** Their shapes are randomly distributed with no preferred shape or orientation, and the dimensions of the pores range from 8.03 to 55 µm. While dolomite crystals show excellent microporosity connectivity, matrix dolomite exhibits very poor connectivity.

5.3.4 Statistical Analysis of Microporosity and Their Associated permeability

Table 5-2 shows statistical analyses of all types of microporosity and associated permeability determined in 65 samples from two stratigraphic sections measured by water saturation method. The average microporosity of these samples is 1.76% and the average associated permeability is 0.357 mD.

Dolomitic wackestones and mudstones are characterized by high microporosity and associated permeability, probably due both to the pore system as well as to the pore morphology and connectivity (see above). Laminated mudstones show less microporosity and permeability. SEM image analyses indicated that the lithofacies is dominated by scaleno-rhombohedral micrite, anhedral compact micrite and fused micrite, with only minor amounts of other types of micrite and sparry calcite cements, and only very low and disconnected amounts of micro pores are present. The other lithofacies are characterized by high to moderate microporosity and permeability. SEM images of these lithofacies show that pores mainly occur between macro and micro sparry cements.

Table 5-2: Summary of microporosity and permeability statistics for 65 core plugs samples measured using water saturation methods.

	Permeability (mD)	Porosity (%)
Min	0.0505	0.36
Max	0.9455	4.35
Mean	0.357926	1.63
St.Dev.	0.191808	0.82
1st Quartile	0.2106	1.00
2nd Quartile	0.3026	1.59
3rd Quartile	0.47165	2.29
Coefficient of variation	0.53	0.50

The coefficients of variation (CV) of microporosity (0.50) and associated permeability (0.53) indicate a degree of heterogeneity in the studied samples. This heterogeneity may be attributed to the different origins of the pore systems. Seven types of pore systems were recognized in the samples. Histograms for both microporosity and associated permeability show a positive skewed to the right distribution (Figure 5-13). This also suggests the heterogeneity of microporosity and associated permeability in the study area.

5.3.5 Microporosity and Permeability Relationship

A cross-plot of microporosity versus log permeability of samples from both the Upper Jubaila Formation and the Arab-D Member is illustrated in Figure 5-14. This plot indicates that the correlation between the two variables is low (the correlation coefficients are 0.17 and 0.25 for the Upper Jubaila and Arab-D Member, respectively). Cantrell and Hangerty (1999) reported a similar scatter plot for porosity and permeability data in the Arab-D reservoir, and attributed this scattering to the non-uniformity of the samples, to rock variations, and to analytical errors.

The microporosity-permeability data are presented in four plots according to lithofacies **(**Error! Reference source not found.**).** On the basis of these grouping, microporosity and permeability relationship improved significantly (Figure 5-15). Correlation coefficients of all groups still remain below 0.55 which although significant (Cantrell and Hangerty, 1999) are still low. Groups II and IV show relatively higher correlation coefficients than the other groups. SEM image analysis of samples from these groups show relatively large micro pores with fairly good connectivity. Group II shows large pore within large dolomitic crystals. Group IV includes all the grain types present in the samples.

Carbonate cements (macro and micro spar) fill all the intergranular macro pores but relatively large micro pores with significant connectivity occur within the cements.

5.4 Discussion

These observations characterize the micro pore systems in the Arab-D reservoir rock analog and show how microporosity can influence petrophysical properties. The study provides a quantitative and qualitative description of micro pore systems in different carbonate grain types, and shows that dolomite crystals exhibit large amounts of microporosity with high values of associated permeability which is attributed to the high micropore connectivity.

Cantrell and Hangerty (1999) in their study of the actual Arab-D reservoir divided Arab-D microporosity into four genetic types: fibrous, matrix, to bladed cements, and microporous equant cements, microporous grains. Micro porous fibrous nor microporous grains were not identified in the present data set, probably due to the total transformation of fibrous early marine cements and skeletal grains from high Mg calcite and aragonite to low Mg calcite.

This study suggests that microporosity and associated permeability are mainly controlled by the morphology of the carbonate cement and micrite, which are mainly post sedimentational processes. This relationship between microporosity and carbonate grains in subsurface reservoirs has been reported in the literature (e.g., Lucia, 1995; Lambert et al., 2006). These studies concentrated on micrite crystallography and associated microporosity and permeability. Microporosity within carbonate cement, dolomite

crystals and dolomite matrix remains poorly understood, although this study provides some observational data on microporosity distribution.

Dolomite crystals appear to contain relatively large amounts of microporosity. The microporosity increases with increasing size of the dolomite crystals. By contrast, the dolomite matrix shows very low amounts of microporosity. Considering that the occurrence of dolomite in the subsurface Arab-D is of three types (fabric preserving, non-fabric preserving and baroque: (Cantrell et al., 2004a), it could be suggested that the last two types of dolomite may be potential zones of microporosity in dolomitic intervals.

The database used in this study was collected from an outcrop analog of the Arab-D reservoir with a similar wide range of lithofacies to that of the actual subsurface reservoir. This database can be used to estimate and predict reservoir quality in terms of microporosity occurrence and distribution. This study assumes zero macroporosity in the samples, and this may not be correct for the actual Arab-D reservoir; however, the system of microporosity modeled in this study may be similar to that present in the actual subsurface reservoir rocks.

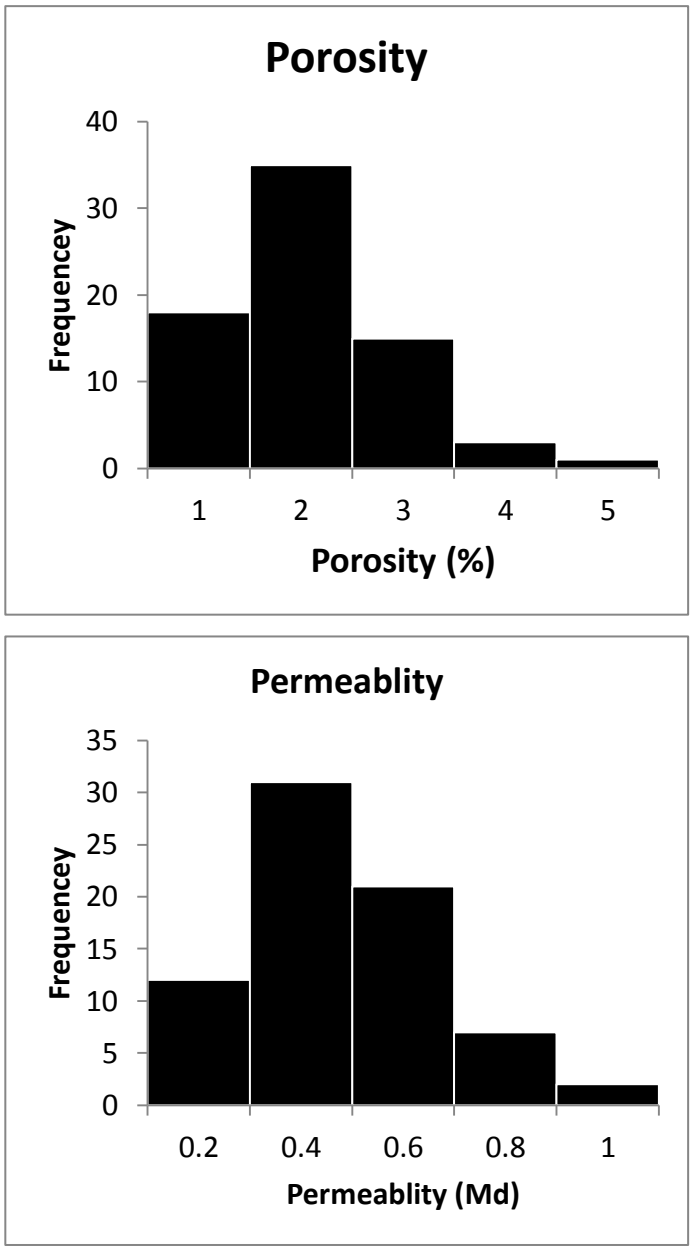

Figure 5-13: Histogram of microporosity (A) and their associated permeability (B) of both the Upper Jubaila and Arab-D Member.

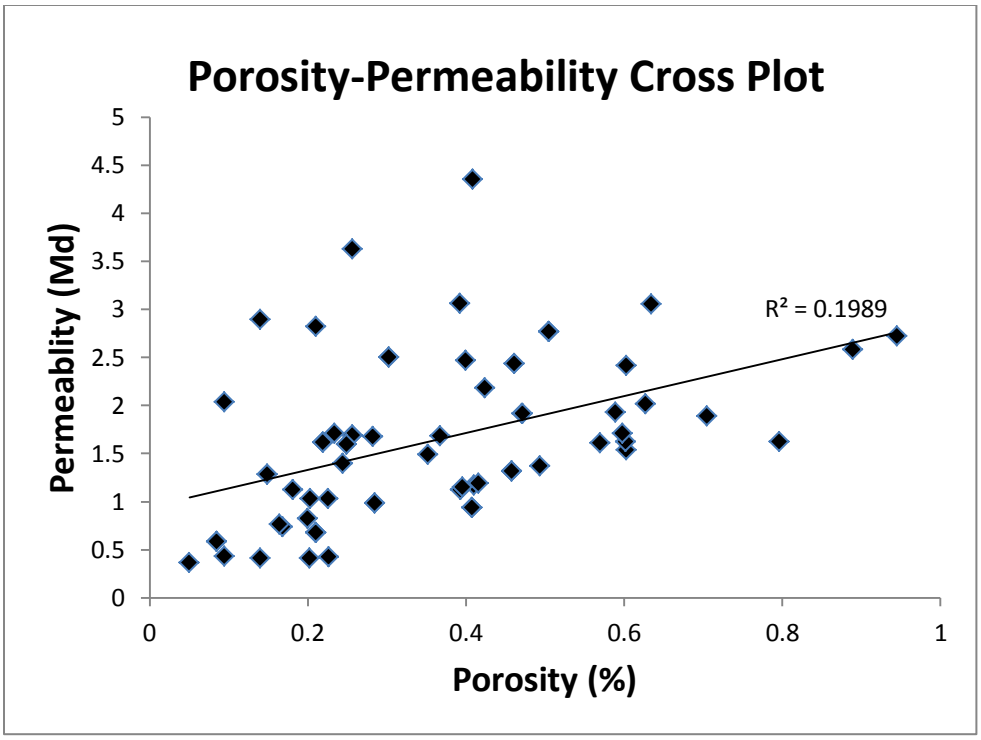

Figure 5-14: Cross plot of porosity and log permeability of both the Upper Jubaila and Arab-D Member.

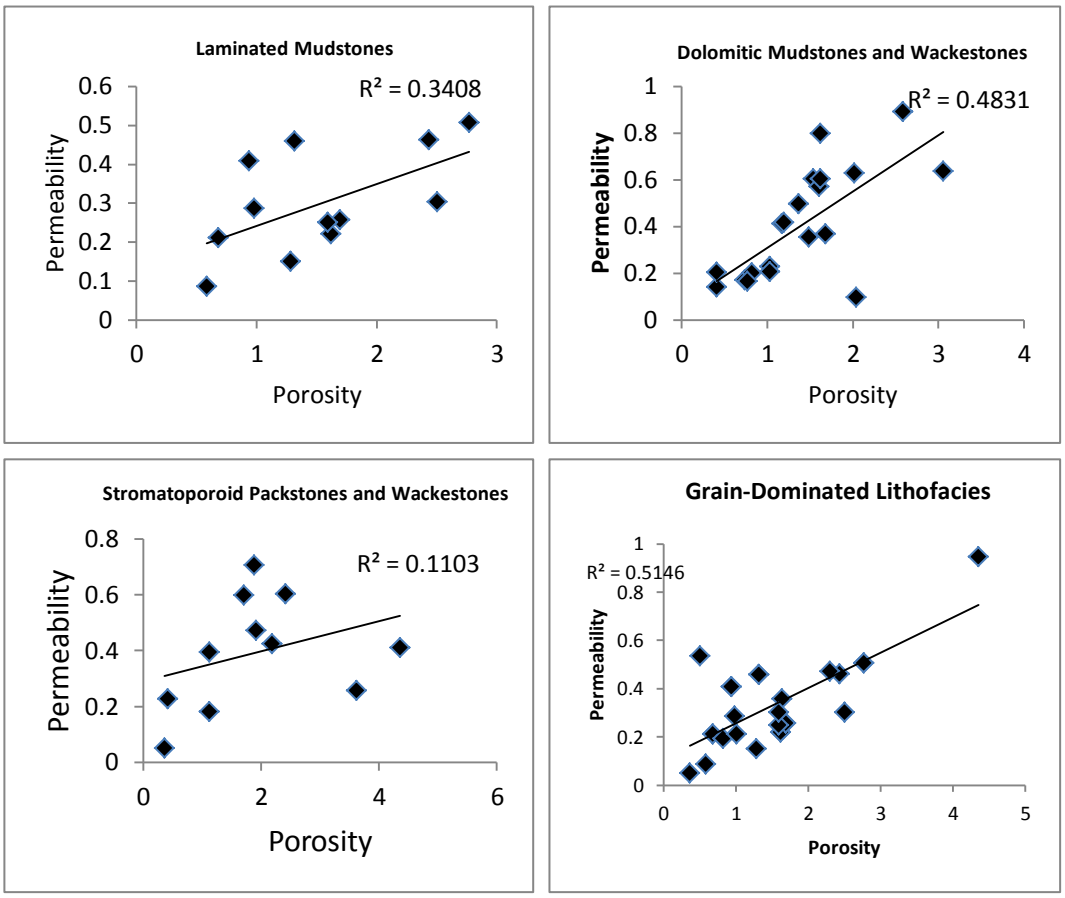

Figure 5-15: Cross plot of porosity and log permeability based on four facies groups.

CHAPTER 6

INTEGRATION OF OUTCROP GAMMA RAY LOGGING AND GEOCHEMICAL ANALYSIS

6.1 Introduction

Investigation of Spectral Gamma Ray (SGR) and Inductively Coupled Plasma-Mass Spectrometry (ICP-MS) geochemical analysis of the study area revealed a strong correlation between the SGR response of the outcrop lithofacies and their elemental content. The two units of the reservoir (the Upper Jubaila Member of the Jubaila Formation and the Arab-D Member of the Arab Formation) show distinctive SGR log profiles controlled mainly by lithofacies associations. Geochemical analysis revealed four groups of elements association: Group-1 includes SiO_2, Al_3O_2, Fe_2O_3, K_2O, TiO_2, Zr, and Zn. This Group has strong relationship with radioactive elements U, K, and Th. Reservoir facies exhibit high concentration of elements in this two group. Group-2 includes CaO, and Sr. High concentration of this group indicates affinity toward pure carbonate facies and less siliciclastic impurities. High concentration of Group-3, which includes only MgO, marked dolomitic zones. The radioactive elements have been assigned to Group-4. The boundary between the Upper Jubaila Member and the Arab-D Member is clearly defined from vertical SGR log profiles, vertical geochemical data logging, and cross plots of Group-1 with the radioactive elements in Group-4. The Upper Jubaila Member geochemical data show a very low concentration of U, K, and Th. Consequently, the SGR

response of the lithofacies was very low. All reservoir lithofacies showed high concentration of elements from Group-1 and Group-4, while all non-reservoir lithofacies show less concentration. The Th/U ratio indicates a general shoaling upward following the same trend of the outcrop lithofacies. A high Th/U ratio represents reservoir lithofacies, while a low Th/U ratio represents non-reservoir lithofacies. Lithofacies and SGR log motifs were related in the measured sections.

6.2 SGR Logging Overview

Spectral Gamma Ray (SGR) logging of outcrops provides an excellent technique for characterizing and Modelling reservoirs. The output from SGR tools are SGR counts per second (CPS), elemental concentrations, and dose rate for potassium (K), thorium (Th), uranium (U), and their total counts (TC). SGR tools have been used effectively by many investigators (Dennison et al. 1997; Krystyniak et al. 2005; Collins et al. 2006; Evans et al. 2007; Koptíková et al. 2010; imicek et al. 2012) to tie gamma ray log signatures to the characteristics of lithofacies at outcrops and extract useful geological information out of these outcrops. There is several information can be extracted from outcrop gamma-ray logging and used for many applications. This includes lithofacies identification, lithofacies correlation, stratigraphic sequences, and paleoenvironment reconstruction. These geological characteristics can increase understanding, with high confidence, the equivalent subsurface reservoir and can greatly enhance the reliability of subsurface well logs interpretation and correlation.

The integration of SGR with the geochemical data of the sedimentary rock has been used effectively for both carbonate and clastic rocks (Svendsen & Hartley 2001). This

integration provides much more information regarding the depositional environment in terms of water depth, oxygen water condition, and terrigenous clastic input. This will help in understanding the vertical and lateral lithofacies stacking pattern, and, ultimately, provide higher order resolution of reservoir characterization.

The Upper Jurassic formations in Saudi Arabia are the most productive oil reservoirs in The general shoaling upward of the whole Upper Jurassic system mask the signature of the Upper Jubaila Member and the Arab-D Member boundary (Al-Dhubeeb 2002; Hughes 2004). This boundary has not been completely understood in the subsurface and requires more criteria for recognition. This is attributed to the fact that the Arab-D reservoir was first defined based on hydrocarbon productivity in the subsurface rather than on the lithostratigraphy or the biostratigraphy of the equivalent outcrop strata (Powers et al. 1966; Meyer et al. 1996). Therefore, construction of accurate outcrop studies SGR and Geochemical signature could bridge the gap in this research venue. This could be performed by identification of different SGR and geochemical log motifs of outcrop equivalent facies, which will allow to subdivide the Arab-D reservoir into two distinctive lithological packages. Moreover, the key components of Arab-D reservoir should be understood to enhance reservoir characterization. This may include the understanding of facies description and their sequence hierarchy and their high resolution stacking pattern, as well as well logging signature of the reservoir lithofacies. Outcrops always used to address the limitation of having low-resolution subsurface logging data and to overcome the challenges associated with reservoir Modelling. Therefore, integration of outcrop SGR logging and geochemical analysis provide valuable information that may help improve reservoir characterization and Modelling.

6.3 SGR Log Motifs

The measured outcrop sections displayed two major SGR profiles of all the logs, U, K, Th, and TC (Figure 6-1). These two profiles represent the Upper Jubaila Member in the lower section and the Arab-D Member in the upper section. The lower section shows general upward increasing in all SGR logs and their TC. Correlation profile through the outcrop show similar pattern for all of the stratigraphic sections that have the Upper Jubaila on it; however, in the area with rocks collapse there might be some changes in the SGR signatures (Figure 6-2 to 6-5). The Upper Jubaila Member was subdivided into four subunits of relatively low SGR levels separated by a sharp peak of a relatively high TC of SGR. These high peaks correspond to Stromatoporoids wackestone and packstone strata in the stratigraphic section. The thicknesses of each of the log packages varied and correspond stratigraphically to the HFSs defined in the stratigraphic section in the Upper Jubaila Member. The U SGR has distinctive four troughs corresponding to the TC and Th SGR peaks. It is also shows general upward increasing with generally lower level of emission reading against high the Th SGR emission reading. The upper section, the Arab-D Member, has a serrated SGR log pattern; however, five peaks of relatively high Th, K, and TC SGR readings are recorded. These peaks correspond to relatively low U SGR log troughs. Peloidal sandy fossiliferous packstone and grainstone and laminated sandy grainstone were observed in the corresponding interval of these K, Th, and TC SGR peaks and U SGR troughs. The boundary between the Upper Jubaila Member and the Arab-D Member exhibited sharp break in the SGR log response, especially for the Th, K, and TC logs.

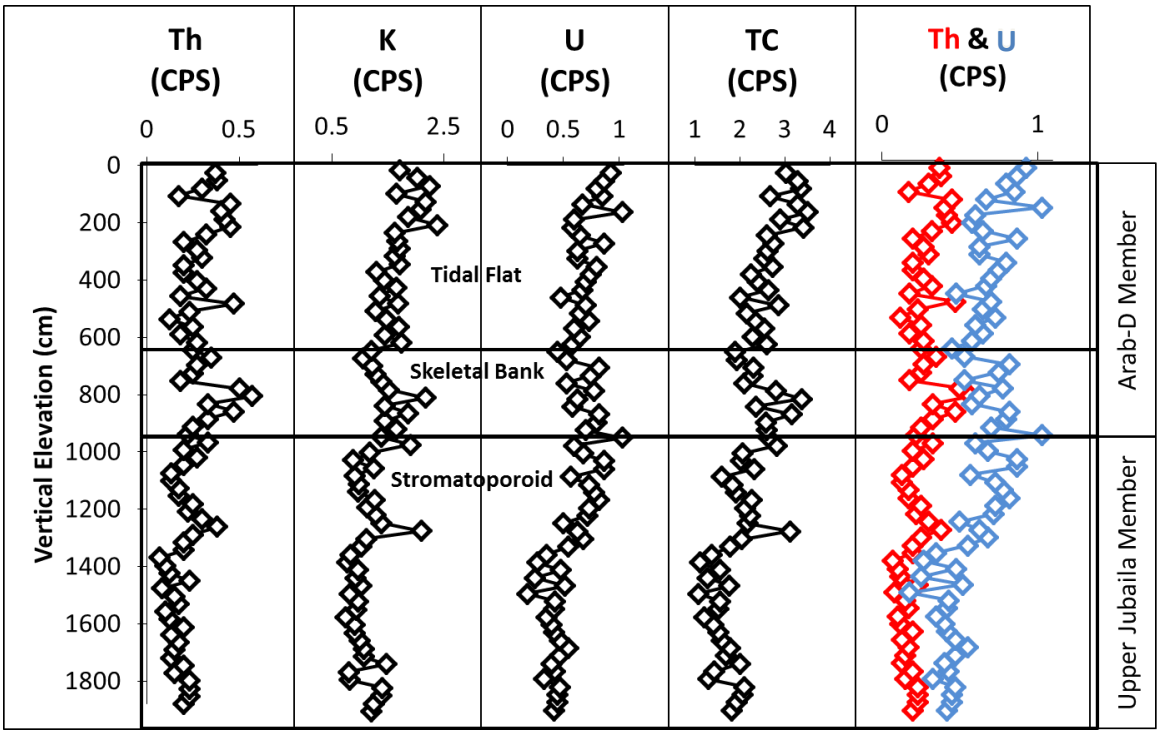

Figure 6-1: SGR Log in section-11 shows SGR distinctive two major units (the Upper Jubaila Member and the Arab-D Member). The Upper Jubaila Member shows four major sharp SGR peaks while the Arab-D Member shows five SGR peaks. These peaks correspond to major troughs in the U SGR log.

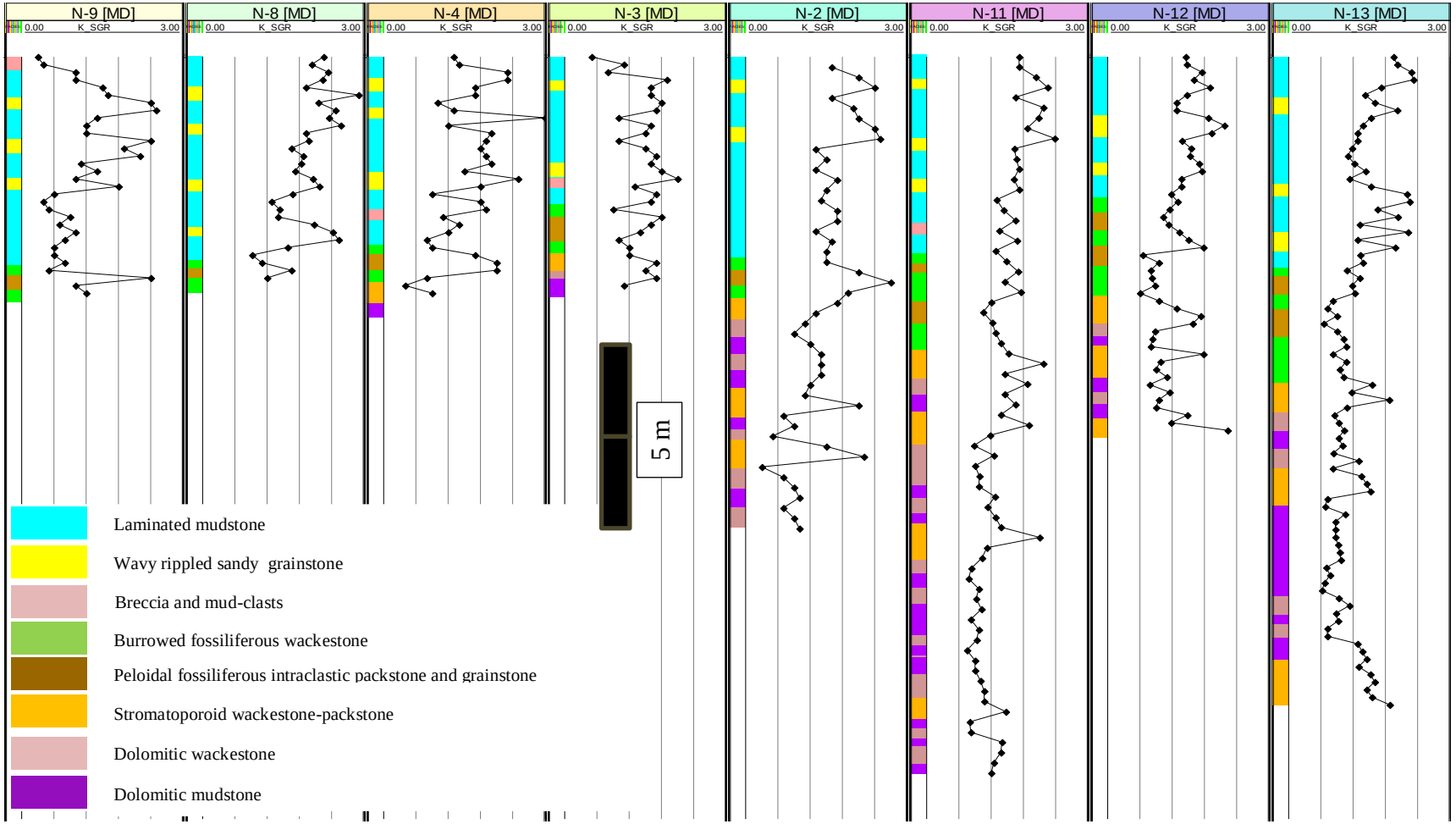

Figure 6-2: Cross section showing K-SGR logs (CPS) in eight stratigraphic sections measured in the outcrop.

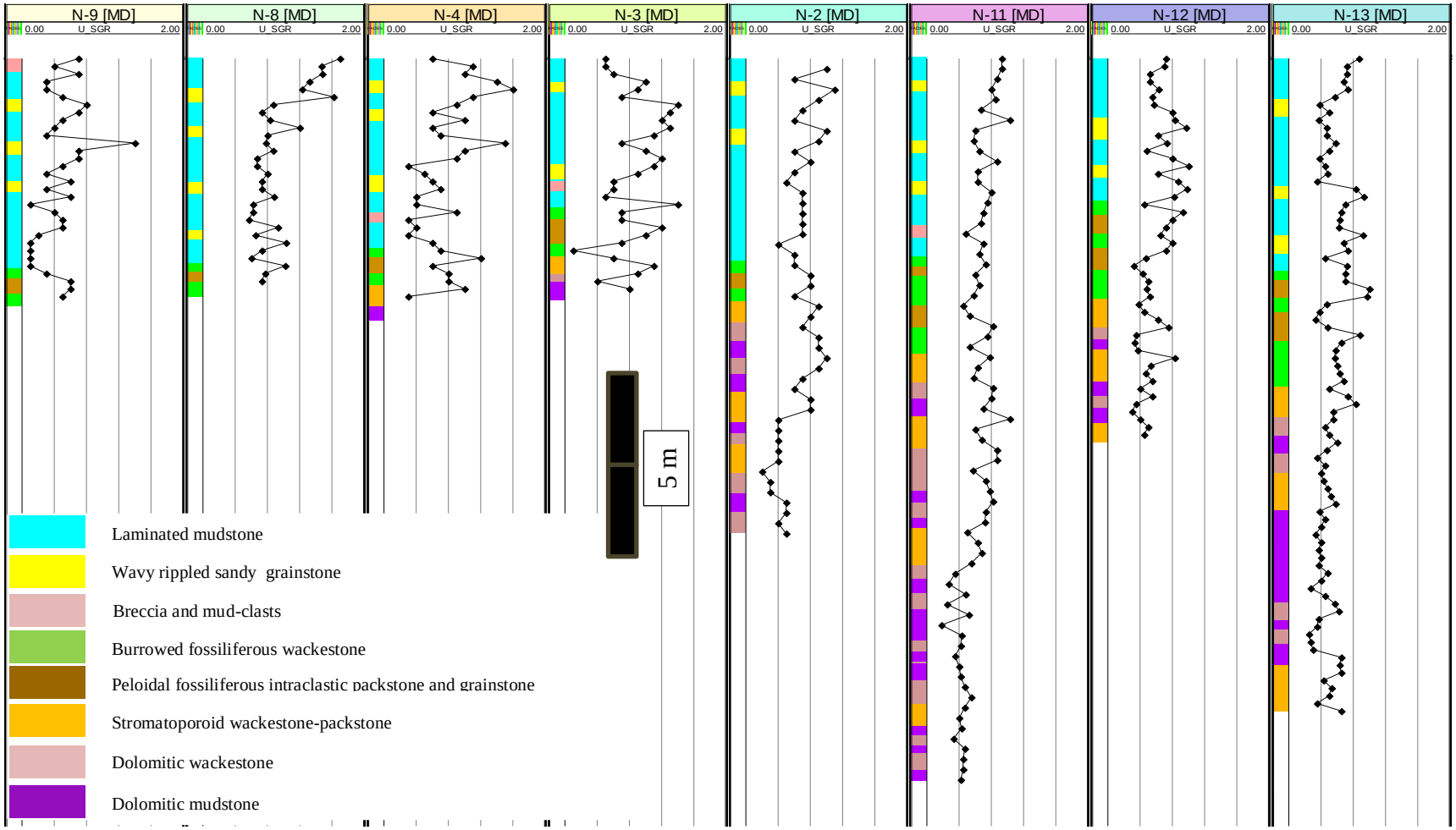

Figure 6-3: Cross section showing U-SGR logs (CPS) in eight stratigraphic sections measured in the outcrop.

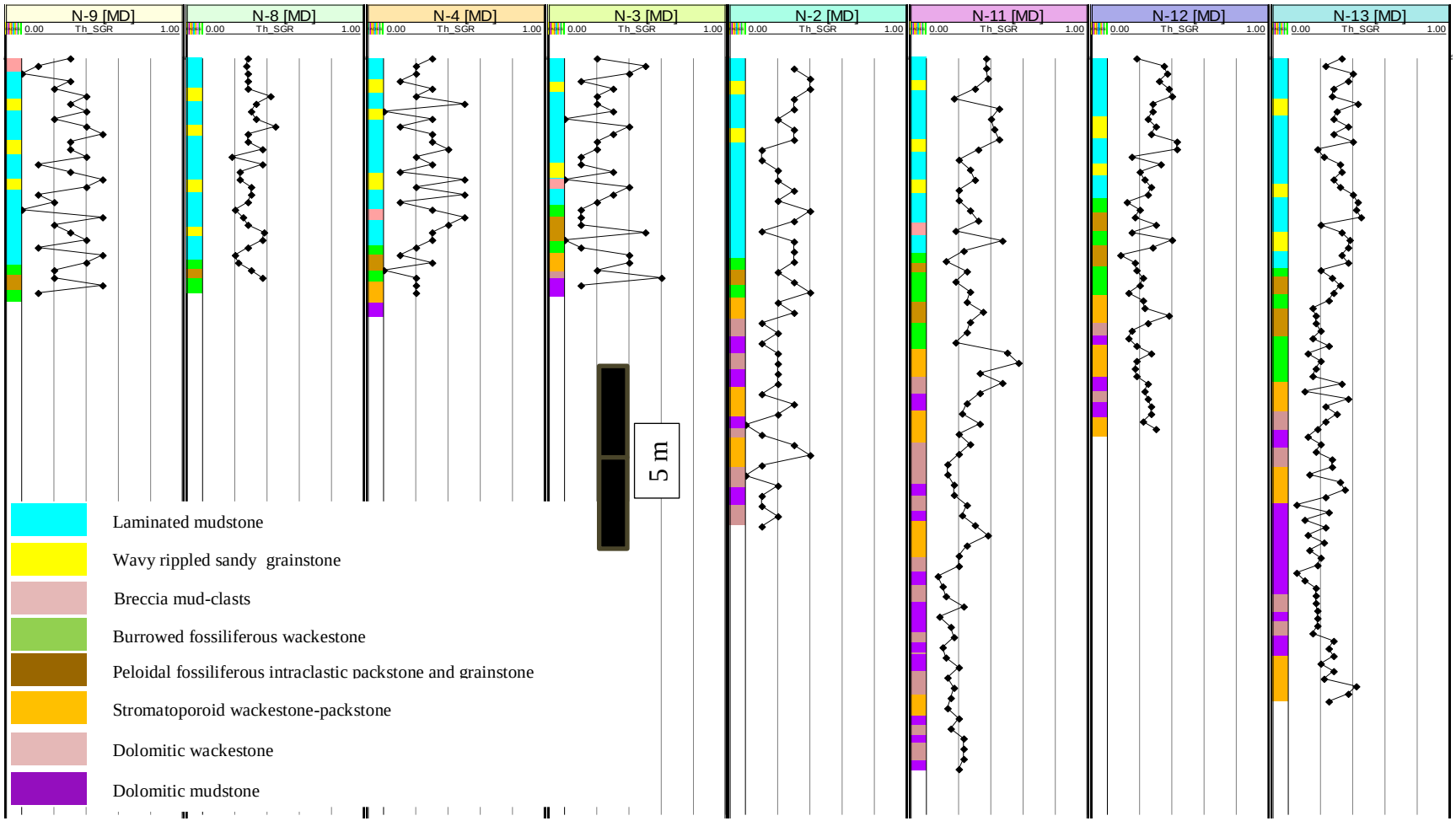

Figure 6-4: Cross section showing Th-SGR logs (CPS) in eight stratigraphic sections measured in the outcrop.

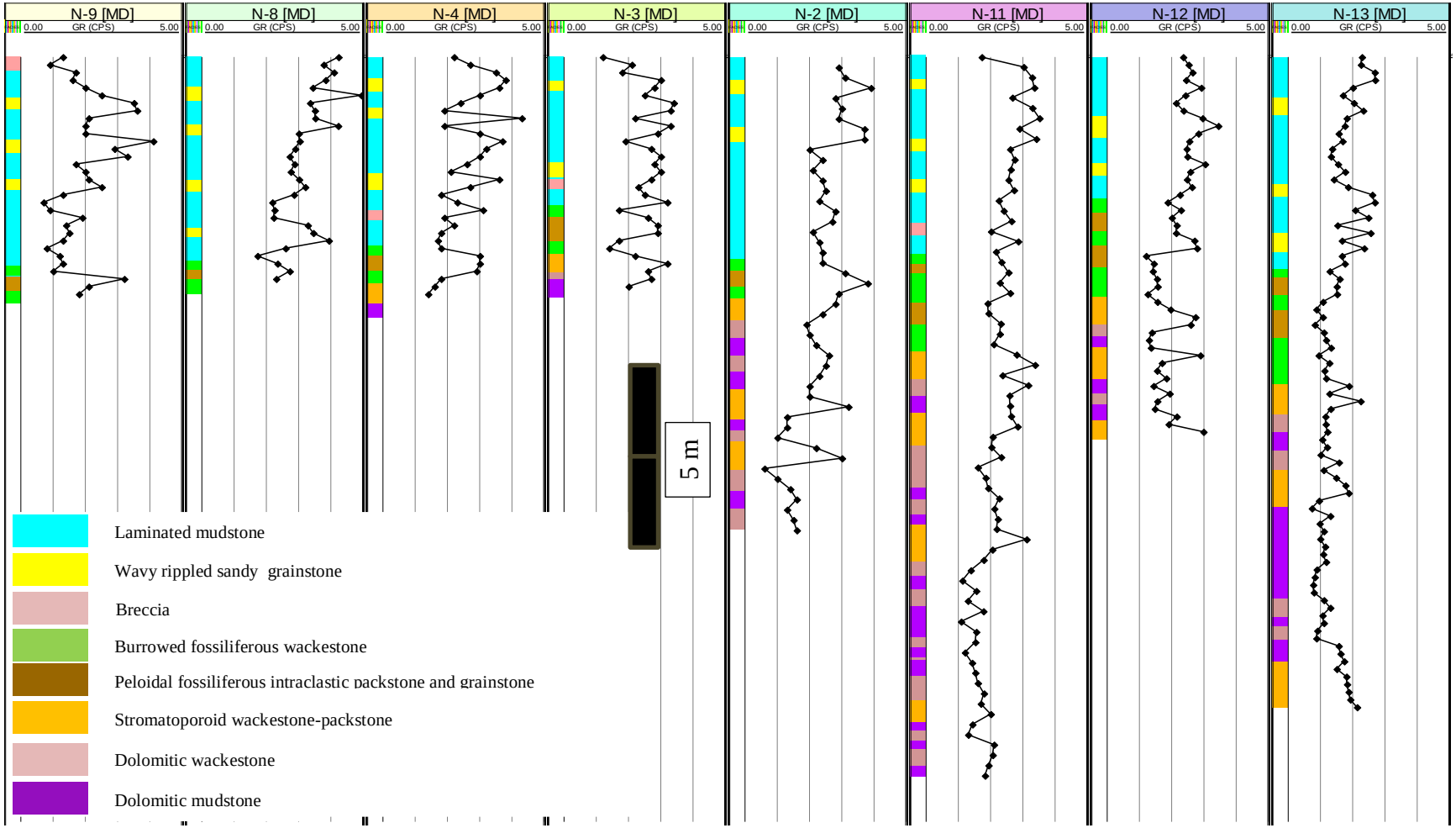

Figure 6-5: Cross section showing Total-SGR logs (CPS) in the eight stratigraphic sections measured in the outcrop.

6.4 SGR Logs 3-D Modelling

6.4.1 Data Analysis

Data analysis was conducted on the SGR logs of the stratigraphic sections of the outcrop in order to choose the suitable geostatistical parameters for the 3-D model. The analysis was conducted on the up-scaled SGR logs, which were processed as continuous variables. The normality of the data was tested by histograms construction of the whole data set to visualize their distribution. The resulting histograms indicated that the data had the shape of non-normal distribution (Figure 6-6). Therefor normality for the data is required because the algorithm used for the 3-D Modelling required the data to be normally distributed and continuous.

Experimental semivariograms were constructed in the major (N-S), minor (E-W), and vertical directions to characterize the spatial behavior of the data set. Figure 6-7 shows examples of a semivariogram for total SGR log together with Modelling parameters. The parameter identification process was repeated for each of the three SGR logs and the Total Count (TC) log. The analysis of these semivariograms led to the definition of the horizontal and vertical ranges for each SGR and the TC GR log used to construct the 3-D model.

6.4.2 3-D Models of SGR Logs

The 3-D model of SGR logs of the Arab-D reservoir in the study area is represented by the same gridding system used for facies Modelling (Chapter-4). The SGR model was generated using a Sequential Gaussian Simulation stochastic approach (SGS). The resulting analyses of the 3-D SGR models for U, K, and Th show difference packages of

Upper Jubaila Member and the Arab-D Member (Figure 6-8, 6-7, and 6-9). There is obvious increasing upward of CPS in all of the three models following the general shallowing upward trend of lithofacies. Stromatoporoid zone showed the lowest CPS values and tidal flat zone showed the highest CPS values while skeletal bank zone represent a transition zone between stromatoporoid and tidal flat zones.

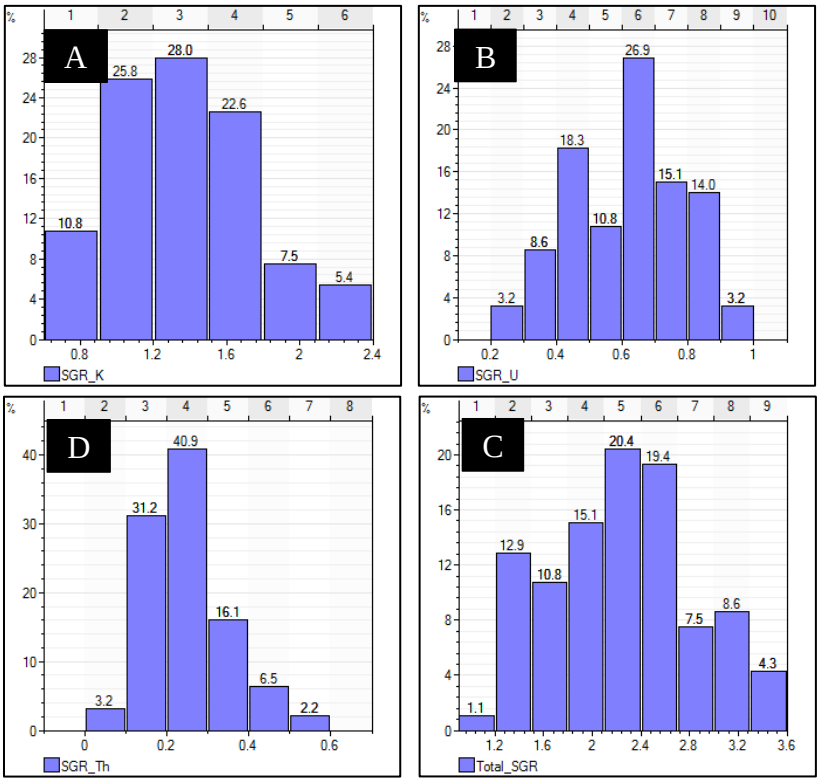

Figure 6-6: Histograms showing count percentage distribution of, (A) K-SGR, (B) U-SGR, and (C) Th-SGR, and (D) Total GR.

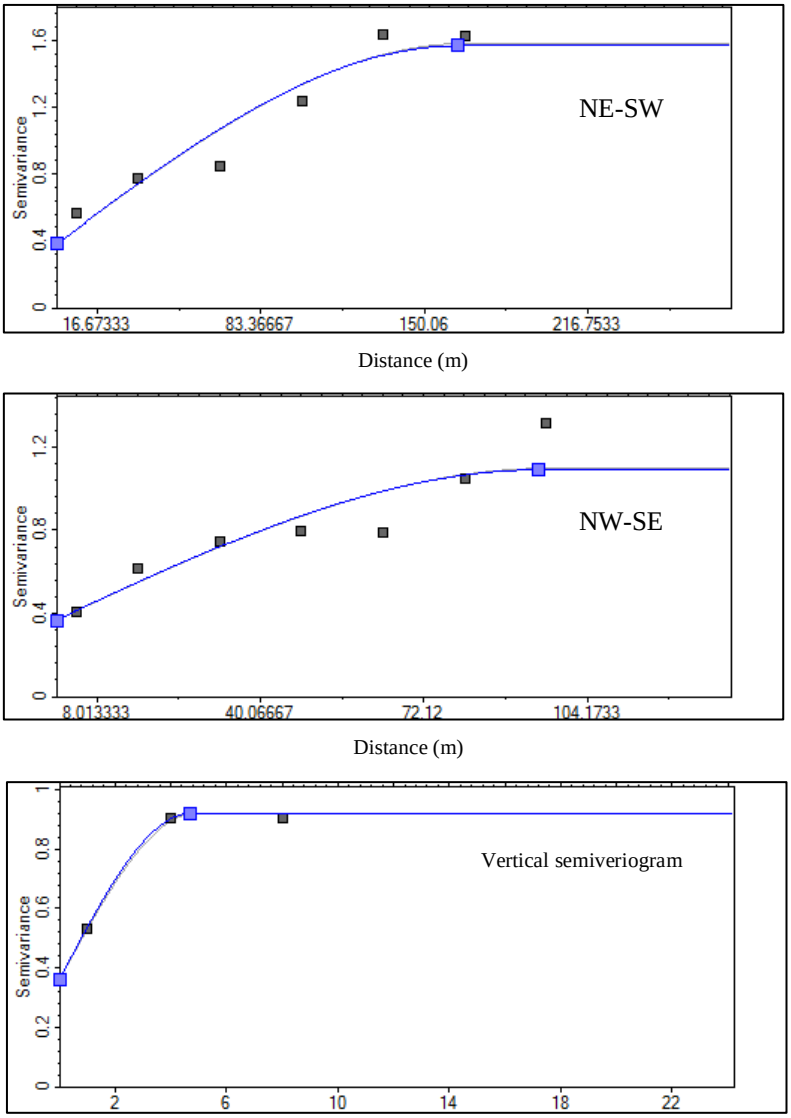

Figure 6-7: Semivariograms for total SGR of N-S (major direction), W-E (minor direction), and vertical direction of K-SGR count per second logs in the study area.

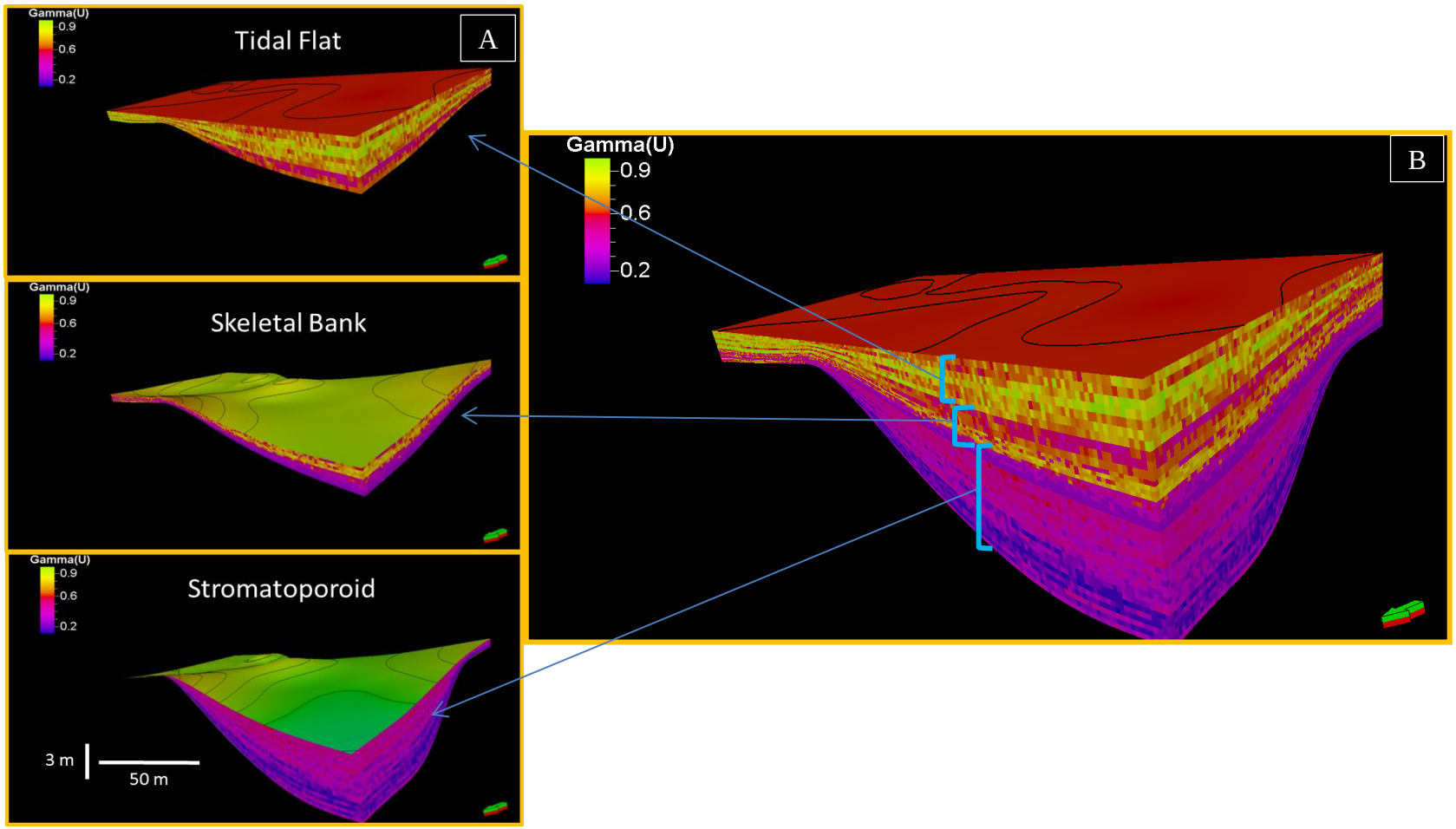

Figure 6-8: 3-D model of U-SGR of the studied outcrop. A) U-SGR values distributed in the 3-D volume of each of the three zones; B) the completed stacked 3-D model for U-SGR logs. Note the increasing upward of U-SGR values in the 3-D model.

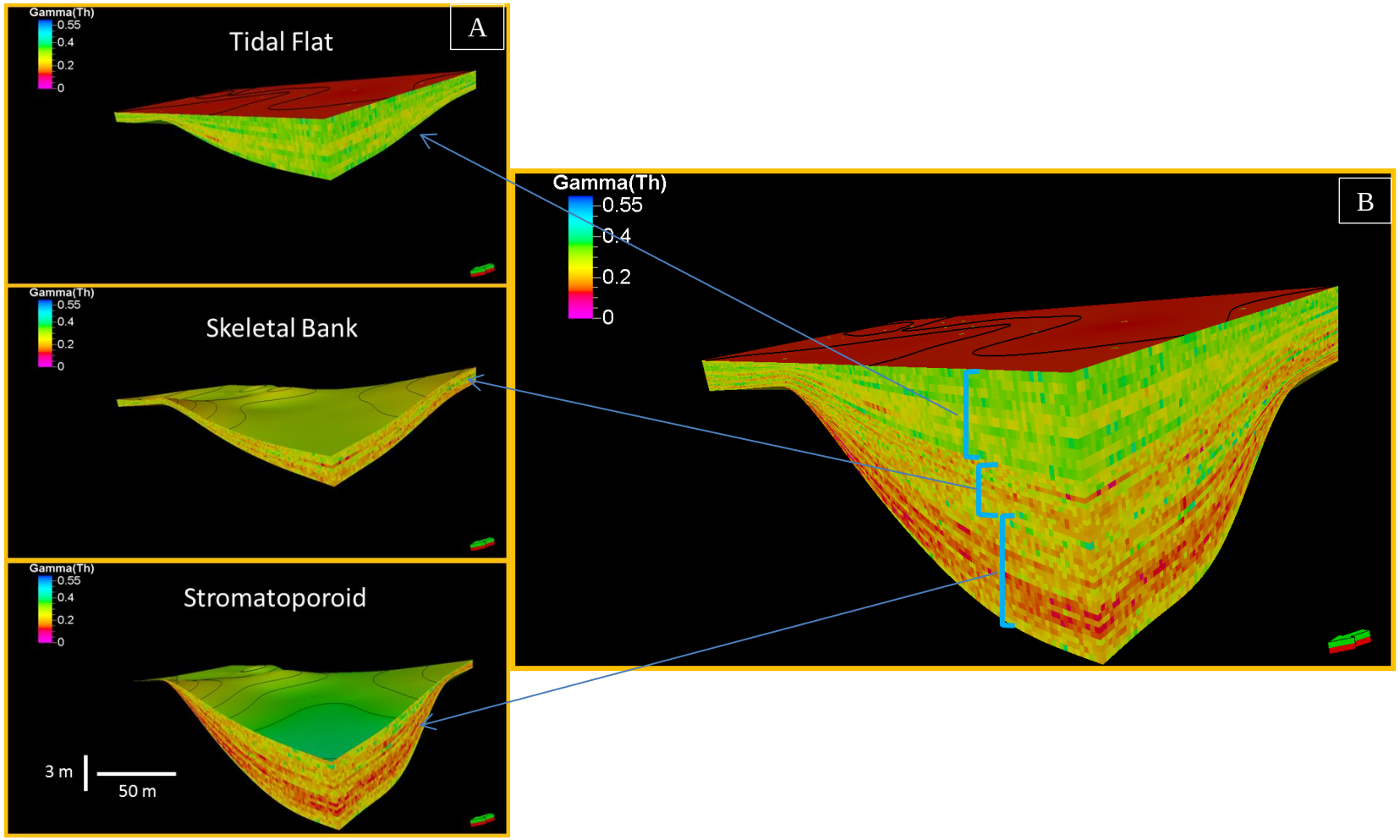

Figure 6-9: 3-D model of Th-SGR of the studied outcrop. A) Th-SGR values distributed in the 3-D volume of each of the three zones; B) the completed stacked 3-D model for Th-SGR logs. Note the increasing upward of Th-SGR values in the 3-D model.

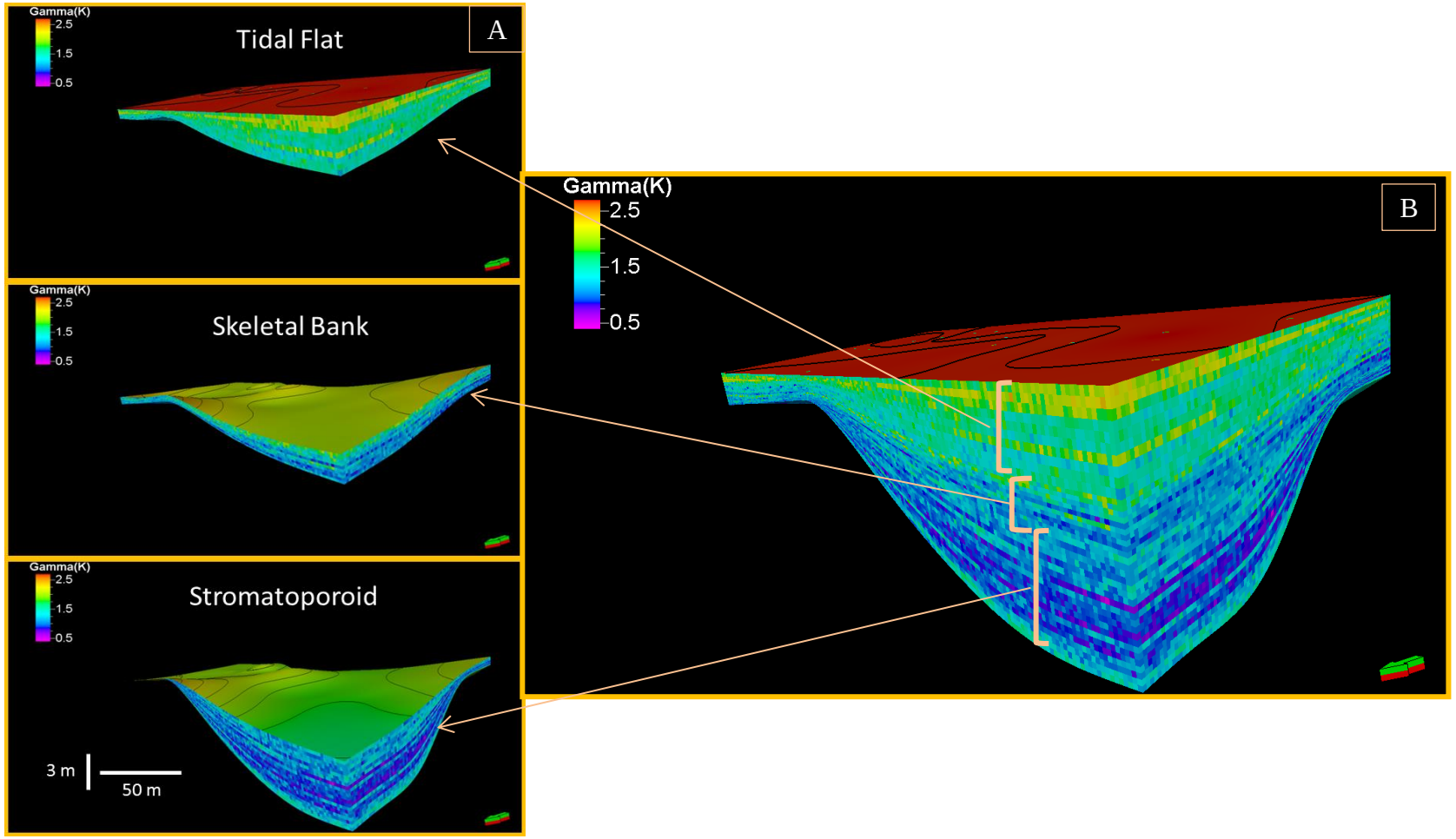

Figure 6-10: 3-D model of K-SGR of the studied outcrop. A) K-SGR values distributed in the 3-D volume of each of the three zones; B) the completed stacked 3-D model for K-SGR logs. Note the increasing upward of K-SGR values in the 3-D model.

6.5 Geochemical Analysis

Whole rock geochemical analysis by ICP-MS revealed four groups of elements and oxides associations that have a significant pattern in the study succession (Figure 6-11).

Group-1 includes SiO_2, Al_2O_3, Fe_2O_3, KO_2, TiO_2, Zr, and Zn. Elements and oxides in this group are associated with detrital sediment fractionated from silicate minerals. Concentration of this group increased upward and had high values in the Arab-D Member and low values in the Upper Jubaila Member. Among the elements and oxides SiO_2 and Zr has exceptionally very high concentration marking the top of HFS-5 and HFS-6 in the Arab-D Member (a good quality reservoir facies). Photomicrographs from the corresponding samples show high quartz content. In contrast, the Upper Jubaila Member in this outcrop showed no differentiation between reservoir rock and non-reservoir rock according to the concentration of this group. If Fe_2O_3 and Zn excluded, the boundary between the Upper Jubaila Member and the Arab-D Member is clearly marked by change from very low to high concentration values of this group.

Group-2 includes CaO, LOI, and Sr. High concentration of this group indicates affinity toward pure carbonate facies and less siliciclastic impurities. Generally, this group has high concentration in all facies association of the study succession, however, relatively low concentrations mixed by relatively high concentration of Group-1 elements were found in the reservoir facies especially in the Arab-D Member.

Group-3 includes only MgO and by definition indicating dolomitic facies. High concentration of this element marked four intervals in the succession. Thin section petrography and SEM-EDS of samples from these intervals confirm the occurrence of dolomitic facies in the same interval. The highest MgO concentration peaks are

associated with zoned dolomite facies occur at the bottom of the Upper Jubaila Member. Other two concentration peaks also occur in the Upper Jubaila Member and associated with . Only one concentration peak of MgO was observed in the Arab-D Member. This peak was associated with fabric preserved dolomitic facies.

Group-4 includes the three radioactive elements K, U, and Th. Elements in this group behave similar to their SGR log response. Concentration values of Th and K show relatively high concentration against lithofacies with good reservoir quality in the stratigraphic succession. In contrast U concentrations show lower values against reservoir facies rocks. Th/U ratio exhibits high values at reservoir facies and low values against non-reservoir facies. Elements concentration in this group and SGR reading from spectrometer shows significant correlation (Figure 6-12, 6-13, and 6-14 and Table 6-1). Other elements in the analysis results do not show any significant indicator and they display with random pattern of peaks and cannot be classified in any of these groups.

6.6 Discussion

6.6.1 SGR Response to Lithofacies Association

Generally, the lithofacies of the studied outcrop could be clearly identified on all of the SGR logs. All log motifs followed a distinctive lithofacies association. The four SGR log profiles in the Upper Jubaila Member were reflected in the four shoaling-upward HFSs of the upper slope to ramp crest deposition environments. The five log profiles of the Arab-D Member reflected on the five shoaling-upward HFSs of the proximal to distal lagoon and skeletal bank deposition environments (Meyer et al. 1996).

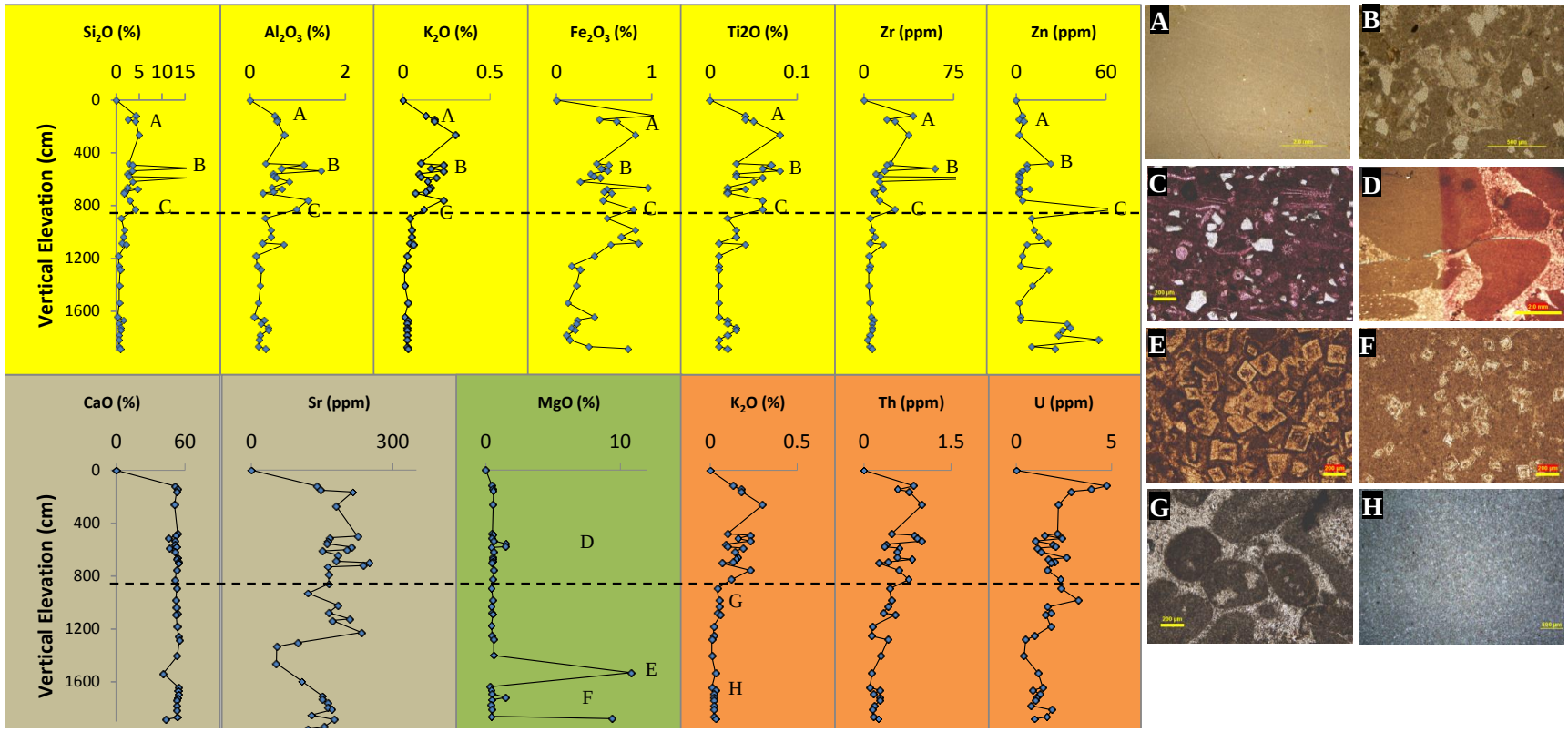

Figure 6-11: SGR log profiles in section 11 show vertical-component results from geochemical analysis for Group 1 (yellow), Group 2 (grey), Group 3 (green), and Group 4 (brown). Reservoir facies are marked by high concentrations of elements from group 1 and 4. The microphotographs on the right show thin sections of selected setion-11 samples. The letters show the corresponding interval in the log profiles. The dashed line represents the boundary between the Upper Jubaila and Arab-D members.

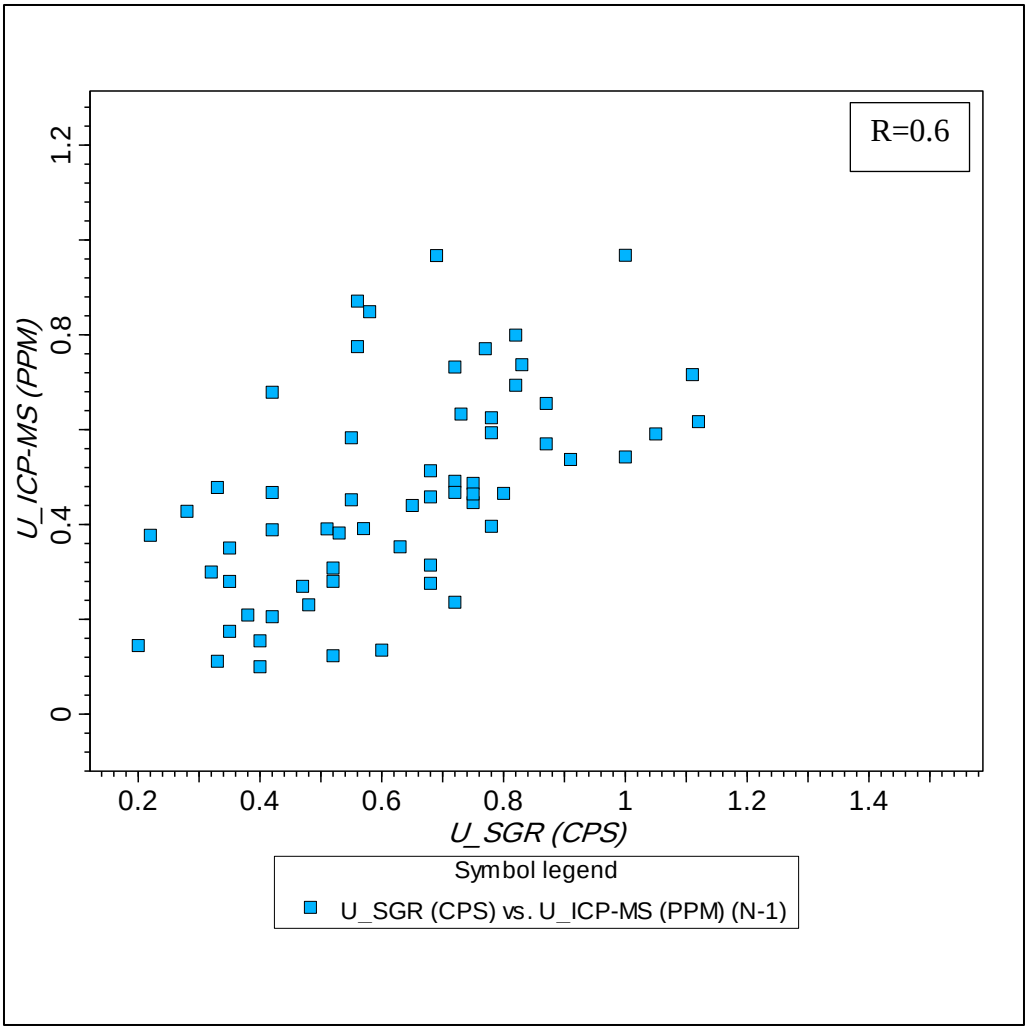

Figure 6-12: Cross plot of U concentrations from ICP-MS versus U from the SGR logs. Note the variation in the relationship which could be attributed to differences between the measurement techniques (ICP-MS measuring points and SGR analysis measuring volume).

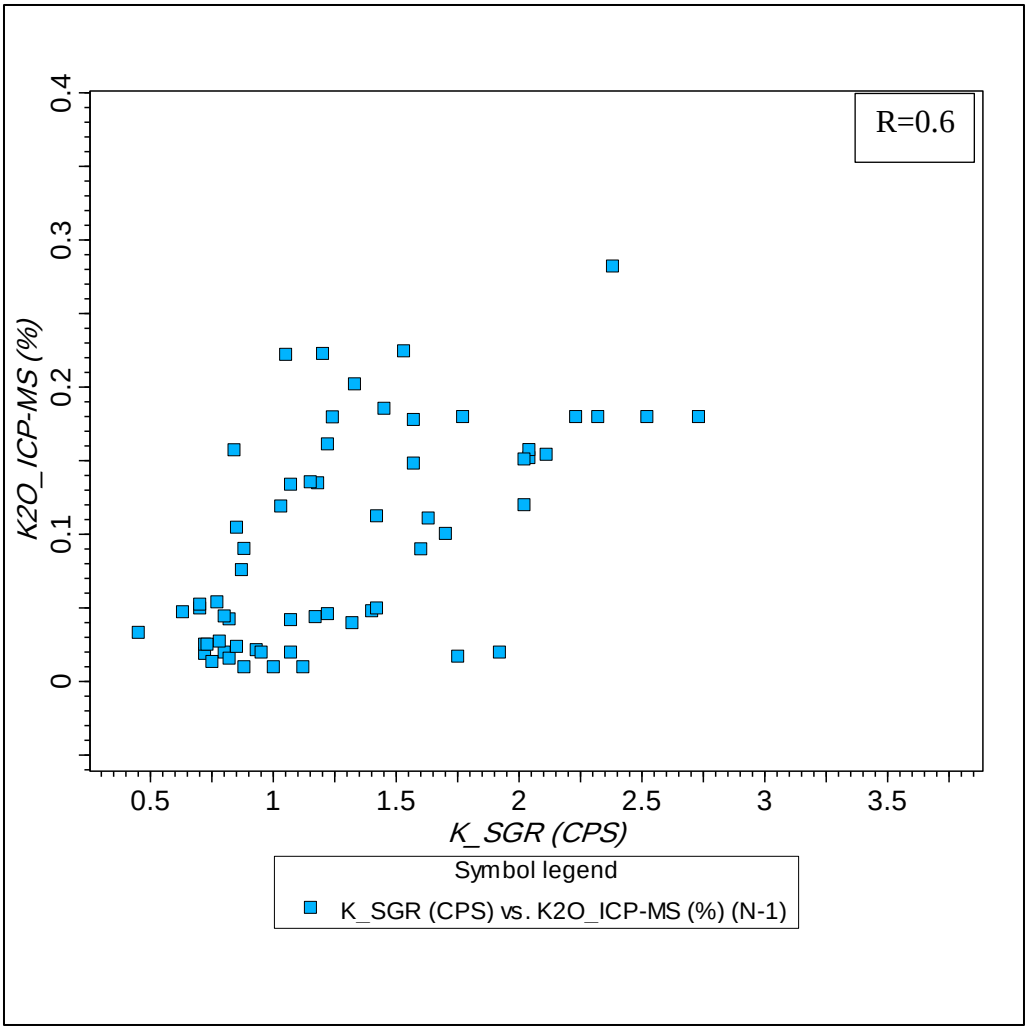

Figure 6-13: Cross plot of K_2O concentrations from ICP-MS versus U from the SGR logs. Note the variation in the relationship which could be attributed to differences between the measurement techniques (ICP-MS measuring points and SGR analysis measuring volume).

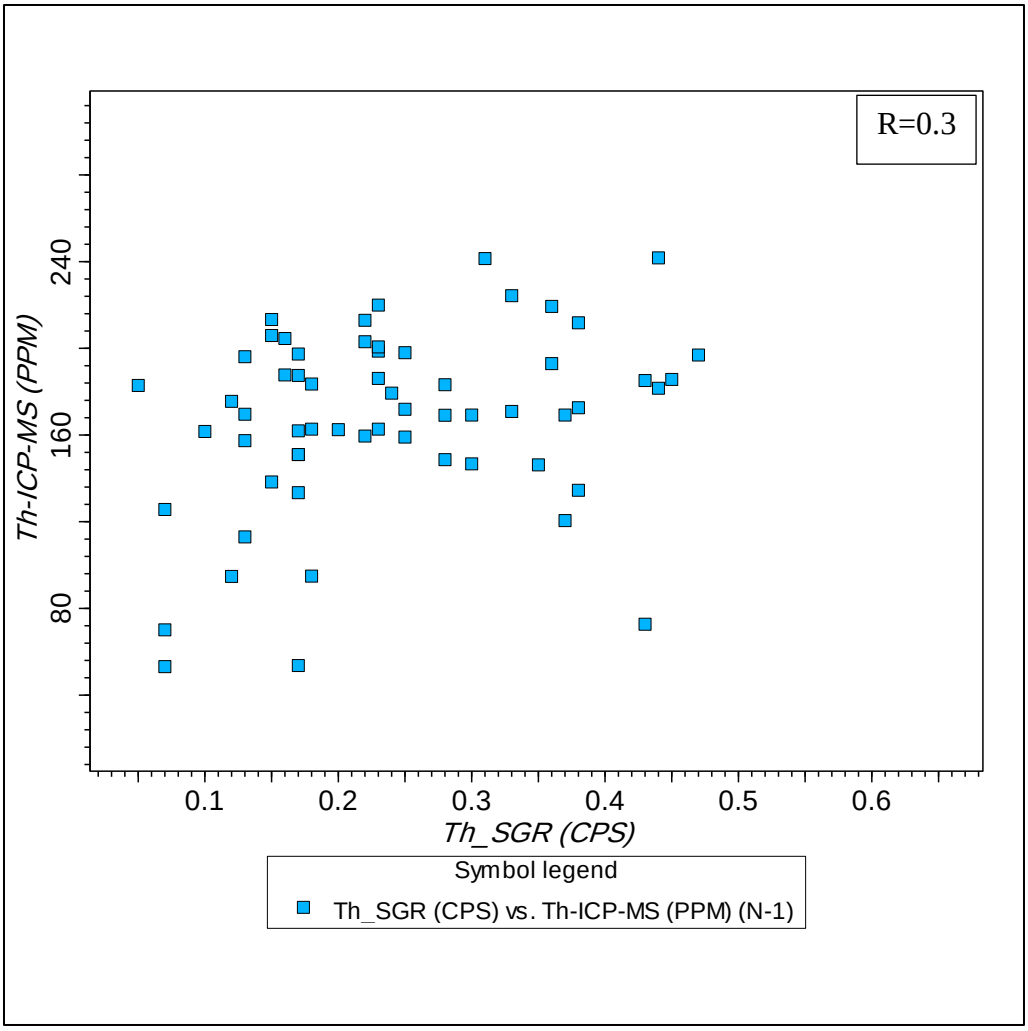

Figure 6-14: Cross plot of Th concentrations from ICP-MS versus Th from the SGR logs. Note the variation in the relationship which could be attributed to differences between the measurement techniques (ICP-MS measuring points and SGR analysis measuring volume).

Table 6-1: Correlation coefficients of the relationship among Group-4 elements measured by two different techniques, SGR logging and ICP-MS.

	K_SGR (CPS)	U_SGR (CPS)	Th_SGR (CPS)	K_2O_ICP-MS (%)	Th-ICP-MS (PPM)	U_ICP-MS (PPM)
K_SGR (CPS)	1.0	0.8	0.8	0.6	0.3	0.6
U_SGR (CPS)	0.8	1.0	0.7	0.7	0.3	0.6
Th_SGR (CPS)	0.8	0.7	1.0	0.6	0.3	0.6
K2O_ICP-MS (%)	0.6	0.7	0.6	1.0	0.5	0.9
Th-ICP-MS (PPM)	0.3	0.3	0.3	0.5	1.0	0.4
U_ICP-MS (PPM)	0.6	0.6	0.6	0.9	0.4	1.0

The Arab-D Member was characterized by higher count per second values of all SGR logs, while the Upper Jubaila Member has relatively very low values. This finding could be attributed to the high content of radioactive elements in the Arab-D Member and was confirmed by elemental analysis from ICP-MS. The four SGR log profiles in the Upper Jubaila Member could be correlated all over the stratigraphic sections that encompass the Upper Jubaila Member. In contrast, correlation of SGR motifs through the Arab-D Member is challenging and show some variation in log motifs.

Because the whole system of the Upper Jurassic formations is shoaling upward (Lindsay et al., 2006) and the Arab-D Member is considered one of the top strata of this system, it is reasonable to find a detrital material input mixed with the carbonate lithofacies in this part of the reservoir. The detrital material input increase upward that reflected in the high SGR reading in the Arab-D Member; however, the detrital material influx did not reach a high enough level to affect the carbonate factory. The angular silt to fine grain quartz (Figure 6-15) in this outcrop suggested that the possible source of these detrital materials is sediments curried by wind current. Arab-D Member of this outcrop may have received more detrital material than the Upper Jubaila Member due to the proximity to the land and shallow depositional environment of the Arab-D Member than the Upper Jubaila Member. Shoaling-upward of Arab-D reservoir system (Wilson 1981; Mitchell et al. 1988; Meyer et al. 1996; Lindsay et al. 2006) could be indicated also by the high concentration of Group-1 elements and oxides. The good correlation between elements in Group-1 and Group-4 as well as data clustering (Figure 6-16) indicates a high terrigenous clastic affinity of lithofacies in the Arab-D Member and a lower terrigenous clastic affinity in the Upper Jubaila Member.

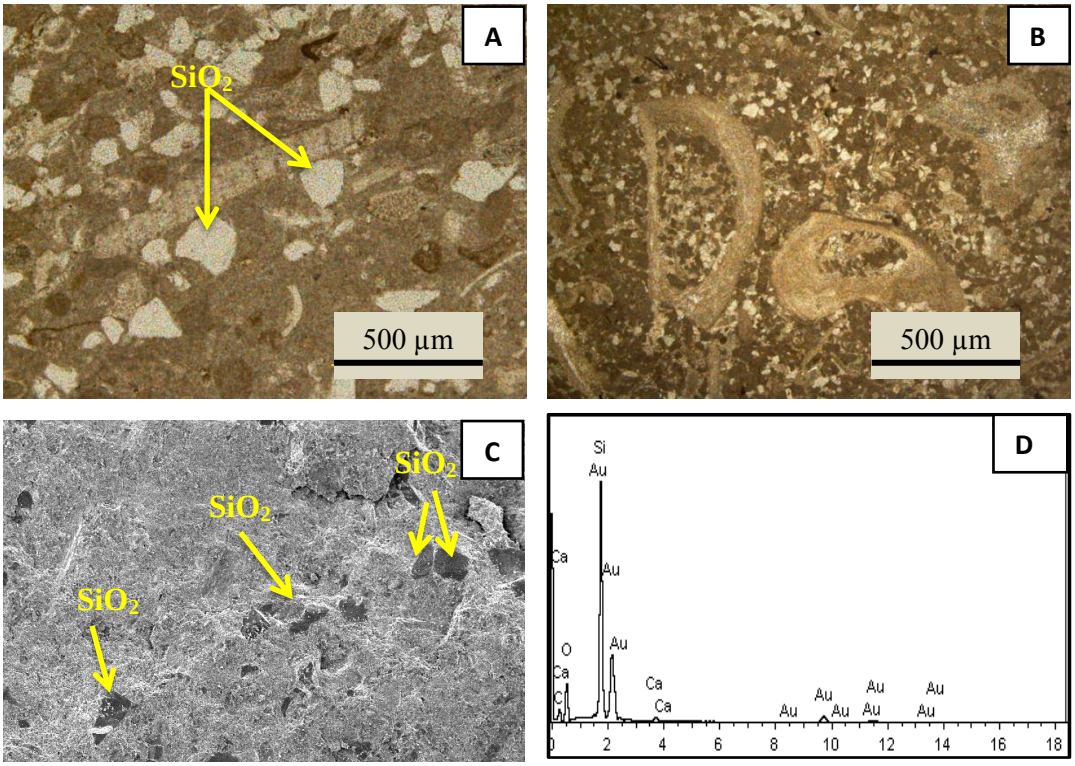

Figure 6-15: Petrographic analysis of samples from the Arab-D Member. A and B) thin-section photographs show quartz grains in silt and fine sand sizes, C) SEM image of the same sample shows quartz grain in dark color, D) EDS peaks for the same sample show a high Si peak indicating the occurrence of quartz. Note that Au was used for coating the samples, and it is not a sample component.

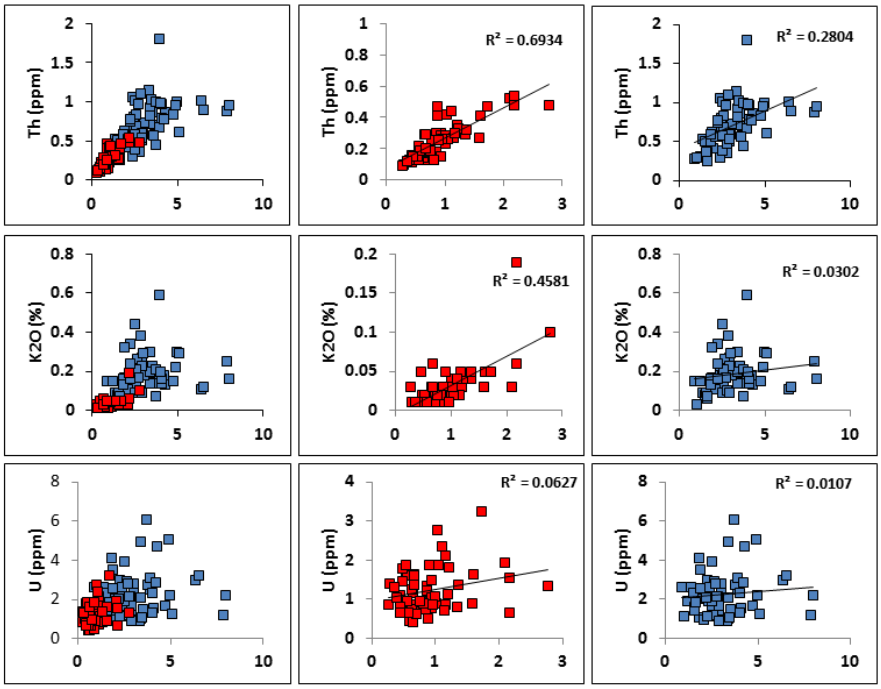

Upper Jubaila Member	K2O (%)	Th (ppm)	U (ppm)
SiO_2 (%)	0.68	0.88	0.28
Al_2O_3 (%)	0.76	0.8	0.08
Fe2O3 (%)	0.23	0.41	0.49
K_2O (%)	1	0.57	0.12
Ti_2O (%)	0.67	0.72	0.09
Zr (ppm)	0.47	0.65	0.19
ZN (ppm)	0.15	0.07	0.02
Sr (ppm)	0.27	0.19	0.5
CaO (%)	0.17	0.09	0.08
MgO (%)	0.01	0.08	0.06
Th (ppm)	0.57	1	0.34
U (ppm)	0.12	0.34	1
K_2O (%)	1	0.57	0.12

Arab-D Member	K2O (%)	Th (ppm)	U (ppm)
SiO_2 (%)	0.13	0.53	0.12
Al_2O_3 (%)	0.53	0.67	0.35
Fe2O3 (%)	0.02	0.3	0.3
K_2O (%)	1	0.62	0.12
Ti_2O (%)	0.54	0.8	0.2
Zr (ppm)	0.18	0.51	0.35
ZN (ppm)	0.28	0.06	0.13
Sr (ppm)	0.24	0.11	0.24
CaO (%)	0.38	0.55	0.11
MgO (%)	0.21	0.09	0.04
Th (ppm)	0.62	1	0.18
U (ppm)	0.12	0.18	1
K_2O (%)	1	0.62	0.12

Figure 6-16: Cross plots of radioactive elements versus SiO_2 from ICP-MS geochemical analysis showing significant correlation between Th and SiO_2 for both the Arab-D (blue squares) and the Upper Jubaila (red squares) members and between K_2O and SiO_2 for the Jubaila Member but not the Arab-D Member. The plot of SiO_2 versus U shows no significant correlation between these variables for either the Arab-D or Upper Jubaila members. The two matrices on the right show linear correlation coefficients (R) for the radioactive elements with other elements and oxides in Group 1 (yellow), Group 2 (grey), Group 3 (green), and Group 4 (brown).

This trend of data confirming the upward shoaling pattern of the system as well as the flux of land detrital materials from same sedimentary sources. Figure 6-17 shows relationship between SiO_2 and the other elements and oxides in Group-1. This figure indicate clear separation between the Arab-D Member and the Upper Jubaila Member in term of elemental content. The associated matrices in Figure 6-17 show statistical parameters for elemental content for both Arab-D and Upper Jubaila members and indicate that higher elemental concentration found in the Arab-D Member.

6.6.2 Reservoir Zonation

The SGR logs values have a unique reflection pattern on the Upper Jubaila Member and the Arab-D Member boundary. Geochemical data analysis showed the same unique reflection pattern on the boundary between the two members. The cross plots conducted in this study reveal two clusters of data The Upper Jubaila Member data concentrate at the bottom of the plot and show very low elemental concentration values, while the data for the Arab-D Member show high elemental concentration values. The plots also show good correlation between radioactive elements and Group-1 elements for both the Arab-D and the Upper Jubaila members. There is a significant correlation between K_2O with SiO_2 for the Jubaila Member and no siginificant correlation with Arab-D Member. The plot of SiO_2 versus U shows no significant correlation between these variables for both the Arab-D and the Upper Jubaila members. This result may indicate that high concentration of detrital material (represented by SiO_2) associated with high values of Th and K SGR logs while for the U SGR this may or may not be correct. As the boundary between the Arab-D and the Upper Jubaila members is a problematic issue in subsurface reservoir mapping, using the SGR logs and elemental reflection pattern and the integrated

Group-1 plots with radioactive minerals could provide a reliable method to determine the exact position of the boundary.

Thorium and potassium are considered as detrital element characterized by relatively high degree of insolubility (Parkinson, 1996; Osmond and Ivanovich, 1992), therefore, high concentration of these two radioactive elements always associated with high concentration of other detrital elements from Group-1. The possible source of these elements fractionated from silicate minerals and indicate proximal shallow depositional environment (high degree of terrigenous clastic input). Uranium is considered more soluble with relatively higher degree of mobilization which allows for leaching and concentration in a deep water condition and always associated with very low concentration of detrital elements (low degree of terrigenous clastic input) (Schnyder et al., 2006). Observations made from sedimentological and stratigraphical analysis at outcrop suggested relatively deeper water depositional environment for the Upper Jubaila Member (Upper to lower slope of ramp platform) and relatively shallower water depositional environment for the Arab-D Member (Lagoon to tidal flat of ramp platform). According to this interpretation the Upper Jubaila Member is most likely will receive less detrital material than the Arab-D Member due to the proximity of the depositional environments. Therefore, the Upper Jubaila Member is supposed to have less content of U, Th, and K than the Arab-D Member. The concentrations of the radioactive elements (U, Th, and K) increase vertically following the same trend of shoaling upward of the outcrop. Figure 6-18 shows U and Th data for seven stratigraphic sections in the studied outcrop. These stratigraphic sections show that the Upper Jubaila Member has relatively lower values of both U and Th SGR than in the Arab-D Member.

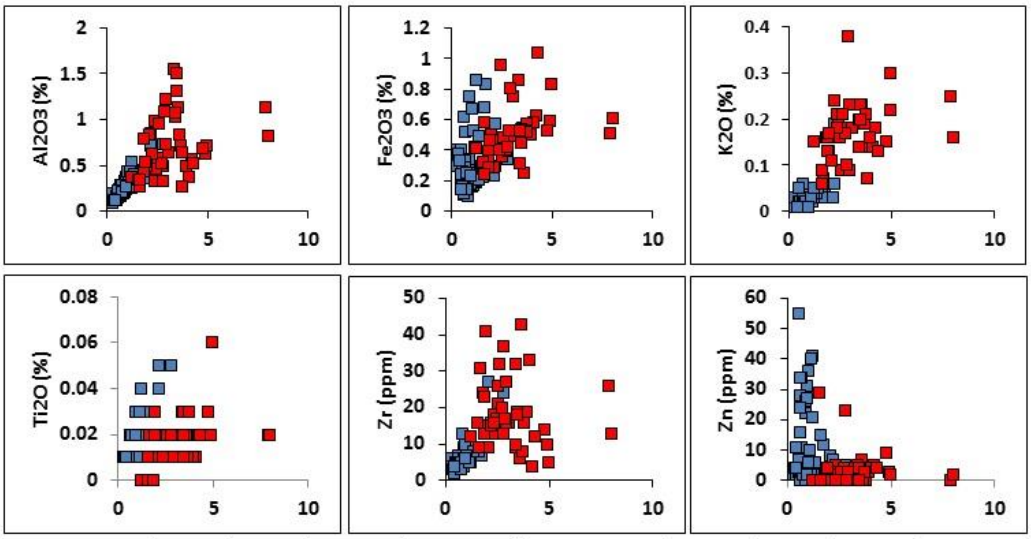

Upper Jubaila Member				
	Max	Min	Mean	St. dev.
SiO_2 (%)	2.78	0.27	0.92	0.53
Al_2O_3 (%)	0.85	0.09	0.29	0.16
Fe2O3 (%)	0.86	0.1	0.3	0.19
K_2O (%)	0.19	0.01	0.03	0.03
Ti_2O (%)	0.05	0.01	0.02	0.01
Zr (ppm)	27	2	6.79	4.73
ZN (ppm)	234	2	11.25	12.34
Sr (ppm)	234	42	132.8	43.86
CaO (%)	56.6	41	53.7	2.4
MgO (%)	10.8	0.22	1.15	2.49
Th (ppm)	0.19	0.01	0.03	0.03
U (ppm)	0.54	0.09	0.25	0.12
K_2O (%)	0.19	0.01	0.03	0.03

Upper Jubaila Member				
	Max	Min	Mean	St. dev.
SiO_2 (%)	2.78	0.27	0.92	0.53
Al_2O_3 (%)	0.85	0.09	0.29	0.16
Fe2O3 (%)	0.86	0.1	0.3	0.19
K_2O (%)	0.19	0.01	0.03	0.03
Ti_2O (%)	0.05	0.01	0.02	0.01
Zr (ppm)	27	2	6.79	4.73
ZN (ppm)	234	2	11.25	12.34
Sr (ppm)	234	42	132.8	43.86
CaO (%)	56.6	41	53.7	2.4
MgO (%)	10.8	0.22	1.15	2.49
Th (ppm)	0.19	0.01	0.03	0.03
U (ppm)	0.54	0.09	0.25	0.12
K_2O (%)	0.19	0.01	0.03	0.03

Figure 6-17: Cross plot of Group-1 oxides and elements versus SiO_2 shows clear data clustering of the Upper Jubaila and Arab-D members. The two matrices at the bottom show minimums, maximums, means, and standard deviations for Group 1 (yellow), Group 2 (grey), Group 3 (green), and Group 4 (brown) for both the Upper Jubaila and Arab-D members.

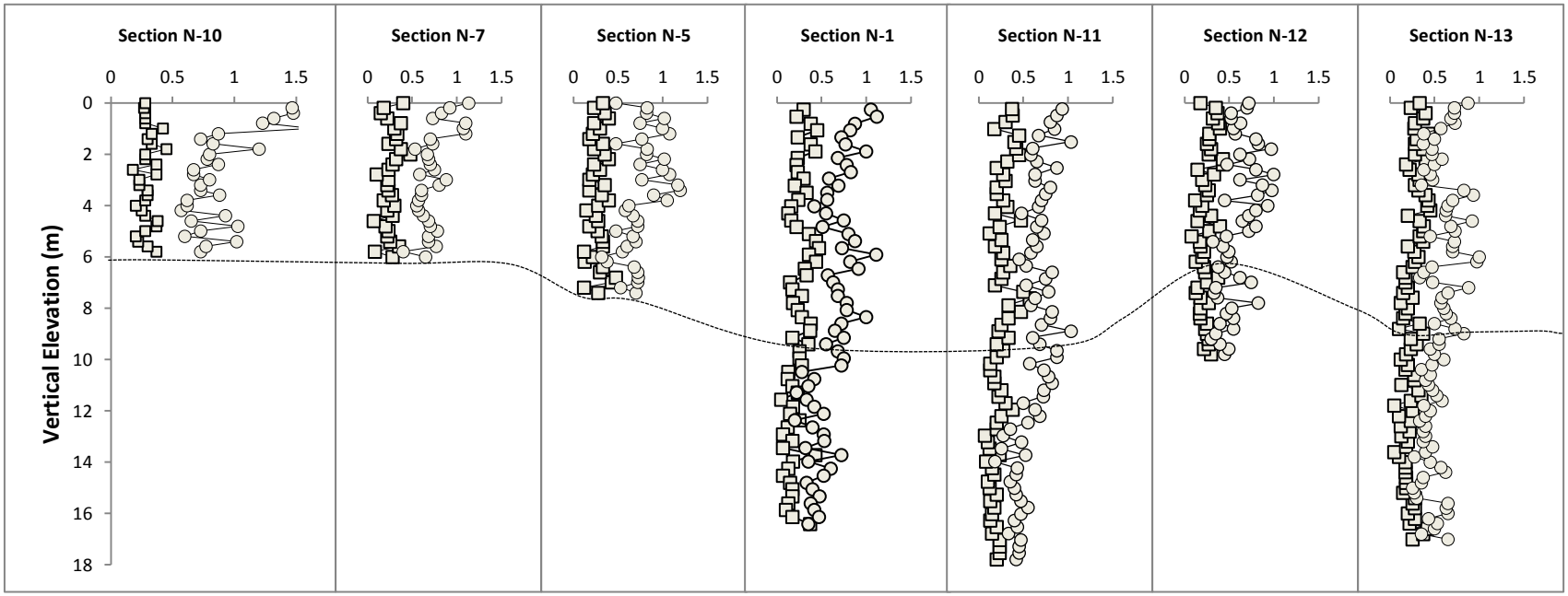

Figure 6-18: U (squared) and Th (circled) SGR logs of 7 stratigraphic sections that encompasses both the Upper Jubaila and Arab-D members. The boundary between the two members is indicated by the dashed line.

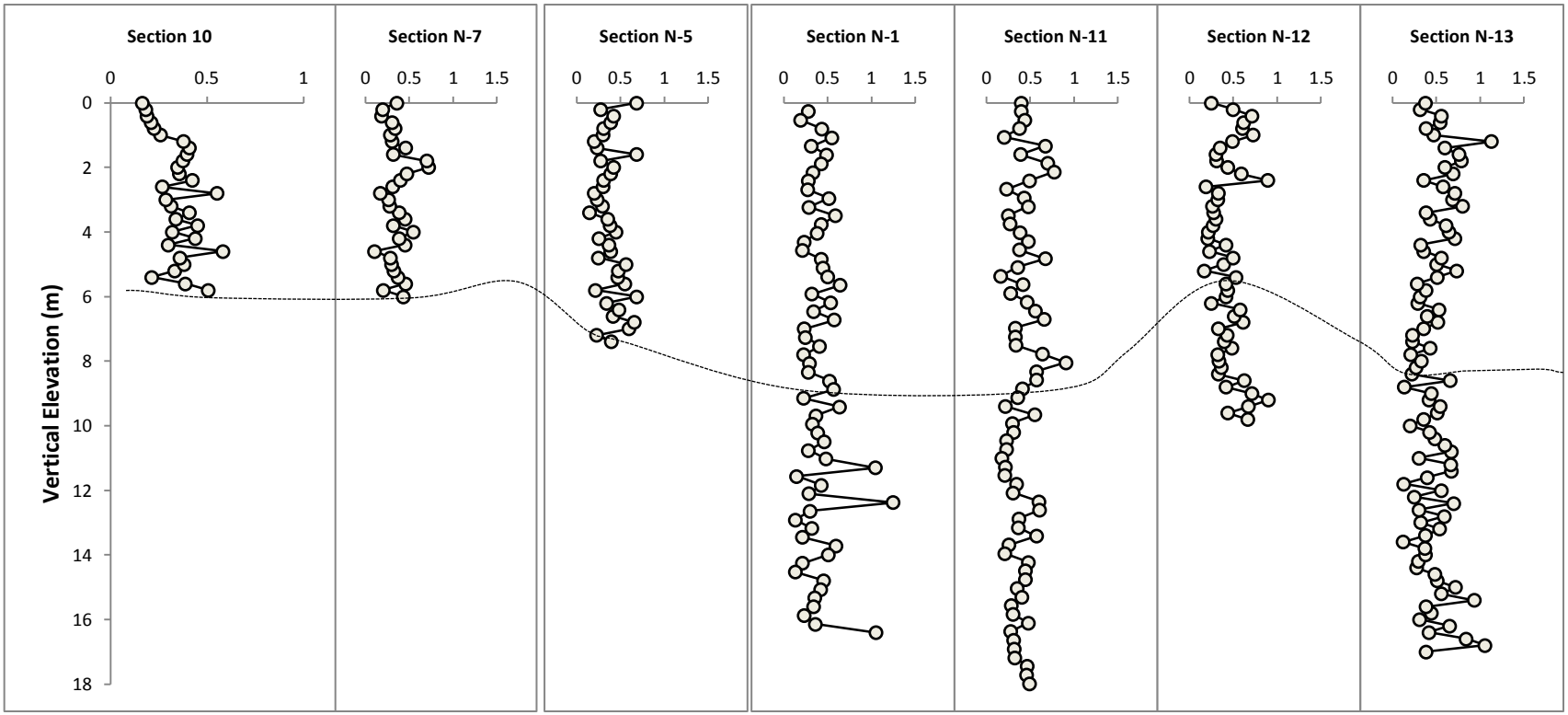

Figure 6-19: Th/U ratio of 7 stratigraphic sections that encompasses both the Upper Jubaila and Arab-D members. The boundary between the two members is indicated by the dashed line.

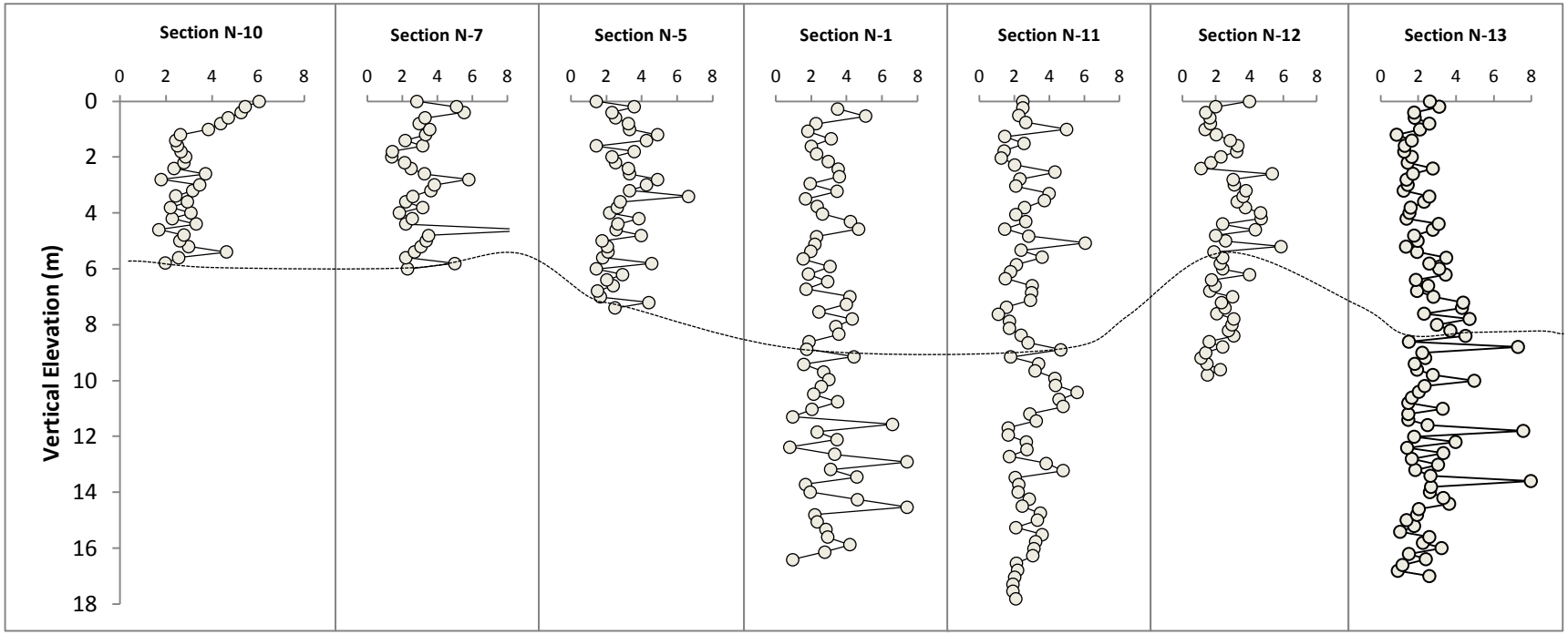

Figure 6-20: U/Th ratio of 7 stratigraphic sections that encompasses both the Upper Jubaila and Arab-D members. The boundary between the two members is indicated by the dashed line.

This Figure also shows that the values of Th and U SGR are varying vertically from one interval to another and not remain constant. This trend is also obvious in Group-4 element concentration vertical distribution shown in Figure 6-18 . This might indicate a change in water chemistry very frequently according to rapid sea level change. Th/U ratio is an excellent indicator of water chemistry in term of oxidizing and reducing conditions (Koptíková et al. 2010), and can be used to interpret the water depth of the depositional environment and the associated lithofacies. The higher ratio of Th/U is related to domination of detrital elements, indicates very shallow and well-oxygenated marine water, while the lowered ratio of Th/U is related to the increase of U solubility, and indicates deep and reducing marine water condition. Th/U ratio could be viewed in a context of sea level rise and fall where the high stand system tracts of the HFSs in the study succession marked by high Th/U ratio, which is supported by coarse, fossiliferous, sandy, laminated carbonate lithofacies of tidal flat and skeletal bank deposits in the corresponding interval of the upper section of the reservoir (Arab-D Member) and by oncoidal packstone and grainstone of ramp crest and shoal deposit in the lower section of the reservoir (the Upper Jubaila Member) (Figure 6-19).

The transgresive system tracts may represented by low Th/U ratio, which characterized by platy laminated mudstone of a deep lagoonal setting in the upper section of the outcrop and dolomitic wackestone, dolomitic mudstone of upper to middle slope in the lower part of the outcrop when inverse this ratio (Th/U to be U/Th) there are a very sharp peaks marks the muddier interval indicating deep water condition (Figure 6-20). Depositional environments change from lower and upper slope to ramp crest into lagoonal setting and finally tidal flats. This change of depositional environments and

shoaling upward system was reflected on the elemental composition of lithofacies comprise the succession. This observation coincides with observed SGR logs and its Th/U ratio. Logs of Group-1 and Group-4 elements show the same results.

With respect to the implications for exploration, the method of integration geochemical analysis with SGR logs is a very useful and economic method for differentiating between reservoir facies and non-reservoir facies because a SGR log is commonly available in logging programs. Once the cutoff of the SGR logs and concentration of elements and oxides in different groups are established the differentiation between reservoir and non-reservoir facies can be applied easily. In this study, it was observed that high concentration values of Group-1 and Group-4 elements along with Th/U ratio indicated all of the reservoir facies (stromatoporoid wackestone and packstone, peloidal sandy fossiliferous intraclastic packstone and grainstone, and laminated sandy grainstone).

CHAPTER 7

DISCUSSION

7.1 Significance of Outcrop Study

The development of reliable models of subsurface reservoirs depends on many geological parameters. These geological parameters define both the geometrical distribution of the reservoir units and the internal heterogeneity of these units (Cantrell and Hagerty, 1999; Lucia, 2004). The regional distribution of reservoirs units is controlled by their special and temporal distribution, their geo-bodies distribution, and their intra-reservoir stratigraphy. On the other hand, the local variability of reservoir parameters is controlled by reservoir facies change, grain types, size, and sorting, sedimentary structure, geochemical signatures, and diagenetic overprints. The heterogeneity of these geological parameters is very high, especially in carbonate setting (Sahin and Saner, 1999; Sahin et al., 2007). Considering the large inter-well area within individual oil field, rare horizontal wells, and the low resolution of seismic data, the characterization and Modelling of these parameters requires more understanding. Poor understanding of the geological parameters of reservoirs will introduce a significant problem in understanding flow units (Meyer et al., 1996) and will, therefore, affect optimum hydrocarbon recovery.

Outcrops are always used, where possible, to address the limitation of having low resolution subsurface data and to overcome the challenges associated with subsurface reservoir Modelling (Pringle et al., 2004). Outcrop analogs have the potential to improve

understanding of the intra-reservoir stratigraphy and thus give valuable information about regional distribution of geological parameters. Outcrop analogs, also, provide rock-based data on the vertical and lateral characteristics of hydrocarbon reservoir lithofacies equivalents in different orientations which will allows the examination of reservoir equivalent rocks on different resolution scales.

7.2 Improvement of geological model of the Arab-D reservoir Using Outcrop Study

The answer of the question what is importance of having outcrop studies for hydrocarbon reservoir is simply to improve exploration and exploitation of hydrocarbon recovery (Stoudt et al., 2004). Carbonate reservoirs are very heterogeneous because of lateral facies changes and digenetic alteration, and commonly yields far less than their estimated reserves. Thus any improvement of these reservoirs would result in a considerable amount of recovery. This study helps to improve reservoir understanding in the following ways:

1. The 3-D facies model for the outcrop allows the heterogeneity of the reservoir lithofacies to be examined at a higher resolution than in the subsurface model. Different scales of lithofacies characterization will significantly enhance Arab-D reservoir understanding.
2. The model is capable of capturing small-scale lithofacies heterogeneities that could influence the distribution of porosity and permeability in the subsurface reservoir.

3. The outcropping strata is reflecting different signatures of spectral gamma ray profile, which might be excellent character for differentiating reservoir units.
4. The geochemical data showed marked differences in characteristics and distribution of different reservoir units and layers, which might help in reservoir zonation.
5. Study of microporosity at an outcrop scale might provide a better understanding and prediction of the quality in subsurface reservoirs.

7.3 Comparison Between Outcrop Results and Published Subsurface Data

This study considered comprehensive research in which different disciplines of reservoir characterization and Modelling were integrated together to build a high-resolution reservoir model. This model has the potential to facilitate the understanding of the available actual reservoir model of the Arab-D reservoir. To illustrate how the studied outcrop analogs are applicable to the actual subsurface Arab-D reservoir, this study was compared to several published data from different areas within Ghawar field and fields in the UAE, given that there is a large amount of published data on the Arab-D reservoir that can be subjected to this type of comparison.

Incorporating outcrop results in subsurface reservoirs models provides an enhancement of the 3-D description of reservoirs and can be performed in several research avenves. These include sharpening the 3-D conceptual model of reservoirs, identifying small scale geological features that could significantly influence the petrophysical parameters of flow

units, or by qualitatively and quantitatively describing different scales of the reservoir stratigraphy and their characteristics. This integration might have a significant implication for the heterogeneity of the intra-stratigraphy of a reservoir at the inter-well scale and provide more understanding of small-scale heterogeneities. The outcrop results should first be compared to the subsurface reservoir to establish a strong relationship between their similarities and to avoid incorporating non-similar geological features in the reservoirs models.

The most important comparison in this study is comparing the strata geometries, the lithofacies association, and the depositional environments observed in different oil fields in Saudi Arabia and UAE to the intra-stratigraphic architectures observed at the outcrop level and discussing the importance and implications for hydrocarbon exploration and production. The comparison procedure encompasses the published results on lithofacies by Mitchell et al. (1988); Meyer and Price (1993); Wilson (1995); Meyer et al. (1996); Handford et al. (2002); Lindsay et al. (2006). For the diagenetic overprint and dolomitization, this study was compared to the published results by Basyuni (1992), Cantrell et al. (2004a), Swart et al. (2005), Cantrell et al., (2007), Cantrell (2008), Basyuni and Khalil (2011), and Muraad et al. (2012). For high resolution sequence stratigraphy, this study was compared to the results of Lindsay et al. (2006). For the bio-components and bio-stratigraphical correlation, this study was compared to the published results by Hughes (1996), (2004a), (2004b), (2009), Al-Debeeb (2005), and Lindsay et al. (2006). For 3-D geostatistical Modelling, this result was compared to the published results by Douglas (1996) and Sahin (1998). The petrophysical parameters were compared to the published results by Saner and Sahin (1999), Cantrell et al. (2001), and

Lucia et al. (2001). The microporosity estimation was compared to the published results by Cantrell and Hagrety (1999) and Deville de Periere et al. (2011).

The major similarities between the study outcrop and the subsurface Arab-D reservoir as indicated by Meyer et al. (1996) are (a) the stacking pattern of the lithofacies as Muddy-Grainy-Muddy and (b) that similar lithofacies types occur in both the subsurface and the outcrop. These types include stromatoporoids, burrowed lithofacies, dolomitic mudstone and wackestone. (c) Dolomitic mudstone and wackestone occur in a position similar to that of the actual Arab-D reservoir. Observation made by this study confirmed the stacking pattern similarity between this outcropping strata and the subsurface Arab-D reservoir. The Ficsher Plot of the outcrop shows characteristics similar to the subsurface Ficsher Plot by Lindsay et al. (2006) with a 1:3 subsurface reservoir to outcrop thickness ratio. Instead of the general shoaling upward pattern of stratigraphic units suggested by Meyer et al. (1996), this study proposed fining upward debris models. The major differences between the study area and the subsurface Arab-D reservoir are (a) the absence of lithofacies such as branched and fragmented Cladocoropsis, skeletal coated grains, and oolitic grainstone lithofacies; (b) the thickness is 60% less than in the actual subsurface reservoir; (c) the outcrop shows more muddier facies than the subsurface reservoir; and (d) the porosity and the permeability are far lower than those values for the subsurface reservoir.

The subsurface lithofacies show lateral changes in the thickness from south to north in Ghawar field (Mitchel, 1995; Hanford et al., 2002). The later authors and Lindsay et al. (2006) interpreted this thickness change as an increase of the evaborite/carbonate ratio toward the north, which was attributed to the change of the depositional environments

from a deep intra-shelf basin in the south to a shallower setting in the north. The same scenario is applicable when comparing the outcropping strata in central Saudi Arabia to the Arab-D reservoir in the eastern Ghawar field. The muddier lithofacies and the scarcity of bifacies component indicated that the outcrop setting is more of a lagoonal and tidal flat setting.

7.4 Reservoir Zonation

The boundary between the two composite sequences of the Arab-D reservoir (the Upper Jubaila and Arab-D Member of the Arab Formation) is not completely understood in the subsurface and requires more accurate criteria for recognition (Al Dhabeeb, 2005) because the Arab-D reservoir was first defined based on hydrocarbon productivity in the subsurface rather than the lithostratigraphy or the biostratigraphy of the equivalent strata (Powers, 1968). The later author stated that the boundary of the Upper Jubaila and Arab-D falls near the middle of the Arab-D reservoir. This boundary is very important because it divides the Arab-D reservoir to two distinctive lithological packages.

This study provides an integrated approach to distinguishing between the two units of the Arab-D reservoir. The integration of spectral gamma ray and trace element data allows identification of the mineralogical differences between the Upper Jubaila and Arab-D members, which could be a very useful tool. The geochemical data of the Arab-D Member in the study area show marked differences in character and distribution from the Upper Jubaila Member. The data reflect the increasing upward concentrations of elements and oxides that possibly fractionated from silicate minerals. This trend is

accompanied by a remarkable increase of $^{87}Sr/^{86}Sr$ compared to the global Upper Jurassic seawater $^{87}Sr/^{86}Sr$ ratio.

With respect to the implications for exploration, the method of integrating geochemical analysis with SGR logs is a very useful and economic method for differentiating between reservoir facies and non-reservoir facies because a SGR log is commonly available in logging programs. Once the cutoff of the SGR logs and the concentration of elements and oxides in different groups are established, the differentiation between reservoir and non-reservoir facies can be applied easily. In this study, it was observed that high concentration values of Group-1 and Group-4 elements and a high Th/U ratio were indicated in all of the reservoir facies (stromatoporoid wackestone and packstone, Peloidal sandy fossiliferous intraclastic packstone and grainstone, and laminated sandy grainstone).

7.5 Limitations

Outcrop studies proved to be a significance proxy for reservoir characterization and Modelling because it provides an approximation of what geologists may encountered in the subsurface reservoirs. In this study, outcrop strata equivalent to the Arab-D reservoir was used to conceptualizing the depositional environments, the paleogeography, the spatial distribution, and the petrophysical 3-D distribution of the reservoir equivalent facies; However, as indicated by White et al. (2004), it is not easy to find perfect outcrop that completely similar to the subsurface reservoir and there are always some limitations of outcrop studies. This emphasis that some geological characters of the hydrocarbon reservoir could be observed both in the subsurface and outcrop, while some may not.

The features that can be observed in the outcropping Arab-D strata and the actual subsurface Arab-D reservoir were compared and discussed in the previous chapters and earlier in this chapter. There are several features present in the actual Arab-D reservoir that cannot be observed in the outcrop. For example, microporosity between marine cementation and in the carbonate grains was totally obliterated due to heavy meteoric diagenesis. Porosity and permeability data of the outcrop doesn't reflect the real characteristic of the actual Arab-D reservoir because all the pore system was completely cemented by meteoric cementation. The lack of sufficient porosity and permeability data from outcrop samples limited the understanding of pore system distribution, pore system connectivity, and porosity-permeability relationship in the outcrop.

Meteoric cementation also changes the isotopic signature of lithofacies and shifted the oxygen and carbon isotopes toward more of negative values. This makes the interpretation of diagentic regime of the Arab-D reservoir in outcrop is not completely understood. These high values of negative oxygen and carbon isotopes also limited the understanding of dolomitization and dedolomitization processes and occurrence in the Arab-D reservoir outcrop analog (Cantrell et al. 2007). Non-fabric preserving dolomite, associated with high flow permeability (super-K interval) in the subsurface Arab-D reservoir, was clearly defined from other dolomitic interval by their isotopic signature (Cantrell 2001; Swart 2005). Conversely, this dolomitic interval could not be distinguished based on isotopic signature in the outcrop although it was petrographically observed. This also attributed to the long exposure of the outcrop and the heavy meteoric cementation. Arab-D outcropping strata showed less biocomponent diversity than that of the actual subsurface reservoir. This may limited the process of reconstruction of

reservoir paleoenvironment in the outcrop. The outcrop locations discussed in this study are all have strike and dip exposure; however, exposures along the strike have the best continuity following the general trend of central Saudi Arabia uplifting. The facies conceptual and geostatistical models discussed in this study is hampered by the limited dip direction exposure of the outcrops. Since there was no proposed shallow drilling program for this study, adding dip direction as additional dimension to the outcrop models remains one of the upcoming tasks.

CHAPTER 8

CONCLUSIONS AND RECOMMENDATIONS

8.1 Conclusions

This study investigates vertical stacking patterns and the lateral continuity of facies in outcropping strata that are equivalent to the Arab-D reservoir in central Saudi Arabia. The study presents sedimentological and petrographic descriptions of lithofacies associations and interprets them within a high order stratigraphic framework using Spectrum Gamma Ray (SGR) logging and geochemical correlations, petrography and micropaleontology. The study could be summarized as the following conclusions:

The sedimentological studies revealed three lithofacies associations:

Stromatoporoid Lithofacies Association include:

- Dolomitic mudstone and dolomitic wackestone
- Stromatoporoid wackestones and packstones

Skeletal Bank Lithofacies Association include:

- Burrowed fossiliferous wackestones
- Peloidal fossiliferous grainstones

Tidal Flat Lithofacies Association Include:

- Laminated mudstones
- Wavy rippled sandy grainstones
- Breccia and mud-clasts

These lithofacies were interpreted to have been deposited in a gentle slope platform environment. A total of 44 cycles were identified using SGR logs, with cycle thicknesses ranging from 15.2 cm to 255 cm. These cycles comprise nine high frequency sequences.

The biocomponents of the study area show a lower degree of diversity than the subsurface Arab-D reservoir; however, some key biofacies are present and provide palaeoenvironmental and reservoir zonation indicators.

The diagenetic features in the outcropping strata equivalent to the Arab-D reservoir include: a) micritization ; b) marine cementation; c) dissolution; d) early dolomitization; e) equant blocky calcite cementation; f) micrite recrystallization; g) Compaction; h) late dolomitization; i) dedolomitization; j) meteoric cementation; and k) fracture filling.

The outcrop analog for the Arab-D reservoir was used to build a high resolution model that captures fine geologic details. Subsurface reservoir lithofacies were matched with those from the studied outcrop, and porosity values derived from published core and well log data from the Ain Dar, Uthmanyah, and Shudgum areas of the Ghawar Field, eastern Saudi Arabia, were then applied to the equivalent lithofacies in the outcrop. Potential reservoir zones were associated with grainstone, packstone and some wackestone layers. Semivariogram analysis of the lithofacies showed good continuity in the N-S direction and less continuity in the E-W direction. The high resolution lithofacies models detected

permeability barriers and isolated low porosity bodies within the potential reservoir zones.

Microporosity and permeability in the analysed samples range from 0.4% to 6.4 % and 0.02 to 1.2 mD, respectively. Three types of microporosity were present: (1) between macro- and micro-sized grains of sparry calcite; (2) between micrite grains of varying morphologies; and (3) within macro-sized dolomite crystals. Microporosity distribution was controlled by sparry calcite cement, micrite grain size, sorting and shape, and the presence of dolomite crystals. The main controls on microporosity are grain-to-matrix ratio and micrite-to-cement ratio, and possibly dolomitization. Statistical analysis of microporosity and its associated permeability exhibits positive skew of the data set, indicating non-normal distributions for both variables. Coefficients of variation indicated high variability for both porosity and permeability, which may be attributed to the high degree of heterogeneity in the pore system. The relationship between microporosity and permeability was characterized by low values of correlation coefficients, indicating scattering of the data set. However, the correlation improves significantly when visualized for individual lithofacies.

Investigation of Spectral Gamma Ray (SGR) and Inductively Coupled Plasma-Mass Spectrometry (ICP-MS) geochemical analysis of the Arab-D reservoir analog revealed a strong correlation between the SGR response of the outcrop lithofacies and their elemental content. The two units of the reservoir (the Upper Jubaila Member of the Jubaila Formation and the Arab-D Member of the Arab Formation) show distinctive SGR log profiles controlled mainly by lithofacies associations. Geochemical analysis revealed four groups of elements association: Group-1 includes SiO2, Al_3O_2, Fe_2O_3, K_2O, TiO_2,

Zr, and Zn. This group has strong relationship with radioactive elements U, K, and Th, which represent Group-4, both with their concentration percentages and their counts per second (CPS) based on spectrometry. Reservoir facies exhibit high concentration of elements of these two groups. Group-2 includes CaO and Sr. High concentration of this group indicates affinity toward pure carbonate facies and less siliciclastic impurities. High concentration of Group-3, which includes only MgO, marked dolomitic zones. The boundary between the Upper Jubaila Member and the Arab-D Member is clearly defined from SGR log profiles, the geochemical data logging and the geochemical data clustering in the cross plots of Group-1 with the radioactive elements in Group-4. The Upper Jubaila Member geochemical data show a very low concentration of U, K, and Th. Consequently, the SGR response of the lithofacies was very low. All reservoir lithofacies showed high concentration of elements from Group-1 and Group-4, while all non-reservoir lithofacies showed less concentration. The Th/U ratio indicates a general shoaling upward following the same trend of the outcrop lithofacies. A high Th/U ratio represents reservoir lithofacies, while a low Th/U ratio represents non-reservoir lithofacies. Lithofacies and SGR log motifs were related in the measured sections. The 3-D models constructed for the SGR indicate significant shoaling-upward cycles of SGR log motifs and provide a good correlation framework with high resolution.

Recommendations

Based on this study the following is recommended:

- Moderate depth drilling and coring program behind the outcrop cliff toward the dip direction could be a suitable way to get much more data for different kind of analysis. This data will not only provide information about lithofacies and

petrophysical properties, but it could also enhance the third dimension for the 3D geostatistical model for the outcrop analog.

- The open boreholes should be logged with different suit of logging. In the lab, variety of analysis could be performed for the cored section like microporosity and micropermeability measurements, petrographic analysis, XRD and SEM-EDS analysis and geochemical analysis. Since this study focused mainly in the qualitative and quantitative analysis of microporosity and micropermeablity, computer tomography (CT) would be crucial step for the core data.
- The methodology of integrating outcrop SGR logging and elemental analysis could be applied in other Jurassic formations (Shuqra Group) to refine their formation tops, sequence stratigraphy, and paleoenvironment.

References

Abu Ali, M., Grover, G., Hwang, R., and Baskin, D., 1995. Geochemical analysis of reservoir continuity and connectivity, Arab-D and Hanifa reservoirs, Abqaiq Field, Saudi Arabia. AAPG Bulletin, 79, 1191.

Adams, E.W., Bellian, J.A., and Reyes, R., 2009. Digital outcrop models reduce uncertainty and improve reservoir characterization. World Oil, 230, 46-49.

Ahr, W.M., 1989. Early diagenetic microporosity in the Cotton Valley Limestone of east Texas. Sedimentary Geology, 63, 275-292.

Al-Dhubbeb, A.G., 2003. Late Jurassic Foraminifera and their palaeoenvironmental significance in the Arab-D Reservoir of the Ghawar Oilfield. Palynology, 27, 252.

Al-Husseini, M.I., 1997. Jurassic sequence stratigraphy of the western and southern Arabian Gulf. GeoArabia (Manama), 2, 361-382.

Al-Husseini, M.I., 2000. Origin of the Arabian Plate structures; Amar collision and Najd Rift. GeoArabia (Manama), 5, 527-542.

Al-Khalifah, M., and Makkawi, M., 2002. The impact of data integration on geostatistical porosity modelling; a case study from the Berri Field, Saudi Arabia. Journal of Petroleum Geology, 25, 485-498.

Alsharhan, A.S., Sadooni, F.N., and Kendall, C.G.S., 2001. Tectono-eustatic controls on the diagenetic evolution of the Middle East platform carbonates. GeoArabia (Manama), 6, 284.

Anselmetti, F.S., Luthi, S., and Eberli, G.P., 1998. Quantitative characterization of carbonate pore systems by digital image analysis. American Association of Petroleum Geologists Bulletin, 82, 1815-1836.

Bábek, O., Kalvoda, J., Aretz, M., Cossey, P.J., Devuyst, F.X., Herbig, H.G., and Sevastopulo, G., 2010. The correlation potential of magnetic susceptibility and outcrop gamma-ray logs at Tournaisian-Viséan boundary sections in Western Europe. Geologica Belgica, 13, 291-308.

Bartley, J.K., Kah, L.C., McWilliams, J.L., and Stagner, A.F., 2007. Carbon isotope chemostratigraphy of the middle Riphean type section (Avzyan Formation, Southern Urals, Russia); signal recovery in a fold and thrust belt. Chemical Geology, 237, 211-232.

Basyoni, M., and Khalil, M., 2011. An overview of the diagenesis of the Upper Jurassic carbonates of Jubaila and Hanifa formations, central Saudi Arabia. Arabian Journal of Geosciences, 1-16.

Bellian, J.A., Kerans, C., and Jennette, D.C., 2005. Digital outcrop models; applications of terrestrial scanning lidar technology in stratigraphic Modelling. Journal of Sedimentary Research, 75, 166-176.

Budd, D.A., 1989. Micro-rhombic calcite and microporosity in limestones: a geochemical study of the lower cretaceous thamama group, U.A.E. Sedimentary Geology, 63, 293-311.

Calvo, J.P., Jones, B.F., Bustillo, M., Fort, R., Alonso Zarza, A.M., and Kendall, C., 1995. Sedimentology and geochemistry of carbonates from lacustrine sequences in the Madrid Basin, central Spain. Chemical Geology, 123, 173-191.

Cantrell, D.L., Swart, P., and Hagerty, R., 2004a. Genesis and characterization of dolomite, Arab-D Reservoir, Ghawar Field, Saudi Arabia. GeoArabia (Manama), 9, 11-36.

Cantrell, D.L., Swart, P., and Hagerty, R., 2004b. Genesis and characterization of dolomite, Arab-D reservoir, Ghawar field, Saudi Arabia. GeoArabia, 9, 11-36.

Cantrell, D.L., Swart, P., Westphal, H., Handford, C.R., and Kendall, C.G.S.C., 2000. Origin of dolomite from the Ghawar Field, Saudi Arabia. GeoArabia (Manama), 5, 65-66.

Cantrell, D.L., 2005. Cortical fabrics of Upper Jurassic ooids, Arab Formation, SaudiArabia: Implications for original carbonate mineralogy. Sedimentary Geology, 186, 156 - 170.

Cantrell, D.L., 2008. Significance of dolomite in a large evaporite-carbonate cycle; Arab-D Reservoir, Saudi Arabia. GeoArabia (Manama), 13, 147.

Cantrell, D.L., Al-Khammash, A., and Jenden, P.D., 2007. Characterization and significance of dedolomite in Wadi Nisah, central Saudi Arabia. GeoArabia 12, 15-30.

Cantrell, D.L., and Hagerty, R.M.p., 1999. Microporosity in Arab Formation carbonates, Saudi Arabia. GeoArabia, 4, 129–154.

Cantrell, D.L., Hagerty, R.M., Handford, C.G., Kendall A., and Westphal, H., 2001. Geology and production significance of dolomite, Arab-D reservoir, Ghawar field, Saudi Arabia. GeoArabia, 6, 45–60.

Cantrell, D.L., and Swart, P.K., 2004b. Enhanced porosity development in the Arab-D as a result of alteration by hydrothermal fluids. Annual Meeting Expanded Abstracts - American Association of Petroleum Geologists, 13, 21.

Choquette, P.W., and Pray, L.C., 1970. Geologic nomenclature and classification of porosity in sedimentary carbonates. The American Association of Petroleum Geologists Bulletin, 54, 207-244.

Cicero, A.D., and Lohmann, K.C., 2001. Sr/Mg variation during rock-water interaction: implications for secular changes in the elemental chemistry of ancient seawater. Geochimica et Cosmochimica Acta, 65, 741-761.

Collins, L.B., Read, J.F., Hogarth, J.W., and Coffey, B.P., 2006. Facies, outcrop gamma ray and C-O isotopic signature of exposed Miocene subtropical continental shelf carbonates, North West Cape, Western Australia. Sedimentary Geology, 185, 1-19.

Debret, M., Sebag, D., Desmet, M., Balsam, W., Copard, Y., Mourier, B., Susperrigui, A.S., Arnaud, F., Bentaleb, I., Chapron, E., Lallier-Vergès, E., and Winiarski, T., 2011. Spectrocolorimetric interpretation of sedimentary dynamics: The new "Q7/4 diagram". Earth-Science Reviews, 109, 1-19.

Dennison, J.M., Filer, J.K., Cavallo, L.J., Drake, R.A., and Middleton, J.D., 1997. Subsurface to surface; use of outcrop gamma-ray logs to interpret structurally complex exposures of Appalachian Devonian strata. AAPG Bulletin, 81, 1549.

Deville de Periere, M., Durlet, C., Vennin, E., Lambert, L., Bourillot, R., Caline, B., and Poli, E., 2011. Morphometry of micrite particles in cretaceous microporous limestones of the Middle East: Influence on reservoir properties. Marine and Petroleum Geology, 28, 1727-1750.

Dewever, B., Breesch, L., Mezini, A., and Swennen, R., 2007. Sedimentological and marine eogenetic control on porosity distribution in Upper Cretaceous carbonate turbidites (central Albania). Sedimentology, 54, 243-264.

Dickson, J.A.D., 1966. Carbonate identification and genesis as revealed by staining. Journal of Sedimentary Petrology, 36, 491-505.

Douglas, J.L., 1996. Geostatistical model for the Arab-D Reservoir, North 'Ain Dar Pilot, Ghawar Field, Saudi Arabia; an improved reservoir simulation model. GeoArabia (Manama), 1, 267-284.

Dravis, J.J., 1989. Deep-burial microporosity in Upper Jurassic Haynesville oolitic grainstones, East Texas. Sedimentary Geology, 63, 325-341.

Dunham, R.J., 1962. Classification of carbonate rocks according to depositional texture. Memoir - American Association of Petroleum Geologists, 108-121.

Dutton, S.P., White, C.D., Willis, B.J., and Novakovic, D., 2002. Calcite Cement Distribution and Its Effect on Fluid Flow in a Deltaic Sandstone, Frontier Formation, Wyoming. AAPG Bulletin, 86, 2007-2021.

Edgell, H.S., 1987. Stratigraphic Control of Oil and Gas Accumulation in Saudi Arabia. . In, Short Course on Hydrocarbon Exploration, , 23.

Enay, R., Le Nindre, Y.M., Mangold, C., Manivit, J., and Vaslet, D., 1987. The Jurassic of central Saudi Arabia; new data on lithostratigraphy, paleoenvironments, ammonite fauna, ages and correlations Le Jurassique d'Arabie Saoudite centrale; nouvelles donnees sur la lithostratigraphie, les paleoenvironnements, les faunes d'ammonites, les ages et les correlations. Geobios, Memoire Special, 9, 13-65.

Evans, R., Mory, A.J., and Tait, A.M., 2007. An outcrop gamma ray study of the Tumblagooda Sandstone, Western Australia. Journal of Petroleum Science and Engineering, 57, 37-59.

Fabuel-Perez, I., Hodgetts, D., and Redfern, J., 2009. A new approach for outcrop characterization and geostatistical analysis of a low-sinuosity fluvial-dominated succession using digital outcrop models: Upper triassic oukaimeden sandstone formation, central high Atlas, Morocco. AAPG Bulletin, 93, 795-827.

Fabuel-Perez, I., Hodgetts, D., and Redfern, J., 2010. Integration of digital outcrop models (DOMs) and high resolution sedimentology - workflow and implications for geological modelling: Oukaimeden Sandstone Formation, High Atlas (Morocco). Petroleum Geoscience, 16, 133-154.

Falivene, O., Arbués, P., Gardiner, A., Pickup, G., Muñoz, J.A., and Cabrera, L., 2006. Best practice stochastic facies Modelling from a channel-fill turbidite sandstone analog (the Quarry outcrop, Eocene Ainsa basin, northeast Spain). AAPG Bulletin, 90, 1003-1029.

Folk, R.L., 1959. Practical petrographic classification of limestones. Bulletin of the American Association of Petroleum Geologists, 43, 1-38.

Frykman, P., 2001. Spatial variability in petrophysical properties in Upper Maastrichtian chalk outcrops at Stevns Klint, Denmark. Marine and Petroleum Geology, 18, 1041-1062.

Galloway, W.E., 1989. Genetic stratigraphic sequences; flooding-surface-bounded depositional units in terrigenous shelves and seaways. International Geological Congress, Abstracts Congres Geologique International, Resumes, 28, Vol. 1, 1-525.

Girard, F., Labourdette, R., and Lopez, M., 2008. Virtual outcrop models and subsurface investigation resolutions; lessons learned from Lodeve Triassic deposits (south of France). Abstracts: Annual Meeting - American Association of Petroleum Geologists, 2008.

Guo, H. and Deutsch, C.V., 2010. Fluvial channel size determination with indicator variograms. Petroleum Geoscience, 16, 161-169.

Halverson, G.P., Wade, B.P., Hurtgen, M.T. and Barovich, K.M., 2010. Neoproterozoic chemostratigraphy. Precambrian Research, 182, 337-350.

Handford, C.R., Cantrell, D.L., and Keith, T.H., 2002. Regional facies relationships and sequence stratigraphy of a super-giant reservoir (Arab-D Member), Saudi Arabia. Program and Abstracts - Society of Economic Paleontologists. Gulf Coast Section. Research Conference, 22, 539-563.

Haq, B.U., Hardenbol, J., and Vail, P.R., 1986. Mesozoic and Cenozoic sea level cycles; towards a complete stratigraphic documentation. Abstracts with Programs - Geological Society of America, 18, 628.

Hughes, G.W., 1996. Environmentally-induced biofacies events in the Arab-D reservoir of Saudi Arabia. GeoArabia (Manama), 1, 150.

Hughes, G.W., 2004a. Middle to Late Jurassic biofacies of Saudi Arabia. Rivista Italiana di Paleontologia e Stratigrafia, 110, 173-179.

Hughes, G.W., 2004b. Palaeoenvironmental and sequence stratigraphic implications of Pseudocyclammina lituus events in the Upper Jurassic (Oxfordian), Hanifa Formation of Saudi Arabia. Grzybowski Foundation Special Publication, 8, 209-216.

Hughes, G.W., Varol, O., Hooker, N.P., and Enay, R., 2008. New aspects of Saudi Arabian Jurassic biostratigraphy. GeoArabia (Manama), 13, 174.

Hughes, G.W., 2009. Using Jurassic micropaleontology to determine Saudi Arabian carbonate paleoenvironments. Special Publication - Society for Sedimentary Geology, 93, 127-152.

Husinec, A., Basch, D., Rose, B., and Read, J.F., 2008. FISCHERPLOTS; an Excel spreadsheet for computing Fischer plots of accommodation change in cyclic carbonate successions in both the time and depth domains. Computers & Geosciences, 34, 269-277.

Kalvoda, J., Bábek, O., Devuyst, F.X., and Sevastopulo, G.D., 2011. Biostratigraphy, sequence stratigraphy and gamma-ray spectrometry of the Tournaisian-Viséan boundary interval in the Dublin Basin. Bulletin of Geosciences, 86, 683-706.

Konert, G., Afifi, A.M., Al-Hajri, S.A., de Groot, K., Al Naim, A.A., and Droste, H.J., 2001. Paleozoic stratigraphy and hydrocarbon habitat of the Arabian Plate. AAPG Memoir, 74, 483-515.

Koptikova, L., Babek, O., Hladil, J., Kalvoda, J., and Slavik, L., 2010. Stratigraphic significance and resolution of spectral reflectance logs in Lower Devonian carbonates of the Barrandian area, Czech Republic; a correlation with magnetic susceptibility and gamma-ray logs. Sedimentary Geology, 225, 83-98.

Koptíková, L., Bábek, O., Hladil, J., Kalvoda, J., and Slavík, L., 2010. Stratigraphic significance and resolution of spectral reflectance logs in Lower Devonian carbonates of the Barrandian area, Czech Republic; a correlation with magnetic susceptibility and gamma-ray logs. Sedimentary Geology, 225, 83-98.

Krystyniak, A.M., Paxton, S.T., and Coffey, W.S., 2005. Detailed outcrop gamma-ray characterization of the Woodford Shale, south-central Oklahoma. Abstracts: Annual Meeting - American Association of Petroleum Geologists, 14, A76.

Labourdette, R., Crumeyrolle, P., and Remacha, E., 2008. Characterisation of dynamic flow patterns in turbidite reservoirs using 3D outcrop analogues: Example of the Eocene Morillo turbidite system (south-central Pyrenees, Spain). Marine and Petroleum Geology, 25, 255-270.

Lambert, L., Durlet, C., Loreau, J.P., and Marnier, G., 2006. Burial dissolution of micrite in Middle East carbonate reservoirs (Jurassic-Cretaceous): Keys for recognition and timing. Marine and Petroleum Geology, 23, 79-92.

Lapponi, F., Casini, G., Sharp, I., Blendinger, W., Fernández, N., Romaire, I., and Hunt, D., 2011. From outcrop to 3D modelling: A case study of a dolomitized carbonate reservoir, Zagros Mountains, Iran. Petroleum Geoscience, 17, 283-307.

Le Nindre, Y.M., Farjanel, G., Giot, D., and Remond, G., 1987. Application of crystalline luminescence properties to the petrography of sedimentary rocks Application des proprietes de luminescence cristalline a la petrographie des roches sedimentaires. Principaux Resultats Scientifiques - Bureau de Recherches Geologiques et Minieres, 1987, 85-86.

Le Nindre, Y.M., Manivit, J., Manivit, H., and Vaslet, D., 1990. Jurassic and Cretaceous sequence stratigraphy of Saudi Arabia Stratigraphie sequentielle du Jurassique et du Cretace en Arabie Saoudite. Bulletin de la Societe Geologique de France, Huitieme Serie, 6, 1025-1034.

Le Nindre, Y.M., Vaslet, D., and Manivit, J., 1996. Quantitative subsidence analysis of the Arabian Shelf during the Jurassic. Conference and Technical Exhibition - European Association of Geoscientists and Engineers, 58.

Lehmann, C., Goff, J., Jones, B.W., and Anastas, A., 2006. Facies distribution and dolomitization along the southeastern shelf margin of the Jurassic Gotnia Basin. Abstracts: Annual Meeting - American Association of Petroleum Geologists, 15, 62.

Leren, B.L.S., Howell, J., Enge, H., and Martinius, A.W., 2010. Controls on stratigraphic architecture in contemporaneous delta systems from the Eocene Roda Sandstone, Tremp-Graus Basin, northern Spain. Sedimentary Geology, 229, 9-40.

Lindsay, R.F., Cantrell, D.L., Hughes, G.W., Keith, T.H., Mueller, H.W., and Russell, S.D., 2006. Ghawar Arab-D; widespread porosity in shoaling-upward carbonate cycles, Saudi Arabia. Abstracts: Annual Meeting - American Association of Petroleum Geologists, 15, 64.

Lucia, F.J., 1995. Rock-fabric/petrophysical classification of carbonate pore space for reservoir characterization. American Association of Petroleum Geologists Bulletin, 79, 1275-1300.

Maliva, R.G., Missimer, T.M., Clayton, E.A., and Dickson, J.A.D., 2009a. Diagenesis and porosity preservation in Eocene microporous limestones, South Florida, USA. Sedimentary Geology, 217, 85-94.

Maliva, R.G., Missimer, T.M., Clayton, E.A., and Dickson, J.A.D., 2009b. Diagenesis and porosity preservation in Eocene microporous limestones, South Florida, USA. Sedimentary Geology, 217, 85-94.

Martinius, A.W., Geel, C.R., and Arribas, J., 2002. Lithofacies characterization of fluvial sandstones from outcrop gamma-ray logs (Loranca Basin, Spain); the influence of provenance. Petroleum Geoscience, 8, 51-62.

Merino-Tomé, O., Porta, G.D., Kenter, J.A.M., Verwer, K., Harris, P.M., Adams, E.W., Playton, T., and Corrochano, D., 2012. Sequence development in an isolated carbonate platform (Lower Jurassic, Djebel Bou Dahar, High Atlas, Morocco): Influence of tectonics, eustacy and carbonate production. Sedimentology, 59, 118-155.

Meyer, F.O., Price, R.C., Al-Ghamdi, I.A., Al-Goba, I.M., Al-Raimi, S.M., and Cole, J.C., 1996. Outcropping strata equivalent to Arab-D reservoir, Wadi Nisah, Saudi Arabia. GeoArabia (Manama), 1, 171-172.

Meyer, F.O., Price, R.C., and Al-Raimi, S.M., 2000. Stratigraphic and petrophysical characteristics of cored Arab-D super-k intervals, Hawiyah area, Ghawar Field, Saudi Arabia. GeoArabia (Manama), 5, 355-384.

Mitchell, J.C., Lehmann, P.J., Cantrell, D.L., Al-Jallal, I.A., and Al-Thagafy, M.A.R., 1988. Lithofacies, diagenesis and depositional sequence; Arab-D Member, Ghawar Field, Saudi Arabia. SEPM Core Workshop, 12, 459-514.

Morad, S., I.S. Al-Aasm, F.H. Nader, A. Ceriani, Gasparrini, M., and Mansurbeg, H., 2012. Impact of diagenesis on the spatial and temporal distribution of reservoir quality in the Jurassic Arab-D and C members, offshore Abu Dhabi oilfield, United Arab Emirates GeoArabia, 17, 17-56.

Moshier, S.O., 1989. Microporosity in micritic limestones: a review. Sedimentary Geology, 63, 191-213.

Murris, R.J., 1981. Seals for major Middle East fields. AAPG Bulletin, 65, 964.

Okla, S.M., 1986. Microfacies and environment of Upper Tuwaiq Mountain Limestone (Upper Jurassic) in central Saudi Arabia. Arab Gulf Journal of Scientific Research, 4, 177-189.

Osmond, J.K. and Ivanovich, M., 1992. Uranium-series mobilization and surface hydrology. Uranium-series disequilibrium; applications to Earth, marine, and environmental sciences, 259-289.

Palermo, D., Aigner, T., Nardon, S., and Blendinger, W., 2010. Three-dimensional facies Modelling of carbonate sand bodies: Outcrop analog study in an epicontinental basin (Triassic, southwest Germany). AAPG Bulletin, 94, 475-512.

Parkinson, D.N., 1996. Gamma-ray spectrometry as a tool for stratigraphical interpretation; examples from the western European Lower Jurassic. Geological Society Special Publications, 103, 231-255.

Pittman, E.D., 1971. Microporosity in carbonate rocks. The American Association of Petroleum Geologists Bulletin, 55, 1873-1878.

Powers, R.W., 1962. Arabian Upper Jurassic carbonate reservoir rocks. 122-192.

Powers, R.W., 1968. International stratigraphic lexicon; volume 3, Asia, part 10 b 1, Saudi Arabia Lexique stratigraphique international; volume III, Asie, fascicule 10 b 1, Arabie Saoudite. 177.

Pringle, J., Gardiner, A. and Westerman, R., 2004. Virtual geological outcrops; fieldwork and analysis made less exhaustive? Geology Today, 20, 67-72.

Pringle, J.K., 2000. 3-D architecture in turbidite systems; integrating digital photogrammetry, outcrop geology and geophysical data in the Ross Formation, County Clare, West Ireland. AAPG Bulletin, 84, 1871-1872.

Pringle, J.K., Howell, J.A., Hodgetts, D., Westerman, A.R., and Hodgson, D.M., 2006. Virtual outcrop models of petroleum reservoir analogues: A review of the current state-of-the-art. First Break, 24, 33-42.

Sahin, A., Ali, A.Z., Saner, S. and Menouar, H., 2007. Permeability Anisotropy Distributions in an Upper Jurassic Carbonate Reservoir, Eastern Saudi Arabia. Journal of Petroleum Geology, 30, 147-158.

Sahin, A. and Saner, S., 2001. Statistical Distributions and Correlations of Petrophysical Parameters in The Arab-D Reservoir, Abqaiq Oilfield, Eastern Saudi Arabia. Journal of Petroleum Geology, 24, 101-114.

Sahin, A., Saner, S. and El-Sahn, H.F., 1998. Statistical distributions and correlation of petrophysical parameters in a carbonate reservoir. GeoArabia (Manama), 3, 151-152.

Saner, S., Al-Hinai, K. and Perincek, D., 2005. Surface expressions of the Ghawar Structure, Saudi Arabia. Marine and Petroleum Geology, 22, 657-670.

Saner, S. and Sahin, A., 1999. Lithological and zonal porosity-permeability distributions in the Arab-D reservoir, Uthmaniyah Field, Saudi Arabia. AAPG Bulletin, 83, 230-243.

Schnyder, J., Ruffell, A., Deconinck, J.-F. and Baudin, F., 2006. Conjunctive use of spectral gamma-ray logs and clay mineralogy in defining late Jurassic–early Cretaceous palaeoclimate change (Dorset, U.K.). Palaeogeography, Palaeoclimatology, Palaeoecology, 229, 303-320.

Senalp, M. and Al-Duaiji, A.A., 2001. Qasim Formation; Ordovician storm- and tide-dominated shallow-marine siliciclastic sequences, central Saudi Arabia. GeoArabia (Manama), 6, 233-268.

Sharland, P., Archer, R., Casey, D., Davies, R., Hall, S., Heward, A., Horbury, A. and Simmons, M., 2000. A proposed sequence stratigraphy for the Phanerozoic succession of the Arabian Plate; Mesozoic and Cenozoic sequences. GeoArabia (Manama), 5, 181.

Sharland, P.R., Boote, D., Casey, D.M., Davies, R.B. and Simmons, M.D., 2001. North Africa and Arabian Plate first and second order sequence stratigraphy. Annual Meeting Expanded Abstracts - American Association of Petroleum Geologists, 12, 156.

Slatt, R.M., Jordan, D.W., D'Agostino, A.E. and Gillespie, R.H., 1992. Outcrop gamma-ray logging to improve understanding of subsurface well log correlations. Geological Society, London, Special Publications, 65, 3-19.

Smith, L.B., Eberli, G.P., Masaferro, J.L. and Al-Dhahab, S., 2003. Discrimination of effective from ineffective porosity in heterogeneous Cretaceous carbonates, Al Ghubar field, Oman. AAPG Bulletin, 87, 1509-1529.

Steineke, M. and Bramkamp, R.A., 1952. Mesozoic rocks of eastern Saudi Arabia. Bulletin of the American Association of Petroleum Geologists, 36, 909.

Stoudt, E. L., and M. A. Raines, 2004, Reservoir characterization in the San Andres Formation of Vacuum field, Lea County, New Mexico: Another use of the San Andres Algerita outcrop model for improved reservoir description, in Integration of outcrop and modern analogs in reservoir Modelling: AAPG Memoir 80, p. 191– 214.

Svendsen, J.B. and Hartley, N.R., 2001. Comparison between outcrop-spectral gamma ray logging and whole rock geochemistry: implications for quantitative reservoir characterisation in continental sequences. Marine and Petroleum Geology, 18, 657-670.

Swart, P.K., Cantrell, D.L., Westphal, H., Handford, C.R. and Kendall, C.G., 2005. Origin of dolomite in the Arab-D reservoir from the Ghawar field, Saudi Arabia: Evidence from petrographic and geochemical constraints. Journal of Sedimentary Research, 75, 476-491.

Vacek, F., Hladil, J. and Schnabl, P., 2010. Stratigraphic correlation potential of magnetic susceptibility and gamma-ray spectrometric variations in calciturbiditic facies (Silurian-Devonian boundary, Prague Synclinorium, Czech Republic). Geologica Carpathica, 61, 257-272.

Vaslet, D., 1990. Upper Ordovician glacial deposits in Saudi Arabia. Episodes, 13, 147-161.

Vaslet, D., Manivit, J. and Le Nindre, Y.-M., 1989. Proposal for new reference sections of the Early Triassic Sudair Shale, Kingdom of Saudi Arabia. Professional Papers - Kingdom of Saudi Arabia, Ministry of Petroleum and Mineral Resources, PP3, 45-59.

Vincent, B., Rambeau, C., Emmanuel, L. and Loreau, J.-P., 2006. Sedimentology and trace element geochemistry of shallow-marine carbonates: an approach to paleoenvironmental analysis along the Pagny-sur-Meuse Section (Upper Jurassic, France). Facies, 52, 69-84.

Volery, C., Davaud, E., Foubert, A. and Caline, B., 2009. Shallow-Marine Microporous Carbonate Reservoir Rocks in The Middle East: Relationship With Seawater Mg/Ca Ratio and Eustatic Sea Level. Journal of Petroleum Geology, 32, 313-325.

Warrlich, G., Bosence, D., Waltham, D., Wood, C., Boylan, A. and Badenas, B., 2008. 3D stratigraphic forward modelling for analysis and prediction of carbonate platform stratigraphies in exploration and production. Marine and Petroleum Geology, 25, 35-58.

Weger, R.J., Eberli, G.P., Baechle, G.T., Massaferro, J.L. and Sun, Y.-F., 2009. Quantification of pore structure and its effect on sonic velocity and permeability in carbonates. AAPG Bulletin, 93, 1297-1317.

Weijermars, R., 1998. Plio-Quaternary movement of the East Arabian Block. GeoArabia (Manama), 3, 509-540.

White, C. D., B. J. Willis, S. P. Dutton, J. P. Bhattacharya, and K. Narayanan, 2004, Sedimentology, statistics, and flow behavior for a tide-influenced deltaic sandstone, Frontier Formation, Wyoming, United States, in Integration of outcrop and modern analogs in reservoir Modelling: AAPG Memoir 80, p. 129 – 152.

Wilson, A.O., 1981. Jurassic Arab-C and -D Carbonate Petroleum Reservoirs, Qatif Field, Saudi Arabia. Society of Petroleum Engineers of AIME, (Paper) SPE, 171-177.

Wilson, P., Gawthorpe, R.L., Hodgetts, D., Rarity, F. and Sharp, I.R., 2009. Geometry and architecture of faults in a syn-rift normal fault array: The Nukhul half-graben, Suez rift, Egypt. Journal of Structural Geology, 31, 759-775.

Ziegler, M.A., 2001. Late Permian to Holocene paleofacies evolution of the Arabian Plate and its hydrocarbon occurrences. GeoArabia (Manama), 6, 445-504.

Vitae

Name: Hassan Abdalla Eltom

Nationality: Sudanese

Date of Birth: 1-2-1976

Email: eltoum5@hotmail.com

Phone: + 966 531579527

Address: Shabia, Khartoum-North, Sudan

Academic Background: MSc Geology